AN EFFECTIVE STRESS CREEP MODEL FOR FROZEN SAND

By

Zhanliang Ji

A Thesis
Submitted to the Faculty of Graduate Studies
in Partial Fulfillment of the Requirements
for the Degree of

DOCTOR OF PHILOSOPHY

Department of Civil & Geological Engineering
The University of Manitoba
Winnipeg, Manitoba

December, 1995

ISBN 0-612-13215-3

Name _____

Dissertation Abstracts International and *Masters Abstracts International* are arranged by broad, general subject categories. Please select the one subject which most nearly describes the content of your dissertation or thesis. Enter the corresponding four-digit code in the spaces provided.

Civil Engineering
SUBJECT TERM

0543
SUBJECT CODE

UMI

Subject Categories

THE HUMANITIES AND SOCIAL SCIENCES

COMMUNICATIONS AND THE ARTS
Architecture 0729
Art History 0377
Cinema 0900
Dance 0378
Fine Arts 0357
Information Science 0723
Journalism 0391
Library Science 0399
Mass Communications 0708
Music 0413
Speech Communication 0459
Theater 0465

EDUCATION
General 0515
Administration 0514
Adult and Continuing 0516
Agricultural 0517
Art 0273
Bilingual and Multicultural 0282
Business 0688
Community College 0275
Curriculum and Instruction 0727
Early Childhood 0518
Elementary 0524
Finance 0277
Guidance and Counseling 0519
Health 0680
Higher 0745
History of 0520
Home Economics 0278
Industrial 0521
Language and Literature 0279
Mathematics 0280
Music 0522
Philosophy of 0998
Physical 0523
Psychology 0525
Reading 0535
Religious 0527
Sciences 0714
Secondary 0533
Social Sciences 0534
Sociology of 0340
Special 0529
Teacher Training 0530
Technology 0710
Tests and Measurements 0288
Vocational 0747

LANGUAGE, LITERATURE AND LINGUISTICS
Language
- General 0679
- Ancient 0289
- Linguistics 0290
- Modern 0291

Literature
- General 0401
- Classical 0294
- Comparative 0295
- Medieval 0297
- Modern 0298
- African 0316
- American 0591
- Asian 0305
- Canadian (English) 0352
- Canadian (French) 0355
- English 0593
- Germanic 0311
- Latin American 0312
- Middle Eastern 0315
- Romance 0313
- Slavic and East European 0314

PHILOSOPHY, RELIGION AND THEOLOGY
Philosophy 0422
Religion
- General 0318
- Biblical Studies 0321
- Clergy 0319
- History of 0320
- Philosophy of 0322

Theology 0469

SOCIAL SCIENCES
American Studies 0323
Anthropology
- Archaeology 0324
- Cultural 0326
- Physical 0327

Business Administration
- General 0310
- Accounting 0272
- Banking 0770
- Management 0454
- Marketing 0338

Canadian Studies 0385
Economics
- General 0501
- Agricultural 0503
- Commerce-Business 0505
- Finance 0508
- History 0509
- Labor 0510
- Theory 0511

Folklore 0358
Geography 0366
Gerontology 0351
History
- General 0578
- Ancient 0579
- Medieval 0581
- Modern 0582
- Black 0328
- African 0331
- Asia, Australia and Oceania 0332
- Canadian 0334
- European 0335
- Latin American 0336
- Middle Eastern 0333
- United States 0337

History of Science 0585
Law 0398
Political Science
- General 0615
- International Law and Relations 0616
- Public Administration 0617

Recreation 0814
Social Work 0452
Sociology
- General 0626
- Criminology and Penology ... 0627
- Demography 0938
- Ethnic and Racial Studies 0631
- Individual and Family Studies 0628
- Industrial and Labor Relations 0629
- Public and Social Welfare 0630
- Social Structure and Development 0700
- Theory and Methods 0344

Transportation 0709
Urban and Regional Planning 0999
Women's Studies 0453

THE SCIENCES AND ENGINEERING

BIOLOGICAL SCIENCES
Agriculture
- General 0473
- Agronomy 0285
- Animal Culture and Nutrition 0475
- Animal Pathology 0476
- Food Science and Technology 0359
- Forestry and Wildlife 0478
- Plant Culture 0479
- Plant Pathology 0480
- Plant Physiology 0817
- Range Management 0777
- Wood Technology 0746

Biology
- General 0306
- Anatomy 0287
- Biostatistics 0308
- Botany 0309
- Cell 0379
- Ecology 0329
- Entomology 0353
- Genetics 0369
- Limnology 0793
- Microbiology 0410
- Molecular 0307
- Neuroscience 0317
- Oceanography 0416
- Physiology 0433
- Radiation 0821
- Veterinary Science 0778
- Zoology 0472

Biophysics
- General 0786
- Medical 0760

EARTH SCIENCES
Biogeochemistry 0425
Geochemistry 0996
Geodesy 0370
Geology 0372
Geophysics 0373
Hydrology 0388
Mineralogy 0411
Paleobotany 0345
Paleoecology 0426
Paleontology 0418
Paleozoology 0985
Palynology 0427
Physical Geography 0368
Physical Oceanography 0415

HEALTH AND ENVIRONMENTAL SCIENCES
Environmental Sciences 0768
Health Sciences
- General 0566
- Audiology 0300
- Chemotherapy 0992
- Dentistry 0567
- Education 0350
- Hospital Management 0769
- Human Development 0758
- Immunology 0982
- Medicine and Surgery 0564
- Mental Health 0347
- Nursing 0569
- Nutrition 0570
- Obstetrics and Gynecology .. 0380
- Occupational Health and Therapy 0354
- Ophthalmology 0381
- Pathology 0571
- Pharmacology 0419
- Pharmacy 0572
- Physical Therapy 0382
- Public Health 0573
- Radiology 0574
- Recreation 0575
- Speech Pathology 0460
- Toxicology 0383

Home Economics 0386

PHYSICAL SCIENCES
Pure Sciences
Chemistry
- General 0485
- Agricultural 0749
- Analytical 0486
- Biochemistry 0487
- Inorganic 0488
- Nuclear 0738
- Organic 0490
- Pharmaceutical 0491
- Physical 0494
- Polymer 0495
- Radiation 0754

Mathematics 0405
Physics
- General 0605
- Acoustics 0986
- Astronomy and Astrophysics 0606
- Atmospheric Science 0608
- Atomic 0748
- Electronics and Electricity 0607
- Elementary Particles and High Energy 0798
- Fluid and Plasma 0759
- Molecular 0609
- Nuclear 0610
- Optics 0752
- Radiation 0756
- Solid State 0611

Statistics 0463

Applied Sciences
Applied Mechanics 0346
Computer Science 0984
Engineering
- General 0537
- Aerospace 0538
- Agricultural 0539
- Automotive 0540
- Biomedical 0541
- Chemical 0542
- Civil 0543
- Electronics and Electrical 0544
- Heat and Thermodynamics ... 0348
- Hydraulic 0545
- Industrial 0546
- Marine 0547
- Materials Science 0794
- Mechanical 0548
- Metallurgy 0743
- Mining 0551
- Nuclear 0552
- Packaging 0549
- Petroleum 0765
- Sanitary and Municipal 0554
- System Science 0790

Geotechnology 0428
Operations Research 0796
Plastics Technology 0795
Textile Technology 0994

PSYCHOLOGY
General 0621
Behavioral 0384
Clinical 0622
Developmental 0620
Experimental 0623
Industrial 0624
Personality 0625
Physiological 0989
Psychobiology 0349
Psychometrics 0632
Social 0451

AN EFFECTIVE STRESS CREEP MODEL

FOR FROZEN SAND

BY

ZHANLIANG JI

A Thesis submitted to the Faculty of Graduate Studies of the University of Manitoba in partial fulfillment of the requirements of the degree of

DOCTOR OF PHILOSOPHY

ABSTRACT

A constitutive creep model for frozen soil is an important component of cold regions engineering and science. There are three fundamental problems remaining unsolved by the existing creep models: (1) most of the existing models were developed from uniaxial creep tests, and did not take into consideration the effects of hydrostatic stress and volume change on the mechanical behaviour the soil, (2) most of the existing models utilized a time-dependent creep rate, and ignored the fact that time is not an intrinsic cause of creep, (3) the existing models treated frozen soil as a single-phase material, and were unable to represent the interaction between the soil skeleton and the pore matrix.

This thesis is a development of a three dimensional strain-hardening, strain-softening, creep model for frozen soil. The stress acting on the frozen soil is separated into a mean normal stress which is associated with volumetric strain and a deviatoric stress which is associated with shear strain and shear induced dilation. Both the mean normal stress and the deviate stress are further separated into components carried by the soil skeleton and components carried by the pore matrix. The creep rate of frozen soil is directly related to the stress actually sustained by the ice matrix. As well, the model relates creep rate to the stress-strain state rather than to time makes it possible to accommodate stress changes during the creep process more rationally and effectively than do the existing models.

The model was verified by comparing the predicted and measured creep curves from both constant mean normal stress and constant cell pressure triaxial creep tests, and the

results showed that the model can represent the creep behaviour fairly well.

The concept of using effective mean normal stresses and effective shear stresses in frozen soils opens a new channel for investigating and modelling the mechanical behaviour of frozen soil.

ACKNOWLEDGEMENTS

The writer wishes to express his sincere gratitude to his advisor, Dr. L. Domaschuk, for his guidance and assistance during the preparation of this thesis.

The writer also wishes to extend special thanks to Dr. D. H. Shields, Dr. N. Rajapakse, Dr. E. Lajtai, who provided helpful suggestions, and encouragements to this work. Appreciation is also expressed to Dr. J. Graham, Dr. R. Frank, and Dr. N. Sinha for their advice and instructions. Thanks also extended to Mr. N. Piamsalee for his support in preparing the experimental equipment.

The writer also wishes to acknowledge the financial assistance provided by the National Science and Engineering Research Council of Canada.

The writer is greatly indebted to his parents for their understanding and encouragement. The writer expresses sincere thanks to his wife, Qingxia Xie, for her support and sacrifices during his education.

TABLE OF CONTENTS

LIST OF FIGURES

Figure

CHAPTER 1

INTRODUCTION

Permafrost extends over a large portion of the Northern Hemisphere. Fig.1.1 shows the distribution of permafrost in the north. It is seen from the figure that a large part of Canada, Russia, and China and the whole of Alaska are covered by permafrost. The population in these cold regions may not be very large, but the natural resources underneath permafrost have received much attention from all over the world. As the world population and the need for these natural resources increases, the exploitation of the cold region seems inevitable. In order to develop the northern area effectively and cause as little damage as possible to the environment of the area, people need to have a comprehensive ecological understanding of the behaviour of permafrost. The mechanical properties of frozen soil is an important aspect of this understanding.

1.1 THE CREEP BEHAVIOUR OF FROZEN SOIL AND THE STATEMENT OF THE PROBLEM

From a mechanics point of view, frozen soil is a particulate composite material composed of four different components. They are the solid mineral and organic grains, pore ice, unfrozen water and air voids. The most significant mechanical characteristic of frozen soil is its time and temperature dependent stress-strain behaviour, which is usually called "creep". The understanding of the creep behaviour of frozen soil is vital to the design of any structure supported by naturally or artificially frozen ground.

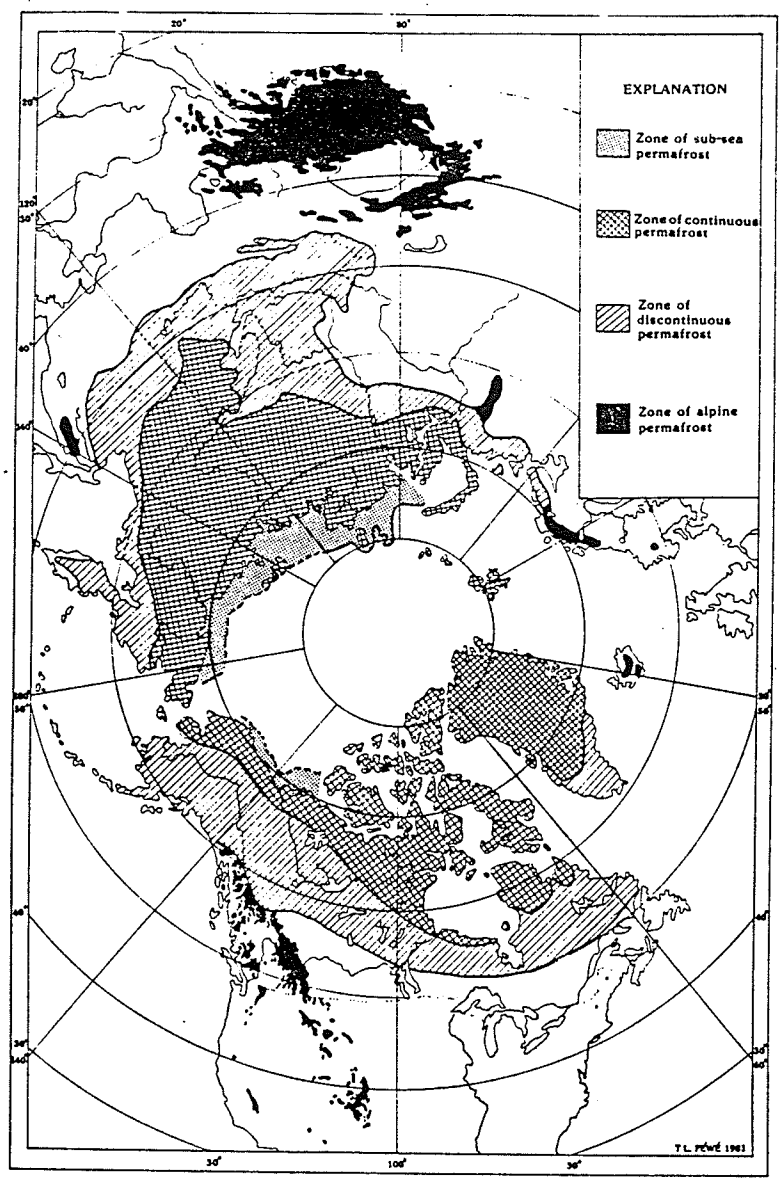

Fig.1.1 Distribution of permafrost in the Northern Hemisphere. (After Pewe, 1983)

Both pore ice and unfrozen water are viscous media. When frozen soils are subjected to stress, these viscous media deform constantly because of creep. The actual stress distribution is extremely complicated and is constantly changing. A proper constitutive model for the creep behaviour of frozen soil has long been a puzzle, and many researchers have tried to solve it. From the methodology point of view, there are two basic approaches to modelling creep behaviour of frozen soil. One is the physical theory which starts with the established laws of physics by considering the directional migration of the molecules/atoms in a stress field. The other is the engineering approach, which is usually called the phenomenological theory, and is based on empirical correlations obtained from creep tests. The former approach takes the micro-structure of the material into consideration, while the latter considers only the macro effects. The former approach was found to be a very useful method in modelling the creep behaviour of metals. For example, there is a well known theory of activation energy and the creep models developed from this theory. The approach, however, was less successful when applied to frozen soil due to the complexity of the material, and so instead, the latter approach was widely adopted. In the development of the creep model in this thesis, the latter approach will be used with the concept from the former approach employed as qualitative guidance.

The following are shortcomings of existing creep models developed for frozen soils.

(A) Most of the existing models were developed from data obtained from *uniaxial* creep tests, and did not take into consideration the effects of hydrostatic pressure and volume change, even though experimental evidence (Chamberlain et. al., 1972; Sayles, 1973;

Parameswaran, 1980; and Domaschuk et. al., 1991) shows that both of them play a significant role in the creep process. The models were extended to a general stress strain state using equivalent stress and strain components under the assumption that the material is isotropic and there is no volume change during creep.

(B) Most of the existing models use a time-dependent creep strain or strain rate. However, time is not an intrinsic cause of creep, rather, it is the imposed stress state and the creep properties of frozen soil that dictate the creep rates. The creep properties change with strain and this change can not be rationally represented by time. Consequently, using time as the variable makes it very difficult to incorporate any changes in applied stress during the creep process.

(C) Most of the existing models treat the frozen soil as a single-phase material and ignore the interaction between the soil skeleton and the ice matrix. However, the reason that frozen soil creeps is because the stress acting on the pore ice causes it to flow under stress. Therefore the creep rate should be related to the stress actually sustained by the ice matrix rather than to the total stress acting on the frozen soil.

1.2 OBJECTIVES AND SCOPE

(A) The primary objective of this thesis was to develop a strain-hardening, strain-softening constitutive creep model for frozen soil. The proposed model differs from existing constitutive models in two fundamental and unique respects. Firstly, the total stress is

separated into a component carried by the soil skeleton and a component carried by the pore ice. Moreover, the stress carried by the pore ice is further separated into an excess component and a sustainable component. Secondly, whereas existing models relate deformation to time, in the proposed model deformation is related to the stress history and the existing stress-strain state. The separation of stress into components carried by the soil particles and the pore ice is a new concept in the mechanics of frozen soil, and the expression of creep rate as a function of prevailing strain makes it possible to compute creep strains under changing conditions of applied stress.

As mentioned previously, the creep characteristics of a frozen soil are dominated by the ice content. The ice content may vary from that of a dry soil to that of a material that is predominantly ice with soil inclusions. In the former case, the behaviour of the soil is basically the same as an unfrozen soil while in the latter case, the behaviour is basically that of ice. Most frozen soils lie between these two extremes and consist of all four phases: mineral solids, ice, unfrozen water, and air. Because of ice segregation, air voids may exist in frozen soil even though the overall degree of ice saturation exceeds 100%. The air voids play an important role in the creep behaviour of such soils in that they provide space into which pore ice may flow thereby resulting in volume reduction and dissipation of excess pore ice stress. The effects of the unfrozen pore water and the pore ice on the creep and strength behaviour of the frozen soil are combined. That is, creep parameters and creep strengths are determined experimentally and thus they include the combined effects of both components. The pore matrix is simply referred to as pore ice since ice constitutes the major portion of the pore matrix.

The majority of the study was devoted to developing the theoretical constitutive creep model. To make the theoretical model applicable to **all** real soils, the model would have to be calibrated for a variety of soil types and a variety of soil temperatures. In this study, the *calibration* of the model was limited to a single soil type and a single temperature. The soil was a sand with a high degree of ice saturation and its temperature was -3°C. This was done because these were the only suitable experimental data that were available for calibrating the model. The data were taken from the triaxial compression creep tests that had been carried out previously by Rahman (1988) in a related study. Generating new or additional experimental creep data was beyond the scope of this thesis because of the inordinate amount of additional time that would have been required.

(B) An overview of the contents of the thesis is given below.

Chapter 2 contains an extensive review of the existing literature on ice and frozen soil mechanics.

Development and calibration of the model required experimental data on the behaviour of the sand in an unfrozen state. Because such data were not available, a series of triaxial compression tests on the sand were carried out by the writer. The details of the tests and the results are presented in Chapter 3.

In developing the constitutive model, the state of stress and strain were separated into volumetric and deviatoric components as presented by Domaschuk and Wade (1969) in their

development of a constitutive model for sand. It is referred to as the K-G model. The creep behaviour of frozen soil under hydrostatic stress was studied by constant mean normal stress isotropic creep tests, and the creep behaviour under deviatoric stress was explored by constant mean normal stress triaxial creep tests. The development of the component of the constitutive equation dealing with a relationship between the mean normal stress and associated volumetric creep strain is given in Chapter 4. The concept of a generalized *effective* mean normal stress is introduced and a relationship between the rate of volumetric creep and the stress-strain state of the frozen sand is developed in the chapter.

The development of the component of the constitutive equation which relates deviatoric or shear stresses with shear creep strains is given in Chapter 5. The development required the following.

(a) Introducing the concept of an *effective* shear stress and an *excess* ice shear stress for frozen soil.

(b) Establishing a relationship between the effective mean normal stress, effective shear stress and shear strain.

(c) Establishing a relationship between the excess ice shear stress and the rate of shear creep.

The two components of the constitutive equation were then coupled to provide a

generalized creep model. The predictive capability of the constitutive model was then examined by using it to predict some experimental triaxial creep data that had not been used in calibrating the model. The results are given in Chapter 6.

A concept fundamental to the constitutive model is that when ice is stressed, it can move through a soil skeleton. To demonstrate this experimentally, two simple tests in which ice was forced into a dry sand were conducted. These results are given in Chapter 7.

Conclusions and recommendations for further research are presented in Chapter 8.

CHAPTER 2

A REVIEW OF MECHANICAL BEHAVIOUR OF ICE AND FROZEN SOIL

2.1 INTRODUCTION

The complicated mechanical behaviour of ice and frozen soil has long been a subject which attracted the interest of many engineers and scientists. The knowledge base of this issue has been greatly broadened by their work. Research on the engineering behaviour of ice and frozen soil was mainly promoted by the industrial development in the northern areas. As well, the requirement for a national defence strategy stimulated research activity. Starting from the early seventies, the development and exploitation of the north demanded by such industries as petroleum and mining greatly accelerated the research on this subject, and a large amount of research articles were published during the seventies and the eighties. The research activities gradually decreased towards the beginning of the nineties because the pace of the industrial development in the north slowed down.

This chapter discusses the current knowledge of the mechanical behaviour of ice and frozen soil. The discussion focuses on the advances made since the eighties.

2.2 MECHANICAL BEHAVIOUR OF ICE

Ice is a major component of frozen soil. The mechanical behaviour of frozen soil is largely dictated by the behaviour of the pore ice, and therefore a summary of the behaviour of ice is appropriate before reviewing frozen soil.

From a mechanics point of view, ice is a non-linear, anisotropic, temperature and time-dependent material. It is impractical to model this type of material without making simplifications, but the simplifications should be made upon a good understanding of the behaviour of the real material. The temperature and time-dependent deformation behaviour, or **creep** as it is usually called, is the most significant mechanical characteristic of ice. Under the temperature and stress levels usually encountered in civil engineering practice, the major portion of the deformation of ice occurs in the form of creep, therefore the discussion in this section will focus on the this aspect.

2.2.1 Physical Properties of Ice

Depending on temperature and pressure at phase change, different types of ice having different arrangements of oxygen and hydrogen atoms may be formed. **Fig.2.1** shows a phase diagram of ice. There are nine different types of ice as shown in the figure. However, the most common type of ice usually encountered in nature is the Ih type of ice. A detailed description of the microstructure of the Ih ice was given by Mellor (1979). Since almost all the pore ice found in frozen soil is of Ih type, the discussion on ice hereafter refers to this type of ice. The following two physical properties have significant effects on the engineering behaviour of ice.

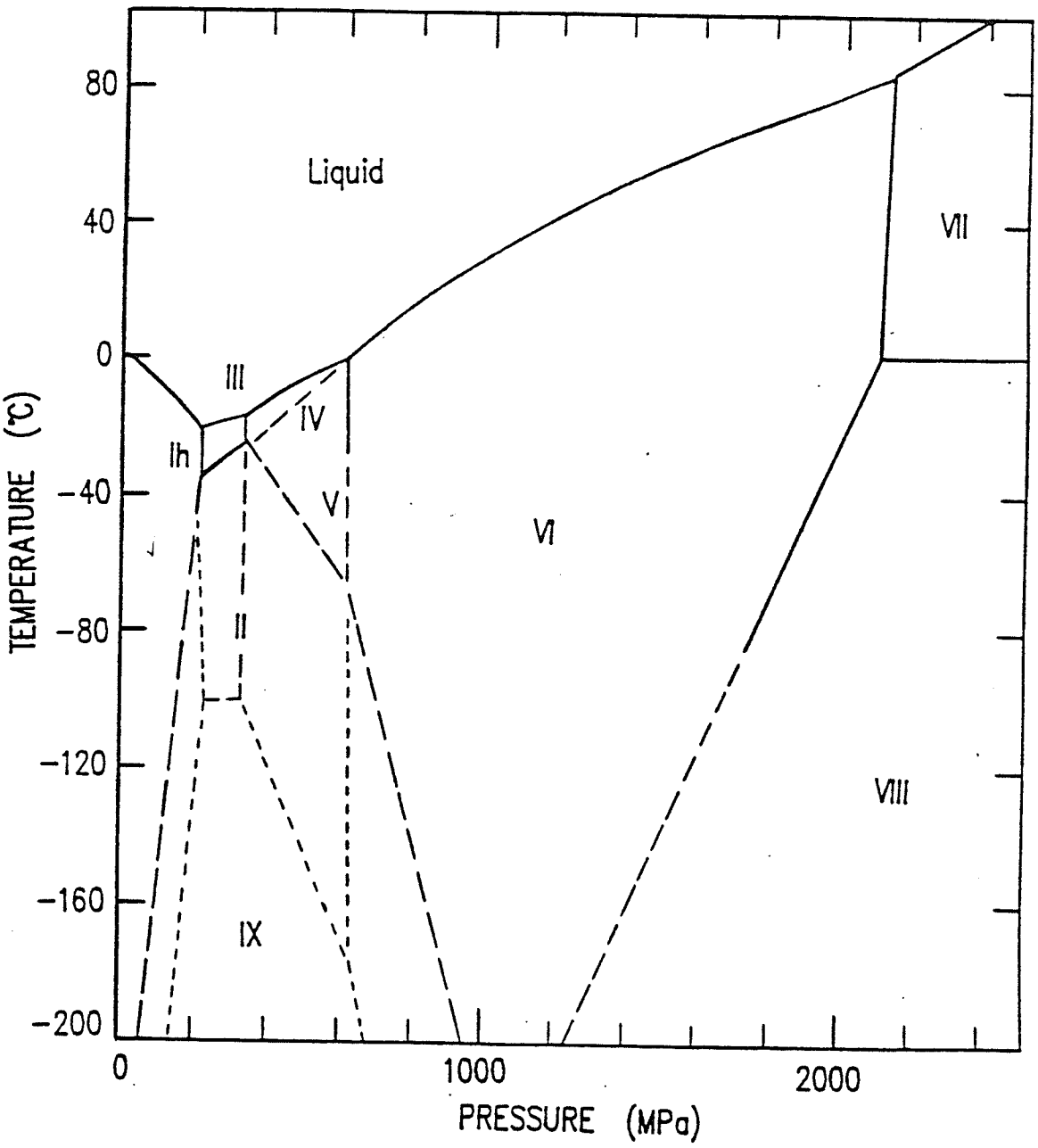

Fig.2.1 Phase Diagram for Ice. (After Mellor, 1979)

(1) The density and latent heat of fusion

The density of ice, at 0°C, is about 0.917 Mg/m^3 and its latent heat of fusion is about 79.6 cal/g. These two physical characteristics affect the thermodynamic equilibrium, mass migration and the volume change during the freezing and thawing of ice. Since the density of ice is different from that of water, the density and the structure of soil may be changed when pore water turns into pore ice.

(2) The anisotropy of ice

Monocrystal ice is anisotropic. The basal plane is usually the glide plane of the crystal lattice. According to Mellor (1979), a shear stress applied parallel to a basal plane produces a shear strain rate of about two orders of magnitude higher than that resulting from shear normal to the basal plane. This anisotropy increases the difficulty in mathematical modelling. Fortunately, natural ice usually exists in an polycrystalline form, and the axes of crystals in polycrystalline ice are randomly oriented. Therefore, when the size of a test specimen or control volume is large compared to the size of ice grains and crystals, polycrystalline ice may be treated as an isotropic material. It should be noted that treating polycrystalline ice as an isotropic material is an approximation which is valid only when microstructural stress and strain are not concerned. Whenever microstructural stress and strain are considered, the anisotropy of the ice structure should be taken into consideration. For example, Sunder and Wu (1990a) suggested that the elastic anisotropy of the ice crystal was the direct cause of crack nucleation in polycrystalline ice. It is generally agreed that pore ice in frozen soil is in polycrystalline form.

2.2.2 Deformation of Ice

(1) Instantaneous Deformation

Like most solid materials, ice, upon application of a stress, shows an instantaneous deformation. For small stresses, the instantaneous deformation is an elastic response. Sinha (1989a) studied the elasticity of several natural types of polycrystalline ice, and concluded that " the elastic properties of various types of ice, in spite of large differences in fabric, are very similar at a constant temperature.". Fig.2.2 shows the results of the measured Young's modulus, E, rigidity (shear) modulus, G, and poisson's ratio, μ, of ice versus temperature.

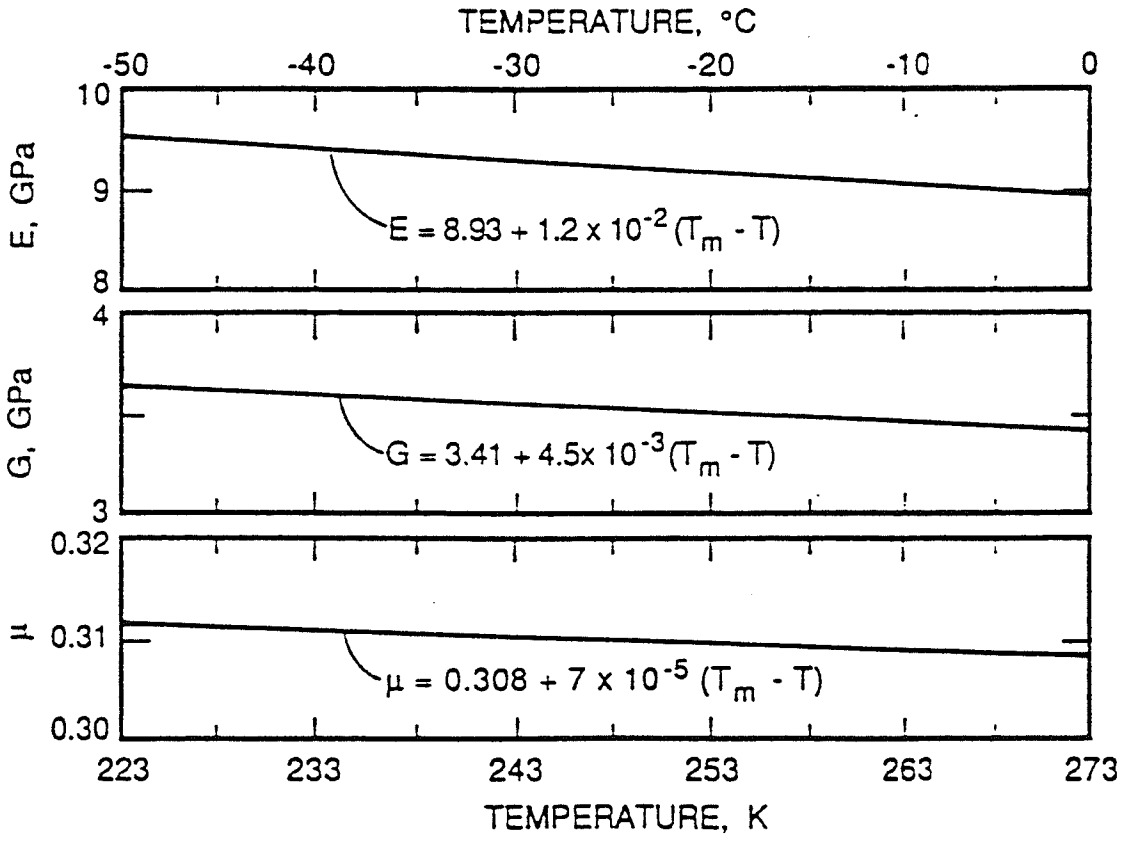

Fig.2.2 Instantaneous Young's modulus, E, rigidity modulus, G, and Poisson's ratio of ice versus temperature. (After Sinha, 1989a)

It is seen from the figure that the variation of E, G and μ due to temperature is not significant. The change of E value due to 50°C of temperature change is only about 6%. The change of E, G, and μ, compared with changes in creep properties caused by the same temperature change, is negligible. Furthermore, the instantaneous deformation constitutes only a very small part of the total deformation for stress levels and time durations normally encountered in civil engineering practice (Mellor, 1979; Sayles, 1988). Therefore, ice may be treated as an isotropic linear material in the analysis of instantaneous deformation.

(2) Creep of Polycrystalline Ice

Experimental evidence from many sources shows that polycrystalline ice under a constant deviatoric stress and at a given temperature exhibits the classical three stages of creep; primary, secondary, and tertiary creep as shown in Fig.2.3 (Mellor, 1979). It should be noted that whether all three creep stages occur depends on the stress level and temperature.

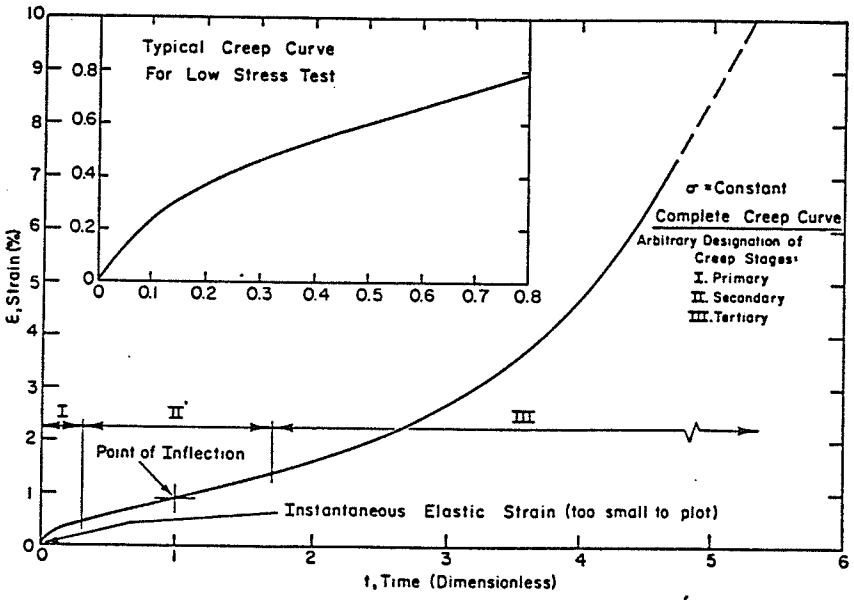

Fig.2.3 A typical creep curve for polycrystalline ice. (after Mellor, 1979)

Ice is a crystalline material which, from a microstructural point of view, is similar to metals. Therefore the creep mechanism of ice is similar to that of metals. Sinha (1989b) compared the creep behaviour of ice and steel, and found similarities between the two. Creep is the global effect of the atoms/molecules' directional migration caused by externally applied stress. Temperature and stress are the two key factors affecting the creep process. It is well known that atoms/molecules are randomly vibrating around their equilibrium positions. From a physics point of view, every atom/molecule has its own free energy. The higher the temperature, the higher the free energy, and higher the free energy, the greater the amplitude of the vibration. The majority of the atoms/molecules in a solid body can only vibrate around their equilibrium positions because they do not have enough energy to leap over the energy barrier. Increasing the temperature increases their ability to overcome the energy barrier and move into new equilibrium positions. If the temperature is sufficiently high, the majority of atoms/molecules start to break away from their equilibrium positions and become free atoms/molecules, and the material then changes from its solid state into its liquid or gaseous state.

When ice is subjected to a stress, a stress field is established on the body. The random vibration of atoms/molecules is subjected to intervention of the stress field, and work done by the stress in the movements of atoms/molecules increases the amplitude of the vibration in the direction of the stress. If the stress level is high enough, some atoms/molecules will be able to leap over their energy barriers and move to new equilibrium positions. The global effect of this directional migration of atoms/molecules under stress constitutes the creep deformation. The temperature dictates the overall ability of the atoms/molecules to overcome

the energy barrier, while the stress helps them to move directionally.

The microstructure of polycrystalline ice also has an effect on the creep behaviour. Polycrystalline ice is composed of monocrystal ice grains. Each ice grain is composed of a certain number of ice crystals which are arranged in a uniform lattice and their basal planes and c-axes have the same orientation. In polycrystalline ice, the axes of ice monocrystals (grains) are usually oriented randomly, therefore polycrystalline ice is usually macroscopically "isotropic". Depending on temperature and stress level, creep takes place in forms of boundary or volume diffusion, dislocation gliding or climbing, grain boundary sliding, or micro-crack propagation etc.. Shoji and Higashi (1978) and Evans and Bilshire (1985) proposed, as shown in Fig.2.4, that volume diffusion occurs at high homologous temperatures and low stress levels, while dislocation creep occurs at a higher level of stress. When stress is further increased, microcracking starts, and dislocation creep is accompanied by microcrack propagation. The definitions and descriptions of such terms as diffusion, dislocation and grain boundary etc., may be found in Evans and Bilshire (1985) and Ĉadek (1988). Mclean (1957) and Chadwich and Smith (1976) studied the structure and properties of grain boundary of metals, while Sinha (1979) studied the grain-boundary sliding of polycrystalline ice. Sinha (1984, 1989c) and Sunder and Wu (1990) discussed the effects of microcracks on the creep process of polycrystalline ice, and presented mathematical models for creep of ice. Their work will be further discussed in subsequent sections. Cole (1986, 1988, 1989) studied the nucleation of microcracks in polycrystalline ice, and evaluated the effect of the grain size, stress and temperature on the cracking process.

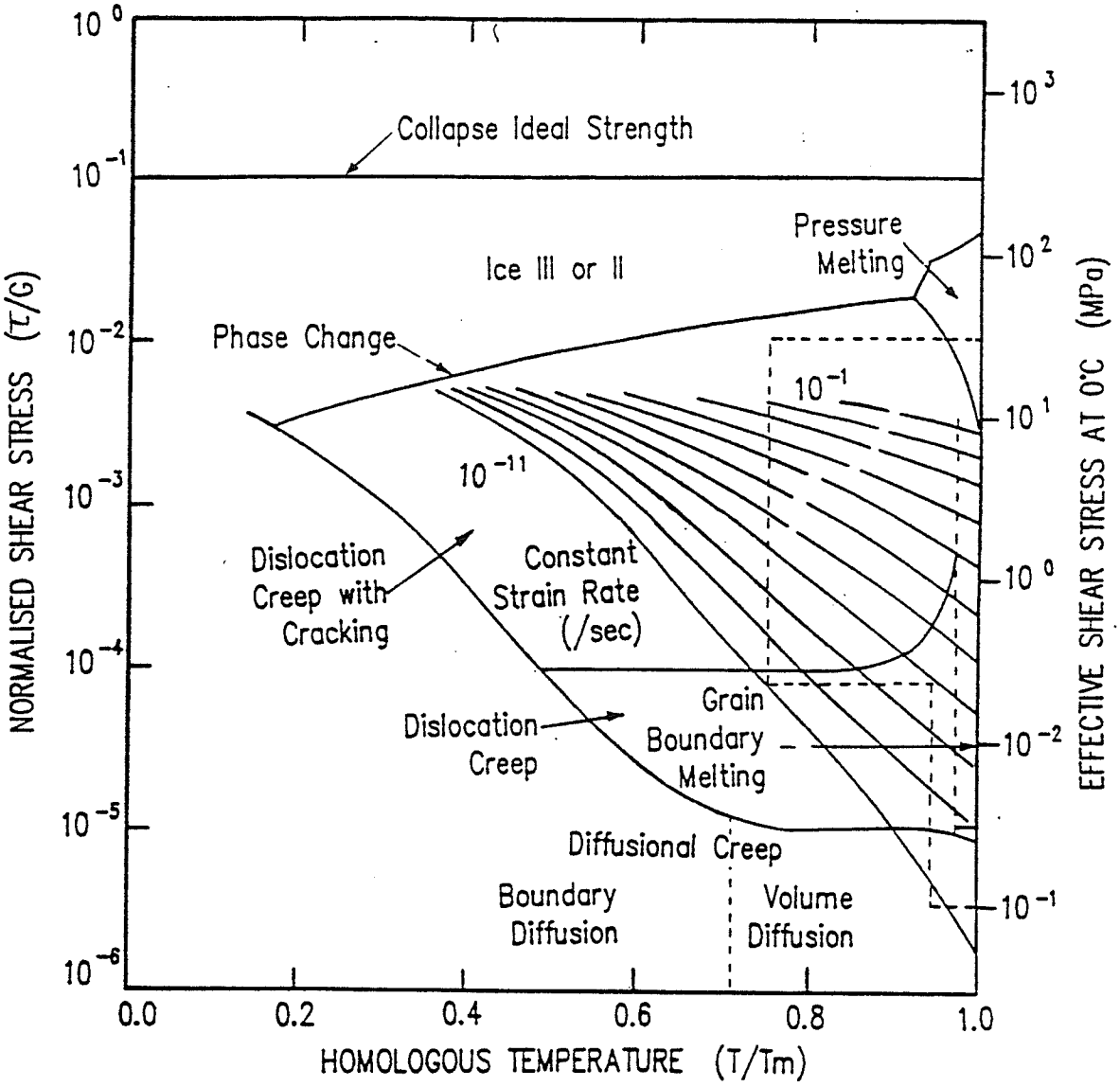

Fig.2.4 Deformation mechanism map for polycrystalline ice of 1mm grain size. (After Shoji and Higashi, 1978)

Generally, there is more than one mechanism involved in the creep process of polycrystalline ice at a given time, However, for a given range of stress and temperature, usually one mechanism is dominant while the others play less important roles. Since different mechanism needed to be modelled by different laws, it is difficult to establish a universal creep model which can accommodate a full stress and temperature regime. That is one of the reasons why there are so many creep models.

2.2.3 Creep Models for Polycrystalline Ice

Various theories have been presented by researchers in the past to model the creep behaviour of ice. From a methodology point of view, there are two categories of models. One is comprised of stochastic models which are developed from established concepts of thermodynamics, and the other is comprised of phenomenological models which are developed by summarizing experimental data and using empirical correlations to represent the data. The models may be one, two or three-dimensional models. Creep models are also classified sometimes according to the creep stages for which the models are valid. Most of the creep models presented by researchers in the past provided a solution in the form of a time-dependent creep strain or creep strain rate for a given range of stresses and temperatures. They were usually expressed in a 1-D form. It is not the writer's intention to list all the creep equations presented in the past, but to present some typical models in each category.

A typical creep model developed on the basis of thermodynamics was presented by

Gold (1973). The steady-state creep strain rate, $\dot{\epsilon}$, was related to stress, σ, temperature, T, and activation energy, E, as

$$\dot{\epsilon} = c\sigma^n exp(\frac{E}{RT}) \tag{2.1}$$

where n and c are constants to be determined experimentally, and R is the universal gas constant (8.31 J/°K mole). This model was a typical application of the Theory of Rate Process presented by Eyring (1936). The model incorporated both stress and temperature effects in a simple equation. It is easy to use and easy to understand. However, the behaviour of ice is more complicated than that described by (2.1). The equation is only valid for steady state creep, and it made no attempt to accommodate multi-dimensional stress-strain states. From an engineering point of view, this model is subject to another inconvenience since the activation energy is not a quantity which is usually measured in engineering practice. Weertman (1973) summarized the values of parameter, n, and activation energy, E, reported by various researchers and found that both of them were subject to large scatter. Actually, it is difficult to determine the activation energy for frozen soils since they are multi-phase materials.

The theory of Rate Process was also applied to develop creep models for other materials such as clay (Pusch, 1979, 1980), frozen soil (Andersland and Akili, 1967), and bitumen (Herrin and Jones, 1963) etc. It is widely used in the study of the creep behaviour of metals.

Generally, the stochastic models have a theoretical base, but they lack capability in

accommodating the complexity of materials and the stress-strain states. Even though these types of models are not very successful in civil engineering practice, they do, however, provide a useful guidance for developing other types of models, such as the empirical models, which will be discussed below.

Assur (1979) proposed an semi- empirical creep model which related the rate of creep strain, $\dot{\epsilon}$, to stress, σ, and time, t, as:

$$\dot{\epsilon} = A \sinh\left(\frac{\sigma}{\sigma_0}\right)^2 \left(\frac{t_m}{t}\right)^{\beta} \exp\left(\frac{\beta t}{t_m}\right) \qquad (2.2)$$

where A, σ_0, and β are constants depending on stress, temperature and the material properties, while t_m is the time taken to reach the minimum creep rate. This is a simple 1-D, time-hardening model which takes no consideration of stress and temperature changes during the creep process into account.

Hult (1966) proposed a power law model for primary creep which related the creep strain, ϵ_c, to stress, σ, and time, t, as

$$\epsilon_c = K \sigma^a t^b \qquad (2.3)$$

where K, a, b, are constants to be determined experimentally. Murat et. al. (1986) used this model to analyze the stress redistribution around a pressuremeter borehole. Azizi (1989) calibrated this model using data from uniaxial creep tests on ice. The model uses a time-hardening law and is only valid when materials are in a primary creep stage. By setting $b=1$,

the equation is able to model secondary creep provided that parameters K and a are calibrated using test data from secondary creep.

Le Gac and Duval (1979) proposed a visco-plastic model which started from the classical theory of non-linear viscosity. The strain rate, $\dot{\epsilon}_{ij}$, was related to deviatoric stress, τ'_{ij}, by a viscosity coefficient, η, as

$$\dot{\epsilon}_{ij} = \frac{\tau'_{ij}}{2\eta} = \frac{B}{2}\tau^{n-1}\tau'_{ij} \tag{2.4}$$

where B and n are constants depending on temperature and τ is the equivalent shear stress defined by:

$$\tau^2 = \frac{1}{2}\sum_{ij}(\tau'_{ij})^2 \tag{2.5}$$

By introducing a tensor state parameter, s_{ij}, and a stress deviator, σ'_{ij}, and a scalar variable σ^*, a creep equation was given as:

$$\dot{\epsilon}_{ij} = \frac{B'}{2}\frac{(\tau^* - \sigma^*)^n}{\tau^*}(\sigma'_{ij} - S_{ij}) \tag{2.6a}$$

and

$$\dot{\epsilon}_{ij} = 0 \quad if \quad \tau^* < \sigma^* \tag{2.6b}$$

where B' is a constant and τ^* may be expressed as

$$\tau^* = \frac{1}{\sqrt{2}} \sqrt{\sum_{ij} (\sigma'_{ij} - S_{ij})^2} \qquad (2.7)$$

This visco-plastic model may be used in analysis of both creep and relaxation. The model was further modified by Sunder and Wu (1990b). The effect of elastic isotropy and microcrack propagation was incorporated into the model. However, the model was further complicated by the modification, and more internal variables were introduced into the model. This is a powerful model provided the material behaves in accordance with the assumptions made in the model. One of the shortcomings which makes the model difficult to use in engineering practice, lies in that ice and many other engineering materials are not ideal visco-plastic materials, and their mechanical behaviour does not always follow a fixed law of viscosity. Specifically, the parameters, n and B' in (2.6a) may depend on stress and strain state. Besides, the model does not consider volume changes during the creep process.

As discussed in the previous section, the creep mechanism depends not only on temperature, but also on stress level and the rate of creep. When stress and creep rate are low, the crack activity in ice is not significant, and creep takes place mainly in forms of diffusion, dislocation or grain-boundary sliding. As stress level increases, so does the creep rate, and the microcracking mechanism becomes more and more dominant. Sinha (1988, 1989b) presented a non-linear viscoelastic creep equation for polycrystalline material. The equation incorporated the effect of microcracking, and it was expressed as

$$\epsilon = \epsilon_e + \epsilon_d + \epsilon_v = \frac{\sigma}{E} + \frac{c_1 d_1}{d}\left(\frac{\sigma}{E}\right)^s \left[1 - exp[-(a_T t)^b]\right]$$

$$+ \int_0^t \dot{\epsilon}_{v0}\left(\frac{\sigma}{\sigma_0}\right)^n \left(1 + \frac{\pi^2}{12x\sqrt{3}} N d^2 \sqrt{n}\right) dt \qquad (2.8)$$

where ϵ, ϵ_e, ϵ_d and ϵ_v are respectively: the total axial, the elastic, the delayed elastic and the viscous strains, E is the Young's modulus, σ is the axial stress, t is time, and c_1, d_1, d, s, a_T, b, $\dot{\epsilon}_{v0}$, σ_0, n and N are constants to be determined experimentally. The parameter N was defined as crack density and was expressed as a function of grain-boundary sliding displacement. This model is still a 1-D time-hardening model. However, it takes the effect of crack activity into consideration, therefore it is able to accommodate high stress levels and high creep rates.

2.2.4 Strength of Polycrystalline Ice

Ice is a material which takes different failure modes under different stress and strain conditions. When the stress level and strain rate are high, ice fails in a brittle mode and shows a clear peak stress, while under low stresses and strain rates, it continues to deform without an explicit failure state. Therefore, the strength of polycrystalline ice is closely interrelated with its deformation and its rate of deformation. The strength of ice is affected by many factors which include the rate of deformation, the temperature, the hydrostatic pressure, the structure or fabric orientation, the grain size, the salinity etc. The effect of some of these factors will be discussed below.

The short-term strength of ice is usually investigated by constant strain rate tests. It is well known that the strength of ice increases with increasing strain rate and decreasing temperature (Gold and Krausz 1971; Hawkes and Mellor, 1972; Sinha, 1978; Mellor, 1979; Gold and Sinha, 1979; Mellor and Cole, 1982 etc.). Strain rate is one of the factors which dictate the failure mechanisms of ice. Kalifa et. al. (1992) performed uniaxial and triaxial tests on polycrystalline ice at -10°C, and studied the effect of microcracking on failure. The influence of confining pressure and strain rate on the shear strength of ice was summarized as shown in Fig.2.5. It is seen from the figure that under a constant confining pressure, the peak shear stress increases with increasing strain rate, while under a given strain rate, the shear strength increases with increasing confining pressure until the confining pressure reaches about 8 MPa for the fine-grained ice and about 6 MPa for the coarse-grained ice. Further increases of confining pressure have little effect on the shear strength of ice. These threshold stress levels depend on the temperature of ice. With a decrease in temperature, there is an increase in the threshold stress levels. The earlier studies presented by Sinha (1988), Sinha (1989c), and Sunder and Wu (1990) showed similar results.

Rist and Murrell (1994) presented experimental data from a series of constant strain-rate triaxial tests on polycrystalline ice. Their research focused on the strength behaviour of ice under high stress (confining pressure up to 50 MPa), low temperature (-20°C to -40°C), and high strain rate (10^{-2} to 10^{-5} 1/s). The effect of confining pressure on failure mode and

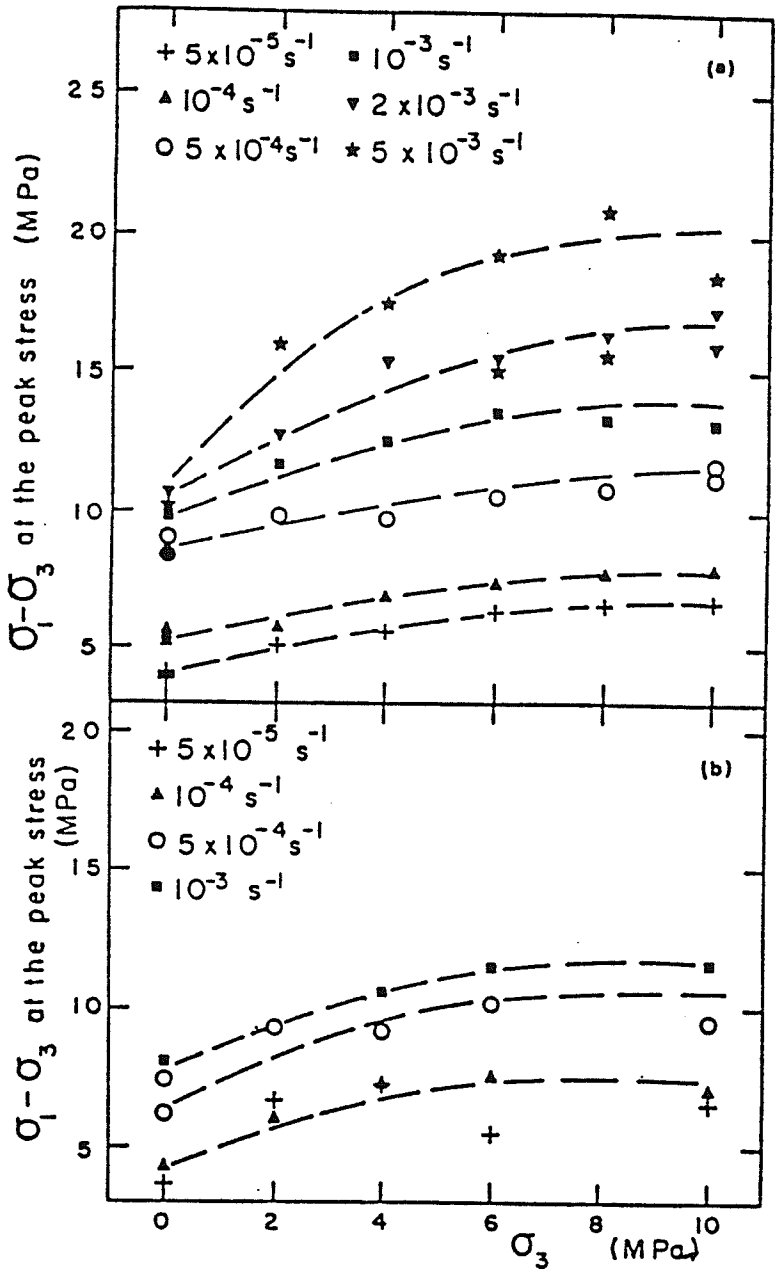

Fig.2.5 Maximum deviatoric stress, $(\sigma_1-\sigma_3)_{max}$, versus confining pressure, σ_3, for two different types of ice under various strain rates, (a) fine-grained ice; (b) coarse-grained ice. (After Kalifa et el., 1992)

shear strength is shown in Fig.2.6. It is seen from the figure that cracking activity increases with increasing strain rate and shows some decrease with increasing confining pressure, especially for the case of high strain rate. As expected, confining pressure has a significant effect on the peak shear strength.

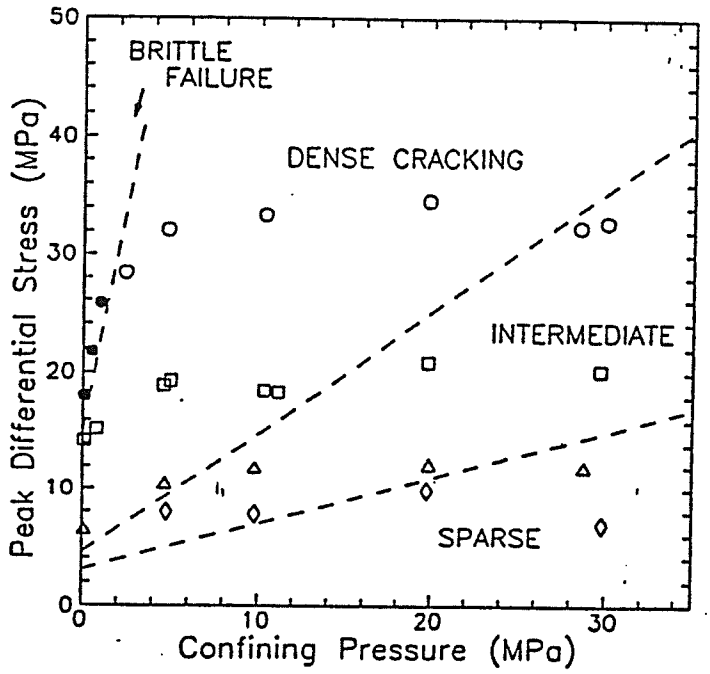

Fig.2.6 Ice-strength and failure mode versus confining pressure at -20°C. Solid symbols denotes brittle-shear fracture; others are ductile failures. Strain rate: ○ = 10^{-2} s^{-1}; □ = 10^{-3} s^{-1}; Δ = 10^{-4} s^{-1}; ◊ = 10^{-5} s^{-1}. (After Rist and Murrel, 1994)

The other aspect of the strength of ice is its long-term strength. The term "ultimate state" is referred to as a state at which creep of ice has ceased or the rate of creep is small enough so that the deformation is negligible. As discussed in **2.2.2(2)**, the fundamental cause of creep of polycrystalline material is the directional migration of atoms/molecules of the material with the help of stress. For a given temperature, there is an associated stress level that is required to maintain the migration. This gives rise to the concept of a threshold stress

or ultimate strength. Stresses lower than the threshold level cannot maintain the migration and therefore creep ceases. This process is synonymous with attenuating creep. Further experimental investigation of the ultimate strength of ice is needed.

The long-term strength of polycrystalline ice is usually investigated by creep tests. Failure is usually defined as the onset of tertiary creep which corresponds to the point of the minimum creep rate in a constant stress, constant temperature creep test. Since creep tests on ice under low stresses are very time-consuming, the long-term strength of ice has not been well explored. Mellor (1979) presented data showing a relationship between stress and minimum strain rate based on the results from uniaxial compression and tension tests on polycrystalline ice at -7°C as shown in Fig.2.7. The long-term strength of ice may be estimated from these data.

The term "strength" discussed above is limited to compressive strength or shear strength. The tensile strength of ice differs somewhat in characteristics. Mellor (1979) reported that the tensile strength of ice is insensitive to changes in strain rate. Ladanyi (1981) suggested that the tensile strength is also insensitive to changes in temperature when the strain rate is high. However, Hawkes and Mellor (1972) proposed that when strain rate is low, both the strength and the deformation of ice in a tensile stress state are greatly affected by its creep behaviour. They suggested that the creep of ice in tension is more or less the same as that in compression. The data given in Fig.2.7 support their suggestion. It is seen from the figure that the line representing the tension test data merged into the line representing the compressive test data when strain rate was lower than about 10^{-6} 1/s.

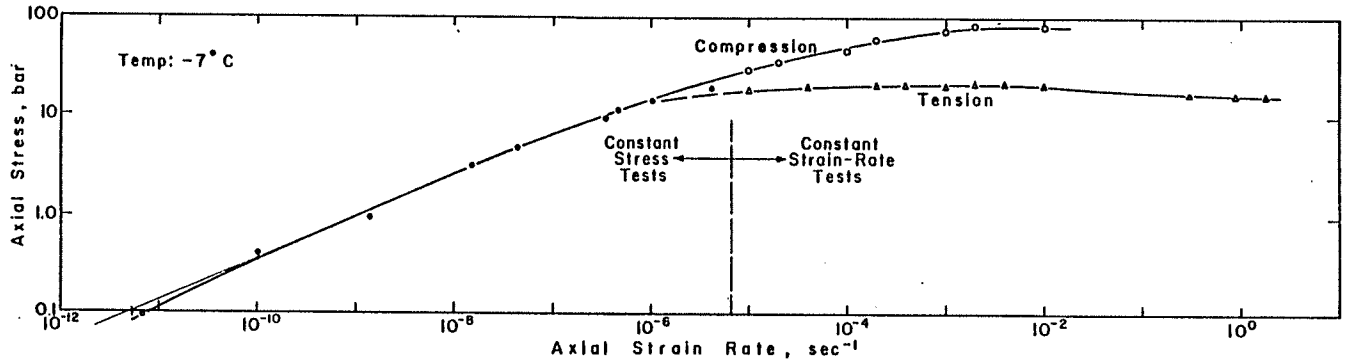

Fig.2.7 Stress/strain-rate data for polycrystalline ice at -7°C in uniaxial tests. (After Mellor, 1979)

2.3 MECHANICAL BEHAVIOUR OF FROZEN SOIL

The mechanical behaviour of frozen soil depends mainly on two aspects of the properties of the soil. One is the physical aspect of the soil which includes the structural fabric of soil grain-ice mixtures, and the respective properties of each. The other is the temperature of the soil. The effect of soil composition on the behaviour of frozen soil has not been extensively documented. The majority of experimental studies were performed on frozen sand, such as those of, Goughnour and Andersland (1968), Sayles (1973), Ting et al. (1983), Zhu et al. (1988), and Domaschuk et al. (1991). Haynes and Karalius (1977), Haynes (1978), Domaschuk et al. (1983) and Zhu and Carbee (1983) studied the creep behaviour of frozen silt. Andersland and Akili (1967), Bourbonnais and Ladanyi (1985b), and Wijeweera and Joshi (1990, 1991) studied frozen clays. Besides soil composition, particle shape and the physicochemical nature of their surfaces also affects the behaviour of frozen soil. Different kinds of minerals carry different cations or ions on their surface, and thus have different electrochemical bonding forces between the soil particles and the water molecules surrounding them. The electrochemical bond dictates the thickness of the unfrozen water layer which in turn affects the mechanical behaviour of the frozen soil. Particle shape directly affects the microscopic stress field around soil particles (Tsytovich, 1975). He proposed that an external stress of 200 kPa could cause an internal stress of as high as 117 MPa at the points of contact of ice and particles. This high level of stress exerts an influence on the creep process of frozen soil.

2.3.1 Soil/Ice Concentration and Classification of Frozen Soil

Most of the previous studies on the mechanical behaviour of frozen soil were carried out on uniform soil-ice mixtures or homogeneous frozen soils. Based on soil grain concentration, Weaver (1979) classified frozen soil into four different types. Type one was called **dirty ice** which is ice with a very low soil concentration and a bulk density between 0.9 to 1.0 Mg/m^3. Type two called **very dirty ice** has a bulk density between 1.0 and 1.7 Mg/m^3. The characteristic of this type of frozen soil is that it has a significant soil concentration but few particle to particle contacts. Type three called **ice-poor frozen soil** refers to a saturated dense frozen soil with a bulk density between 1.7 and 2.0 Mg/m^3. The particle to particle contacts of this type of frozen soil are well established. Type four called **ice-rich frozen soil** refers to a frozen soil with a high level of ice segregation. The segregated ice is distributed in the frozen soil quite uniformly and therefore the frozen soil may be treated as a homogeneous material from a macroscopic point of view. All four types of frozen soil are essentially saturated. There are also unsaturated frozen soils which in an extreme situation may be a dry soil at below zero temperatures.

2.3.2 Strength and Deformation of Frozen Soil

The strength and deformation of frozen soil are affected by many factors, such as the properties of the soil itself, the temperature, the magnitude of strain or stress, the rate of strain or stress application, and the degree of confinement. Since the strength and deformation of frozen soil are closely interrelated, they will be discussed together in the following sections.

(1) The Source of Shear Strength of Frozen Soil

Ting et al. (1983) summarized the work by Goughnour and Andersland (1968),

Andersland and AlNouri (1970), Chamberlain et al. (1972), Hooke et al. (1972), Alkire and Andersland (1973), Rein et al. (1975), Smith and Cheatham (1975), and Ting (1981), and proposed a mechanism map for unconfined compressive strength of frozen Ottawa sand as shown in Fig.2.8. According to Ting et al. (1983), the strength of frozen sand has the following four sources: (1) ice strength and strengthening due to interaction with soil, (2) soil strength, (3) dilatancy effects, and (4) structural hinderance between the soil and the ice matrix. These four sources may be combined into two. One is the strength of ice which contributes to the strength of frozen soil in a similar way to the cohesion of cohesive unfrozen soils. The "strengthening due to interaction with soil" may be explained by the different grain size and different arrangements of ice crystals or ice grains in pore ice from that in bulk ice.

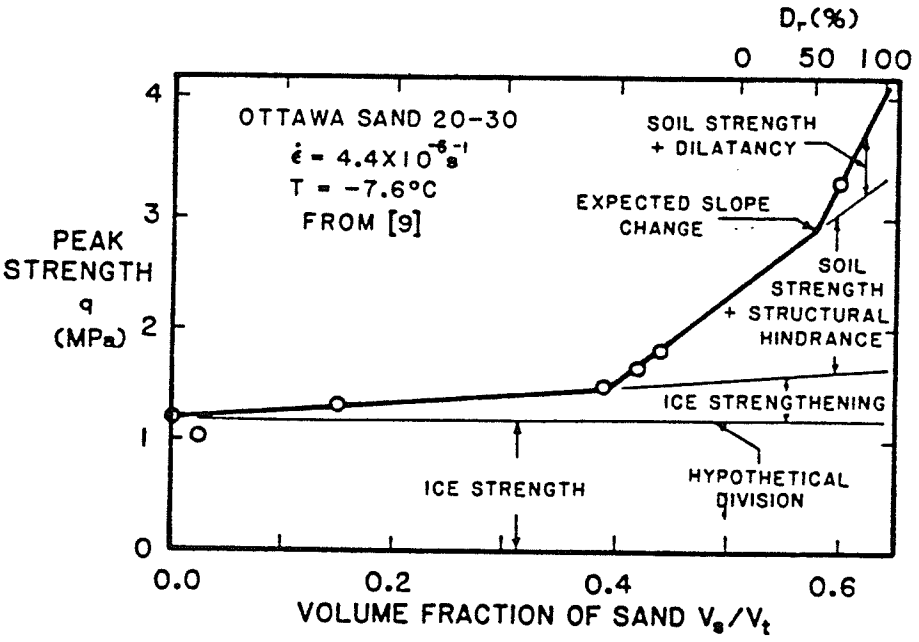

Fig.2.8 Proposed mechanism map for unconfined compressive strength of frozen Ottawa sand at -7.6°C and a strain rate of 4.4x10^{-4} s^{-1}. (After Ting et al., 1983)

The hindering effect of soil particles on the formation of slip surfaces in pore ice may also contribute to the increase in strength in pore ice. Therefore, pore ice is usually stronger than bulk ice at the same temperature. The other source of strength is the interparticle friction and particle interlocking provided by the soil skeleton, which depends on soil properties and the effective confinement of the soil. The dilatancy effect mentioned by Ting et al. (1983) may be taken as a part of this source. The effective confinement acting on the soil skeleton includes both the externally applied confining pressure and the internal confinement provided by the ice matrix (Ladanyi and Morel, 1990). The two sources of strength may be combined into a Mohr-Coulomb type of strength criteria for unfrozen soil as:

$$\tau_f = c_f + \sigma_f' \tan\phi_f' \qquad (2.9)$$

where subscript f stands for frozen soil, c_f represents the strength provided by pore ice, $\tan\phi_f'$ represents the contribution from inter-particle friction, τ_f' is the shear strength, and σ_f' is the effective normal stress acting on the skeleton of frozen soil, which includes both external and internal confinements.

(2) Factors Affecting Strength and Deformation

(a) Soil Concentration

According to Goughnour and Andersland, 1968; and Hooke et al. 1972, very low concentrations of soil grains in ice had a weakening effect on the ice. When the soil particle concentration was about 1 to 3% by volume, the frozen soil (slightly dirty ice) deformed at a slightly higher rate than did the clear ice under the same stress and temperature. When soil

concentration was gradually increased, the soil particles showed a strengthening effect on the ice. The higher the soil concentration, the higher the strength (Goughnour and Andersland, 1968; Hooke et al., 1972; and Baker, 1979). Soil concentration also affects the deformation and the failure modes of frozen soil. Sayles and Carbee (1981) showed that as soil concentration increases, the failure mode gradually changes from brittle failure at small strains to more ductile failure at larger strains. Ting et al.(1983) proposed a mechanism map for a frozen fine sand in uniaxial compressive creep tests as shown in Fig.2.9. The map was constructed using data from unconfined compressive creep tests at a given stress level and a given temperature. The figure shows that the creep rate decreases with increasing sand concentration.

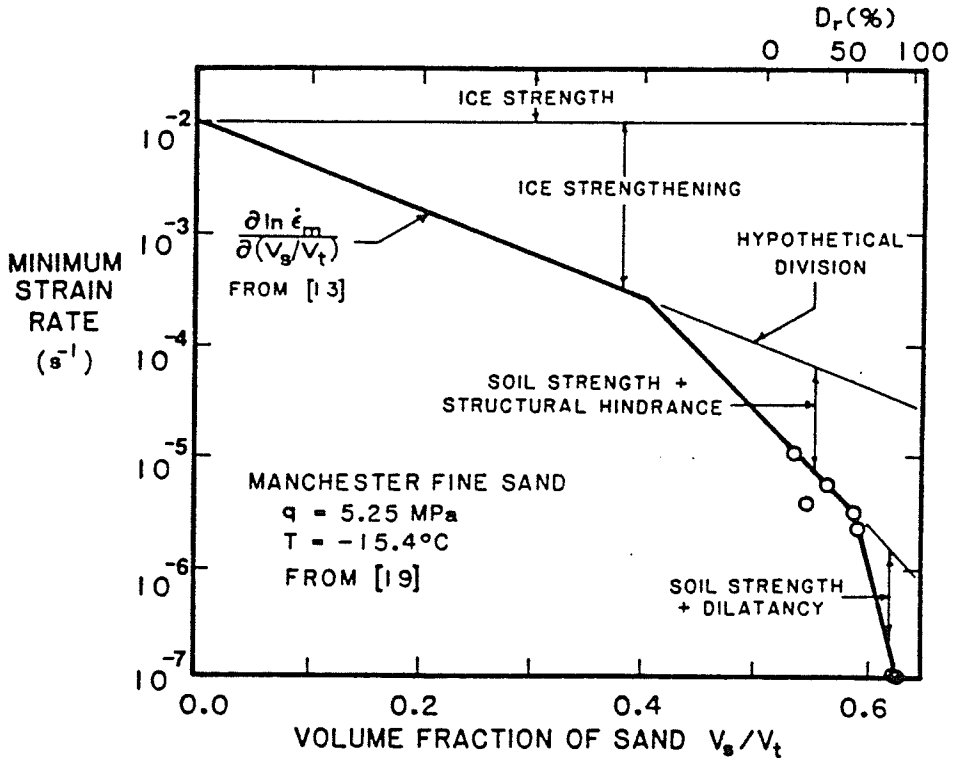

Fig.2.9 Proposed mechanism map for unconfined compressive creep of frozen Manchester fine sand at -15.4°C under an axial stress of 5.25 MPa. (After Ting et al., 1983)

(b) Temperature

It is well known that decreasing the temperature increases the strength and decreases the creep rate of frozen soil, and this is irrespective of soil types. This observation is supported by the experimental data presented by such researchers as Andersland and Akili (1967), Sayles (1968), Haynes and Karalius (1977), Haynes (1978), Sayles (1988), Wijeweera and Joshi (1990) etc. However, when the temperature is very low, different types of frozen soils behaves differently. Bourbonnais and Ladanyi (1985a, 1985b) studied the behaviour of frozen soil under very low temperatures (down to -160°C). Fig.2.10 shows the dependence of the uniaxial compressive strength on temperature. The figure shows that the strength of frozen sand increases with decreasing temperature until about -110°C. A further decrease in temperature causes the strength to decrease. The authors suggested that thermal microcracking during cooling, which was caused by the mismatch of thermal expansion between sand grains and pore ice, was the cause of this phenomenon. It is also interesting to see from the figure that at higher temperatures, for example higher than about -80°C, the strength of frozen sand was higher than that of frozen clay. However, when temperatures dropped further down to about -100°C to -110°C, the strength of frozen clay became much higher than that of frozen sand. Besides the effect of thermal microcracking suggested by the authors, lack of plasticity in frozen sand at very low temperature may also be a reason for this behaviour.

(c) Strain Rate

The effect of strain rate on strength of frozen soil has been investigated by Sayles (1973), Perkins and Ruedrich (1973, 1974), Parameswaran (1980), Haynes et al. (1975),

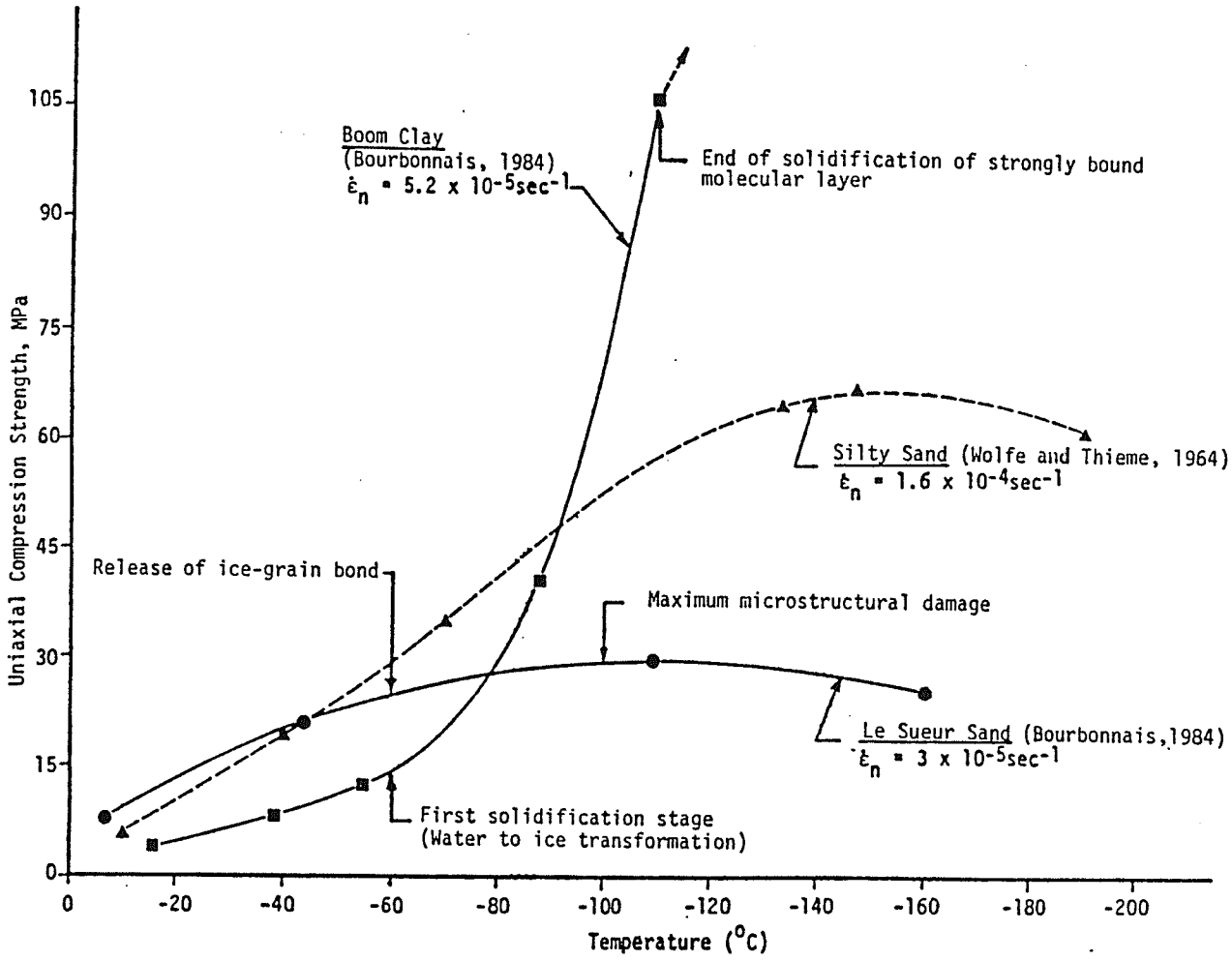

Fig.2.10 Effect of temperature and soil type on uniaxial compressive strength of three typical frozen soils. (After Andersland and Ladanyi, 1994)

Haynes and Karalius (1977), Bragg and Andersland (1980), Zhu and Carbee (1984), and Zhu et al. (1988). It was found that the compressive or shear strength of frozen soil increases significantly with increasing strain rate, while the tensile strength increases with increasing strain rate only when the strain rate is low. For high strain rates, the specimen under tensile stress fails at small strains, and the strength is virtually independent of strain rate.

Strain rate also affects the failure mode of frozen soil. By summarizing the test results from Perkins and Ruedrich (1973, 1974), Parameswaran (1980) and their own data, Bragg and Andersland (1980) presented a relationship between failure strain and strain rate for frozen sand as shown in Fig.2.11. This work cleared up the misconception that failure strain of frozen sand was always close to 1%. It is seen from the figure that the small failure strain of about 1% is associated with high strain rates and a brittle failure mode. However, when the strain rate is low, the failure mode is ductile, and the failure strain is between 4 to 7%. It should be noted that the data shown in Fig.2.11 were obtained from uniaxial tests. The failure strain may be even higher when frozen soil is subjected to confining stresses.

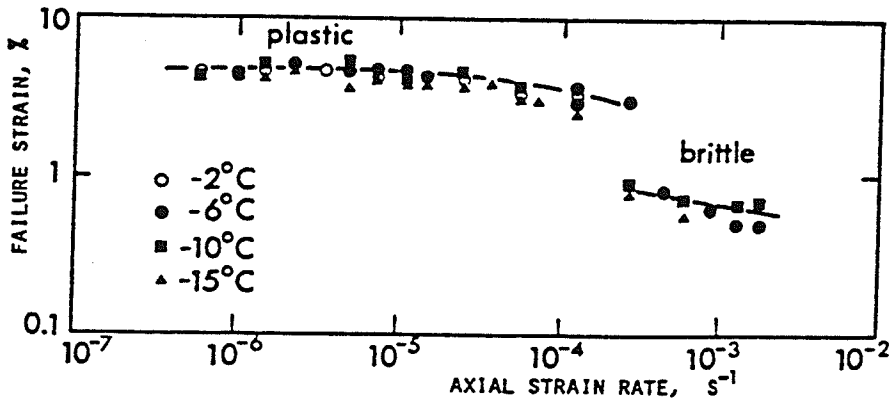

Fig.2.11 Failure strain versus strain rate relationship for a frozen sand in uniaxial compression tests at different temperatures. (After Bragg and Andersland, 1980)

(d) Confining Pressure

The effect of confining pressure on the deformation and strength of frozen soil has been studied by Chamberlain et al. (1972), Sayles (1973), Alkire and Andersland (1973), Jones and Parameswaran (1983), Rahman (1988), and Domaschuk et al. (1991). Confining pressure has a more significant effect on coarse-grained frozen soil with higher soil concentrations than on fine-grained soil with lower soil concentrations. Fig.2.12 provides an overall view of the effect of confining pressure. It is seen from the figure that, firstly, the

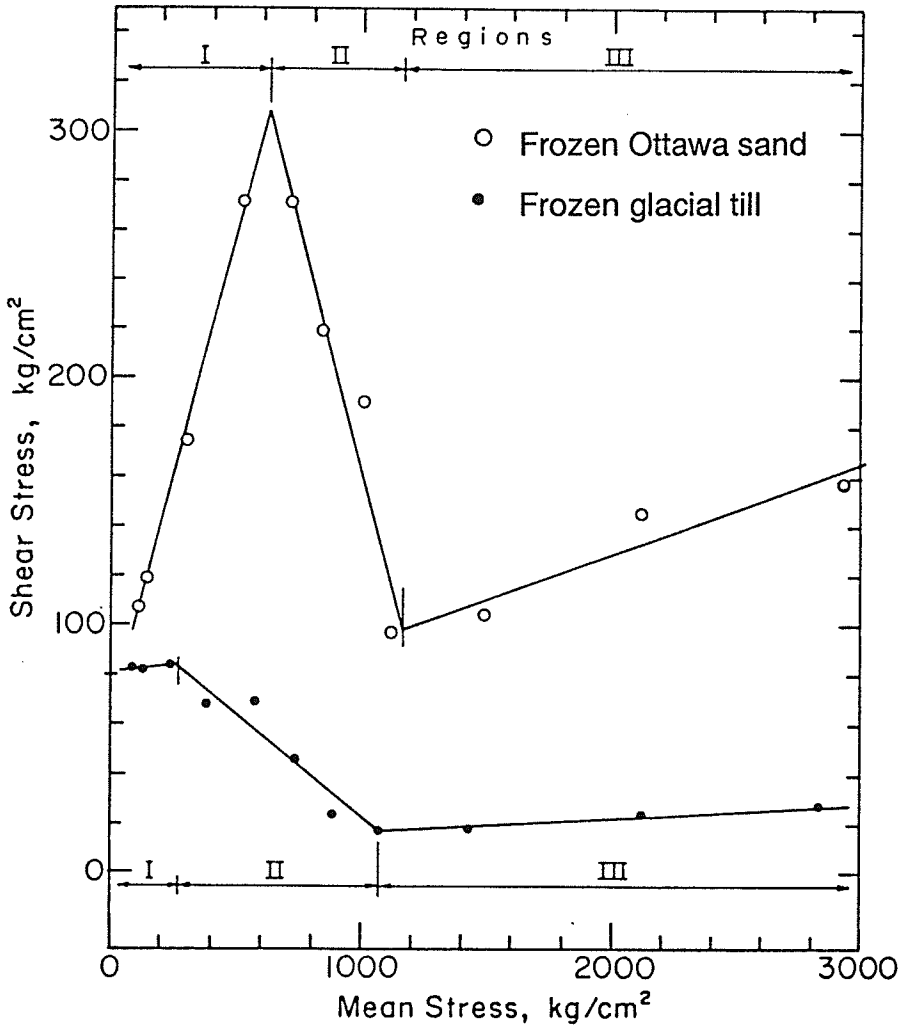

Fig.2.12 Shear stress, $[(\sigma_1 - \sigma_3)/2]$, versus mean normal stress, $[(\sigma_1 + \sigma_3)/3]$, relationship from high stress triaxial compression tests on frozen sand. (After Chamberlain et al., 1972)

effect of confining pressure has a more significant effect on frozen sand (OWS) than on frozen glacial till (WLT), and secondly, for a given frozen soil at a given strain rate, the shear strength increases with increasing confining pressure in Region I, decreases in Region II, and increases again in Region III. In Region I, the increase in shear strength with increasing confining pressure was mainly due to interparticle friction and particle interlocking. The coarse-grained frozen Ottawa sand was able to develop significant interparticle friction and interlocking, therefore its shear strength increased with increasing confining pressure significantly, while the fine-grained frozen till could not generate very much friction and interlocking, and therefore confining pressure had very little effect on it. In Region II, the shear strength decreased with increasing confining pressure. This was because the increasing confining pressure caused pressure melting, therefore weakened the bond between ice and soil particles and among ice grains. Another possible reason was that the increasing unfrozen water content increased pore water pressure, and resulted in a decrease in effective mean normal stress. In Region III, since the confining pressure was so high that the majority of pore ice turned into water, and since the system did not allow the water to drain, the shear strength was reduced to approximately the undrained shear strength of the soil in an unfrozen state. This research mainly focused on the strength of frozen soil under very high stress levels. These stress-strain conditions are not usually encountered in engineering practice. The research, however, provided a global picture of the effect of confining pressure on the strength of frozen soil.

2.3.3 Constitutive Equations of Frozen Soil

The previous section discussed the factors which influence the mechanical behaviour

of frozen soils. In order to apply that knowledge to engineering practice, mathematical expressions which represent the influence of those factors on the strength and deformation of frozen soil had to be established. Since the behaviour of frozen soil is complicated, at the present time there is no single constitutive model able to represent all aspects of the mechanical behaviour of the soil. It is common practice that the strength is represented by one set of empirical equations, while the deformation is represented by another set of equations, and the compatibility between the two sets of equations is not well established. Since the deformation of frozen soil under the stress-strain and temperature conditions usually encountered in engineering practice takes place mainly in the form of creep, the majority of constitutive equations for frozen soil focus on the creep deformation and time-dependent strength. This is the topic that will be discussed in the following sections.

2.3.3.1 Creep Strength of Frozen Soil

Creep strength of frozen soil is usually defined as the maximum stress that the soil can sustain in a finite period of time without failure. When dealing with experimental data, failure is usually referred to as the onset of tertiary creep in constant stress creep tests or the attainment of peak resistance in constant strain rate tests. In constant strain rate tests, the peak resistance can be easily identified. In constant stress creep tests, the long-term strength of frozen soil may be determined as shown in Fig.2.13. For a given frozen soil at a given temperature, creep tests were performed with different stress level, σ', σ'', σ''', and a time to failure (the point of minimum strain rate) was obtained for each stress level (Fig.2.13a). Strength-time plot can then be produced as shown in Fig.2.13b with the instantaneous strength, σ_{inst}, and the ultimate strength, *ult* σ_{II}, determined by extrapolation.

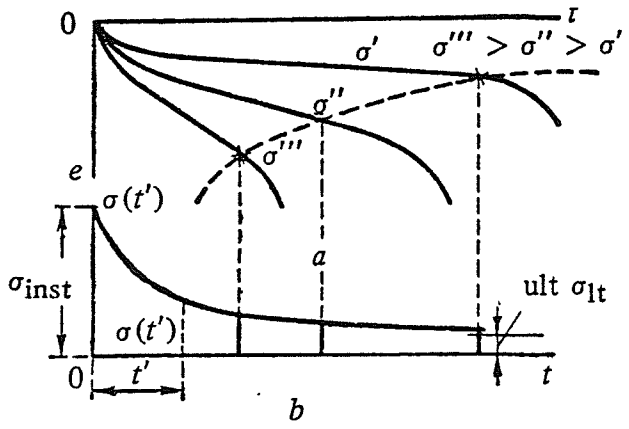

Fig.2.13 Plotting of long-term strength graph for frozen soil from sustained-creep curves. (After Tsytovich, 1975)

Vialov (1959) proposed that the creep strength of frozen soil be expressed as

$$\sigma_f = \frac{\beta}{ln\frac{t_f}{B}} \qquad (2.11)$$

where β and B are parameters depending on soil properties and temperature, β having units of stress and B having units of time. The parameters σ_f and t_f are the creep strength and the associated time taken to reach failure respectively. Fig.2.14 shows a comparison by Sayles (1988) between his measured time-dependent uniaxial compressive strengths and that predicted by (2.11). It is seen from the figure that the equation fairly fitted the experimental data.

Eq.(2.11) was proposed on the basis of uniaxial creep tests. There were attempts to use it in predicting the shear strength of frozen soil under triaxial stress states. Sayles (1973) conducted triaxial tests on frozen Ottawa sand and compared the measured creep

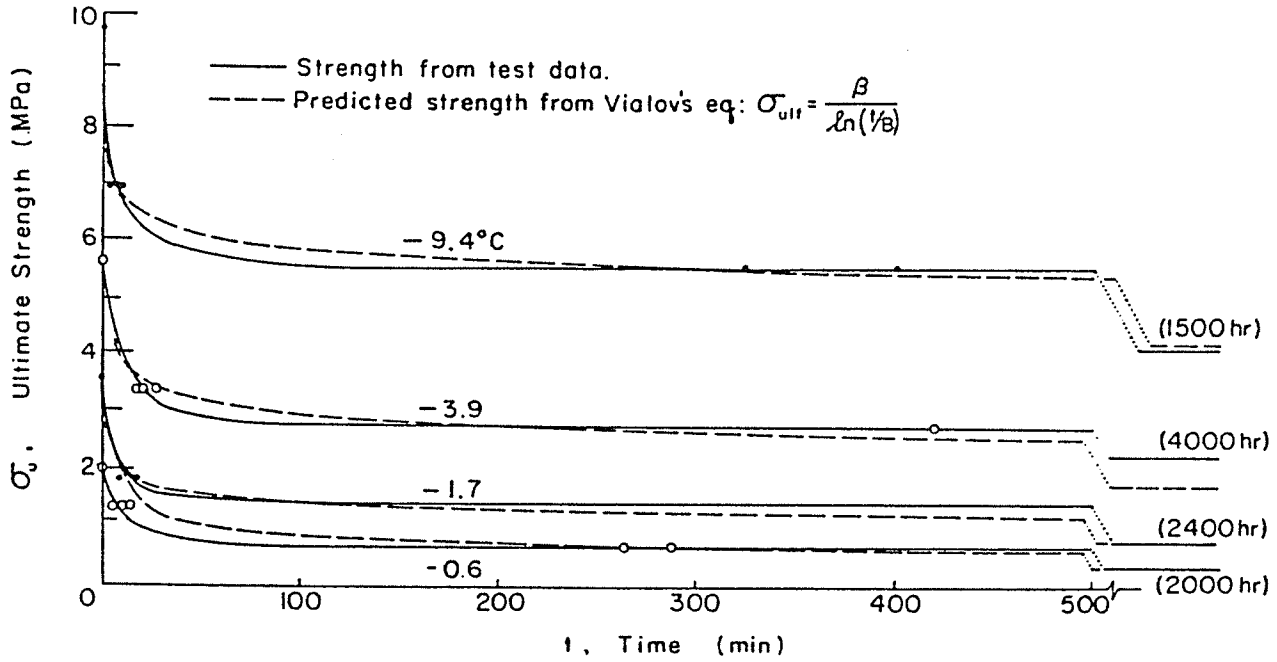

Fig.2.14 Creep strength versus time for frozen Ottawa sand at different temperatures. (After Sayles, 1988)

strength of the sand with that predicted by (2.11) as shown in Fig.2.15. The figure shows that the shear creep strength, $(\sigma_1 - \sigma_3)_{max}$, increases with increasing confining pressure. The equation represented the shear strength quite well for the two cases with the higher σ_3 values but not as well for the case of the lowest σ_3.

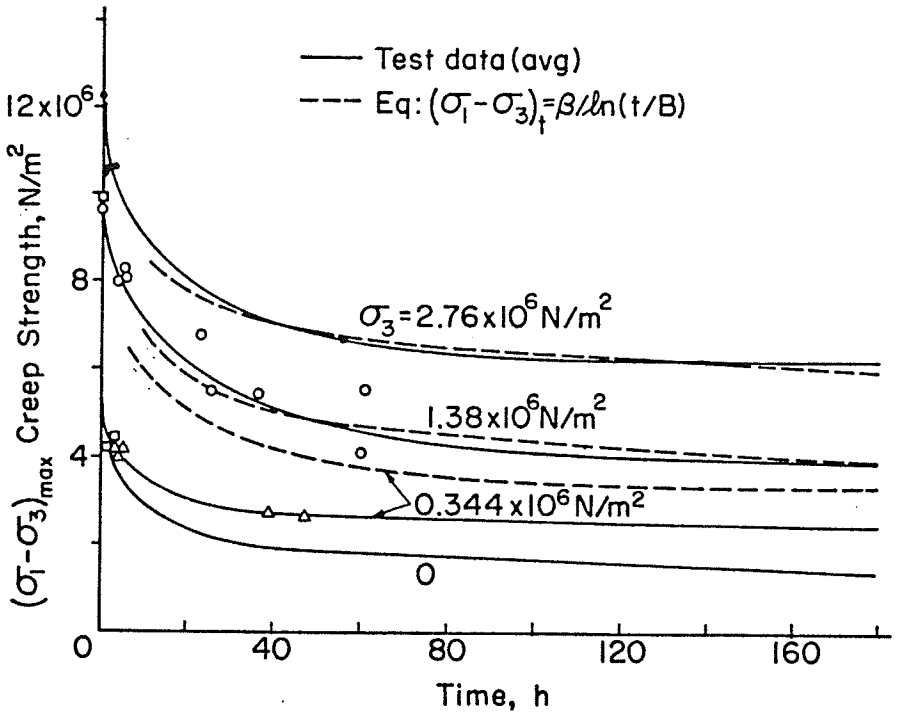

Fig.2.15 Creep strength versus time to failure for frozen Ottawa sand. (After Sayles, 1973)

Sayles (1973) proposed that "the long-term, ultimate creep strengths of frozen sands can be estimated by drained triaxial tests on sand under the same stress conditions and unit weights as those of the in situ material". He suggested that Mohr-Coulomb strength criteria be used for frozen sand.

$$\tau = c + \sigma_n \tan\phi \qquad (2.12)$$

where c is unit cohesion, σ_n is normal stress, and ϕ is the angle of internal friction for the sand. Fig.2.16d shows Mohr-Coulomb strength envelopes for different times based on constant strain rate triaxial tests performed on frozen Ottawa sand by Sayles (1973). No quantitative conclusion was drawn from the limited data. This work was an attempt to use Mohr-Coulomb criteria for the long-term strength of frozen soil.

Ladanyi (1972) suggested that the relationship between time to failure, t_f, and the applied stress, σ, be expressed by a power function as

$$t_f = \frac{\epsilon_f}{\dot{\epsilon}_c (\sigma/\sigma_c)^n} \qquad \textbf{(2.13)}$$

where ϵ_f is the failure strain, $\dot{\epsilon}_c$, σ_c, and n are parameters depending on the soil properties and temperature. This equation may rewritten as

$$\sigma_f = \sigma_c \left(\frac{\epsilon_f}{t_f \dot{\epsilon}_c} \right)^{\frac{1}{n}} \qquad \textbf{(2.14)}$$

where σ_f represents the creep strength of frozen soil. Eq.(2.14) is similar to (2.11) except that a power function is used in (2.14) , while a logarithmic function is used in (2.11). Both of them are empirical equations. Eq.(2.14) is applicable to ice-rich frozen soil in the stress and temperature range where secondary creep dominates the deformation. It usually produces poor prediction in other situations.

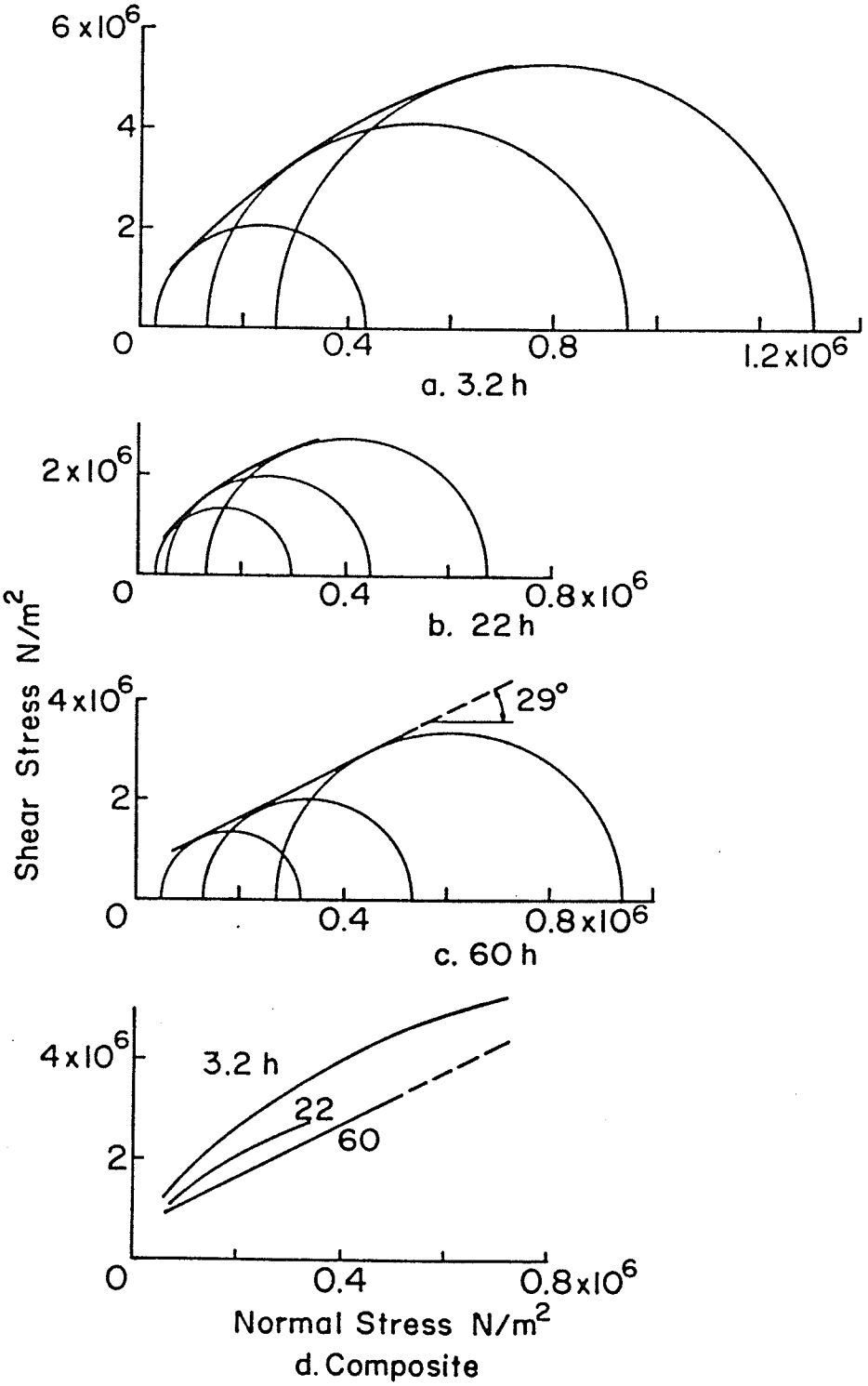

Fig.2.16 Mohr-Coulumb's envelopes for creep strength of Ottawa sand. (After Sayles, 1973)

Fish (1983, 1987), Ting (1983), and Gardner et al. (1984) studied the shape of creep curves, and suggested that the strain, strain rate and time to the point of inflection are the key parameters for characterizing a creep curve. Fish (1983, 1985) proposed a relationship between the time to the point of minimum strain rate, t_m, and the applied stress, σ, as

$$t_m = t_0 \left(\frac{\sigma}{\sigma_0} \right)^{-m} \tag{2.15}$$

where t_0 is the mean duration of the "settled life" of an elementary particle in position of equilibrium (Frenkel, 1946), and σ_0 is the stress that causes failure at time t_0, while m is a parameter depending on soil properties and temperature. Eq.(2.15) is essentially the same as (2.13) except that the parameters in (2.15) are given physical interpretations while that in (2.13) are not. Eq.(2.15) can only be used in cases where tertiary creep occurs. Similar form of equations has been used by Sayles and Haines (1974), Tsytovich (1975), and Zhu and Carbee (1987).

Wijeweera and Joshi (1990, 1991) studied the strength of frozen clays and proposed a simple power law relationship between peak uniaxial compressive strength, σ_m, and temperature, θ, as

$$\sigma_m = A(\theta/\theta_0)^m \tag{2.16}$$

where A and m are parameters depending on soil properties, and θ_0 is a reference temperature. The dependency of strength on time was not studied in this research. As

discussed in 2.3.3.5, when strain rate is higher than a certain level, the strength of frozen fine-grained soil is almost independent of strain rate (or time). Eq.(2.16) focuses on the short-term strength of frozen clays, which depends mainly on temperature.

2.3.3.2 Creep Models for Frozen Soil

Andersland and Akili (1967) studied the effect of stress, σ, on creep rates, $\dot{\epsilon}$,of frozen clays by uniaxial multi-stage creep tests, and suggested that the effect be expressed by

$$\dot{\epsilon} = c' \sinh(B\sigma) \tag{2.17}$$

where c' and B are two constants to be determined experimentally. For creep deformation involving more influencing factors, they suggested that the following general equation proposed by Kauzmann (1941) and Conrad (1961) be used.

$$\dot{\epsilon} = \sum C_i(\sigma,T,s) \exp\left[\frac{-\Delta F_i(\sigma,T,s)}{RT}\right] \sinh(B_i(T,s)\sigma) \tag{2.18}$$

where C_i is the frequency factor, ΔF_i is the activation energy, B_i is the stress factor, R is the Universal gas constant, T is the temperature, and s represents the soil properties. This equation was developed on the basis of rate process theory. It can accommodate varying stress and temperature. However, it is not a convenient creep equation for engineering practice since it is in the form of a progression which has many constants to be determined. Also, the equation is valid only for creep dominated by secondary creep under an uniaxial stress condition. This equation was developed for creep of metals instead of frozen earth materials and therefore one cannot expect it to be very successful when applied to frozen

soils.

Goughnour and Andersland (1968) and Andersland and AlNouri (1970) studied the mechanical behaviour of frozen sand using triaxial tests, and proposed a creep equation as

$$\dot{\epsilon} = A\exp(\frac{-L}{T})\exp(ND)\exp(-m\sigma_m) \tag{2.19}$$

where A, L, N, and m are parameters to be determined experimentally, T is temperature, while D and σ_m are deviatoric and mean normal stress respectively. This equation is a simplified form of (2.18).

Ladanyi (1972) proposed a simple creep equation for steady state creep as

$$\epsilon = \frac{\sigma}{E} + \epsilon_k(\frac{\sigma}{\sigma_k})^k + \dot{\epsilon}_c(\frac{\sigma}{\sigma_c})^n t \tag{2.20}$$

where ϵ and σ are strain and stress respectively, E is Young's modulus, ϵ_k, σ_k, k and $\dot{\epsilon}_c$, σ_c, n are constants depending on temperature and soil properties, while t is time. The first term of the right hand side of (2.20) represents the instantaneous and delayed elastic strain, while the second term represents the instantaneous plastic strain, and the third term stands for creep strain. The limitation of this equation is obvious. It is valid only for steady state creep and completely ignores the change of strain rate during creep process. The advantage of (2.20) is its simplicity.

Odqvist (1966) proposed a constitutive equation for multi-axial stress-strain state, based on the theory of plasticity, as

$$\frac{d\epsilon_{ij}}{dt} = \frac{3}{2}\left[\frac{d}{dt}\left(\left(\frac{\sigma_e}{\sigma_c}\right)^{n-1}\frac{S_{ij}}{\sigma_c}\right) + \left(\frac{\sigma_e}{\sigma_c}\right)^{n-1}\frac{S_{ij}}{\sigma_c}\right] \tag{2.21}$$

where ϵ_{ij} and S_{ij} are strain and deviatoric stress tensors respectively, σ_e is the equivalent stress, σ_c is a proof stress, n is the exponent of Norton-Bailey power law creep equation (Norton, 1929), and t is time. This equation gives a complete constitutive relationship for materials which meet the following hypotheses: (1) the material is incompressible, and the creep rate is independent of hydrostatic pressure, (2) it is homogeneous and isotropic, (3) it follows the associated flow rule, and the (4) Norton-Bailey creep law holds in uniaxial stress condition. Since no frozen earth material completely meets these hypotheses, (2.21) has very few applications in permafrost engineering practice.

Viylov (1973), based on his study on long-term strength of frozen soil, proposed a creep equation as

$$\epsilon_c = \left(\frac{C_\infty}{w(1+\theta)^k}\right)^{\frac{1}{m}}\left(\frac{\sigma_c t^\alpha}{C_\infty + \sigma_m \tan\phi_\infty}\right) \tag{2.22}$$

where ϵ_e and σ_e are equivalent creep strain and stress, σ_m is the mean normal stress, C_∞ and ϕ_∞ are respectively cohesion and friction angle of frozen soil at $t = \infty$, which depend on temperature and soil properties, θ is the relative temperature, t is time, and w, k, m and α are parameters to be determined experimentally. This creep equation focuses on the long-term

deformation of frozen soil under low stress level. It relates the creep strain to stress, ultimate strength, unfrozen water content, w, and time.

Based on the Theory of Rate Process (Eyring, 1936; Glasston et al., 1941; and Frenkel, 1946), Fish (1980, 1982, 1983, 1985) studied the creep behaviour of frozen soil and ice, and proposed the following creep equation which was similar to (2.19) but more general.

$$\dot{\epsilon} = \check{C}\ \frac{kT}{h} exp\left(-\frac{E}{RT}\right) exp\left(\frac{\Delta S}{k}\right)\left(\frac{\sigma}{\sigma_0}\right)^{n+m} \qquad (2.23)$$

where $\dot{\epsilon}$ is the axial strain rate, σ is the stress applied, σ_0 is the ultimate strength depending on soil properties and temperature, k is Boltzmann's constant, h is Planck's constant, R is Universal gas constant, E is the activation energy of frozen soil, ΔS is the change in entropy, and $\check{C}$, $n \geq 0$ and $m \geq 1$ are dimensionless constants depending on soil properties but independent of temperature. This equation is able to make good predictions for ice-rich frozen soils under a stress level higher than its ultimate long-term strength but not so high as to cause massive microcracking. The deformation of ice-rich frozen soil under such stress conditions is dominated by a prolonged apparent steady state creep. On the other hand, (2.23) is not good for dense frozen sand since several mechanisms of deformation jointly affect the deformation.

Ting (1983) proposed an empirical equation, (2.24), to fit creep curves for frozen sand.

$$\dot{\epsilon} = At^{-m} exp(\beta t) \qquad (2.24)$$

where A, m, and β are parameters depending on soil properties, temperature and stress acting on frozen soil. Fish and Assur (1984) suggested that (2.24) was actually a special case of a family of equations used by Zaretskiy and Vialov (1971), Assur (1979), and Fish (1980, 1982) as (2.23). This equation describes a creep curve with the creep rate first decreasing with time to a minimum strain rate point and then increasing with time to failure.

Gardner et al. (1984) proposed a creep equation which, like (2.24), also describes creep curves from primary creep to the minimum strain rate point and then to tertiary creep as

$$\frac{\epsilon_c}{\epsilon_m - \epsilon_0} = \left(\frac{t}{t_m}\right)^c exp\left[(\sqrt{c} - c)\left(\frac{t}{t_m} - 1\right)\right] \qquad (2.25)$$

where ϵ_c is creep strain, ϵ_m is the creep strain at the point of minimum strain rate, while t_m is the time taken to reach ϵ_m, ϵ_0 is the instantaneous strain, t is time, and c is a parameter to be determined experimentally. This equation also belongs to the same family of equations as that used by Zaretskiy and Vialov (1971), Assur (1979) and Fish (1980, 1982) etc.

Among the seven creep models discussed herein, the Odqvist (1967) model was developed on the basis of the theory of plasticity, the Ladanyi (1972) and Vyalov (1973) models are empirical, while all the other models are more or less based on the Theory of Rate Process and incorporate a time-dependent or constant creep rate. The shortcomings of these

models are as follows.

(1) Most of them considered uniaxial stress conditions only.

(2) The effect of volumetric deformation was ignored, and most of them also ignored the effect of confining pressure.

(3) The behaviour of soil particles was not separated from the behaviour of ice matrix, and a single equation was used to represent the effect of both components.

Rahman (1988) and Domaschuk et al. (1991) proposed a K-G model for frozen sand based on the K-G model developed by Domaschuk and Wade (1969) for unfrozen sand. A method of separating the effect of mean normal stress from that of deviatoric stress was proposed. The model considered the effect of confining pressure and volumetric strain. A time-hardening law was used, and the interaction between soil particles and ice matrix was not considered. The details of their work will be discussed in subsequent chapters.

CHAPTER 3

EXPERIMENTAL DATA

The experimental data required for development of the model were taken from two sources. Firstly, creep data were taken from the results of triaxial compression tests on a frozen sand as reported by Rahman (1988). Secondly, because the model required data on the behaviour of the same sand in an unfrozen state, a series of conventional constant strain rate triaxial tests were performed by the writer on the sand in an unfrozen state. The details and results of these two series of tests are presented in the following sections.

3.1 TRIAXIAL CREEP TEST ON FROZEN SAND (Rahman 1988)

The results of 10 triaxial creep tests were taken, which included one multi-stage isotropic creep test, IC1, five long-term multi-stage constant mean normal stress creep tests, MST1, MST2, MST3, MST4, and MST5, three short-term multi-stage constant mean normal stress creep tests, MST7, MST8, and MST9, and one long-term multi-stage constant cell pressure creep test, MST13. The soil tested was a medium to dense sand at a temperature of -3°C. Reference should be made to Rahman (1988) for details of the test program and the data. The creep curves for the tests mentioned above are shown in Fig.3.1 through Fig.3.10 as cumulative strain versus cumulative time. These will be discussed in detail in the subsequent chapters when the data are used.

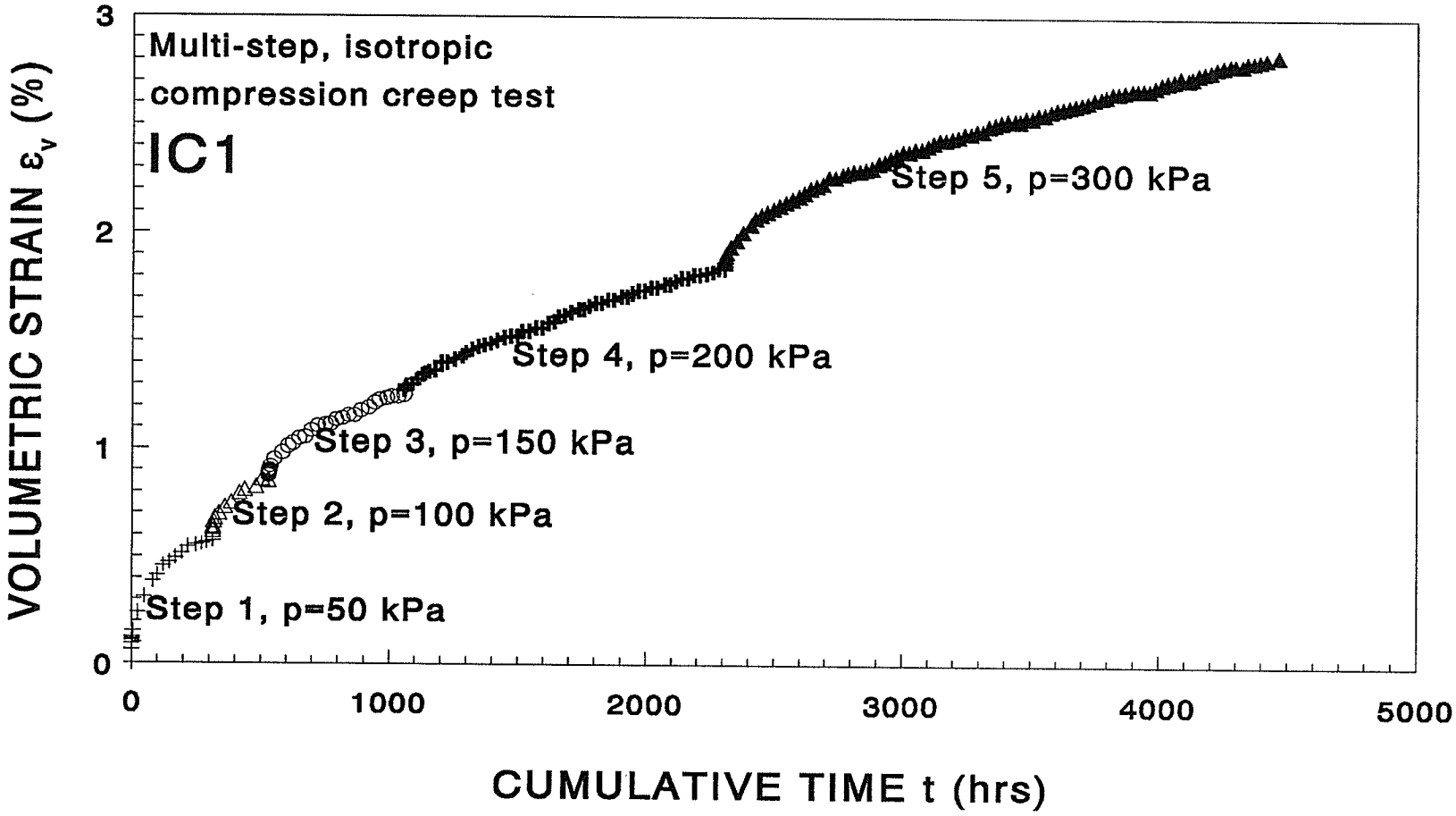

Fig.3.1 Creep curve for forzen sand at -3°C in a multi-step, isotropic compression creep test: Test IC1. (After Rahamn, 1988)

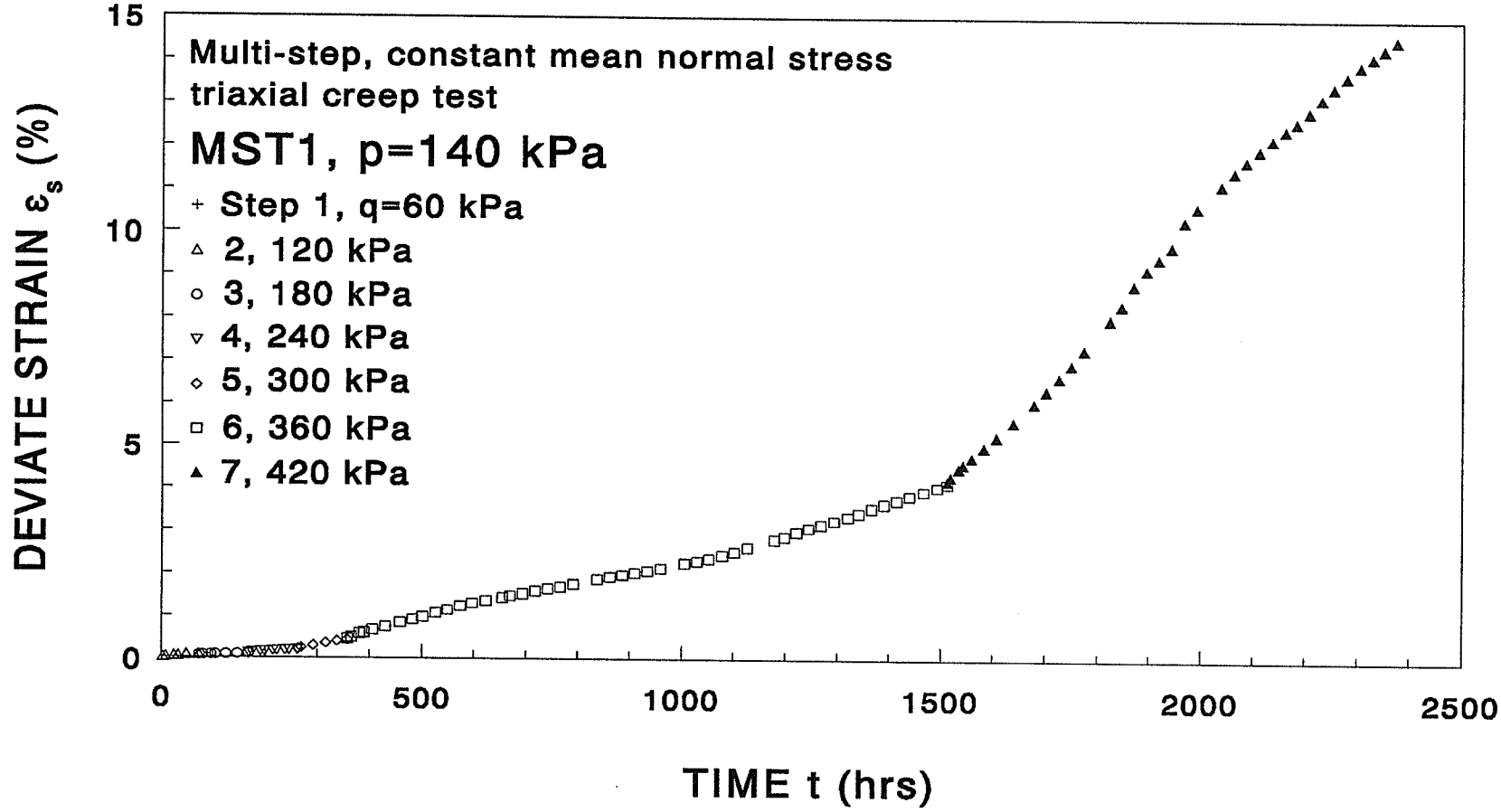

Fig.3.2 Creep curve for frozen sand at -3°C in a multi-step, constant mean normal stress, triaxial creep test: Test MST1. (After Rahman, 1988)

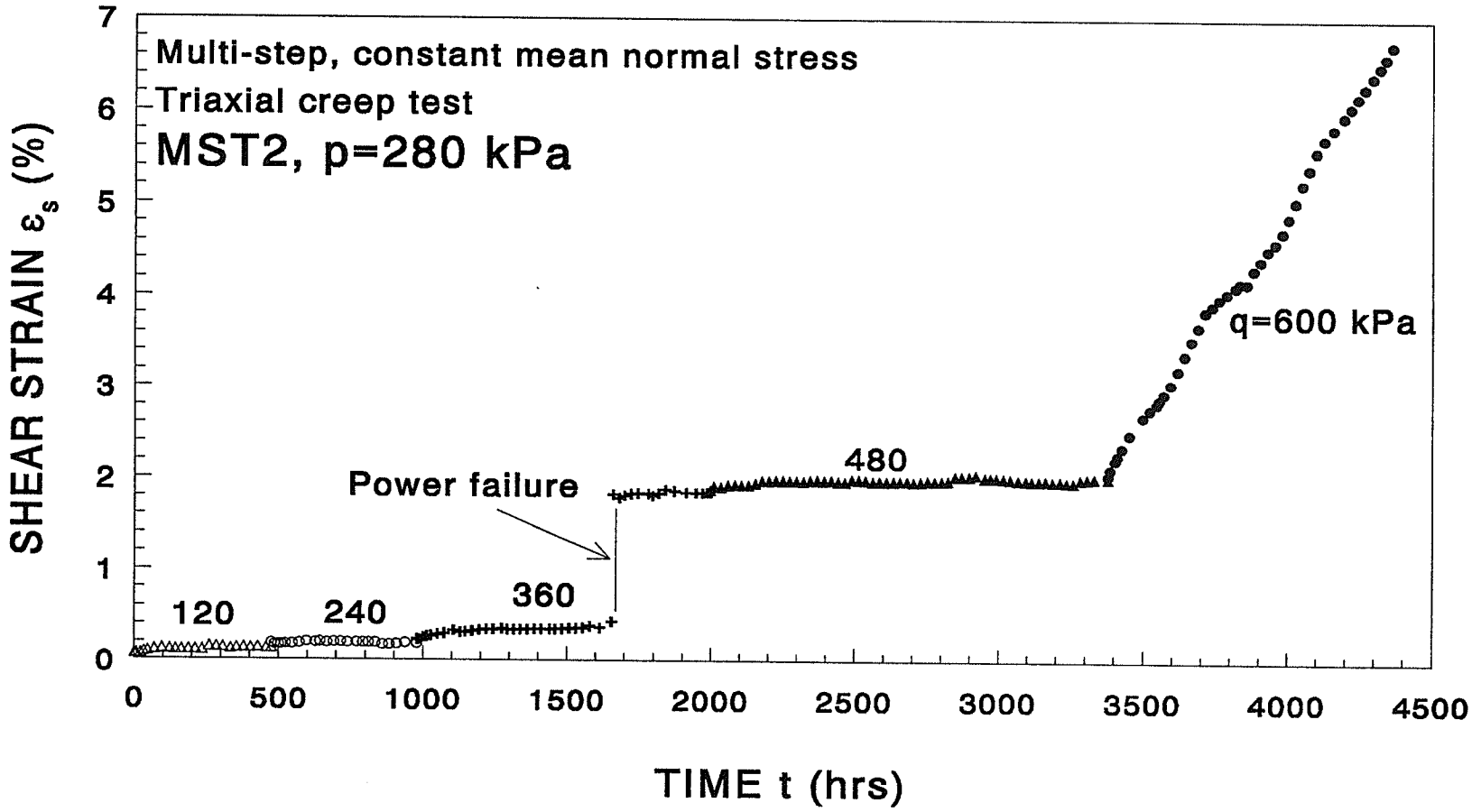

Fig.3.3 Creep curve for frozen sand at -3°C in a multi-step, constant mean normal stress, triaxial creep test: Test MST2. (After Rahman, 1988)

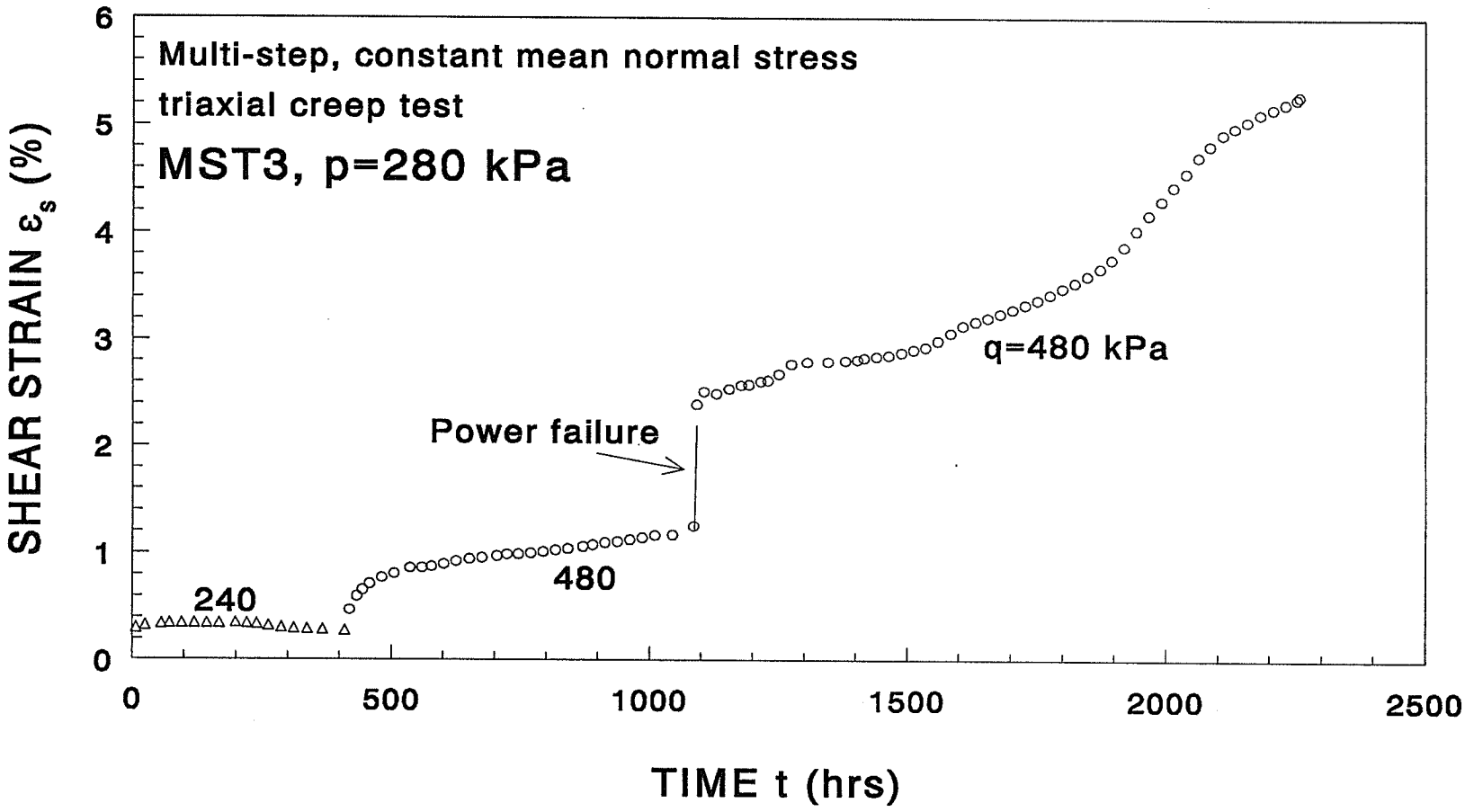

Fig.3.4 Creep curve for frozen sand at -3°C in a multi-step, constant mean normal stress, triaxial creep test: Test MST3. (After Rahman, 1988)

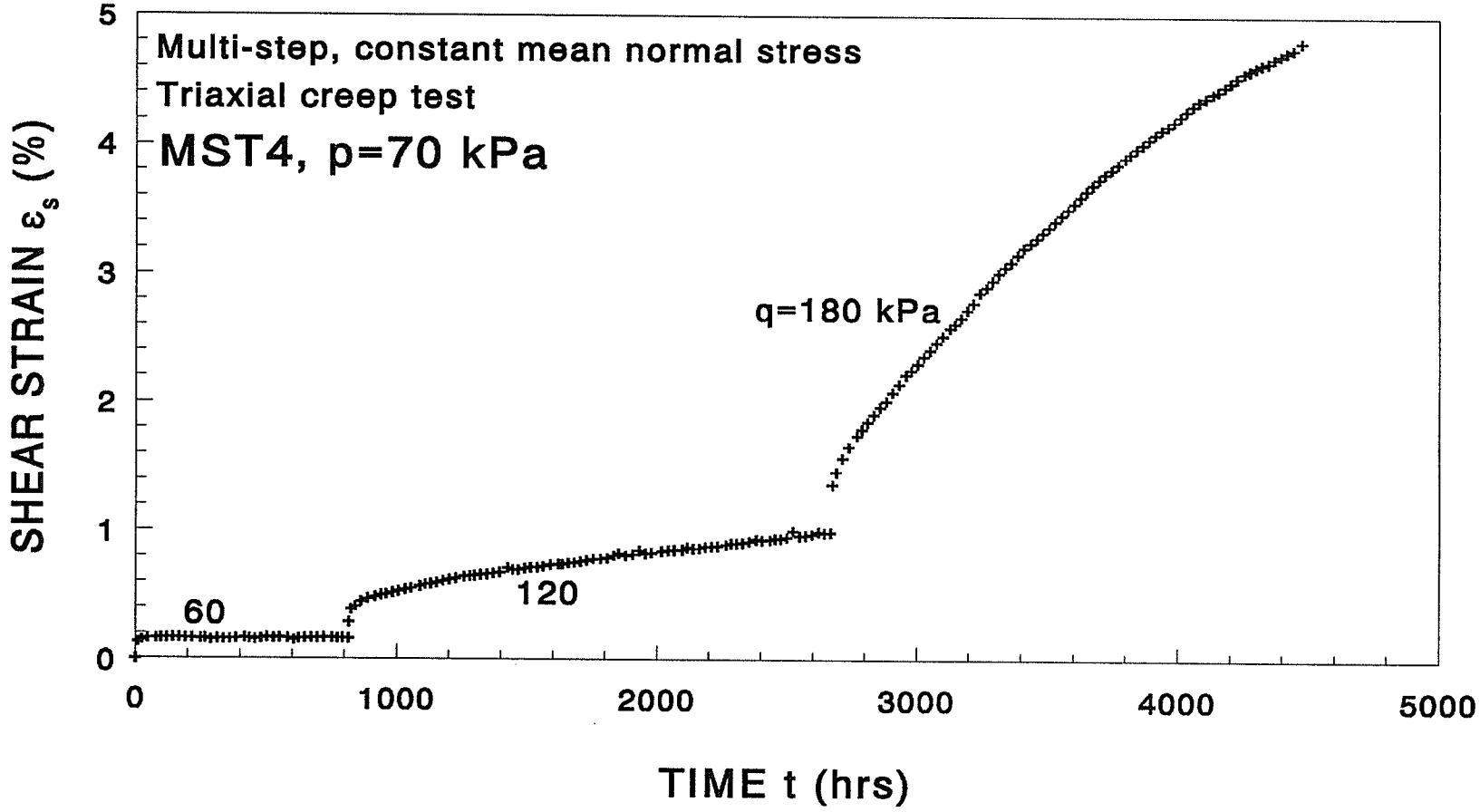

Fig.3.5 Creep curve for frozen sand at -3°C in a multi-step, constant mean normal stress, triaxial creep test: Test MST4. (After Rahman, 1988)

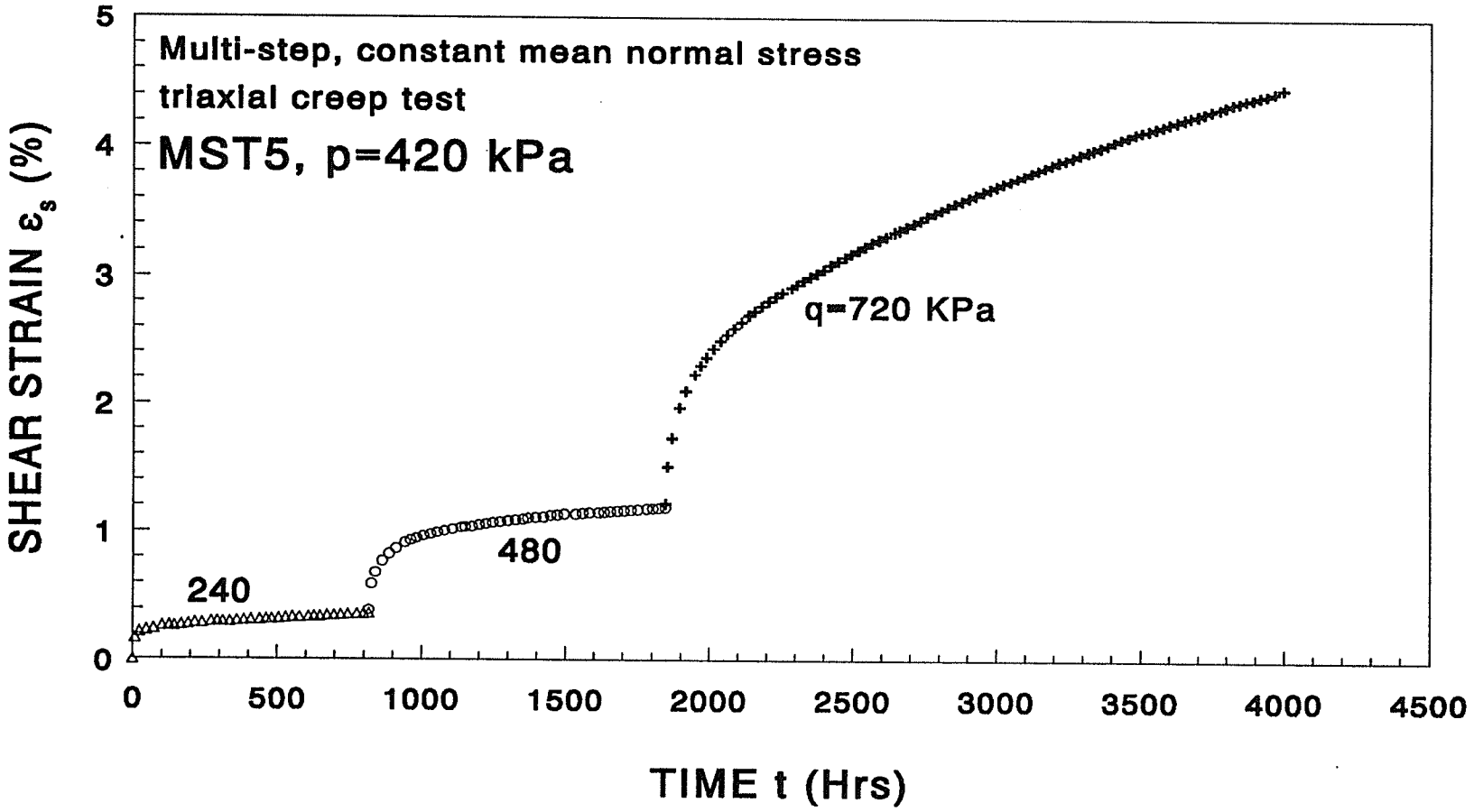

Fig.3.6 Creep curve for frozen sand at -3°C in a multi-step, constant mean normal stress, triaxial creep test: Test MST5. (After Rahman, 1988)

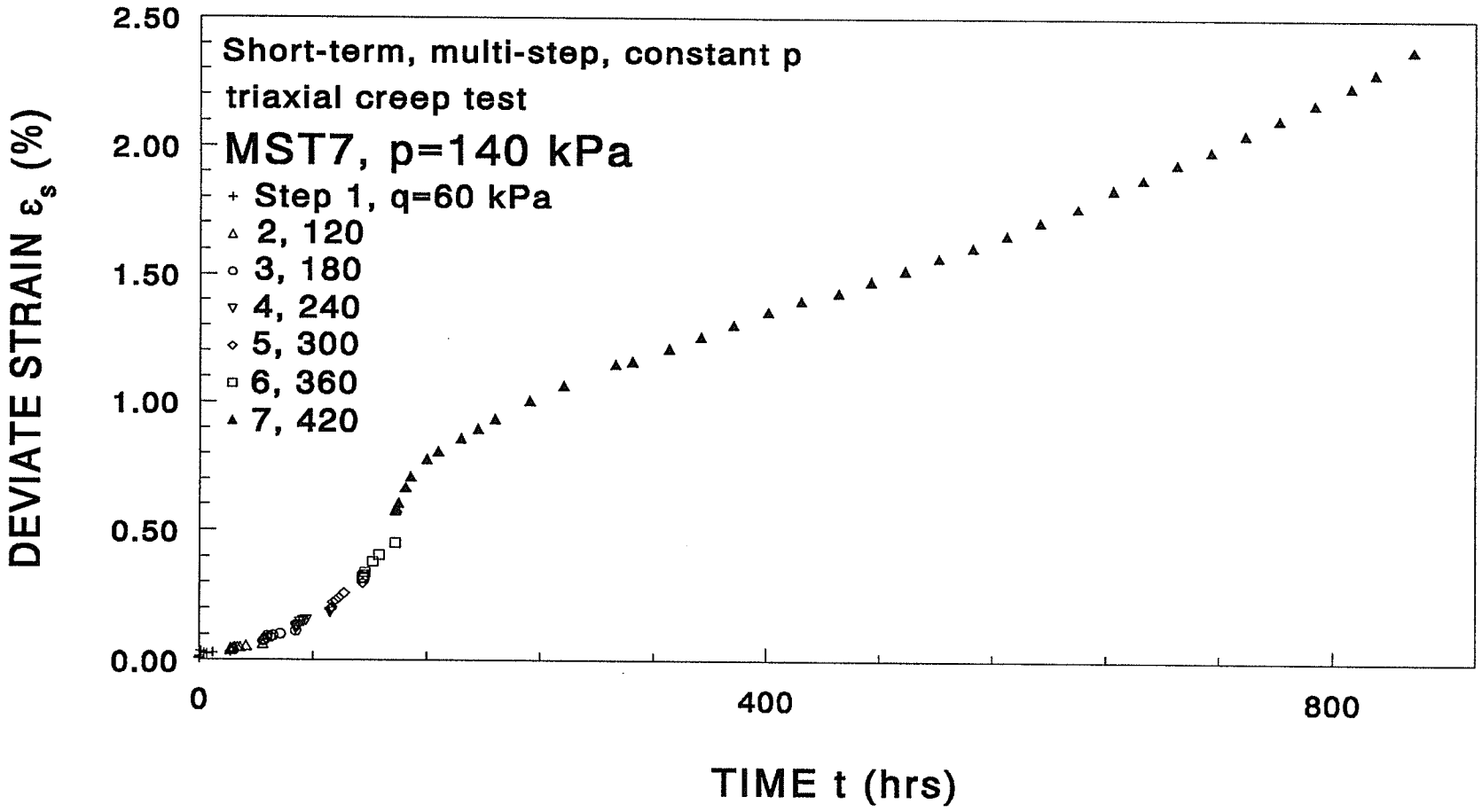

Fig.3.7 Creep curve for frozen sand at -3°C in a short-term, multi-step, constant mean normal stress, triaxial creep test. Step 1 through 6 each lasted for about 24 hours, step 7 lasted for about 720 hours: Test MST7. (After Rahman, 1988)

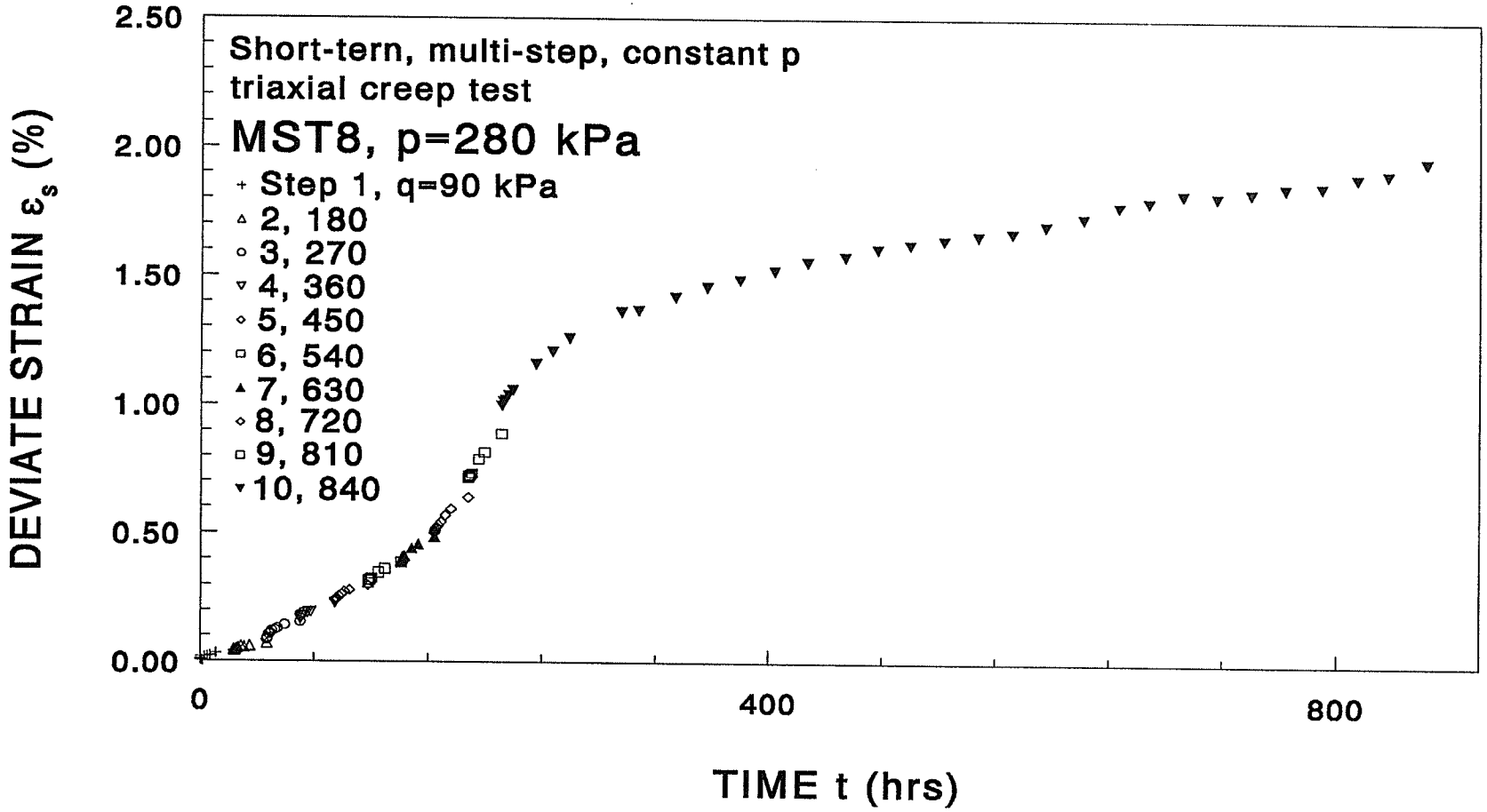

Fig.3.8 Creep curve for frozen sand at -3°C in a short-term, multi-step, constant mean normal stress, triaxial creep test. Step 1 through 9 each lasted for about 24 hours, step 10 lasted for about 650 hours: Test MST8. (After Rahman, 1988)

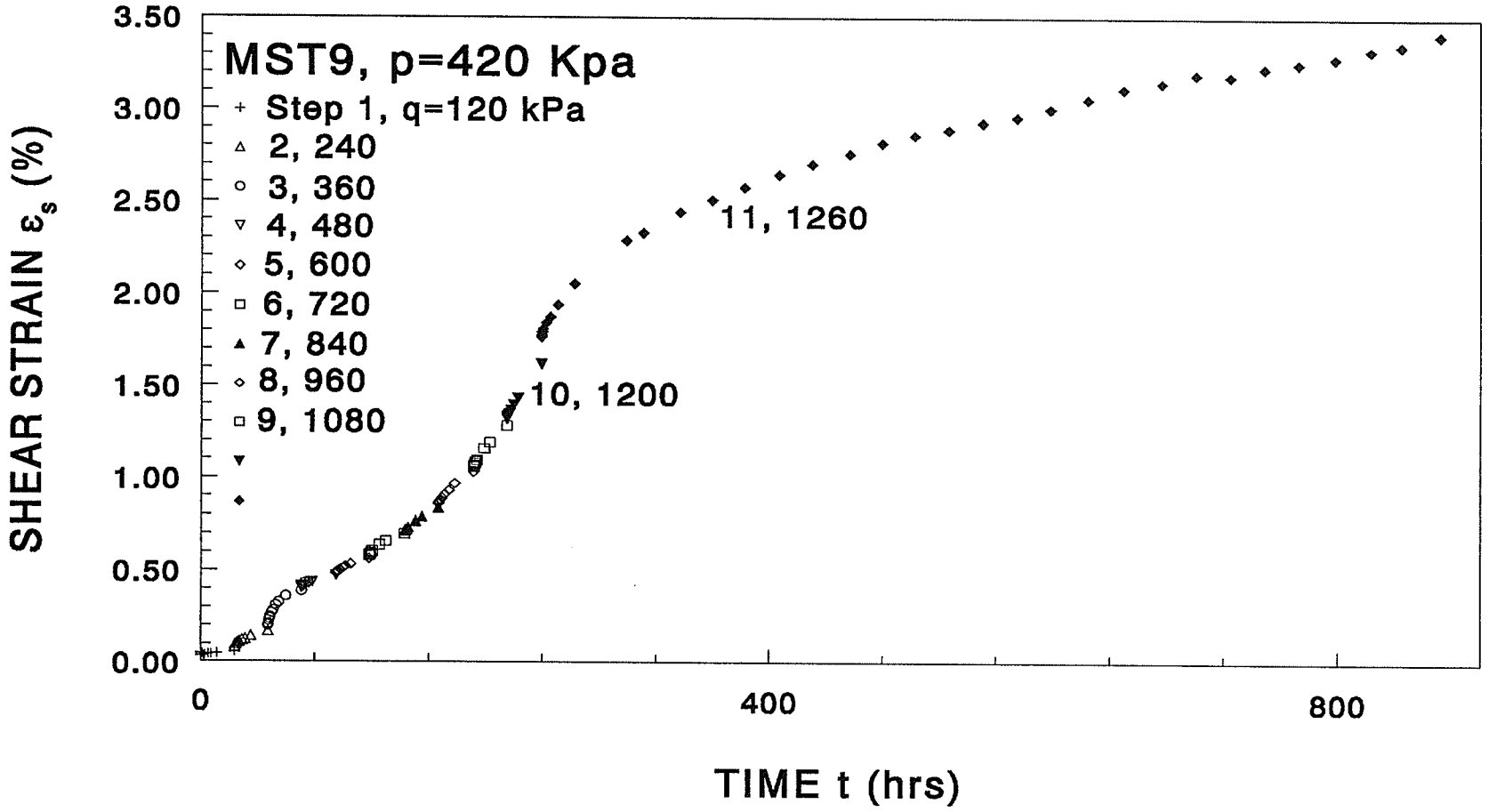

Fig.3.9 Creep curve for frozen sand at -3°C in a short-term, multi-step, constant mean normal stress, triaxial creep test. Step 1 through 10 each lasted for about 24 hours, step 11 lasted for about 630 hours: Test MST9. (After Rahman, 1988)

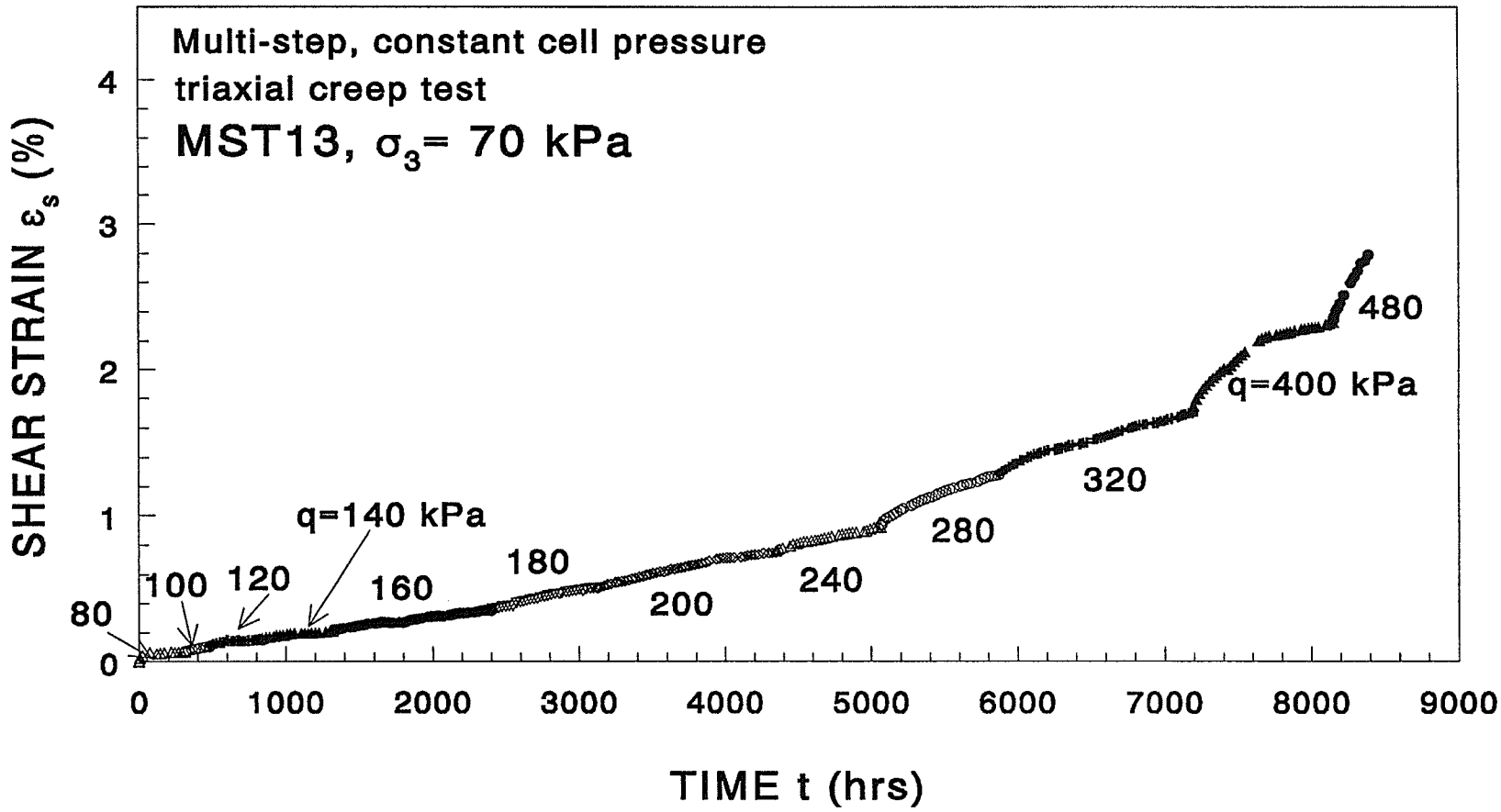

Fig.3.10 Creep curve for frozen sand at -3°C, multi-step, constant cell pressure, triaxial creep test: Test MST13. (After Rahman, 1988)

3.2 CONVENTIONAL TRIAXIAL TEST ON UNFROZEN SAND

The sand tested was the same as that used by Rahman (1988). It consisted of an uniform, quartz-carbonate medium-grain sand with an uniformity coefficient (D_{60}/D_{10}) of 2.0 and a specific gravity of 2.70. The grain size distribution of the sand is shown in Fig.3.11. The test specimens were about 36 millimetres in diameter and 72 millimetres in height, and were prepared by spooning moist sand into a mould, layer by layer, and lightly compacting each layer. A schematic of the test set-up is shown in Fig.3.12.

In order to achieve saturation, distilled water was introduced through the bottom porous stone and was allowed to flow upward through the specimen under a vacuum pressure of 50 kPa for about five hours. After that, the vacuum pressure was gradually decreased to 15 kPa, and the drainage line connected to the bottom of the specimen was closed. The dimensions of the specimen were measured at this stage. Prior to testing, the suction was removed, the drainage line to the top of the sample was closed, and the drainage line to the bottom of the specimen was connected to either the device for measurement of the volume change in a drained test or to a gauge for measurement of pore water pressure in an undrained test.

The axial load was applied and measured by means of a proving ring. The axial displacement was measured with a dial gauge.

In the drained tests, the specimen was first isotropically consolidated to a preset

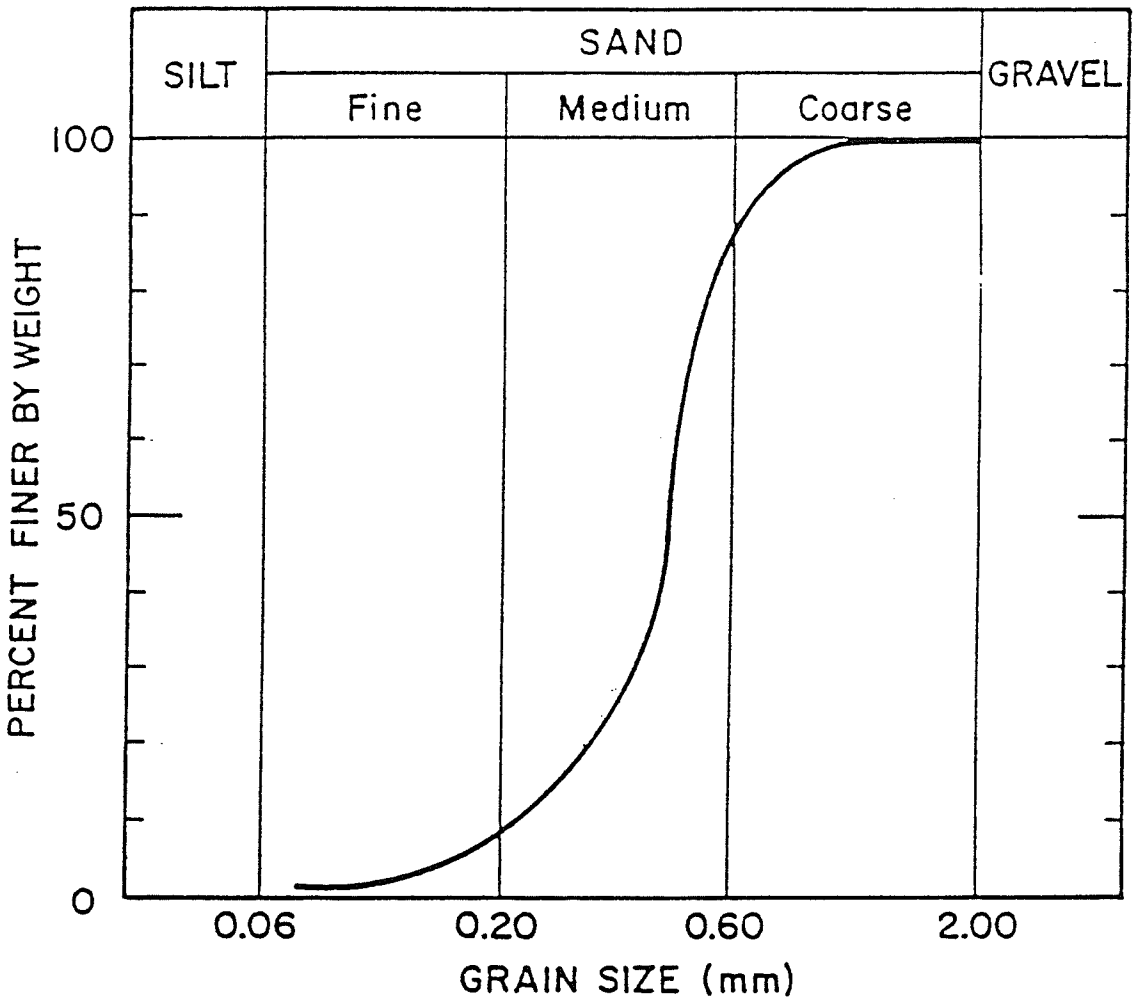

Fig.3.11 Grain size distribution of the sand. (After Rahman, 1988)

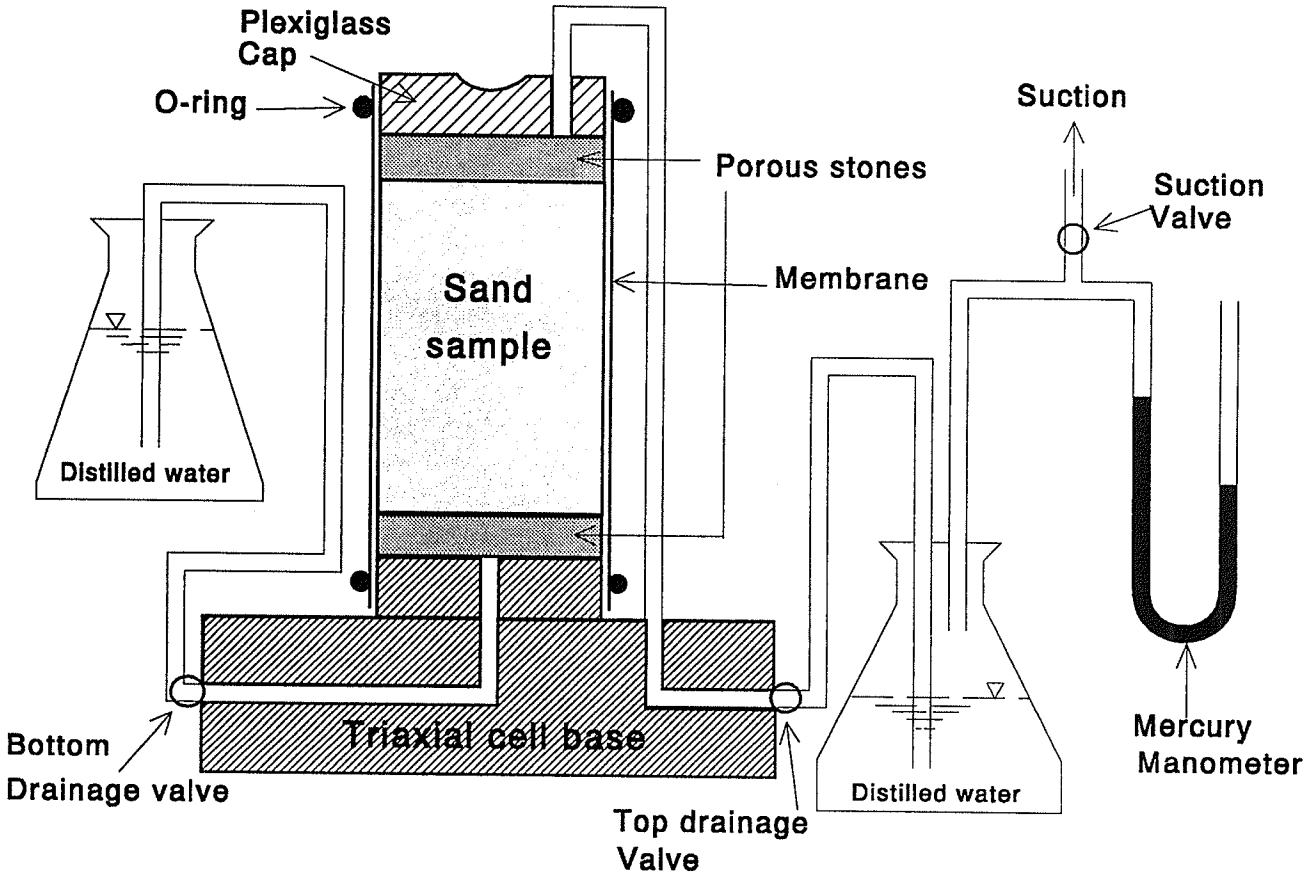

Fig.3.12 A schematic of the test setup for conventional triaxial tests on the sand in an unfrozen state.

effective mean normal stress, and then sheared under a constant rate of vertical displacement of 0.04572 millimetres per minute. It took about four hours to develop an axial strain of about 15%, at which point the tests were terminated. The vertical displacement, the axial load, and the volume change were recorded for every 0.2 mm of vertical displacement. A total of twelve drained, constant cell pressure, triaxial tests were performed, and were numbered as DT1 through DT12. The measured stress-strain-volume change data are given in Fig.3.13 through Fig.3.16, and will be discussed in a subsequent chapter when the data are used.

In the undrained test, the specimen was first consolidated to a preset effective mean normal stress, and then the back pressure and the cell pressure were increased simultaneously until the desired back pressure was reached. The specimen was then sheared at a vertical displacement rate of 0.04572 mm per minute with the drainage closed. The recorded data included vertical displacement and the pore water pressure. A total of twelve undrained, constant cell pressure, triaxial tests were performed, and were numbered as UT1 through UT12. The measured stress-strain-pore pressure data are shown in Fig.3.17 through Fig.3.28, and will be discussed when the data are used in a subsequent chapter.

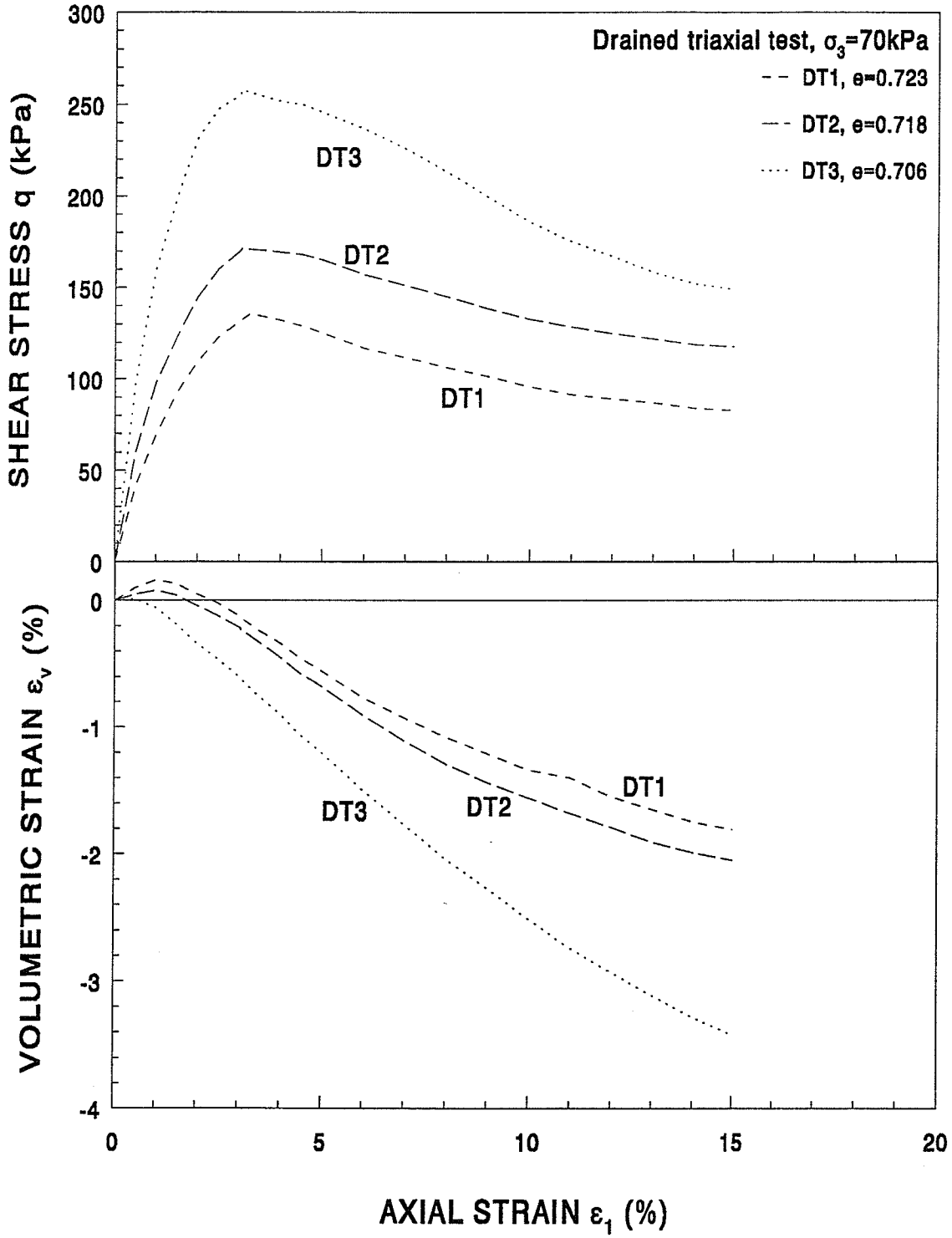

Fig.3.13 Shear stress and volumetric strain for unfrozen sand in constant cell pressure, constant strain rate, drained triaxial tests: DT1, DT2 and DT3.

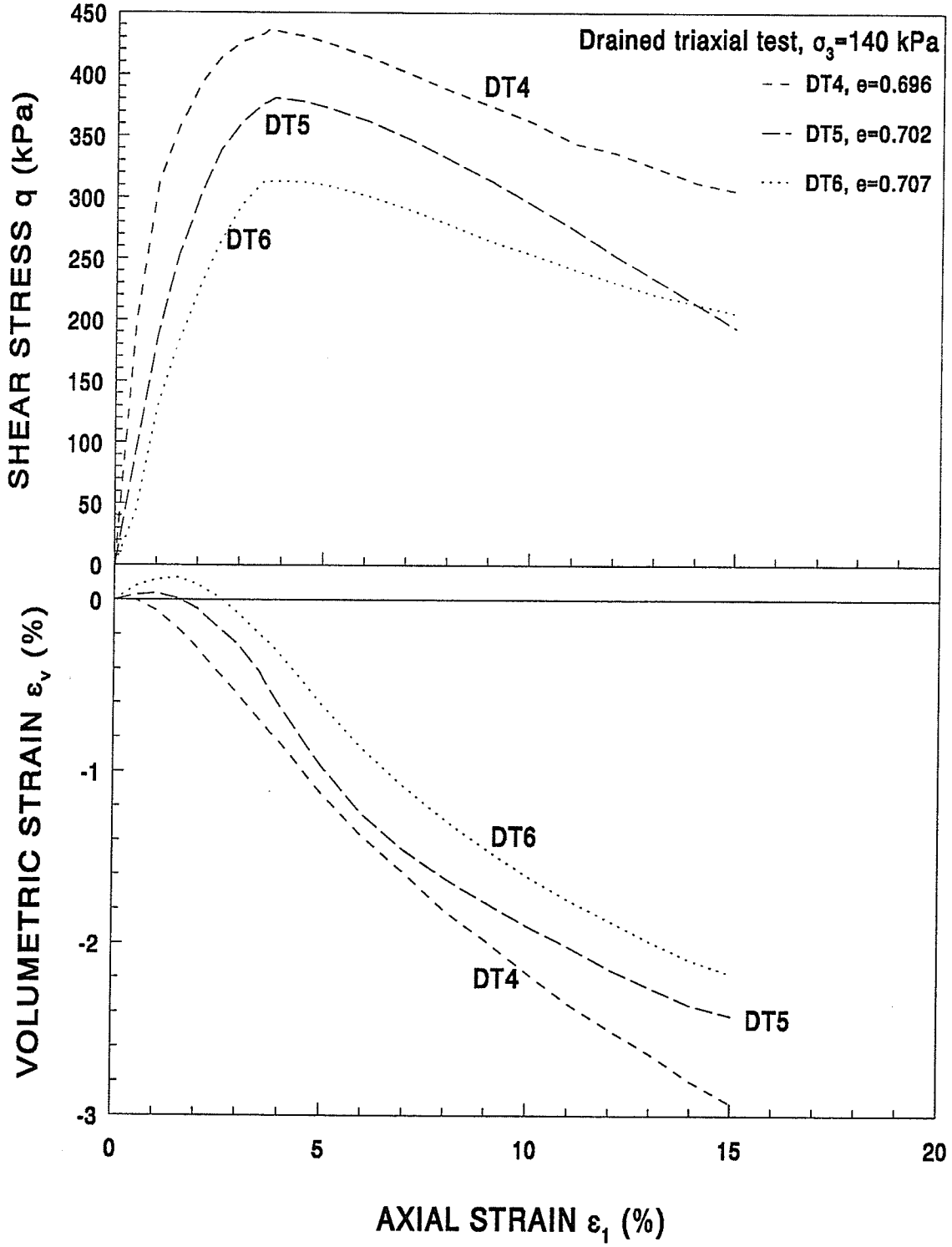

Fig.3.14 Shear stress and volumetric strain for unfrozen sand in constant cell pressure, constant strain rate, drained triaxial tests: DT4, DT5, and DT6.

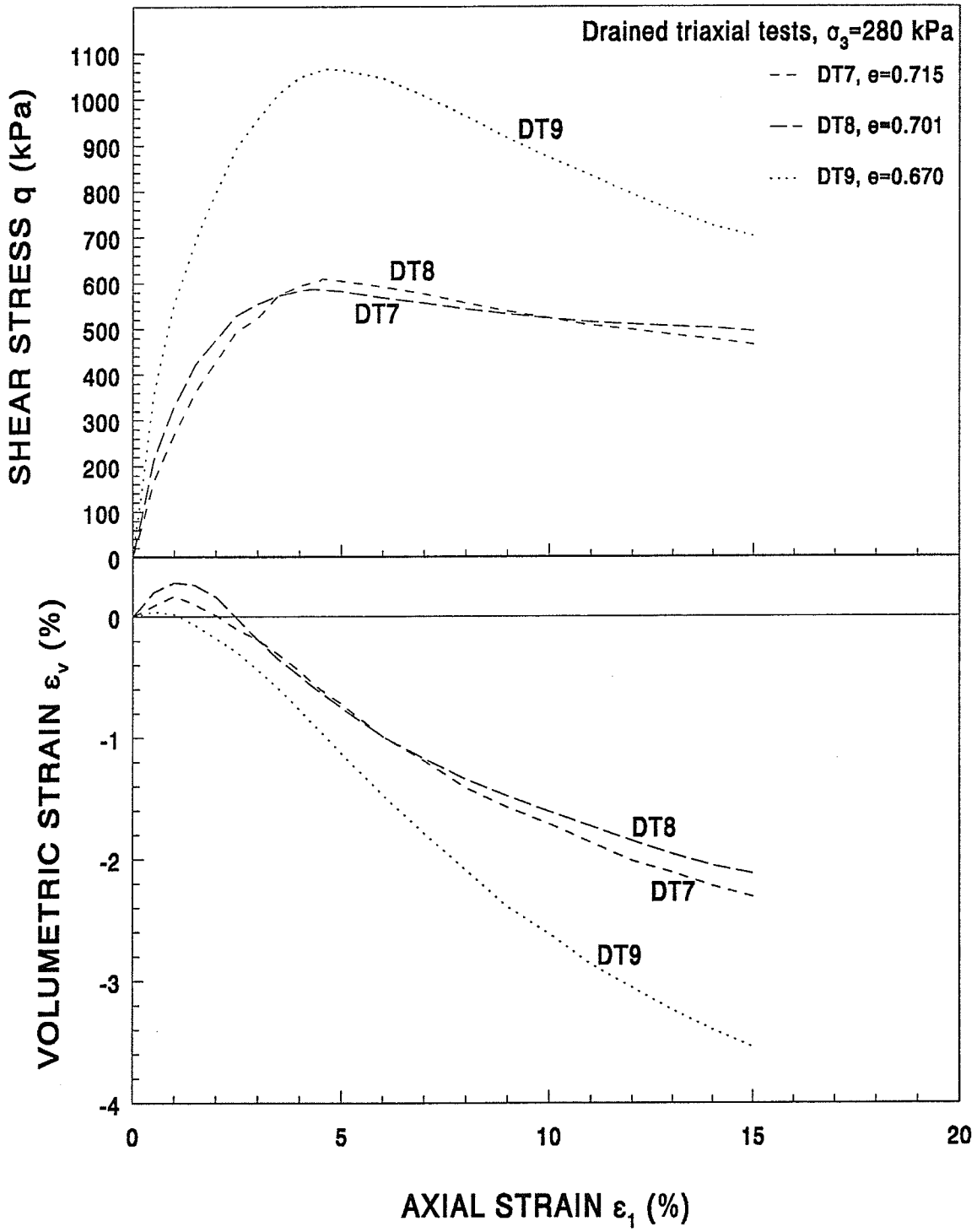

Fig.3.15 Shear stress and volumetric strain for unfrozen sand in constant cell pressure, constant strain rate, drained triaxial tests: DT7, DT8 and DT9.

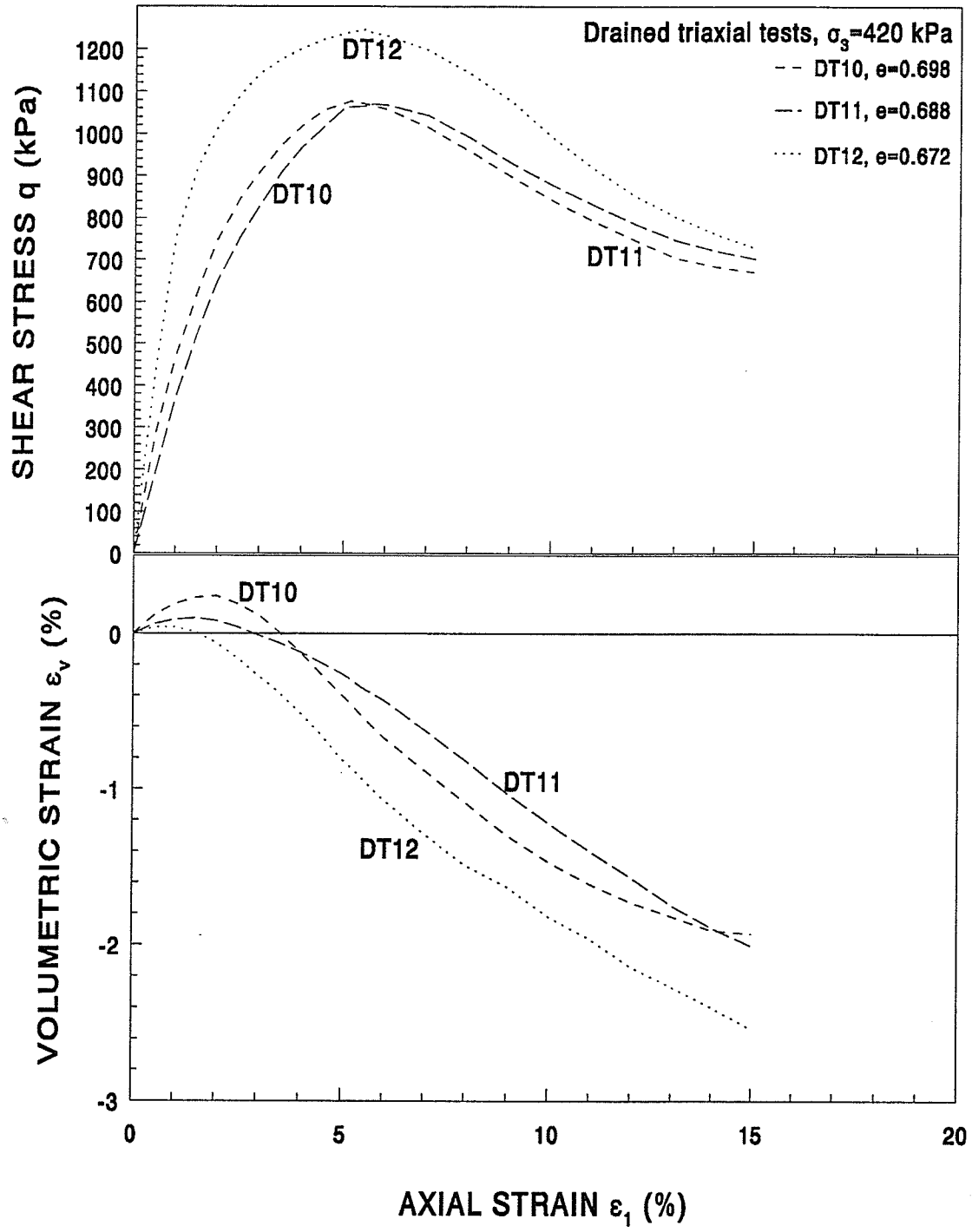

Fig.3.16 Shear stress and volumetric strain for unfrozen sand in constant cell pressure, constant strain rate, drained triaxial tests: DT10, DT11 and DT12.

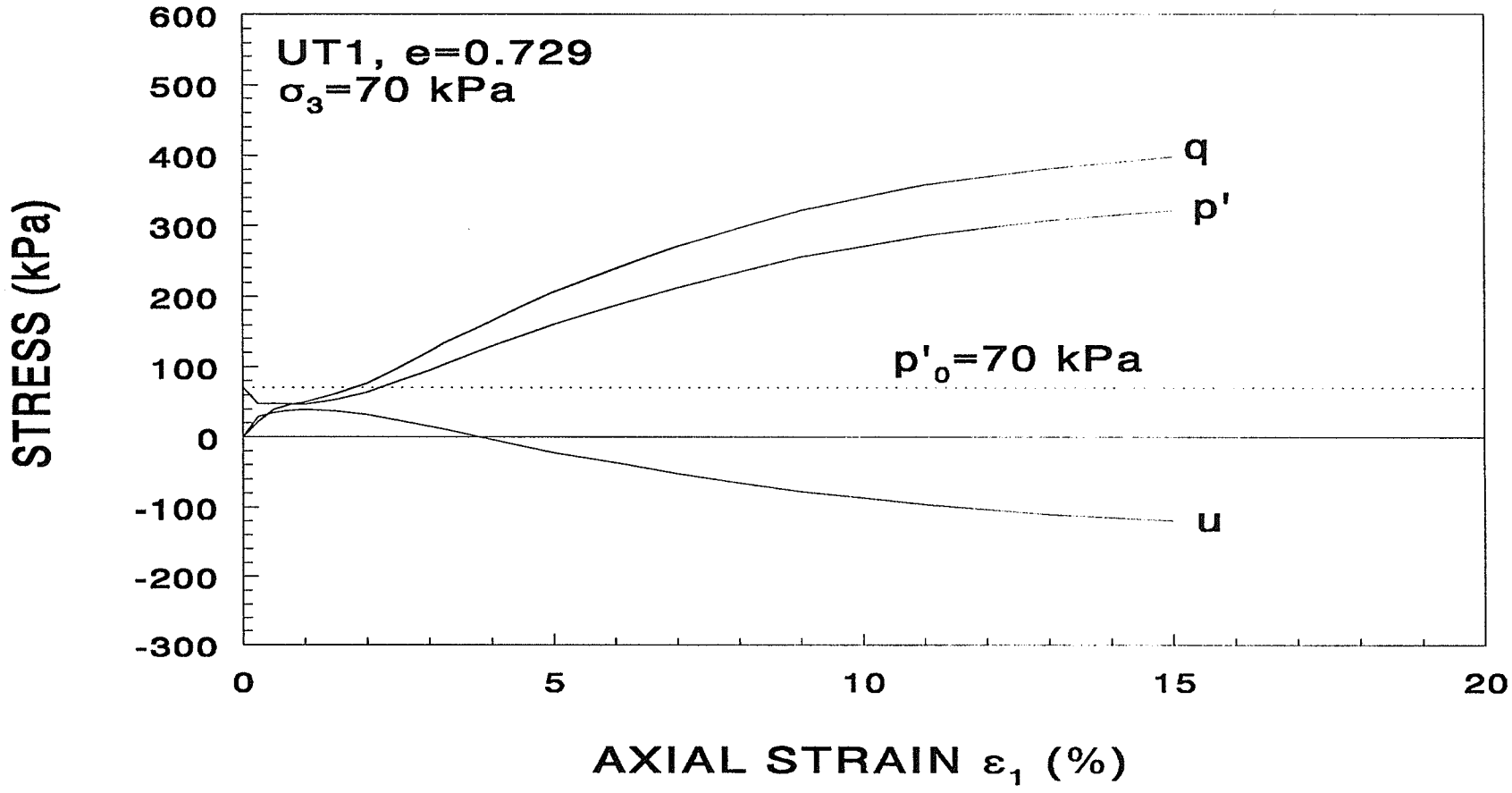

Fig.3.17 Shear stress q, effective mean normal stress p', and excess pore water pressure u for the unfrozen sand, a constant cell pressure, constant strain rate, undrained triaxial test: Test UT1.

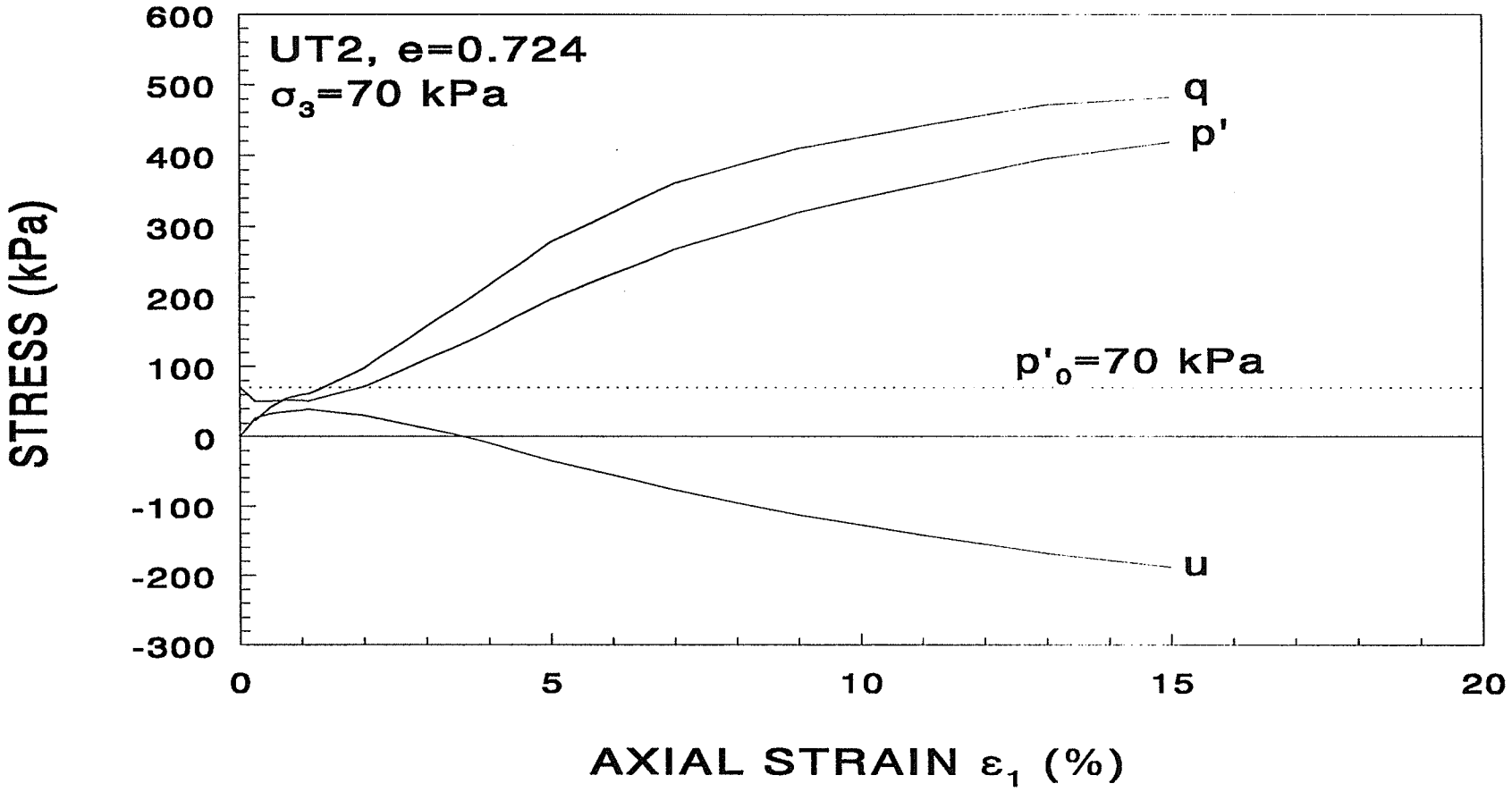

Fig.3.18 Shear stress q, efffective mean normal stress p' and excess pore water pressure u for the unfrozen sand, a constant cell pressure, constant strain rate, undrained triaxial test: Test UT2.

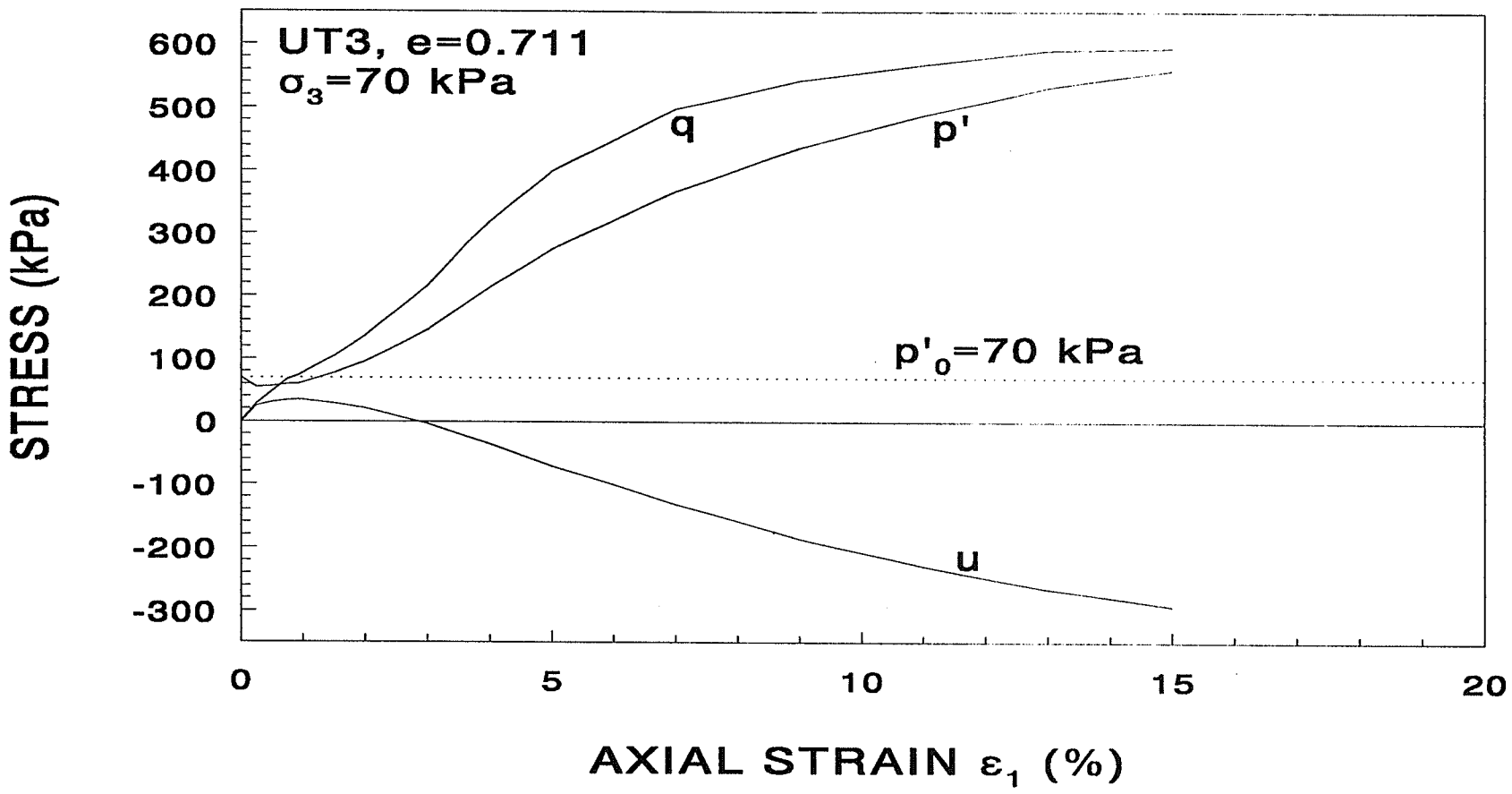

Fig.3.19 Shear stress q, effective mean normal stress p' and excess pore water pressure u for the unfrozen sand, a constant cell pressure, constant strain rate, undrained triaxial tsets: Test UT3.

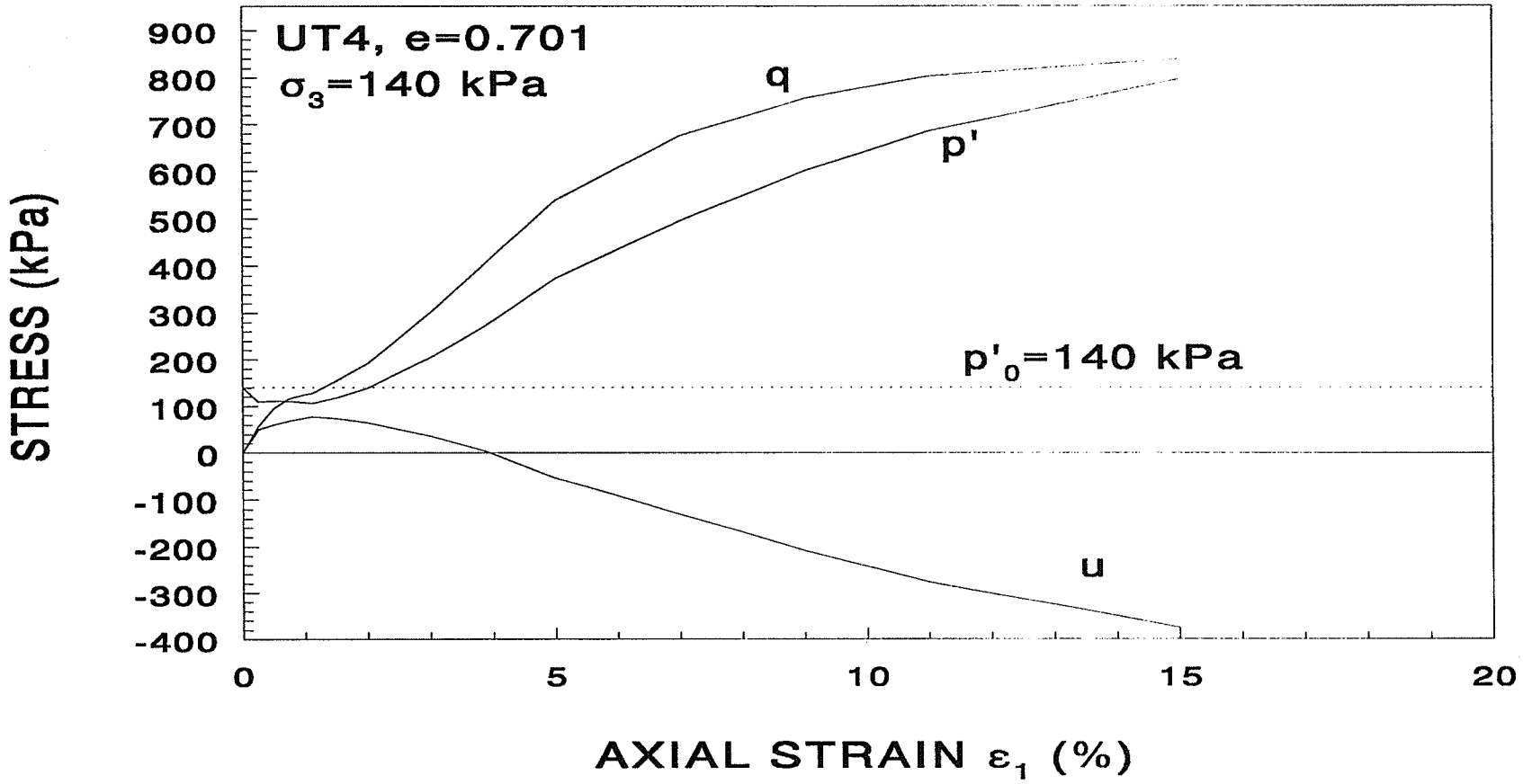

Fig.3.20 Shear stress q, effective mean normal stress p' and excess pore water pressure u for the unfrozen sand, a constant cell pressure, constant strain rate, undrained triaxial test: Test UT4.

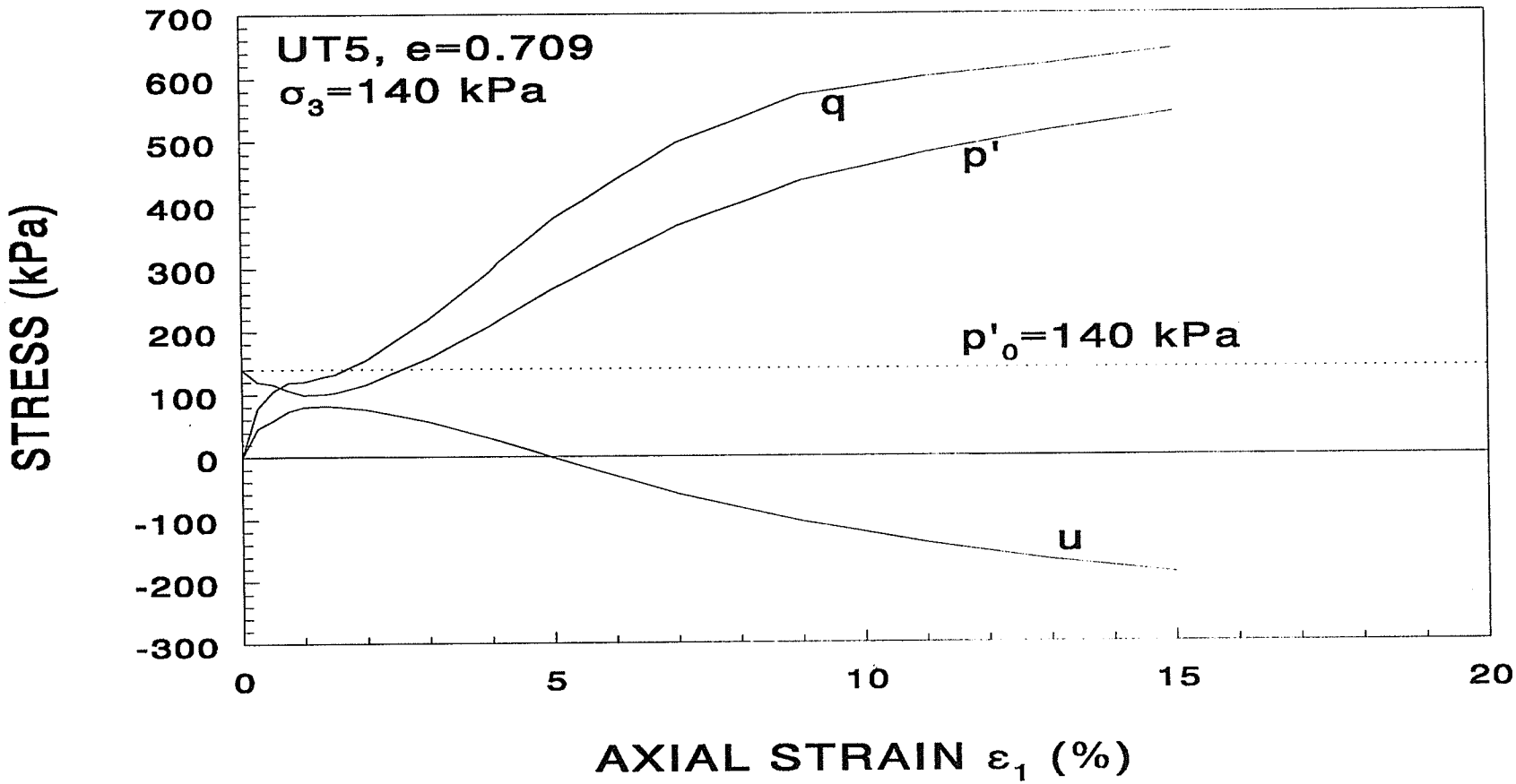

Fig.3.21 Shear stress q, effective mean normal stress p' and excess pore water pressure u for the unfrozen sand, a constant cell pressure, constant strain rate, undrained triaxial test: Test UT5.

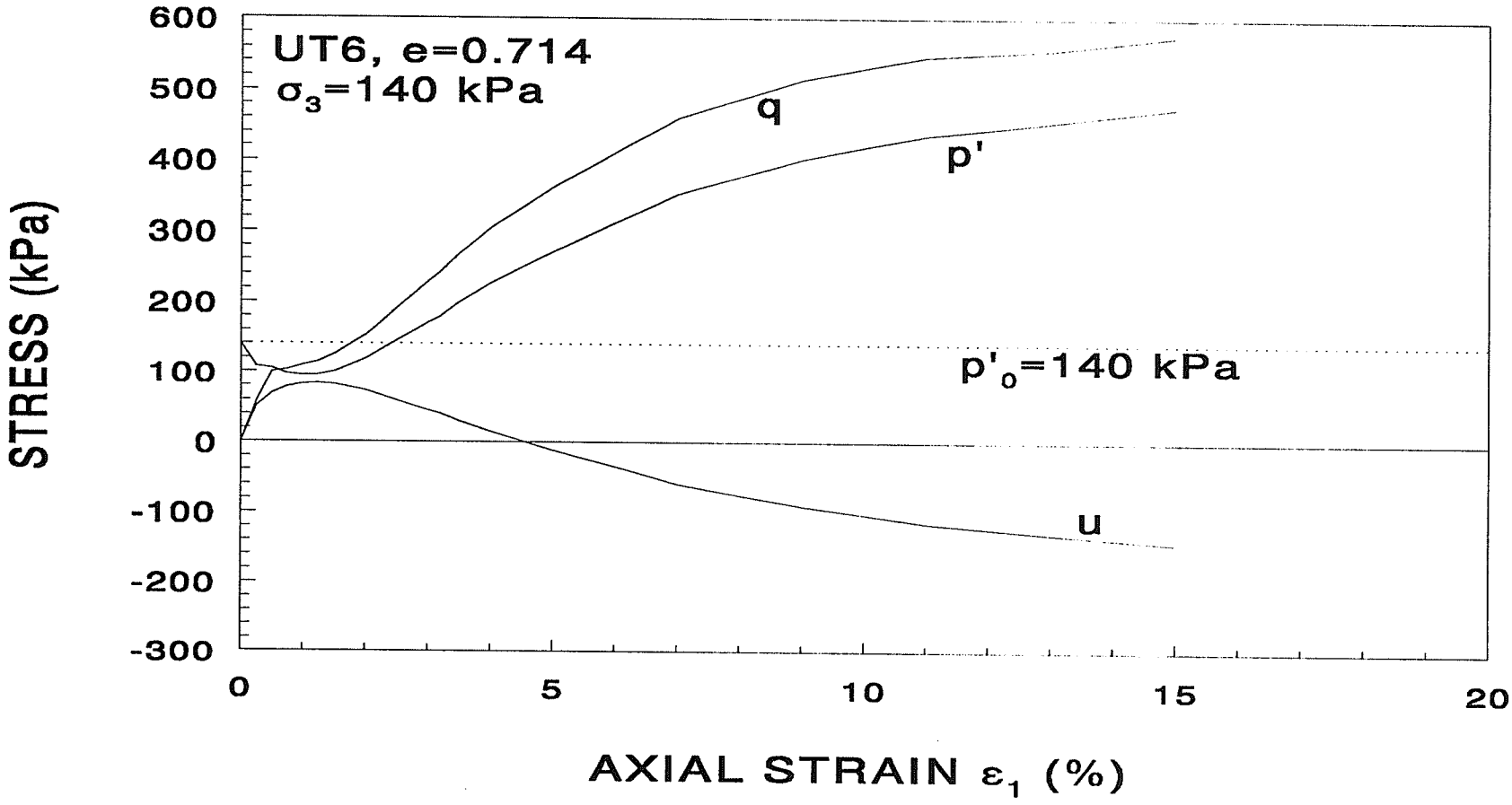

Fig.3.22 Shear stress q, effective mean normal stress p' and excess pore water pressure u for the unfrozen sand, a constant cell pressure, constant strain rate, undrained triaxial test: Test UT6.

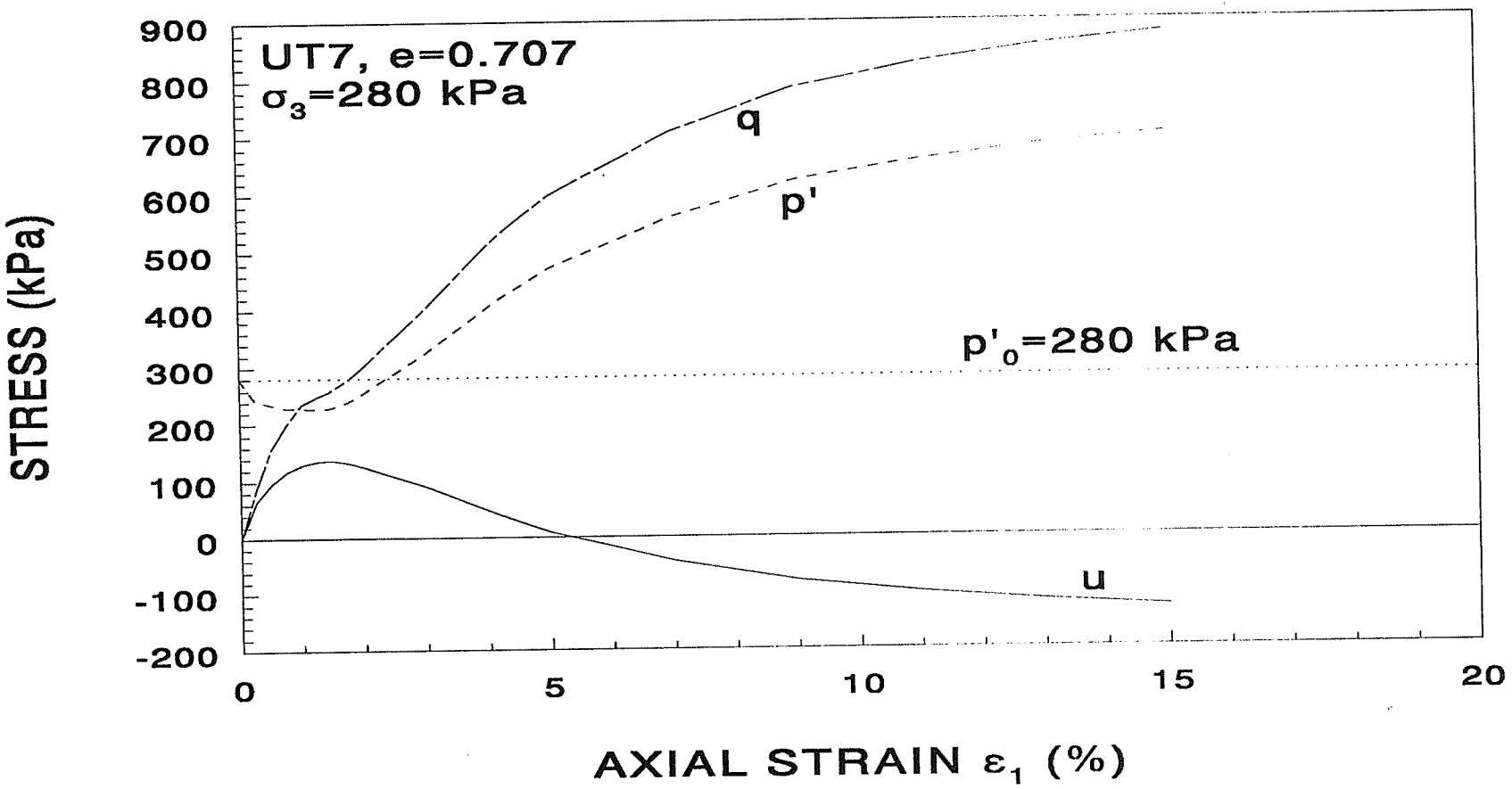

Fig.3.23 Shear stress q, effective mean normal stress p' and excess pore water pressure u for the unfrozen sand, a constant cell pressure, constant strain rate, undrained triaxial test: Test UT7.

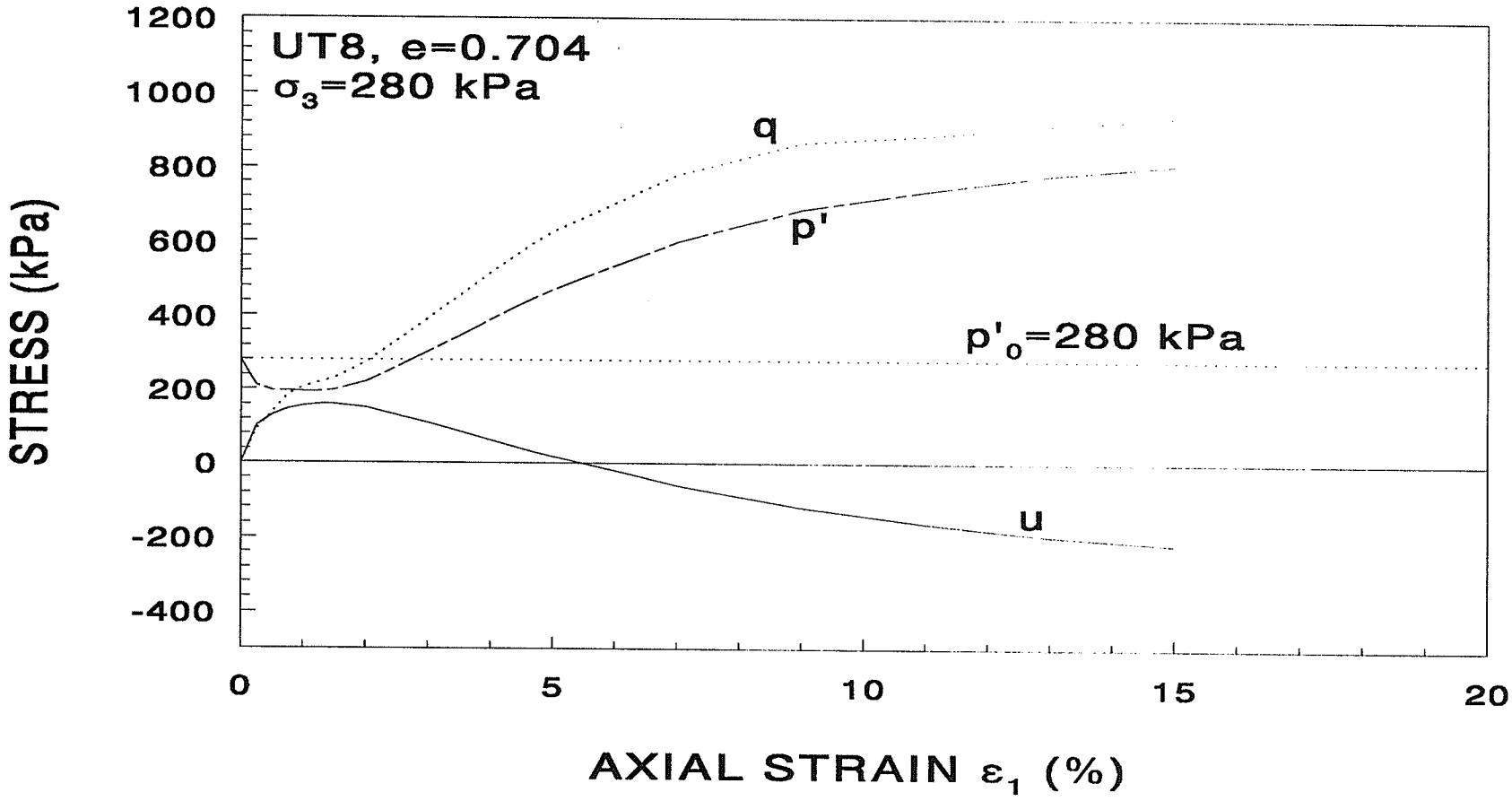

Fig.3.24 Shear stress q, effective mean normal stress p' and excess pore water pressure u for the unfrozen sand, a constant cell pressure, constant strain rate, undrained triaxial test: Test UT8.

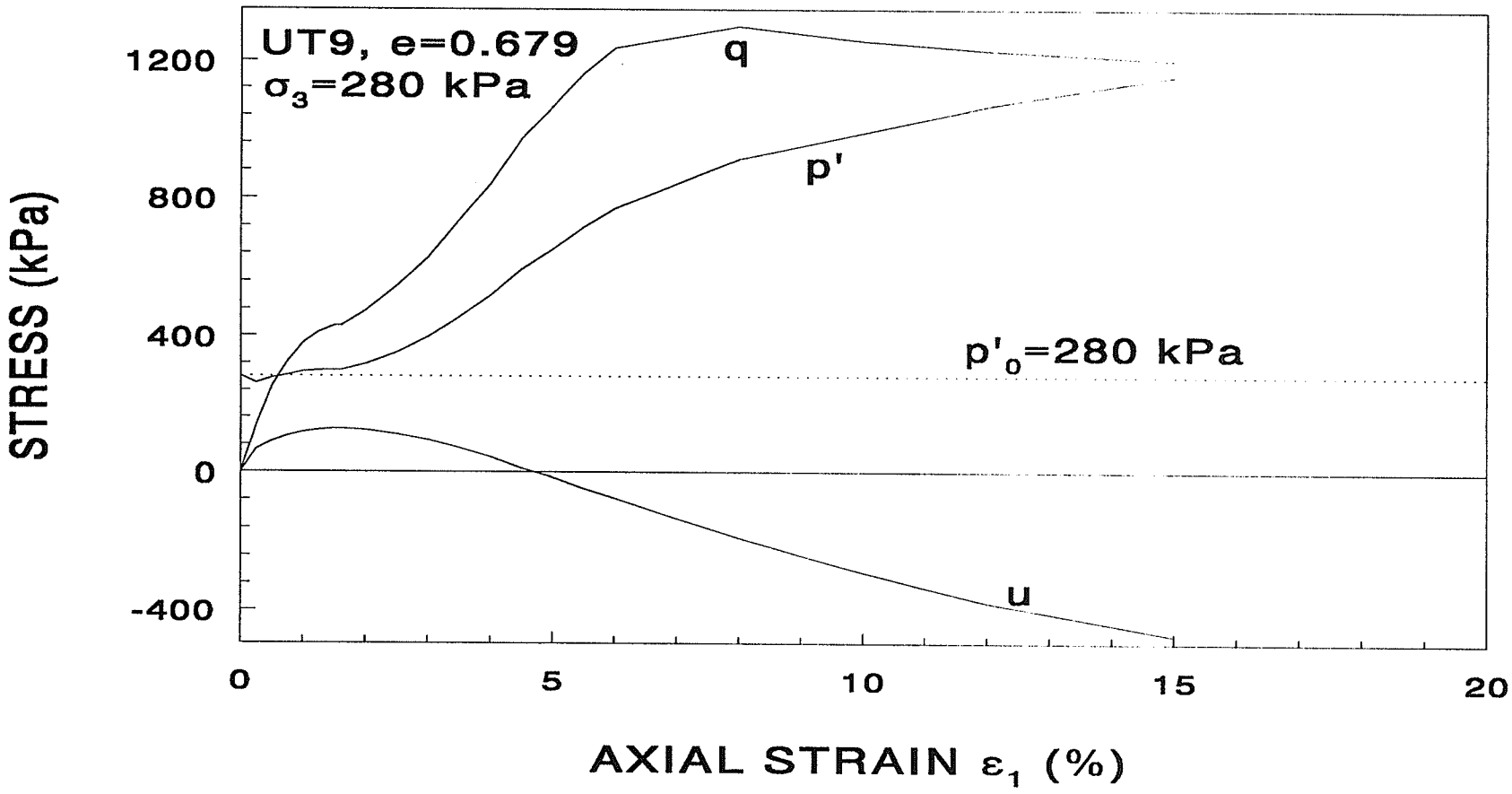

Fig.3.25 Shear stress q, effective mean normal stress p' and excess pore water pressure u for the unfrozen sand, a constant cell pressure, constant strain rate, undrained triaxial test: Test UT9.

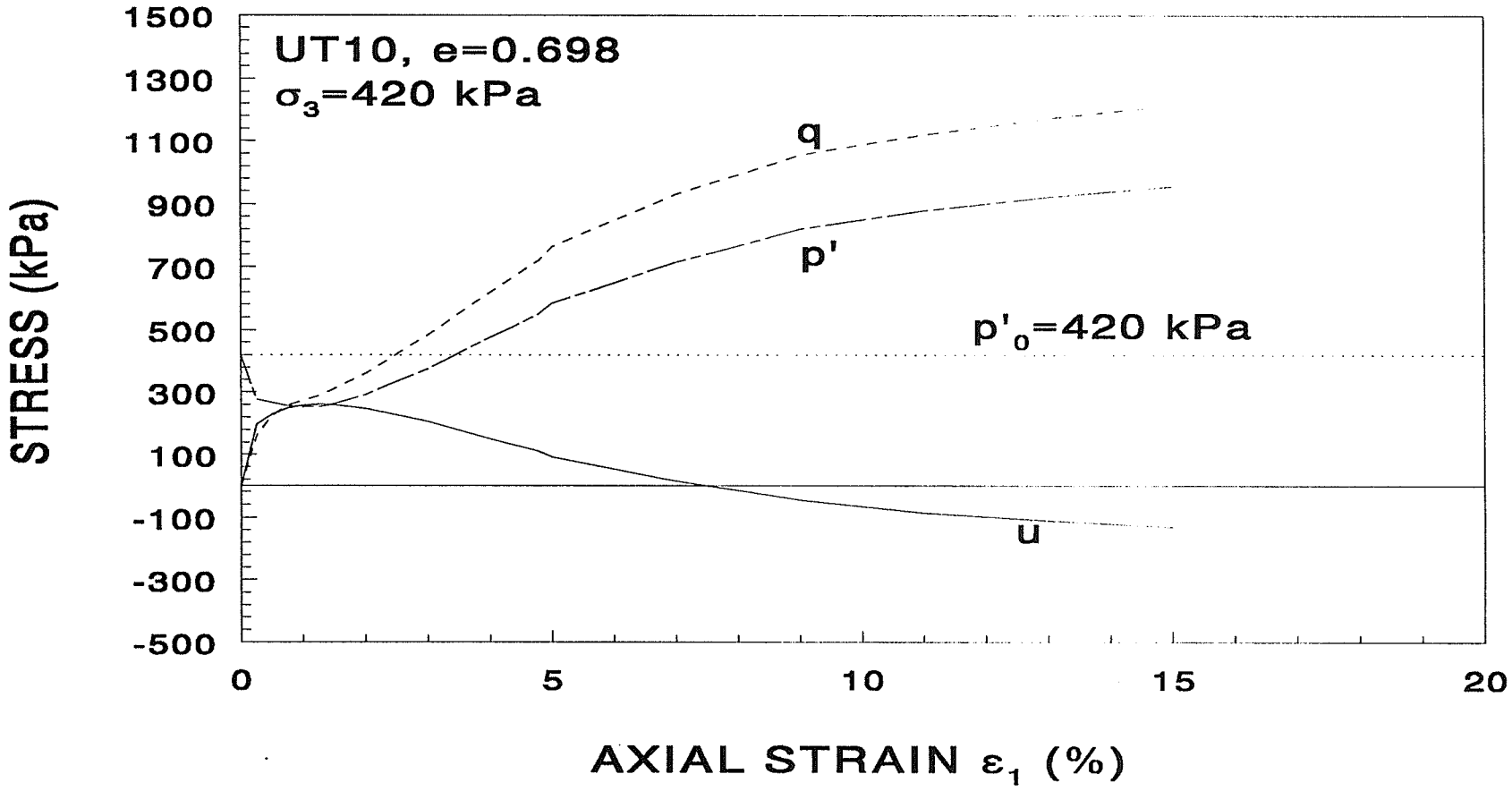

Fig.3.26 Shear stress q, effective mean normal stress p' and excess pore water pressure u for the unfrozen sand, a constant cell pressure, constant strain rate, undrained triaxial test: Test UT10.

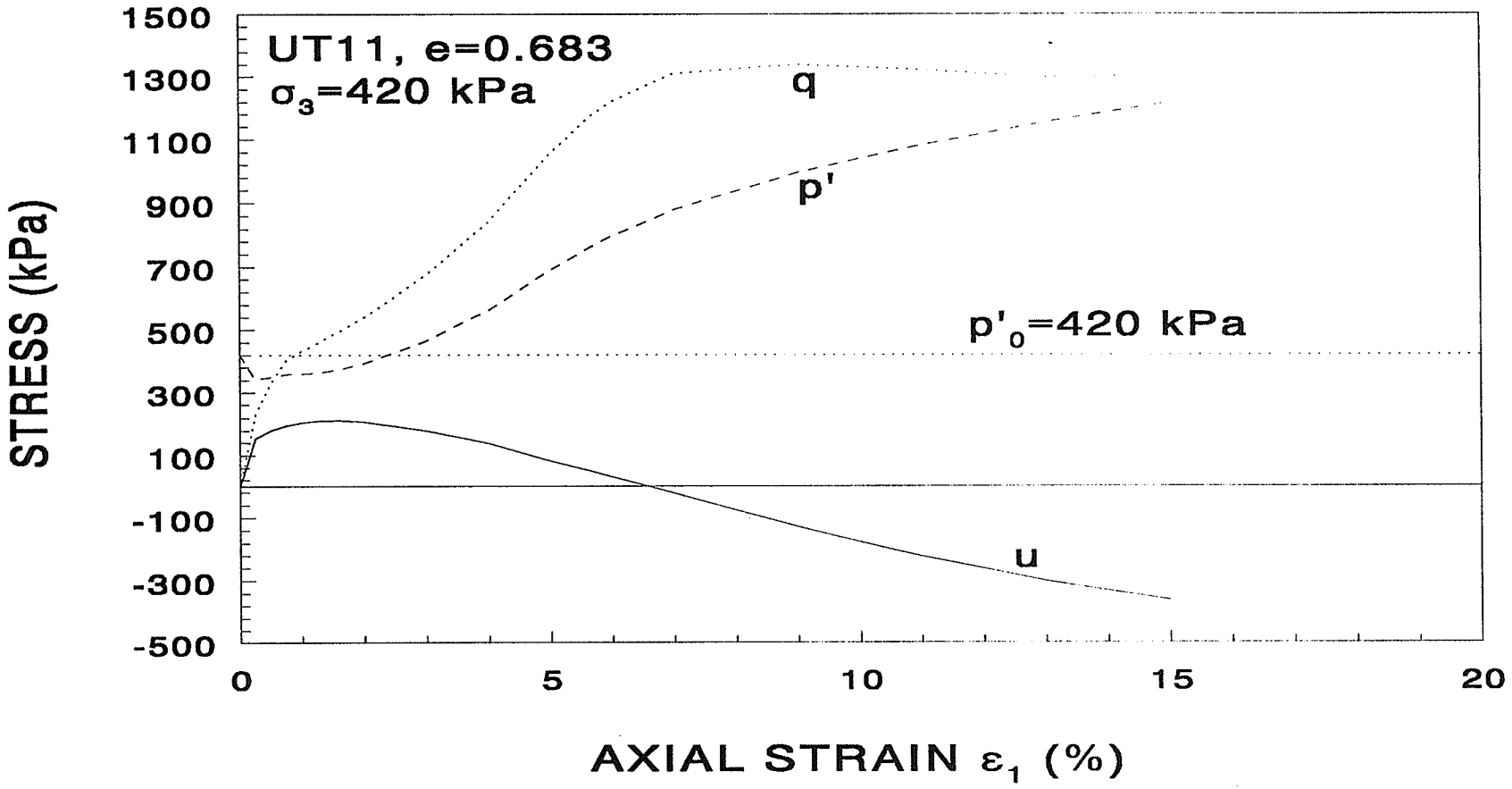

Fig.3.27 Shear stress q, effective mean normal stress p' and excess pore water pressure u for the unfrozen sand, a constant cell pressure, constant strain rate, undrained triaxial test: Test UT11.

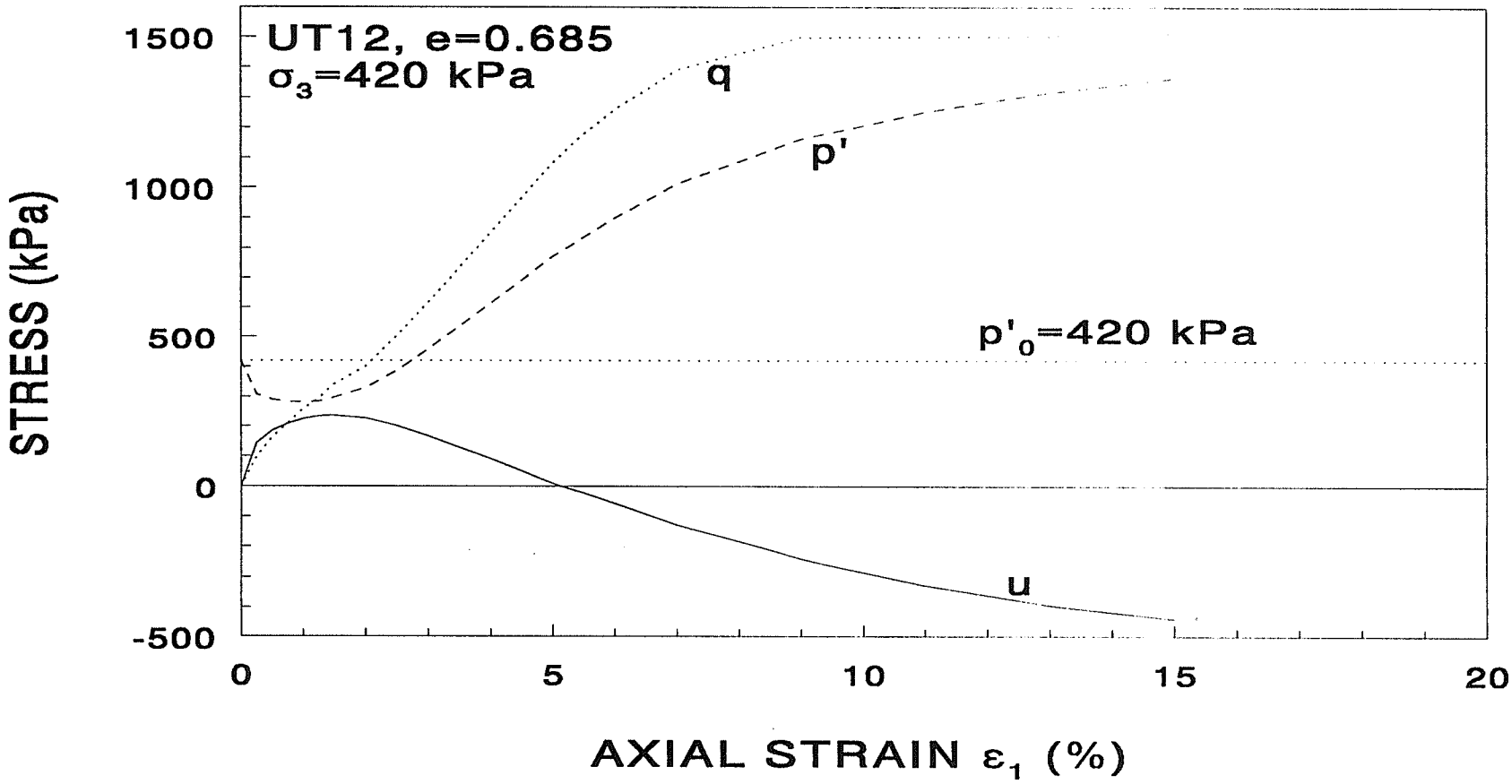

Fig.3.28 Shear stress q, effective mean normal stress p' and excess pore water pressure u for the unfrozen sand, a constant cell pressure, constant strain rate, undrained triaxial test: Test UT12.

CHAPTER 4

MODELLING VOLUMETRIC STRAIN OF FROZEN SOIL UNDER HYDROSTATIC PRESSURE

4.1 MECHANISM OF VOLUMETRIC CREEP OF FROZEN SOIL UNDER HYDROSTATIC PRESSURE

Volumetric deformation under hydrostatic pressure comes mainly from the following three sources.

1. The instantaneous compression of: soil particles, unfrozen water, and the pore ice.

2. Movement of soil particles and pore ice into air voids.

3. Flow of pore ice under pore ice stress gradients from highly stressed zones to zones of lesser stress.

The latter two sources give rise to volumetric creep strains associated with hydrostatic pressures. Unfortunately it is impossible to separate and quantify the individual contributions of these two sources. From an engineering point of view, ice may be likened to a non-Newtonian fluid having a very high viscosity. Under high shear stresses, flow occurs by virtue of microscopic sliding along the boundaries of ice crystals. Although the overall state of stress

may be hydrostatic, high shear stresses are induced in the ice particularly at the points of contact between ice and the soil particles. In non-saturated soils, ice may flow into void spaces, which are small zones of zero ice stress, giving rise to large stress gradients in their vicinities. Expulsion of pore ice may occur at drainage boundaries where the stress gradients would also be very high. The rate of flow depends on the magnitude of stress gradient in the pore ice, the void characteristics of the soil skeleton, and the viscosity of the ice. The viscosity increases with a decrease in temperature which explains why creep rates decrease as soil temperatures are lowered. Since the viscosity of ice is several orders higher than that of water, flow of ice is several orders slower than that of water with all other factors being equal.

It is hypothesized that when frozen sand is stressed, the total stress is carried by the ice matrix and the soil skeleton. Flow of the pore ice results in a volume reduction and a transfer of stress from the pore ice to the soil skeleton. The process continues until the stress in the ice is reduced to a magnitude, ie. a threshold, that will not cause any further flow. This threshold increases with a decrease in soil temperature. Thus the flow of ice in soil differs from that of water in that the flow rate of ice is several orders slower due to its higher viscosity and in that ice is able to sustain a finite value of shear stress with no accompanying shear strain. It should be noted that the microscopic stress field in a frozen soil is very complicated. The actual interparticle stresses and the stresses in the ice matrix vary considerably from point to point. The statistical mean value of these stresses is used in constitutive modelling for engineering purposes.

4.2 MODELLING THE VOLUMETRIC STRAIN

The development of the model is based on data from triaxial isotropic compression tests. However the equations and concepts developed may be modified for the case of anisotropic compression. When a frozen sand sample is subjected to a hydrostatic pressure p, the volumetric strain ϵ_v may be divided into instantaneous strain ϵ_{vi}, and creep strain, ϵ_{vc}.

$$\epsilon_v = \epsilon_{vi} + \epsilon_{vc} \tag{4.1}$$

The instantaneous strain, ϵ_{vi}, may be related to the pressure, p, by the instantaneous bulk modulus, K_i.

$$\epsilon_{vi} = \frac{p}{K_i} \tag{4.2}$$

Fig.4.1 shows schematically a representative family of creep curves generated by isotropic compression creep tests. At any given time, the volumetric creep strain of a given frozen soil increases with increasing stress, and at any given stress, the rate of volumetric creep decreases with increasing time. Finally the creep rate approaches zero and the volumetric creep strain reaches an ultimate value, ϵ_{vcu}. The ultimate value, ϵ_{vcu}, depends only on the magnitude of isotropic stress for a given frozen soil at a given temperature. It may be empirically related to stress by a power law as:

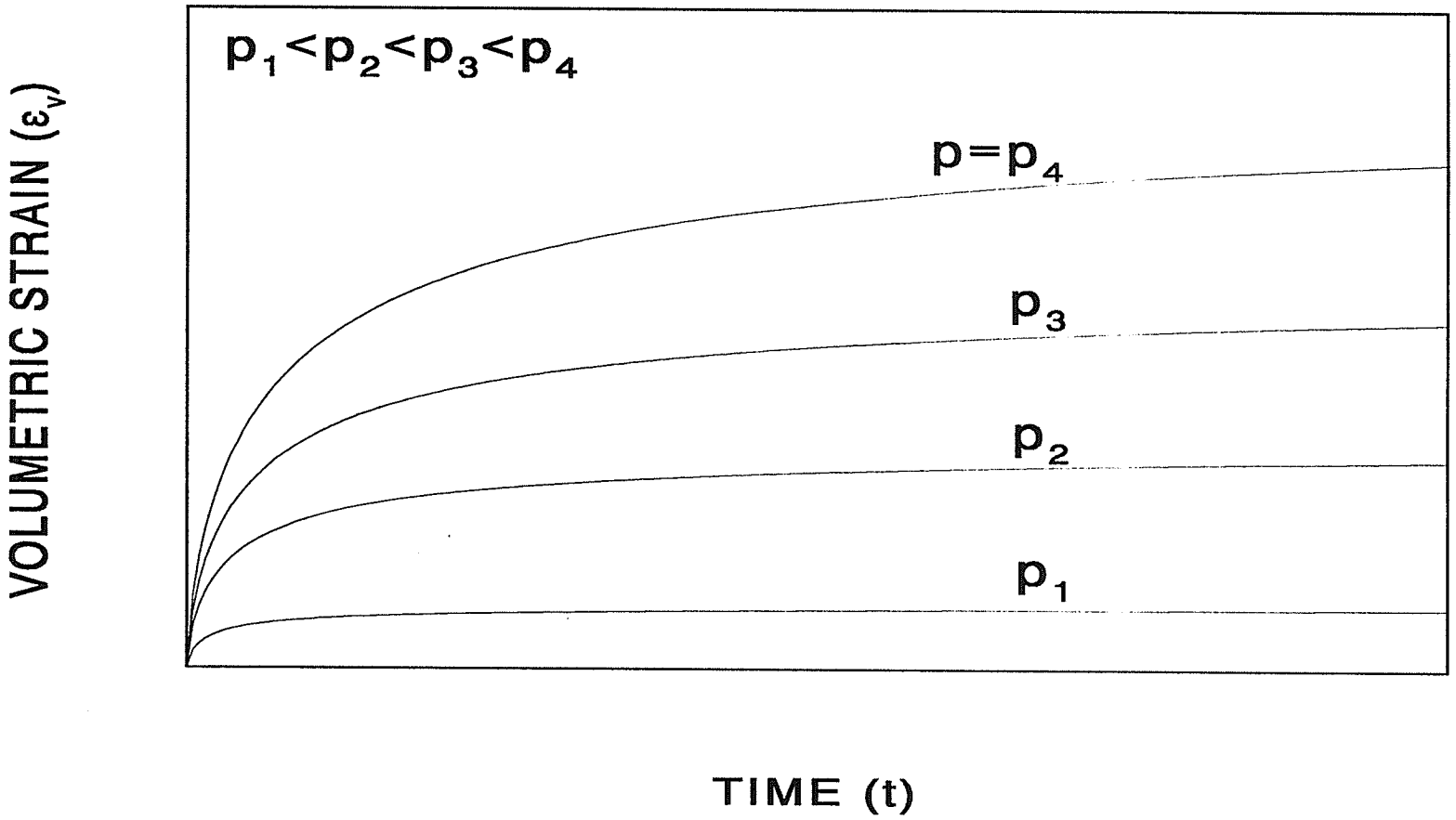

Fig.4.1 A schematic of a family of creep curves from isotropic compression creep tests for a given frozen soil under different hydrostatic pressures p.

$$\epsilon_{vcu} = \epsilon_{vc0}\left(\frac{p}{p_0}\right)^m \tag{4.3}$$

where p_0 is a small reference stress and ϵ_{vc0} is the corresponding volumetric strain. The parameter, m, characterizes the rate of change in the ultimate volumetric strain, ϵ_{vcu}, with pressure. The volumetric creep strain, ϵ_{vc}, at any time, t, may be expressed by a hyperbola as:

$$\epsilon_{vc} = \epsilon_{vcu}\frac{\bar{t}^{\alpha}}{1+\bar{t}^{\alpha}} \tag{4.4}$$

where $\bar{t} = t/t^*$ is a normalized time, t^* is a reference time defined as the time taken to reach one-half of the ultimate creep strain, and t is the real time. The exponent, α, is a constant which reflects the shape of the creep curve.

Based on the concept that the volumetric strain is made up of an instantaneous and a creep component, the relationship between total volumetric strain, ϵ_v, and the hydrostatic stress, p, is shown schematically in Fig.4.2. Line [1] represents the instantaneous state and Line [2] represents the ultimate state for the frozen soil. Line [3] represents the ϵ_v - p' relationship for the same soil in an unfrozen state. The "ultimate state" refers to a state in which the consolidation or volumetric creep process is complete. The difference between Lines [2] and [3] stems from the fact that in the case of the frozen soil, some of the stress is still being carried by the ice at the end of consolidation and hence its volumetric strain is less than that of the unfrozen soil. Lines [1] and [2] provide the initial and the ultimate ϵ_v - p

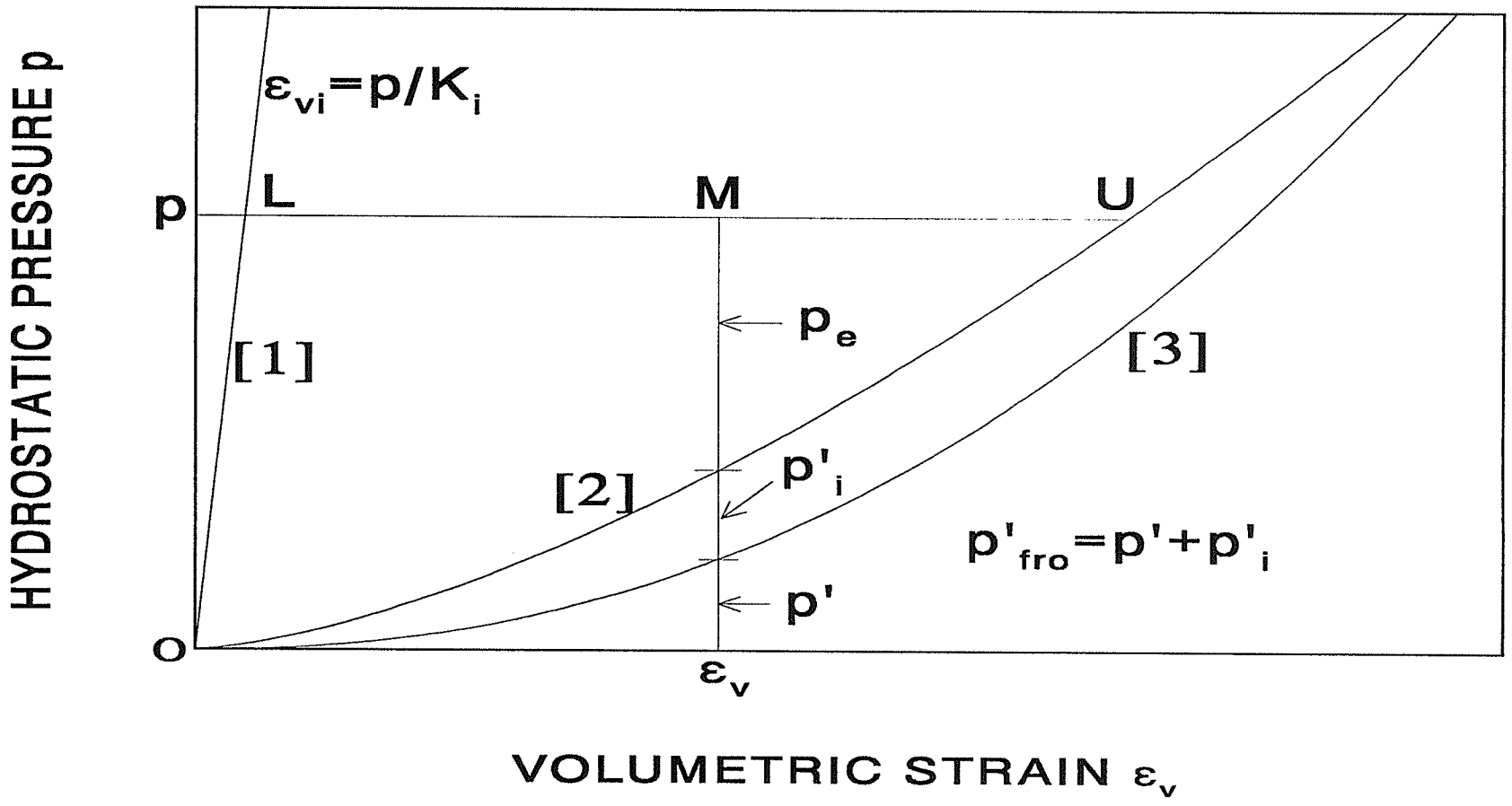

Fig.4.2 A schematic of the instantaneous and ultimate state relationships between hydrostatic pressure and volumetric strain of frozen soil.

relationships, and the space between these two lines is the margin for creep. Thus if a hydrostatic pressure of magnitude p is applied, the stress-strain path is O-L-M-U as shown on the figure. The total stress at any time may be considered to be made up of three components.

1. The stress sustained by the soil skeleton, p', which is represented by Line [2].

2. The stress ultimately sustained by the ice, p'_i, which is the difference between the ultimate stresses of the soil in the frozen and unfrozen states.

3. The excess ice pressure, p_e, which is equal to the difference between the total stress and the sum of the two previous components, ie:

$$p_e = p - (p' + p'_i) \tag{4.5}$$

The stress sustained by the soil skeleton and the ultimate stress in the ice may be combined into a single component $p'_{fro}=p'+p'_i$. This component represents the source of the effective shearing resistance of frozen soils at any given time. The stress, p'_{fro}, **is called the generalized effective mean normal stress** of frozen soil, which is defined as the mean normal stress sustained by the frozen soil at the end of the consolidation process. During the process, it is assumed to be given by Line[2]. The stress p'_{fro} is referred to as simply effective stress hereafter and the component p'_i **is called the effective ice pressure**. The component p_e **is called the excess ice pressure** which is the true driving force of the volumetric creep.

Consolidation continues until p_e goes to zero. It should be noted that if a significant amount of unfrozen water is present in a frozen soil, the corresponding excess pore ice pressure, p_e, should include contributions from both the unfrozen water and the pore ice.

Using the above concept of stresses, a strain-hardening model for volumetric creep of frozen soil was developed. The rate of creep may be directly related to the stress-strain state instead of to time. Firstly, a general expression for volumetric strain ϵ_v may be obtained by combining (4.1), (4.2), (4.3), and (4.4) to give:

$$\epsilon_v = \frac{p}{K_i} + \epsilon_{vc0}\left(\frac{p}{p_0}\right)^m \frac{\bar{t}^{\alpha}}{1+\bar{t}^{\alpha}} \tag{4.6}$$

By differentiating (4.6) , the rate of the volumetric creep may be expressed as

$$\dot{\epsilon}_v = \frac{1}{K_i}\frac{dp}{dt} + \epsilon_{vc0}\frac{d}{dt}\left(\left(\frac{p}{p_0}\right)^m \frac{\bar{t}^{\alpha}}{1+\bar{t}^{\alpha}}\right) \tag{4.7}$$

Considering only step-wise changes in stress, p, then $dp/dt=0$ when p is constant, and for incremental changes in p at any time $t=t_j$, $dp/dt=\delta(t_j)$, where $\delta(t_j)$ is a pulse function. It may be shown that for an incremental stress change, Δp, there will be a corresponding instantaneous volumetric strain $\Delta\epsilon_v=\Delta p/K_i$ and a new creep rate given by:

$$\dot{\epsilon}_v = \dot{\epsilon}_{vc} = \epsilon_{vc0}\left(\frac{p}{p_0}\right)^m \frac{\alpha \bar{t}^{\alpha-1}}{(1+\bar{t}^{\alpha})^2}\frac{1}{t^*} \tag{4.8}$$

where p is the new total stress. From Fig.4.3, the volumetric strain ϵ_v may also be expressed

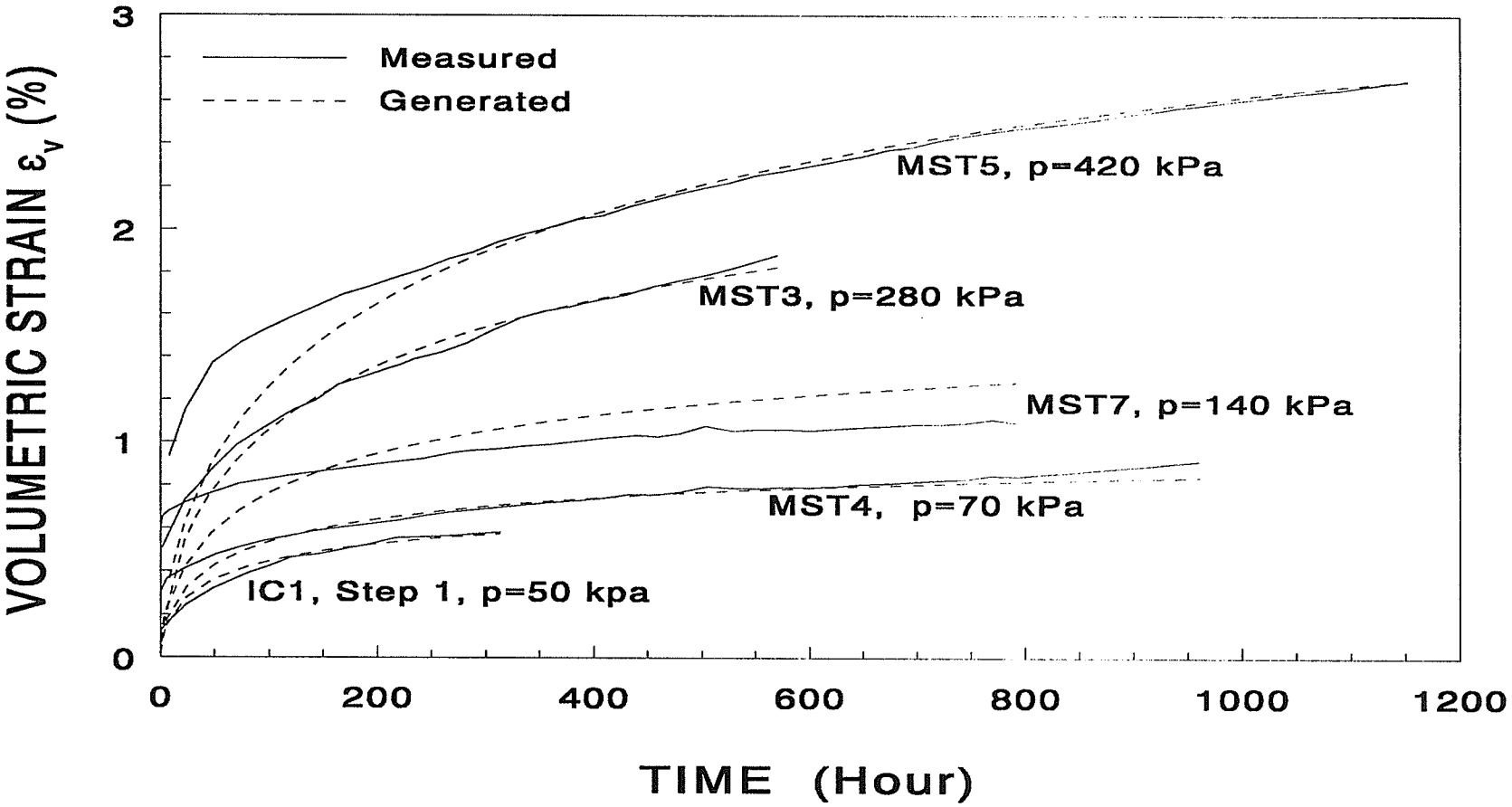

Fig.4.3 Measured and reproduced volumetric creep curves of the frozen sand in single-stage, constant *p*, triaxial compression creep tests.

in terms of effective stress p'_{fro}, in accordance with (4.9):

$$\epsilon_v = \frac{p'_{fro}}{K_i} + \epsilon_{vc0}\left(\frac{p'_{fro}}{p_0}\right)^m \tag{4.9}$$

Combining (4.6) and (4.9) produces:

$$\frac{\bar{t}^{\alpha}}{1+\bar{t}^{\alpha}} = \left(\frac{p'_{fro}}{p}\right)^m \left(\frac{\epsilon_v - \frac{p}{K_i}}{\epsilon_v - \frac{p'_{fro}}{K_i}}\right) = U_c \tag{4.10}$$

The term $\bar{t}^{\alpha}/(1+\bar{t}^{\alpha})$ may be represented by U_c which is called the generalized degree of consolidation. Substituting $p_e = p - p'_{fro}$ into (9) and rewriting it, U_c may be expressed as a function of the excess ice pressure p_e as:

$$U_c = \left(1 - \frac{p_e}{p}\right)^m \left(\frac{p - K_i\epsilon_v}{p - p_e - K_i\epsilon_v}\right) \tag{4.11}$$

From (4.10) we have $\bar{t}^{\alpha} = U_c/(1-U_c)$ which substituted into (4.8) gives:

$$\dot{\epsilon}_v = \frac{\alpha\,\epsilon_{vc0}}{t^*}\left(\frac{p}{p_0}\right)^m U_c^{\,1-\frac{1}{\alpha}}(1-U_c)^{1+\frac{1}{\alpha}} \tag{4.12}$$

which is an equation for creep rate in terms of excess ice pressure rather than time. The generalized degree of consolidation, U_c, may be expressed as a function of time, but it can also be made to depend only on the stress-strain state as long as the excess ice stress is taken into consideration. The parameter t^*, previously defined as the time corresponding to one-half of the ultimate creep strain, is a characteristic of the creep curve and can only be determined experimentally. By analyzing the isotropic compression creep data given by Rahman (1988), t^* may be empirically related to stress by a power function as indicated in (4.13).

$$t^* = t_0^* \left(\frac{p}{p_0} \right)^{\theta} \tag{4.13}$$

where θ is a constant to be determined experimentally, p_0 is a reference stress and t_0^* is the value of t^* when $p = p_0$. Substituting (4.13) into (4.12) and rearranging terms provides:

$$\dot{\epsilon}_v = \dot{\epsilon}_{v0} (p/p_0)^{m-\theta} U_c^{\,1-\frac{1}{\alpha}} (1-U_c)^{1+\frac{1}{\alpha}} \tag{4.14}$$

which relates the creep rate to the stress-strain state rather than to time. In (4.14) $\dot{\epsilon}_{v0} = \alpha \epsilon_{vc0} / t_0^*$ is a characteristic strain rate of the frozen soil which depends on the soil, the temperature and the drainage conditions. This equation makes it more convenient for incorporating stress changes during the creep process as compared to a model in which time is a variable. When stress p has an increment Δp at any time, there will be an instantaneous increase of volumetric strain $\Delta \epsilon_v = \Delta \epsilon_{vi} = \Delta p / K_i$ and a new creep rate which may be obtained by substituting the new stress into (4.14). The volumetric strain ϵ_v may be obtained by

integrating the creep rate over time. For continuously changing stress, a step-wise approximation may be used.

4.3 CALIBRATION OF THE CONSOLIDATION MODEL

The data from isotropic compression creep tests conducted by Rahman (1988) on a frozen sand were used to calibrate the mathematical model presented. The data used were taken from the first step of Test IC1 and the isotropic compression part of Tests MST3, MST4, MST5 and MST6 with hydrostatic pressures ranging from 50 to 420 kPa, and the void ratios of the sand specimens in the order of 0.72. The temperature of the frozen soil was -3°C. For details of the test procedure and equipment, reference should be made to Rahman (1988). The isotropic creep curves from the tests stated above are shown in Fig.4.3. It is worth mentioning that the initial density plays an important role in the consolidation process of frozen soil. The samples used in the tests mentioned above did not have an identical initial density, and therefore there was some scatter of the data.

The instantaneous bulk modulus K_i was chosen as 9.0×10^6 kPa which is the value of the bulk modulus of "solid" ice according to Meller (1979). To calibrate the model, the first step was to curve-fit the creep curves shown in Fig.4.3, using (4.6). This provided a set of α, ϵ_{vcu} and t^* values for each mean normal stress p. Since there was only a limited amount of data available, parameter α was assumed to be independent of stress, and its values from the different sets were averaged. The curve-fitting was then repeated using this average value of α, and a new set of ϵ_{vcu} and t^* values were obtained. These parameters were related to the

hydrostatic stress as shown in Fig.4.4 and Fig.4.5. Taking p_0=1.0 kPa as the reference stress, the corresponding expression for the ultimate volumetric strain ϵ_{vcu} was:

$$\epsilon_{vcu}=0.04\times p^{0.77} \tag{4.15}$$

and the time taken to reach one-half of the ultimate volumetric strain, t^* was:

$$t^*=2.83\times p^{0.82} \tag{4.16}$$

where strain is in percent, time in hours and stress in kPa. The parameters K_i, α, m, and θ are the four parameters required for the model. They were determined as described above as K_i=9.0×10^6 kPa, α=0.6, m=0.77 as shown in Fig.4.4 and θ=0.82 as shown in Fig.4.5. In Fig.4.3 the creep curves generated by introducing these parameters into (4.6) are included with the experimental curves and it is seen that there is a reasonable agreement between the two.

To test the model, the four parameters were introduced into (4.14) to obtain a general expression for the rate of volumetric creep. This equation was then used to generate creep curves for the multi-stage creep test IC1. Five stress levels of 50, 100, 150, 200, and 300 kPa were used in the test. The total duration of the test was 4466 hours (186 days), and a total volumetric strain of 2.8% occurred. The predicted volumetric strains were obtained by integrating the expression for creep rate, step by step, and adding the instantaneous strains. The experimental and predicted creep curves are shown in Fig.4.6. Generally the agreement between the predicted and the experimental creep curves was very good considering the scatter of the test data. The maximum relative variation between predicted and experimental data was 6%.

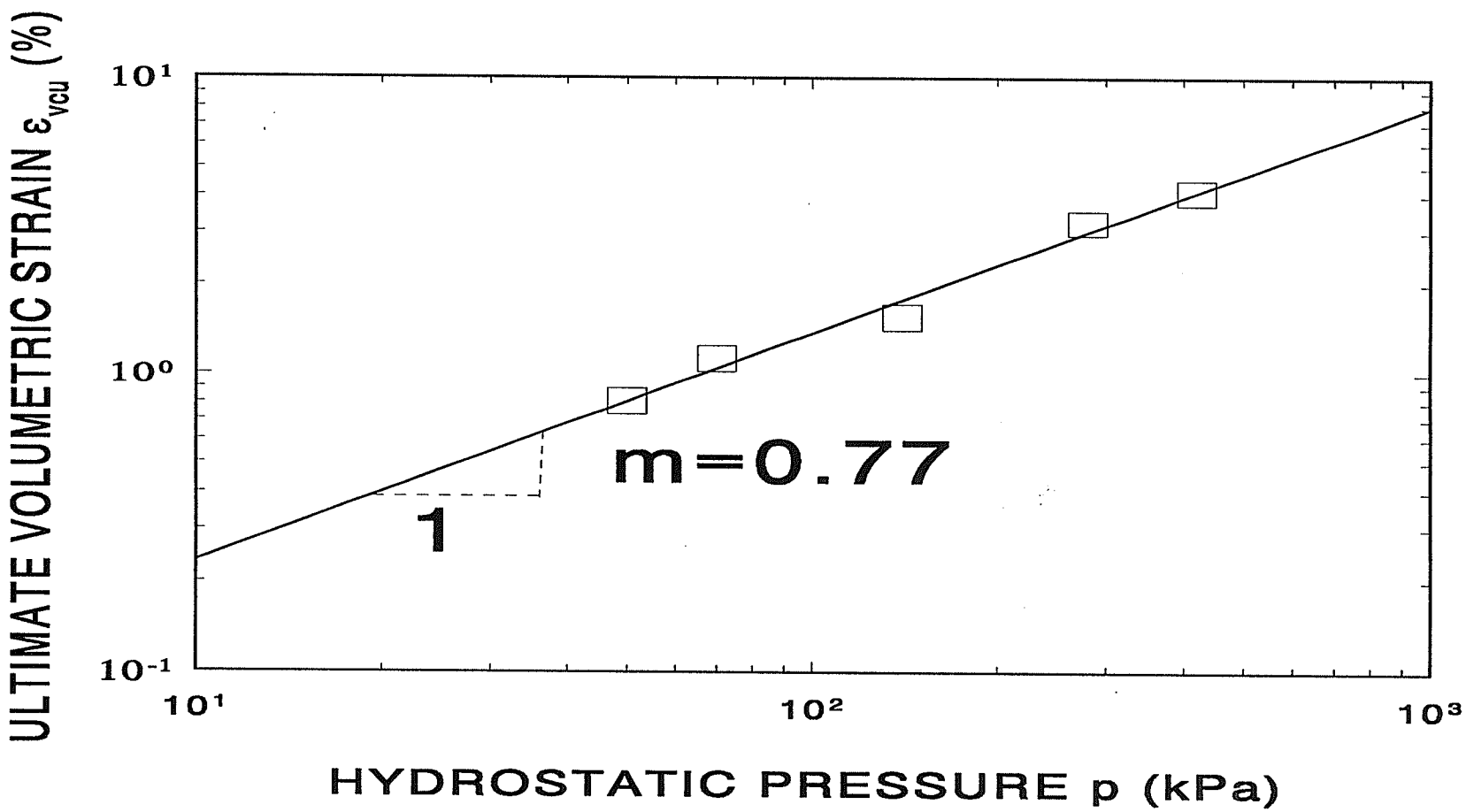

Fig.4.4 The ultimate volumetric creep strain, ϵ_{vcu}, obtained by curve-fitting the creep curves from single-stage, constant p, isotropic compression creep tests of the frozen sand.

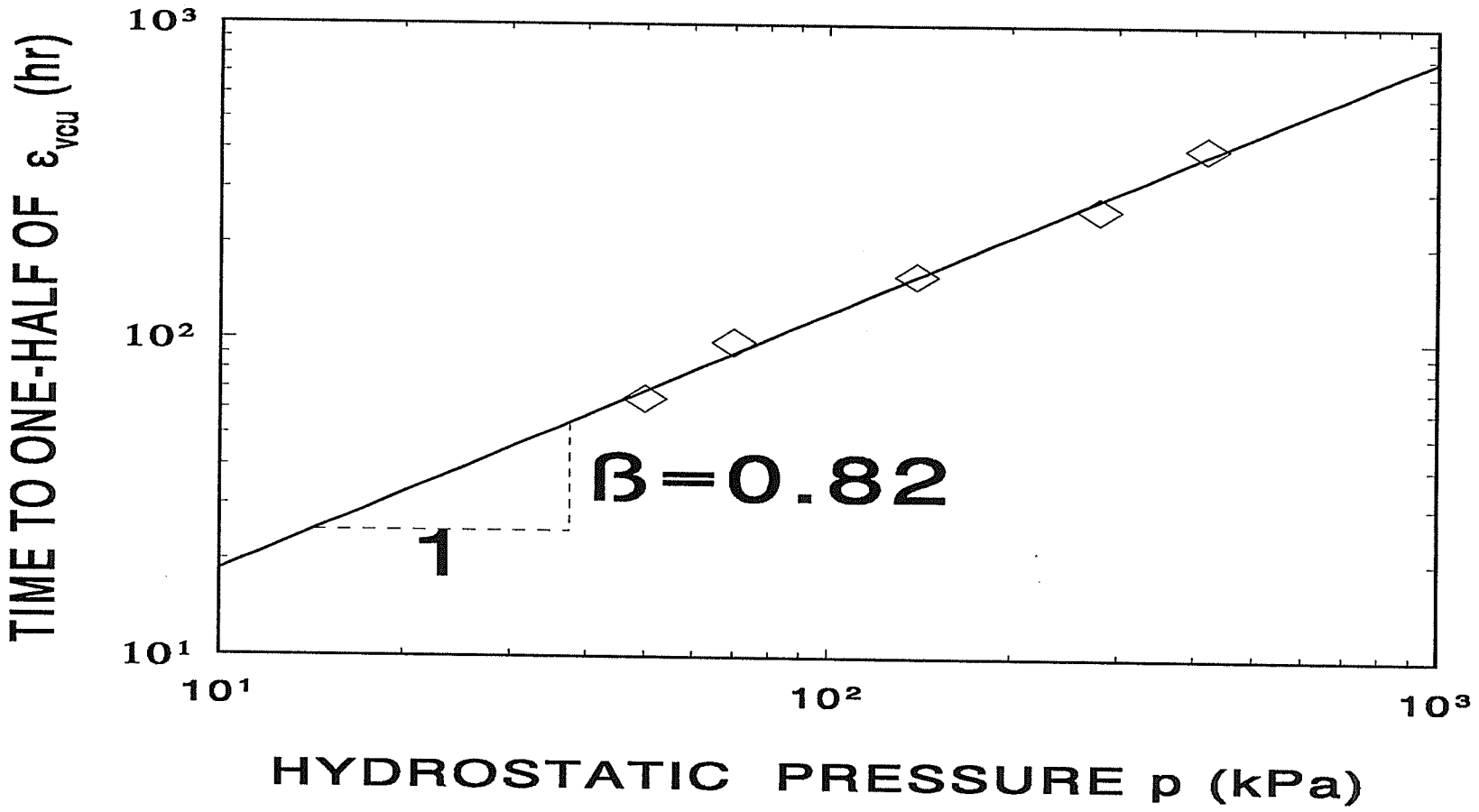

Fig.4.5 The relationship between the time taken to reach one-half of the ultimate volumetric strain and the hydrostatic stress acting on the frozen sand.

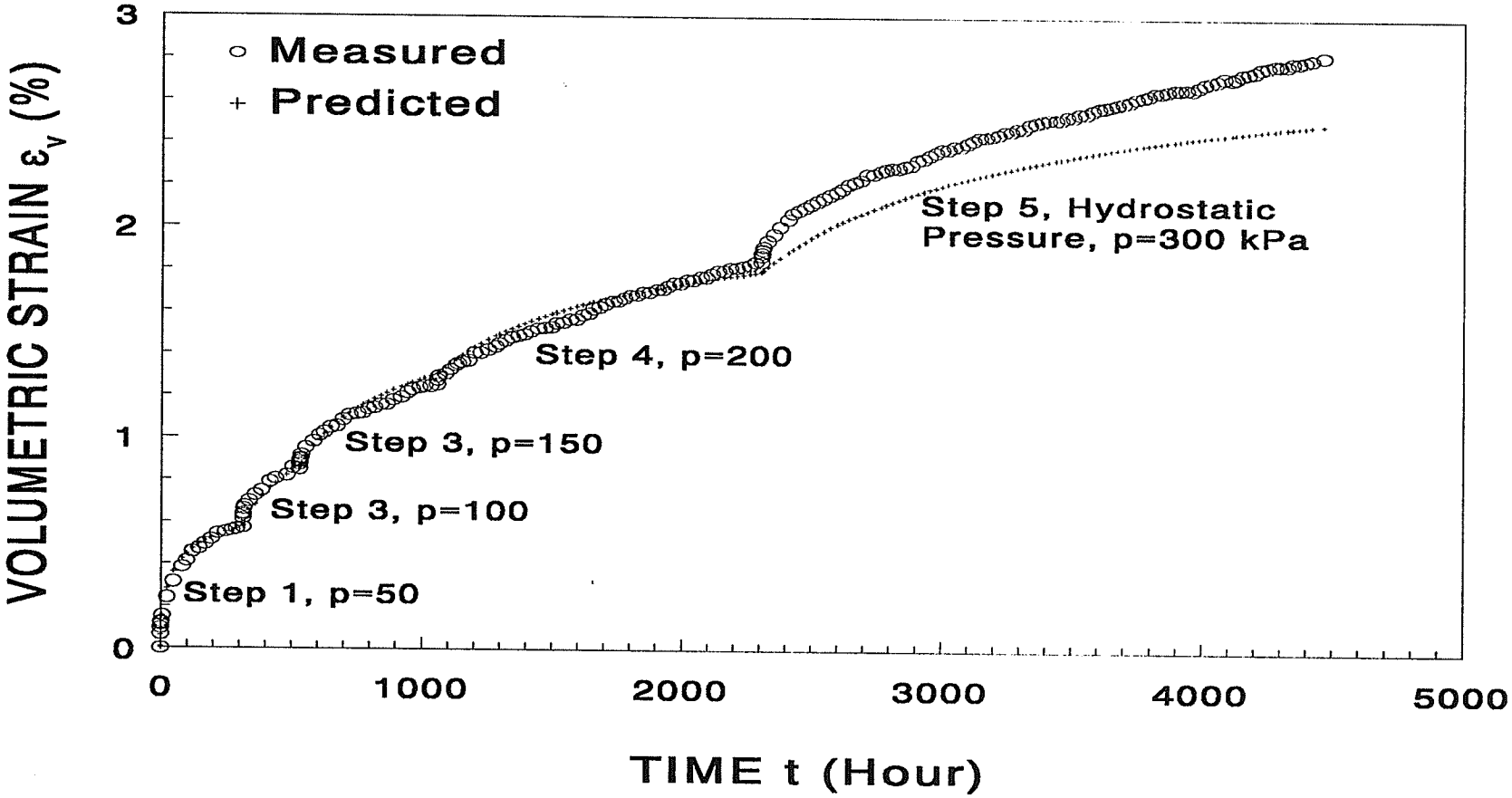

Fig.4.6 The measured and predicted volumetric creep curves of the frozen sand in a multi-stage, constant p, isotropic compression creep test: Test IC1.

4.4 SUMMARY

The behaviour of frozen soil under hydrostatic pressure was discussed in this chapter, and a strain-hardening creep model for consolidation of frozen soil was presented. The model presented here is based on the concept of separating the total mean normal stress into an effective mean normal stress and an excess pore ice pressure with the former depending only on the properties of the material. It is simple in concept and is easy to use with only four parameters required, all of which can be determined by isotropic compression creep tests. The model which was developed from single-stage tests was used to generate creep curves for an independent multi-stage test, and the comparison between the predicted and the experimental curves was fairly good.

A good understanding of the consolidation behaviour is an important step towards the understanding of the creep behaviour of frozen soil under shear since the shearing resistance of frozen soil is closely related to the confining pressure and the volumetric deformation of the soil. The consolidation model is a part of a general strain-hardening, strain-softening creep model which is discussed in the following chapter, and it will also be used to analyze the consolidation process during shear creep.

CHAPTER 5

CREEP BEHAVIOUR OF FROZEN SOIL UNDER SHEAR

5.1 INTRODUCTION

The previous chapter discussed the relationship between the volumetric deformation and the hydrostatic stress of frozen soil. The concept of an effective mean normal stress and excess pore ice pressure was introduced. In this chapter, the behaviour of frozen soil under shear will be discussed and the total shear stress will be separated into an effective and an excess component as well.

Shear stress acting on the pore ice causes a frozen soil to creep. Therefore determining the shear stress that is actually sustained by the ice matrix becomes vitally important to the modelling of the creep behaviour. In order to obtain a clear picture of the stress transformation between the sand skeleton and the ice, it is important to separate and to model the behaviour of the soil in both the unfrozen and the frozen states. Thus the present work includes an extensive study of the behaviour of the unfrozen sand, and an associated constitutive model is established for it.

By analyzing the creep mechanism and the data from tests on both frozen and unfrozen sand, a strain-hardening, strain-softening creep model for frozen soil under shear is developed in this chapter.

5.2 STRESS DISTRIBUTION BETWEEN SOIL SKELETON AND ICE MATRIX

This section discusses the distribution of shear stress between the sand skeleton and the ice matrix, and its effect on the creep process. The discussion is limited to macroscopic stress and strain. The stress and strain quoted here is in compliance with the definition commonly used in soil mechanics.

5.2.1 Effective Shear Stress and Excess Ice Shear Stress

When unfrozen soil is stressed, the total mean normal stress is shared by the soil skeleton and the pore water, while the total shear stress is sustained wholly by the soil skeleton. This statement is the key pillar of the "principle of effective stress" presented by Terzaghi (1923), which is one of the most important discoveries in modern soil mechanics. It is based on the fact that the shearing resistance of water is practically negligible. However, if the pore liquid is not water but a fluid with significant shearing resistance, such as bitumen or ice, this statement is no longer valid. When a frozen sand is stressed, both the mean normal and the shear stresses are shared by the soil skeleton and the ice matrix. It is the stress sustained by the ice that dictates the creep characteristics of the soil, rather than the magnitude of the total stress. The following section discusses the distribution of shear stress between the sand skeleton and the ice matrix. The discussion will be limited to the triaxial stress-strain state as the first step since all the data that will be used to develop the model are from triaxial tests. The stress and strain components involved are mean normal stress, $p=(\sigma_1+2\sigma_3)/3$, volumetric strain, $\epsilon_v=(\epsilon_1+2\epsilon_3)$, deviate stress, $q=(\sigma_1-\sigma_3)$, and deviatoric strain $\epsilon_s=2(\epsilon_1-\epsilon_3)/3$. The components q and ϵ_s are called shear stress and shear strain

respectively hereafter for simplicity.

Fig.5.1 shows a schematic of a typical family of creep curves from triaxial creep tests on a frozen soil with p held constant and q varied. The creep under low q values attenuates while under high q values it goes from primary to secondary and then to tertiary stages. The total shear strain ϵ_s may be divided into an instantaneous component, ϵ_{si}, and a creep component, ϵ_{sc},

$$\epsilon_s = \epsilon_{si} + \epsilon_{sc} \tag{5.1}$$

The instantaneous shear strain, ϵ_{si}, may be related to shear stress, q, by an instantaneous shear modulus, G_i, as

$$\epsilon_{si} = \frac{q}{3G_i} \tag{5.2}$$

where G_i depends on the soil properties and temperature. For attenuating creep, ϵ_{sc} may be expressed by a hyperbola as

$$\epsilon_{sc} = \epsilon_{scu} \frac{\bar{t}^{\xi}}{1+\bar{t}^{\xi}} \tag{5.3}$$

where t is real time, and $\bar{t} = t/t_s$ is a normalized time in which t_s is the time taken to reach one-half of the **ultimate state** creep shear strain, ϵ_{scu}, and ξ is a parameter which depends on

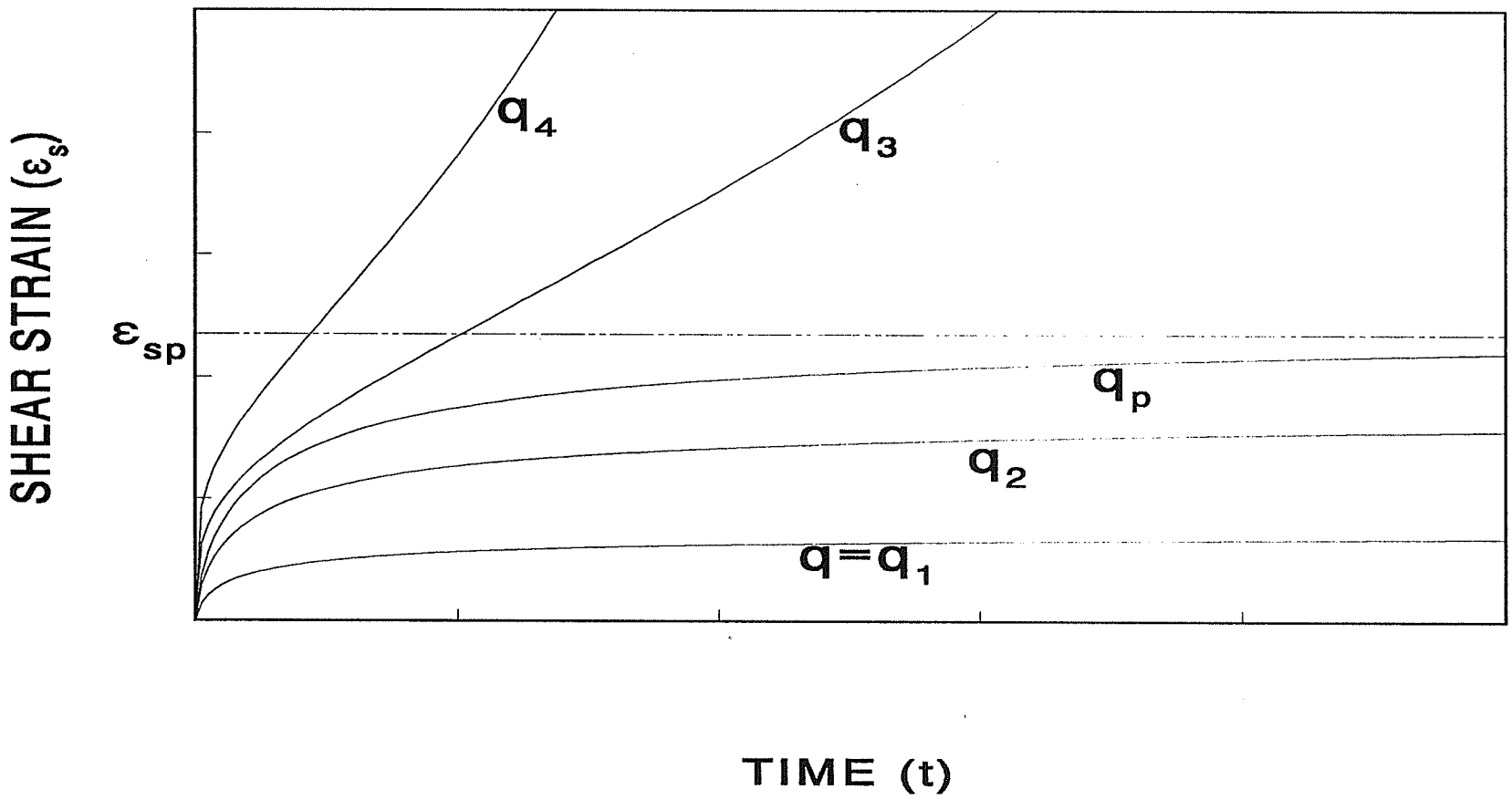

Fig.5.1 A schematic of a family of creep curves for frozen sand under the same mean normal stress but different shear stresses.

the shape of the creep curve. The "**ultimate state**" is referred to as a state in which the rate of creep approaches zero. For each attenuating creep curve, there is a given value of ϵ_{scu} which depends on the shear stress q. Fig.5.2 shows a schematic of the instantaneous and the ultimate state q-ϵ_s relationships. Line [1] represents the instantaneous q - ϵ_s relationship which is given by (5.2), and Line [2] gives the ultimate state q - ϵ_s relationship, of which the first section, OP, corresponds to attenuating creep, and the second section, PS, corresponds to non-attenuating creep. Line [3] is the q - ϵ_s relationship for the same sand in an unfrozen state. The space between Line [1] and Line [2] is the margin for creep. The difference between Lines [2] and [3] represents the ultimate state shear resistance of ice. It is the shear stress that ice can sustain without any further creep, and it depends on the temperature of the soil. As the temperature increases, the shearing resistance of ice decreases, and Line [2] approaches Line [3]. When a consolidated frozen sand is stressed by a constant shear stress q_1 which is smaller than the peak ultimate shear resistance, q'_p, its stress-strain path on the q - ϵ_s space is O-L-U as shown on Fig.5.2. The total stress, q_1, can be separated into three components by Lines [2] and [3]. Component q' represents the shear stress sustained by the soil skeleton, while q'_i gives the difference in shearing resistance between unfrozen and frozen soil at the ultimate state. The combination of q' and q'_i constitutes the ultimate state shear resistance of the frozen soil. We **define q'_{fro}=q'+q'_i as the generalized effective shear stress of frozen soil and simply call it as effective shear stress, hereafter.** The third component, **q_e is called the excess ice shear stress** and is equal to the difference between the total and the effective shear stresses, i.e. $q_e = q - q'_{fro}$. The component q_e is the true driving force of shear creep of frozen soil. As shown in Fig.5.2, q_e is large at the start of the creep process, and therefore the creep rate is also high at that time. The component q_e decreases as the shear

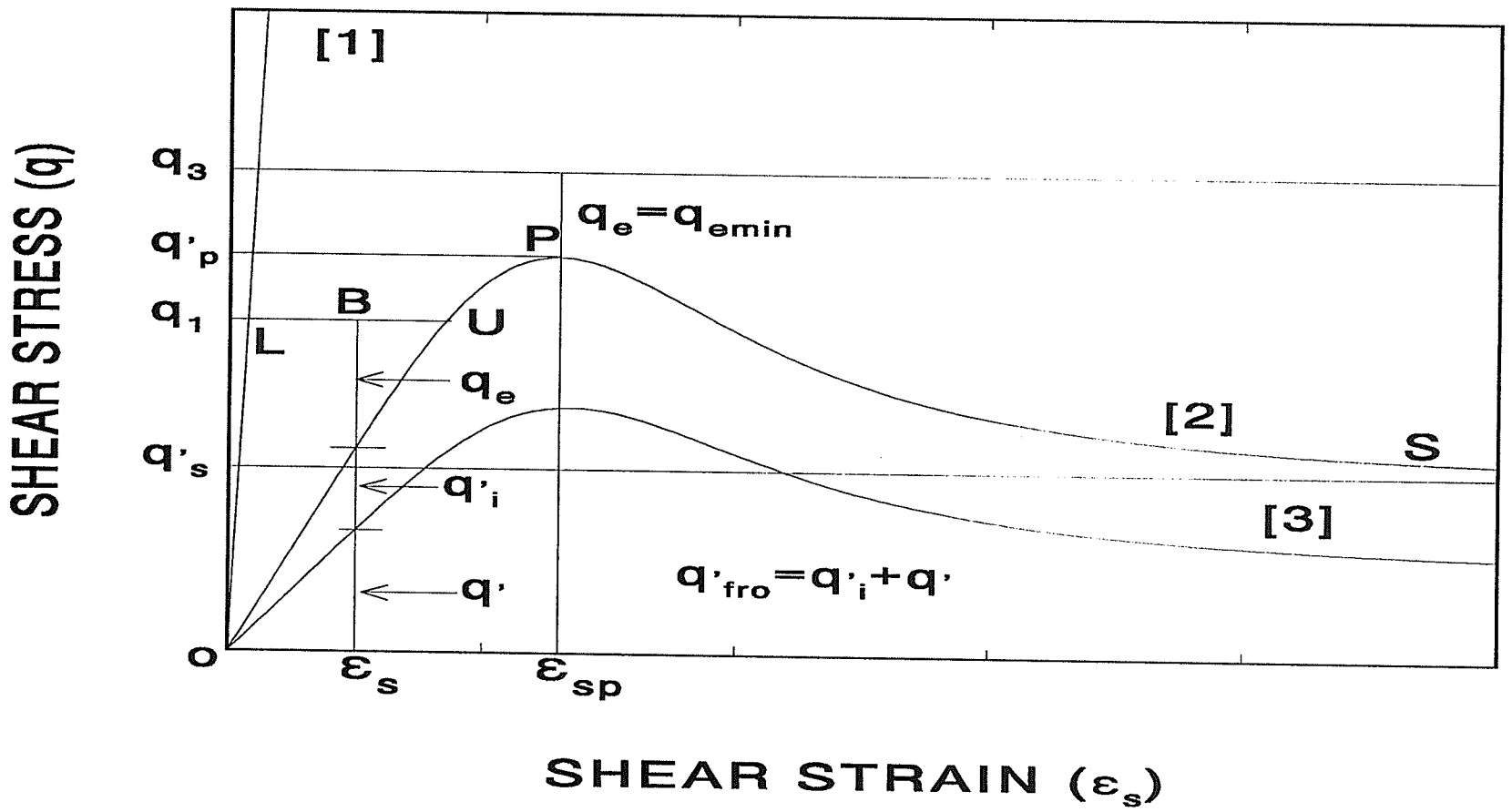

Fig.5.2 A schematic of the instantaneous and the ultimate state relationships between shear stress and shear strain for frozen sand.

resistance of the soil skeleton is gradually mobilized with increasing shear strain, and consequently the creep rate decreases as well. At the end of the shear creep (point U), q_e goes to zero and the rate of creep goes to zero also. For the case of high total shear stresses, such as q_3 which is greater than the peak shear stress, q'_p, q_e decreases with increasing shear strain until $\epsilon_s=\epsilon_{sp}$, at which point the effective shear stress q'_{fro} reaches its maximum value, q'_p, and q_e reaches its minimum value. After the peak, the effective shear stress decreases with increasing shear strain as depicted by Line [2] in Fig.5.2, and the material goes into its strain-softening stage which corresponds to the tertiary creep stage.

The effective shear stress of frozen soil, q'_{fro}, depends on the properties of the soil. Line [2] in Fig.5.2 shows a schematic of q'_{fro} for a medium to dense sand which has a peak shear resistance greater than the large strain shear resistance. As shown in the figure, q'_{fro} is composed of two components which are q', the shearing resistance provided by the soil skeleton, and q'_i , the ultimate sustainable or effective shearing resistance of pore ice. Both of these components depend on the soil composition. For example, for pure ice, q' is zero and q'_{fro} is equal to q'_i. Under a constant total shear stress $q > q'_i$, after a certain amount of creep, the excess ice shear stress, $q_e= q - q'_{fro} = q - q'_i$, which is the true driving force of shear creep, remains constant, and therefore the creep rate also remains constant. This helps to explain why, if the stress level is within a certain range, the creep process of pure ice often includes a relatively long period of secondary creep. On the other hand, if the total shear stress, q, is smaller than the effective ice shear stress, q'_i, there will still be some creep since a certain amount of shear strain is needed to mobilize the effective shear resistance of ice. However, the creep will attenuate when the excess ice shear stress, q_e, approaches zero.

When q is larger than q'_i but is not so large that the integrity of the ice structure is damaged, the creep process of ice will include both a primary creep stage and a long period of secondary creep. This phenomenon can be observed in the movement of some glaciers, which move at an almost constant rate for many years, even decades. If, however, the level of total shear stress is so high that a large amount of micro cracks occur, the mechanism of shear creep is changed, and the macro stress components used here are no longer able to represent the real stress state of the ice. Therefore a modification to the definition of the effective ice shear stress q'_i needs to be made before the model can be applied to this situation. The creep process of pure ice under very high shear stresses often includes primary and tertiary stages only, and the creep process is governed mainly by the formation and development of micro cracks inside the ice (Sinha, 1988a, 1989c; and Zhan, Evgin and Sinha, 1994).

For those frozen soils which are classified as "dirty ice" (ice with very small quantities of solid grain impurities) q'_i may be lower than that of the pure ice because the solid grain impurities weaken the bond between the ice crystals. Therefore the creep rate of "dirty ice" may be higher than that of pure ice under the same stress and at the same temperature (Goughnour and Andersland 1968; Hooke et al., 1972). Other than "dirty ice", the ice - soil mixture is usually "stronger" than pure ice. At a soil grain concentration of about 11% by volume, which corresponds to very ice-rich frozen soil, the solid grains inside the ice matrix start to show their strengthening effect on the creep behaviour of the frozen soil (Baker 1979). From the stress distribution point of view, q', which is the shearing resistance provided by the soil skeleton, is still zero. However, the effective ice shear stress q'_i is usually larger than that of the pure ice because the soil grains change the micro stress-strain field of frozen

soil. Consequently it requires more external energy to develop a weak sliding plane in this frozen soil than in pure ice. Thus the creep rate of ice with soil is lower than that of pure ice under the same stress and temperature even though the soil grain concentration is low and there is no particle to particle contact inside the frozen soil. With increasing soil grain concentration, the ice-soil mixture becomes stronger and the creep rate becomes lower.

The model developed here is based on test data derived from tests on a medium to dense frozen sand. However, it is seen from the above explanation that the concept of an effective shear stress and an effective ice shear stress may also be applied to any ice-rich frozen soil or pure ice within the framework of the model. However, the relationship between the effective shear stress q'_{fro} and the shear strain ϵ_s needs to be determined experimentally for each individual material.

5.2.2 Effective Shear Resistance Surface in q'_{fro}-p'_{fro}-ϵ_s Space

The previous section introduced the concept of an effective shear stress and an excess ice shear stress of frozen soil. It is known that the shearing resistance of unfrozen soil depends on the soil properties and the effective normal stress acting on the soil. The effective shear stress of frozen soil, q'_{fro}, includes the contribution from both the ice matrix and the soil skeleton. It therefore also depends on the effective normal stress. The effective mean normal stress of frozen soil, p'_{fro}, was discussed in detail in Chapter 4. We will hereby relate effective shear stress q'_{fro} to the effective mean normal stress p'_{fro}. Fig.5.3 shows a schematic of q'_{fro}-p'_{fro} - ϵ_s relationship which may be obtained experimentally. This surface is defined as the **Ultimate State Shear Resistance Surface of Frozen Soil, or will be referred to as simply**

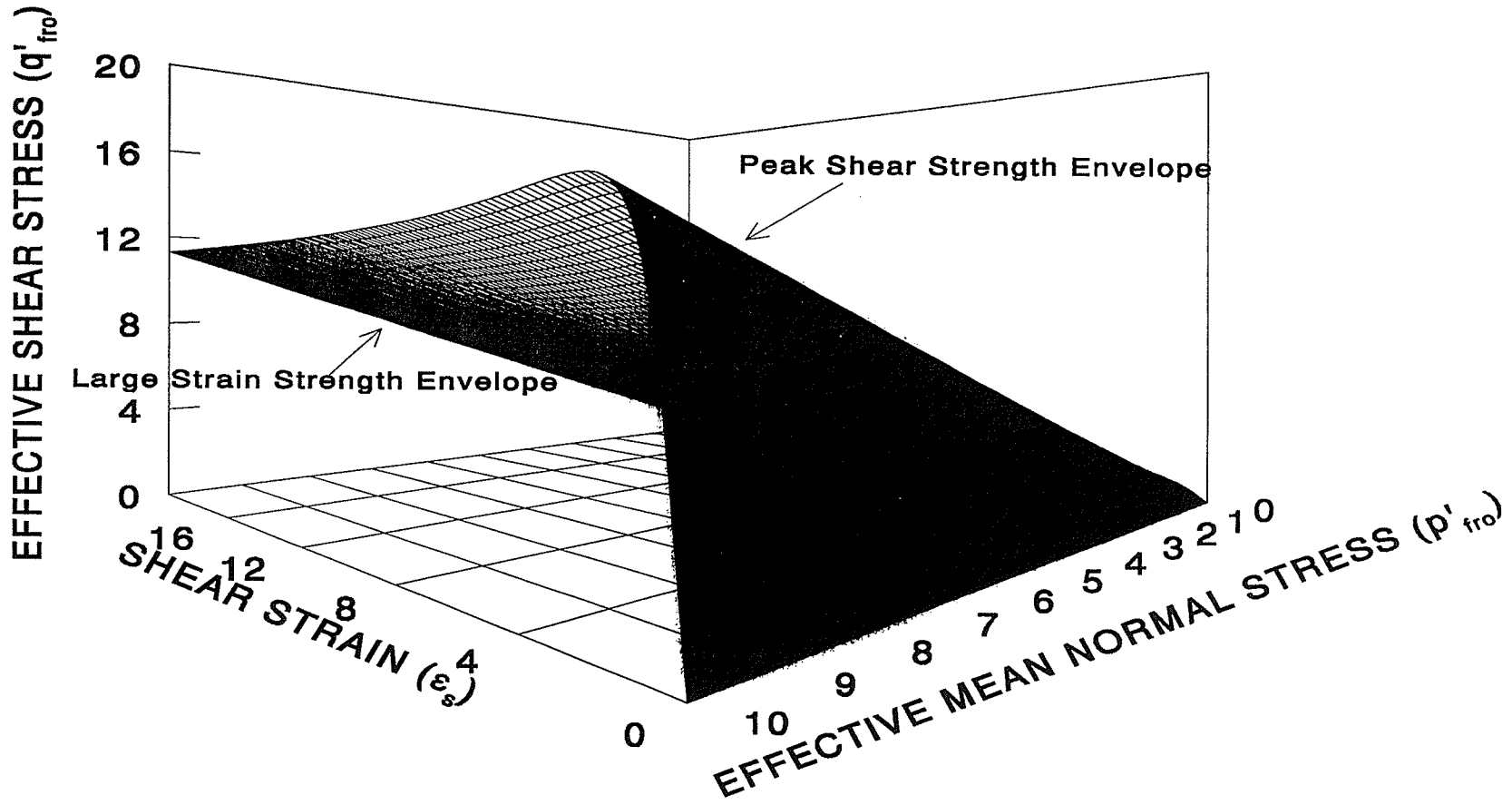

Fig.5.3 A three dimensional view of the Effective Shear Resistance Surface (**ESRS**) of frozen soil.

the Effective Shear Resistance Surface(ESRS). From an engineering point of view, **ESRS** may be determined by establishing the following three relationships.

1. A relationship between the effective mean normal stress, p'_{fro}, and the peak effective shear stress, q'_p, given by (5.4). This corresponds to the Mohr-Coulomb peak shear strength envelope of unfrozen soil, and is identified by the subscript P:

$$q'_p = C_p + M_p\, p'_{fro} \tag{5.4}$$

2. A relationship between the shear strain, ϵ_{sp}, corresponding to the peak shear stress and the effective mean normal stress, p'_{fro}, as given in (5.5).

$$\epsilon_{sp} = \epsilon_{sp0} + \epsilon_{s0}\left(\frac{p'_{fro}}{p'_0}\right)^{\zeta} \tag{5.5}$$

where ϵ_{sp0}, ϵ_{s0}, p'_0, and ζ are parameters to be determined experimentally. Parameter p'_0 is introduced to normalize the equation and to ensure compatibility of units.

3. A relationship between q'_L which is the effective shear stress at the "large strain" state (or steady state, critical state) and the effective mean normal stress, p'_{fro} as given in (5.6). This relationship corresponds to the large strain Mohr-Coulomb envelope of unfrozen soil, and is identified by the subscrept L:

$$q'_L = C_L + M_L\, p'_{fro} \tag{5.6}$$

The above three relationships are used to generate a curved surface in q'_{fro}- p'_{fro} - ϵ_s space,

which is schematically shown in Fig.5.3 for a medium to dense frozen sand. At a given value of effective mean normal stress p'_{fro}, the q'_{fro} - ϵ_s relationship takes the shape of Line [2] in Fig.5.2 while the values of q'_p , q'_L, and ϵ_{sp} are given by (5.4), (5.6) and (5.5) respectively.

5.2.3 Shear Induced Excess Pore Ice Pressure During Creep Process

It is well known that shear deformations can cause excess pore water pressure in unfrozen soil due to the fact that the soil has a tendency to change its volume during shear deformation. This property is usually called dilatancy (Rowe, 1962). Similarly, shear strain of frozen soil causes excess pore ice pressure, except that the process of the development and dissipation of excess pore ice pressure is more complicated, and pore ice pressure cannot be measured directly. In a constant stress triaxial creep test, the total mean normal stress and total shear stress remain constant, while the effective mean normal stress and effective shear stress change continuously during the creep process. The excess pore ice pressure p_e approaches zero towards the end of the consolidation process as shown in Fig.4.3. It, however, can be regenerated due to dilatancy upon application of the shear stress. A newly generated positive excess pore ice pressure triggers a new round of volumetric creep, which in turn, results in a reduction of the excess pore ice pressure. As the shear creep goes on, the dilatancy and the consolidation jointly affect the excess pore ice pressure. In order to determine the shear induced excess ice pressure during a creep process, **an assumption** is made that **the shear induced excess ice pressure in a frozen sand under a fully undrained condition is the same as the excess pore water pressure that is generated in the unfrozen soil under the same state and stress conditions.** Based on the above assumption, Figs.5.4(a) and (b) show schematically the shear induced excess pore ice pressures and the

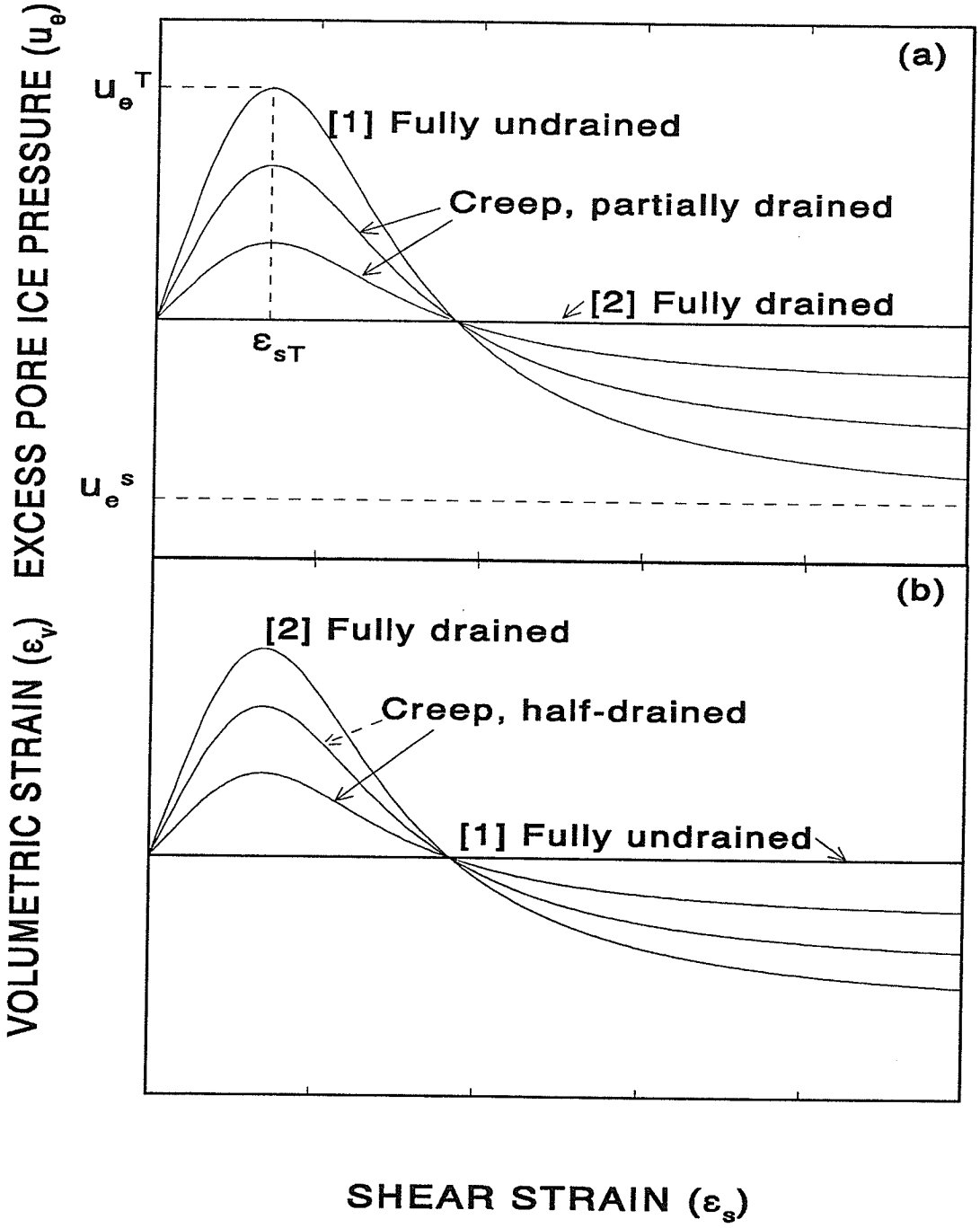

Fig.5.4 A schematic of the shear induced excess pore ice pressure and volumetric strain during the creep process of frozen sand.

volumetric strains of a medium to dense frozen sand respectively. Line [1] corresponds to the fully "undrained" condition where excess pore ice pressure is fully developed because volume change is prevented, while Line [2] corresponds to the fully "instantaneously drained" condition where there is no restraint on volume change and therefore no excess pore ice pressure is mobilized. Lines [1] and [2] are the two extreme cases, while the actual shear induced excess pore ice pressure, Δu_{ef}, lies between these two extremes, and depends on the relative magnitudes of the rates of shear creep and volumetric creep. The ice matrix provides a resistance to volume change of the sand skeleton, but as creep occurs volume change takes place. The resistance to volume change provided by the ice matrix was called *internal confinement* by Ladanyi and Morel (1990). Lines [1] and [2] may be obtained from triaxial tests, while changes in the volumetric creep strain and the excess pore ice pressure may be calculated using the isotropic creep model developed in Chapter 4. A stepwise iteration is needed to calculate Δu_{ef}, and that will be discussed in the following sections.

5.3 DEVELOPMENT AND CALIBRATION OF THE MODEL

This section discusses the results from the creep tests on frozen sand and from the constant strain rate triaxial tests on unfrozen sand. The discussion will focus on the determination of excess ice shear stress since it is the true driving force of shear creep. A good understanding of the behaviour of the sand in an unfrozen state is a necessary step in modelling the behaviour of frozen sand. The relationship between the rate of shear creep and the excess ice shear stress is established after the process of stress distribution and transformation between sand skeleton and ice matrix is clearly understood and mathematically

expressed.

5.3.1 Triaxial Creep Tests on Frozen Soil

As mentioned earlier, the triaxial creep test data used were taken from the work of Rahman (1988) who had performed the tests for a related study. A total of 9 triaxial creep tests had been performed. Five of them, MST1, MST2, MST3, MST4 and MST5, were long term multi-stage, constant p tests, three of them, MST7, MST8, and MST9, were short term, multi-stage, constant p tests, and one, MST13, was a long term, constant cell pressure test. The creep curves from the tests were presented in Fig.3.2 through Fig.3.10. The data from MST4, MST5, MST7, MST8 and MST9 were used to calibrate the model and, the calibrated model was then used to predict the creep curves for tests MST1, MST2, MST3 and MST13.

As seen on the creep-curve figures, there was some scatter in the test data. In order to obtain representative creep rates, the curves were smoothed before differentiation was made. To smooth the data, the attenuating creep curves for each loading step were fitted by the following hyperbola.

$$\epsilon_s = \epsilon_{si} + \epsilon_{scu}\left(\frac{t^{-\xi}}{1+t^{-\xi}}\right) \qquad (5.7)$$

Equation (5.7) is the combination of (5.2) and (5.3), and the parameters used are defined as before. A comparison of the best-fit curves with the test data is shown in Fig.5.5 through Fig.5.9 as cumulative shear strain versus incremental time. The constants in equation (5.9) which represent the curves are given in Table 1 and Table 2 of Appendix A. The creep rates

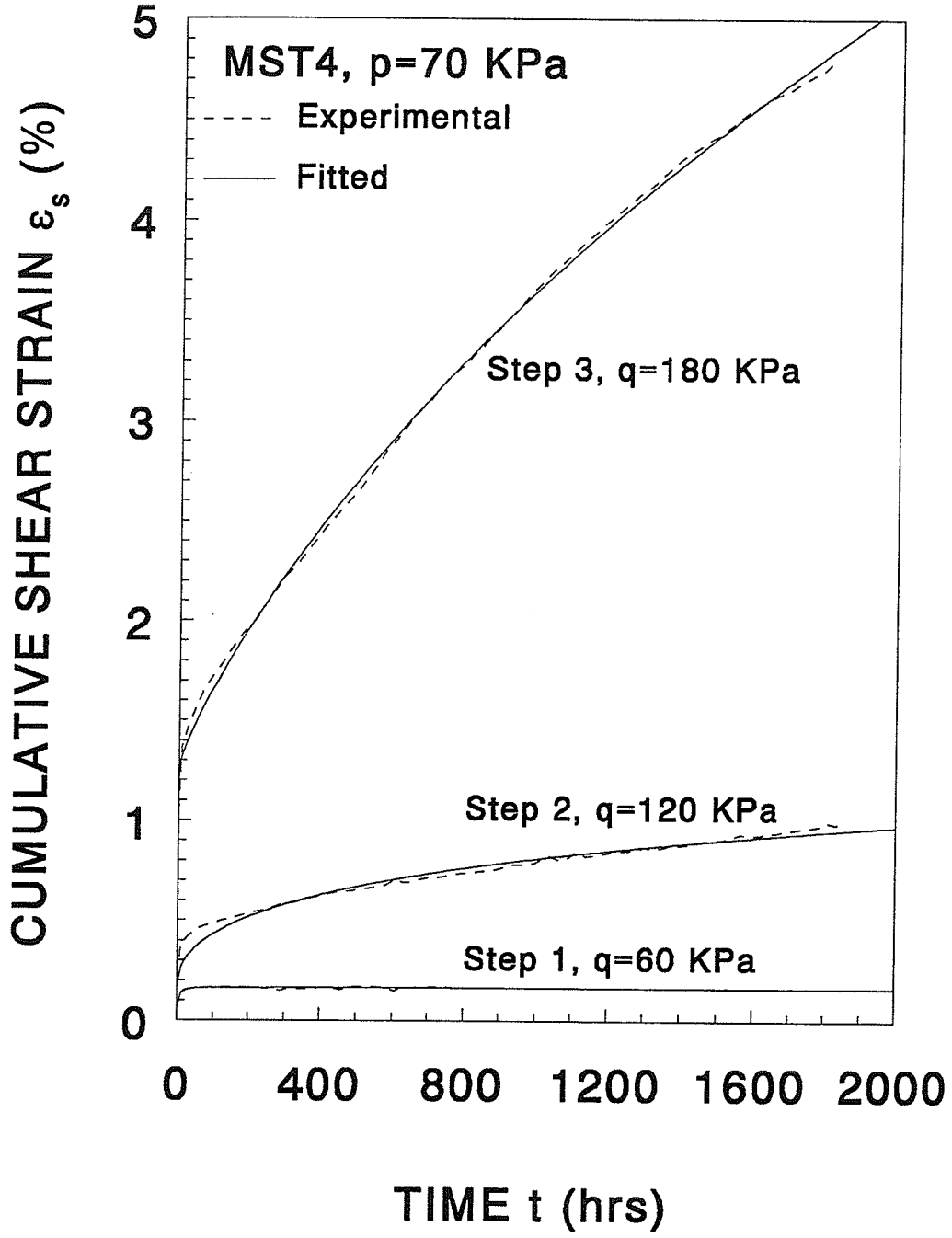

Fig.5.5 Experimental and fitted cumulative shear strain versus time for constant *p*, multi-stage, triaxial creep test MST4.

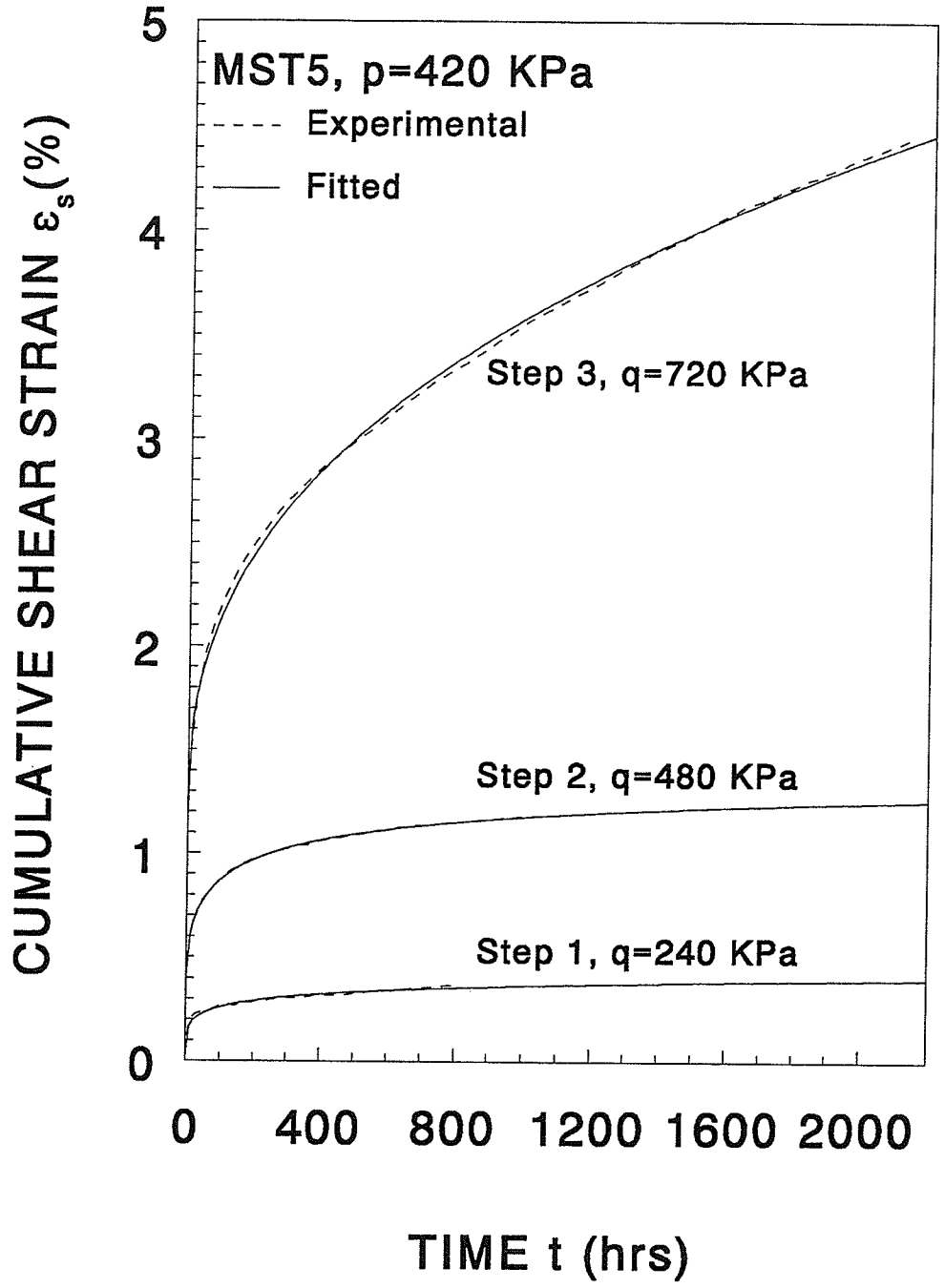

Fig.5.6 Experimental and fitted cumulative shear strain versus time for constant *p*, multi-stage, triaxial creep test MST5.

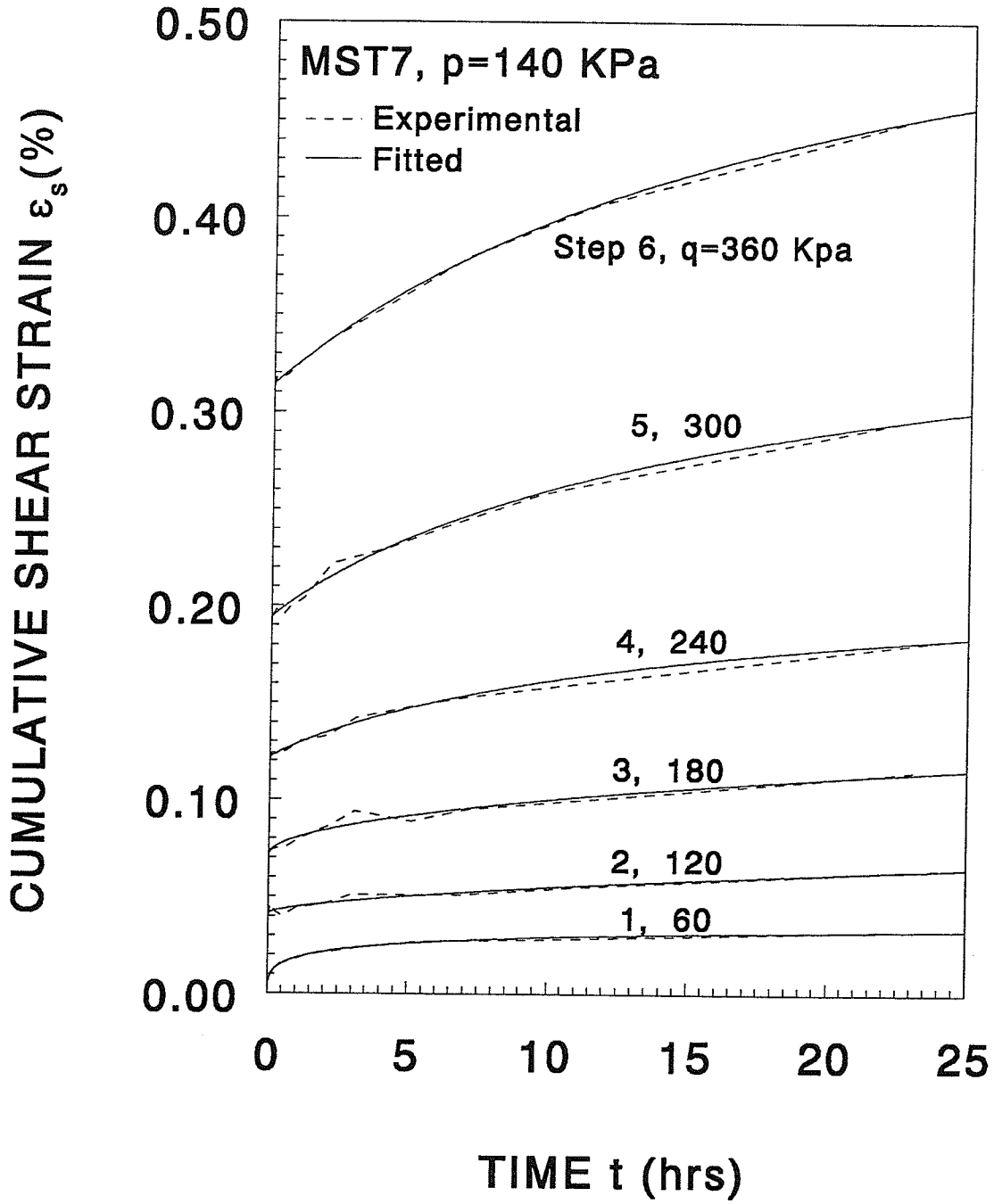

Fig.5.7 Experimental and fitted cumulative shear strain versus time for short-term, constant *p*, multi-stage, triaxial creep test MST7.

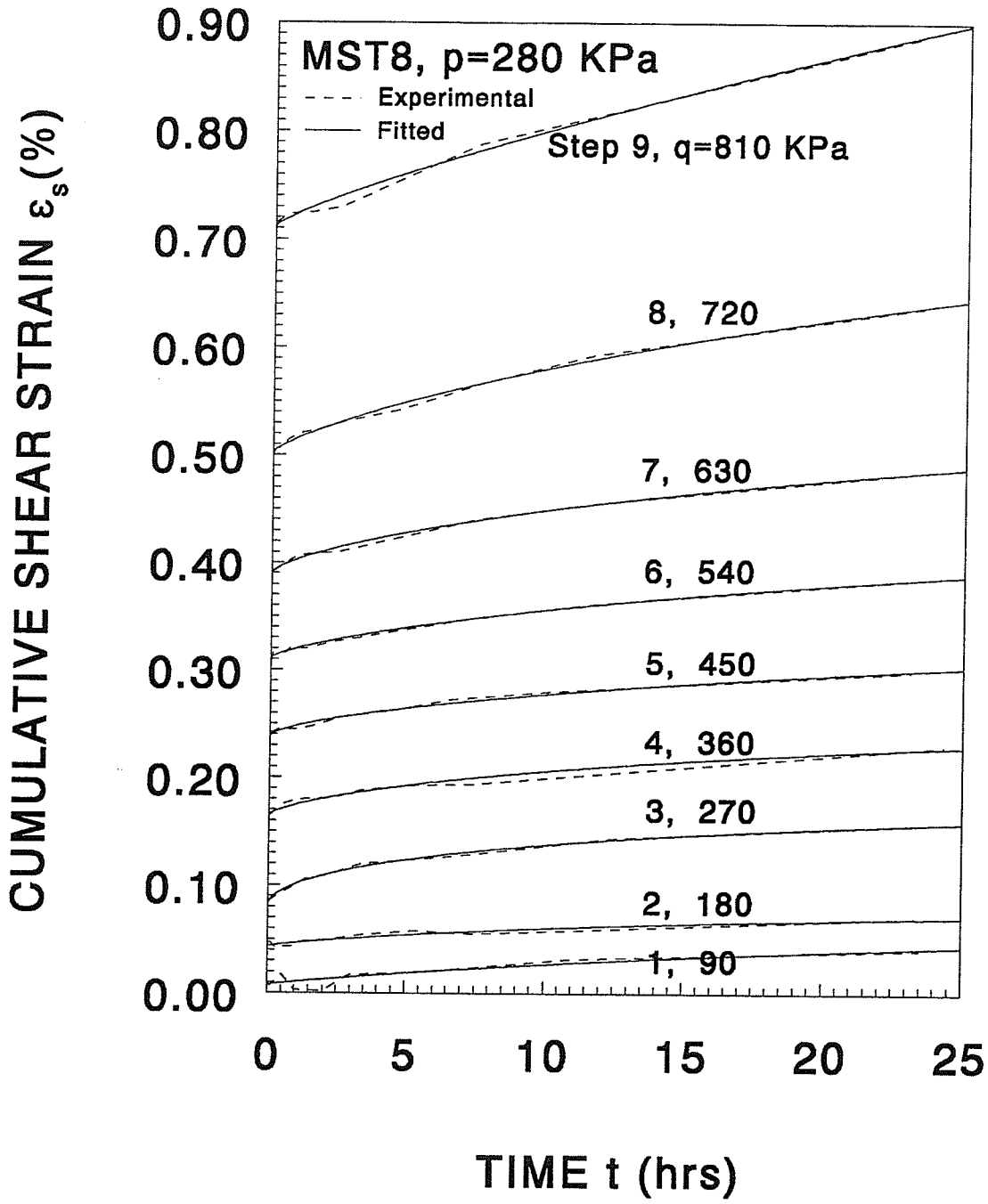

Fig.5.8 Experimental and fitted cumulative shear strain versus time for short-term, constant *p*, multi-stage, triaxial creep test MST8.

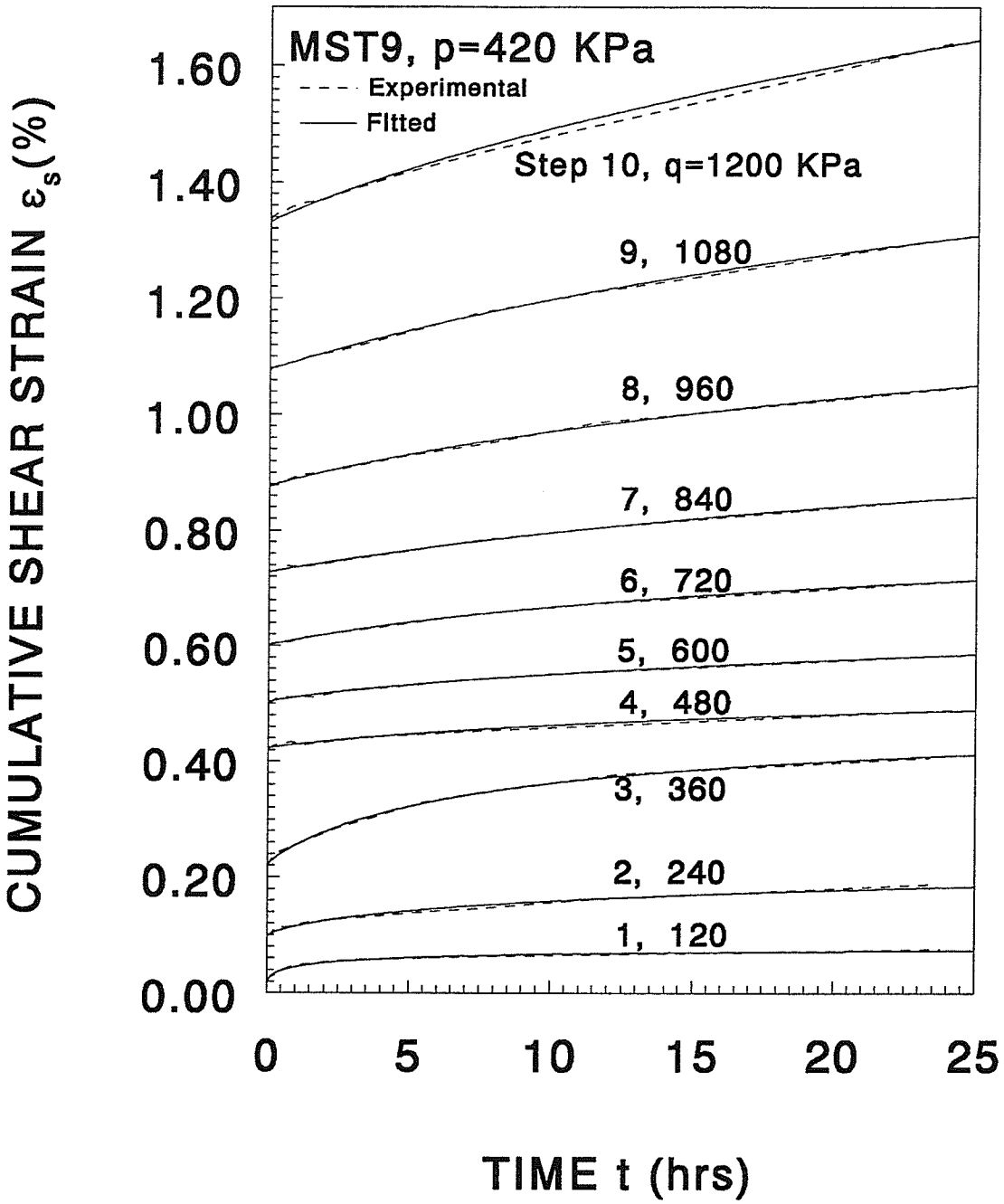

Fig.5.9 Experimental and fitted cumulative shear strain versus time for short-term, constant *p*, multi-stage, triaxial creep test MST9.

were obtained by differentiating the equations over time.

5.3.2 Instantaneous Shear Modulus

The instantaneous shear modulus, G_i was determined from the test data using the shear strain at $t = 0.01$ hour, which was the earliest recording of shear strain for each stress increment. Fig.5.10 shows the ϵ_{si} - q relationship from which a value of $G_i = 205$ MPa was determined by regression analysis.

5.3.3 Establishment of the Effective Shear Resistance Surface

According to its definition, the effective shear stress, q'_{fro}, is the shear stress sustained by the frozen soil at the end of the shear creep. If a sufficient number of creep tests were performed systematically with different magnitudes of mean normal stress p and shear stress q, the ESRS could be obtained by plotting the q'_{fro} - ϵ_s curve for every given p'_{fro} and then combining those curves into a curved surface in q'_{fro} - p'_{fro} - ϵ_s space. This would take an inordinate amount of time, thus rendering the approach impractical for engineering purposes. Consequently, the following alternative method for generating the surface was developed.

The effective shear stress, q'_{fro}, includes the contributions, q', from the sand skeleton, and, q'_i, from the ice matrix

$$q'_{fro} = q' + q'_i \qquad (5.8)$$

The shear stress sustained by the sand skeleton may be determined by conventional triaxial tests on unfrozen sand. The effective ice shear stress depends on the soil properties and the

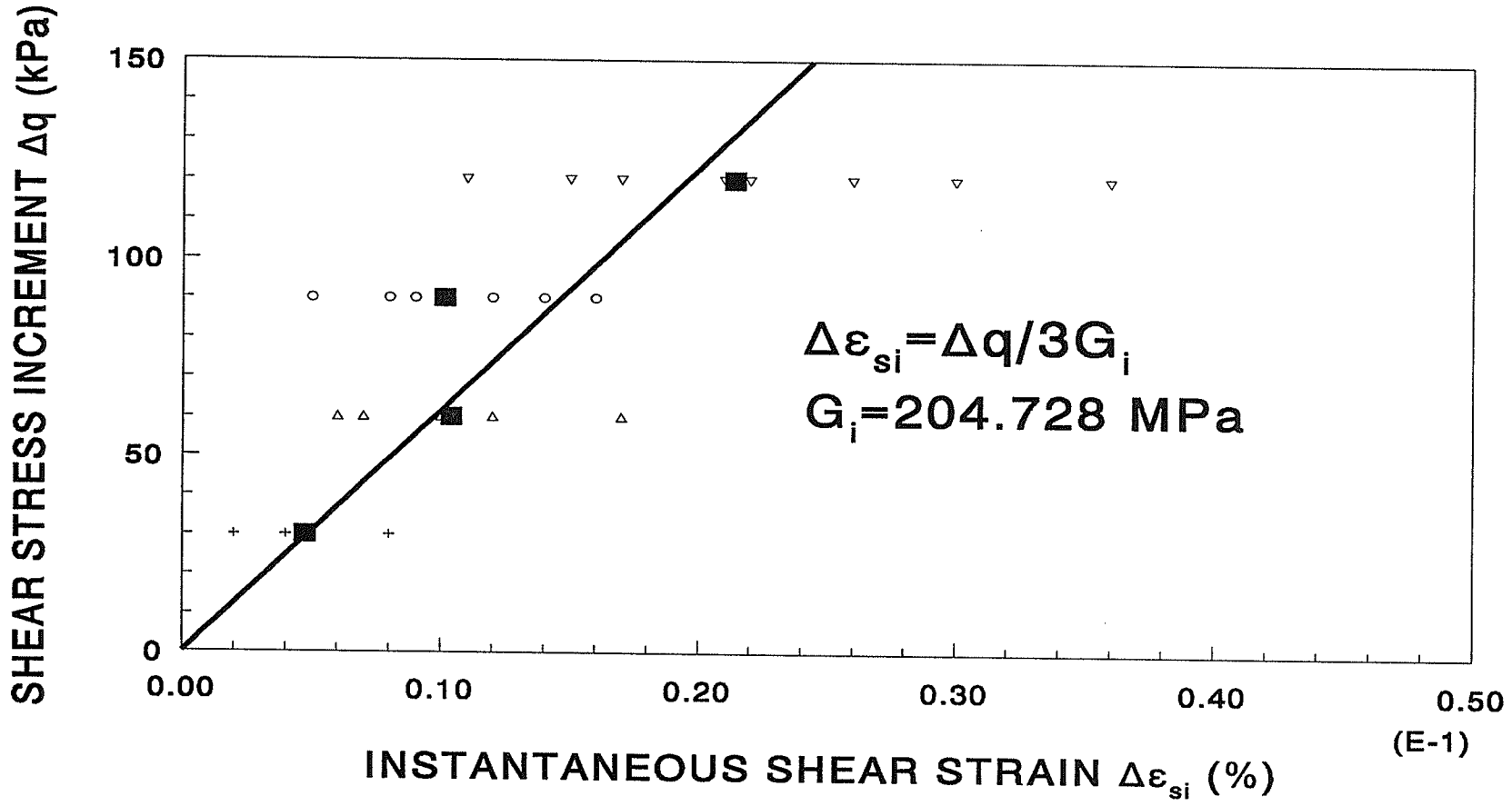

Fig.5.10 Calibration of the instantaneous shear modulus, G_i, of the frozen sand.

temperature, and is assumed to be independent of the shear strain. In order to generate the **ESRS** of the frozen sand, the first step was to determine q' by establishing the **ESRS** for the sand in an unfrozen state, and then to determine q'_i from the frozen sand creep test data. The detailed procedure is explained in the following subsections.

5.3.3.1 The Effective Shear Resistance Surface of the Unfrozen Sand

As mentioned in Chapter 3, a series of conventional constant cell pressure, drained and undrained triaxial tests on the sand in an unfrozen state were performed. The results of the drained tests DT1 through DT12 were shown in Fig.3.13 through Fig.3.16 and the results of the undrained tests UT1 through UT12 in Fig.3.17 through Fig.3.28. The shear resistance at the peak and at the large strain states were obtained from those data, and the corresponding modified Mohr-Coulomb strength envelopes are shown in Fig.5.11. They may be expressed as:

$$q_p = M_p\, p' \qquad \textbf{(5.9)}$$

$$q_L = M_L\, p' \qquad \textbf{(5.10)}$$

with M_p = **1.42** for the peak state and M_L = **1.07** for the large strain state. The shear resistance at the state of phase transformation is also shown in the figure and it will be discussed in 5.3.4.2. The strain ϵ_{sp} which is the shear strain taken to reach the peak shear stress is shown in Fig.5.12. The relationship between ϵ_{sp} and p' may be empirically expressed as

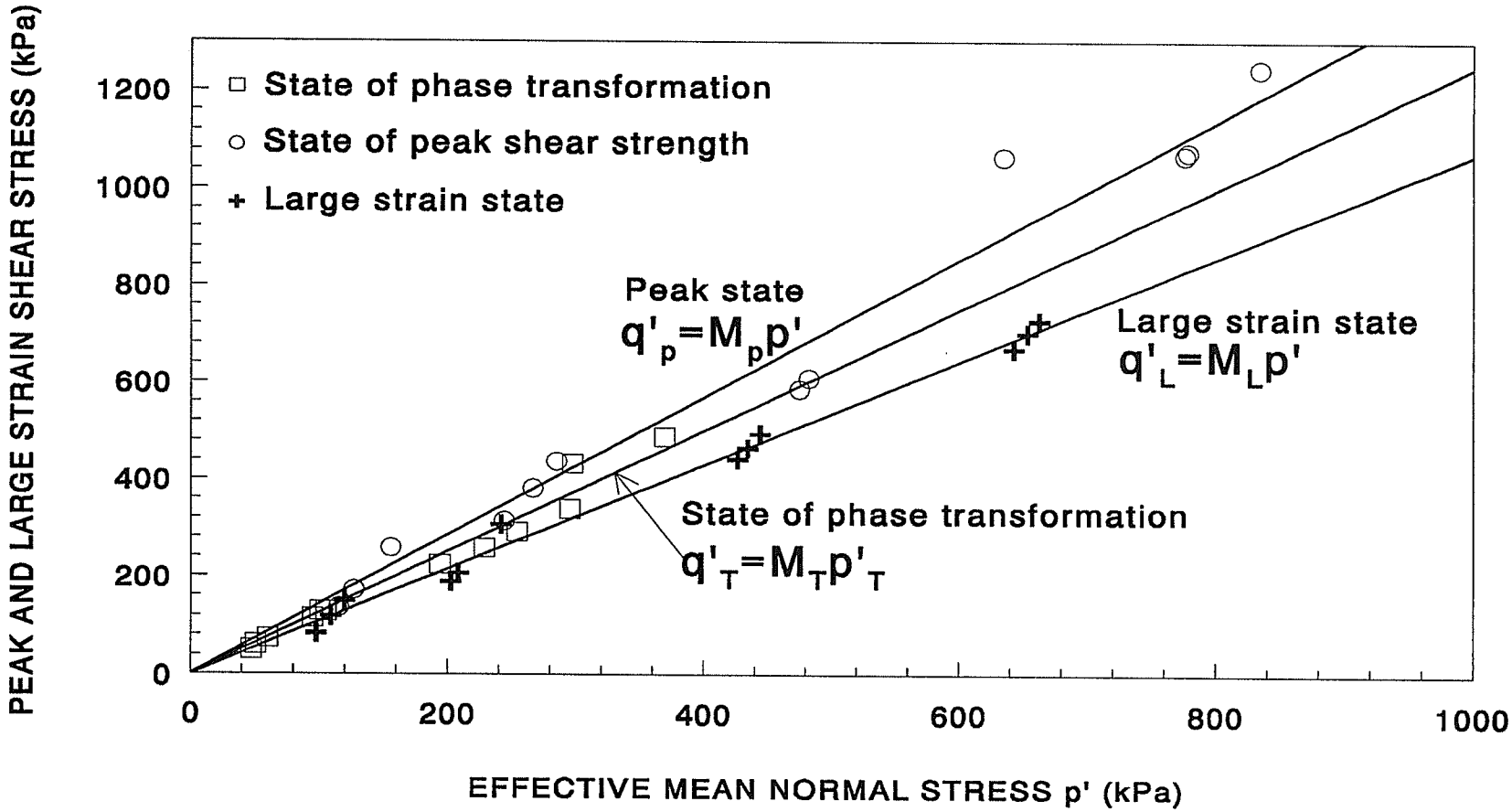

Fig.5.11 Relationships between shear stress and effective mean normal stress at the state of phase transformation, the state of peak shear strength, and the large strain state for the sand in an unfrozen state.

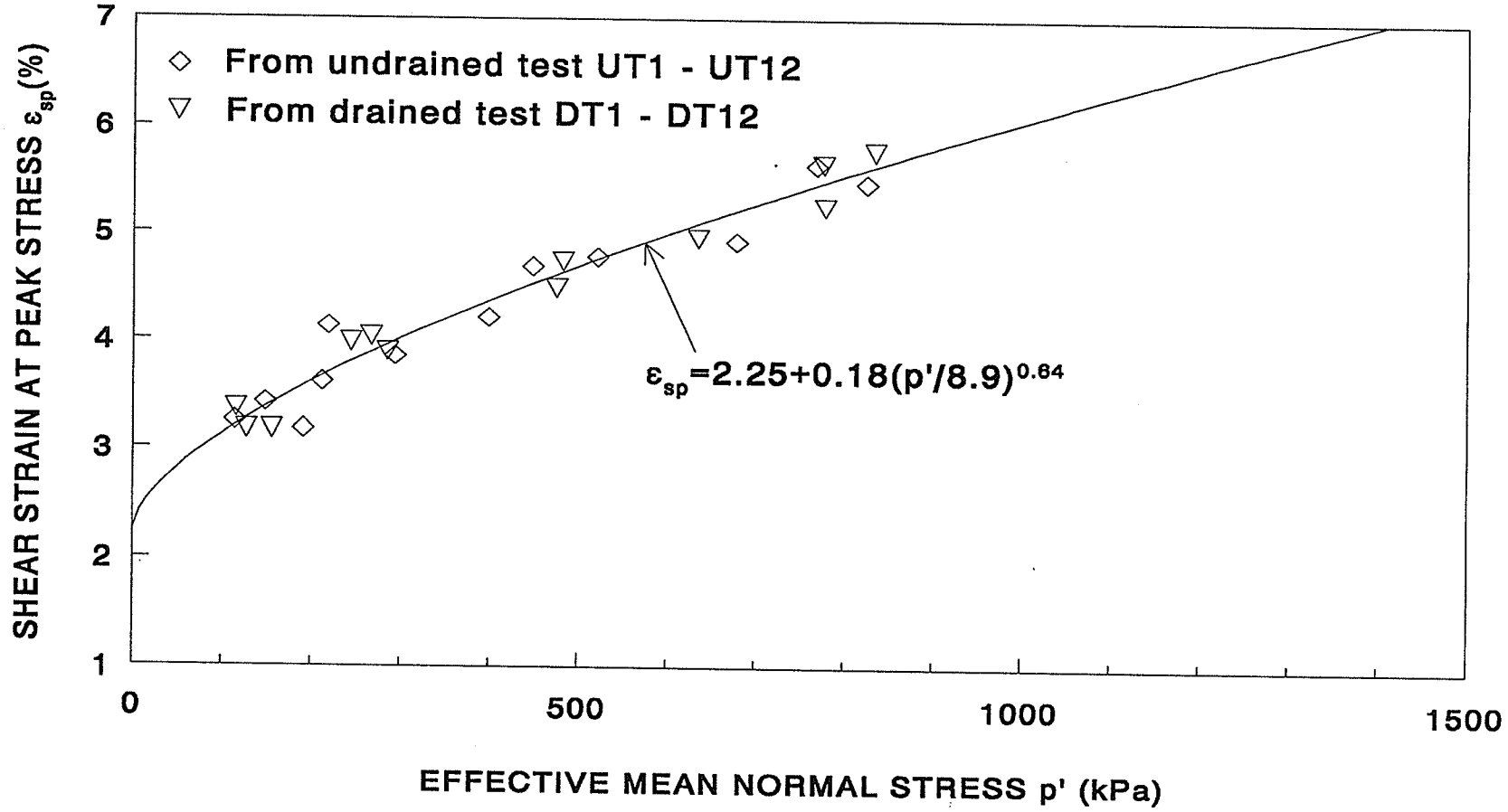

Fig.5.12 The relationship between the shear strain and the effective mean normal stress at the peak shear stress point for the sand in an unfrozen state.

$$\epsilon_{sp} = \epsilon_{sp0} + \epsilon_0 \left(\frac{p'}{p_0} \right)^{\zeta} \qquad \textbf{(5.11)}$$

For the stress range and the sand tested here, ϵ_{sp0}=2.253%, $\epsilon_0 = 0.1837\%$, $p_0 = 8.896$ kPa and $\zeta = 0.642$ as shown in Fig.5.12.

A relationship between effective shear stress, q', shear strain, ϵ_s, and effective mean normal stress, p', may be established on the basis of (5.9), (5.10) and (5.11). The test results shown in Fig.3.13 through Fig.3.16 are in the form of ϵ_1 versus q, and ϵ_1 versus ϵ_v under constant cell pressure, σ_3. The shear stress, q, in those figures is the same as q' defined here. The relationship required is ϵ_s versus q', and ϵ_s versus ϵ_v under constant mean normal stress, p'. The conversions were made and a group of ϵ_s - q' curves under constant p' are shown in Fig.5.13. The curves may be empirically expressed by the following equation:

$$q' = q_L^* \frac{\epsilon_s^2 + c\epsilon_s^{\beta}}{\epsilon_s^2 + d^2} \qquad \textbf{(5.12)}$$

where q_L^*, c, d and β are constants. The first three constants may be determined from the following three known conditions:

(1) The q' - ϵ_s curve must pass through the peak shear strength point (ϵ_{sp}, q'_p)

$$\textit{i.e.} \quad q' = q_p \quad \textit{when} \quad \epsilon_s = \epsilon_{sp} \qquad \textbf{(5.13)}$$

(2) The q' - ϵ_s curve must pass through the "large strain" shear strength point (ϵ_{sL}, q'_L)

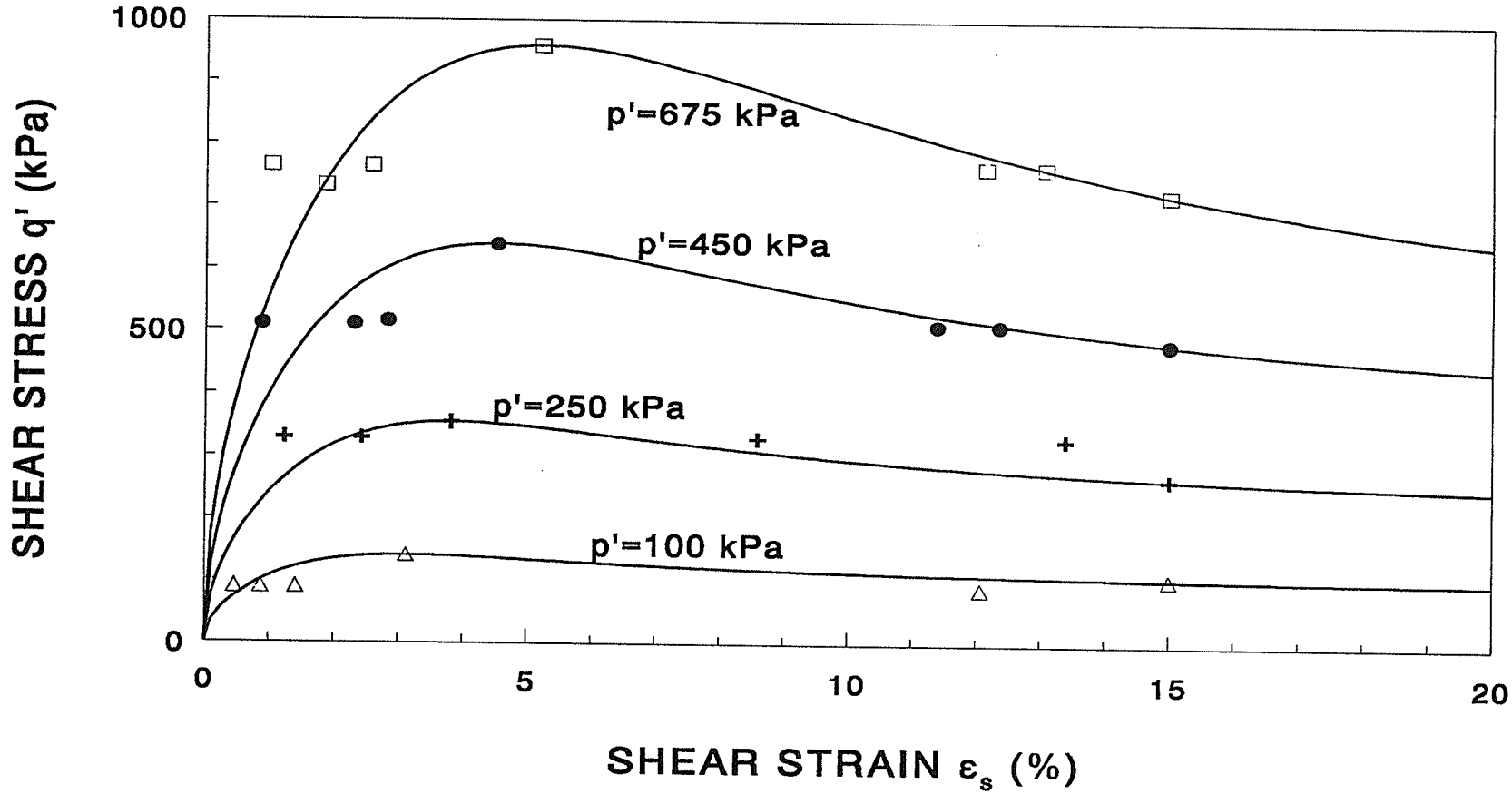

Fig.5.13 The shear stress - shear strain relationships of the sand in an unfrozen state under different effective mean normal stresses.

$$i.e. \quad q' = q_L \quad when \quad \epsilon_s = \epsilon_{sL} \tag{5.14}$$

(3) The shear stress, q', must attain its maximum value at the peak shear strength point (ϵ_{sp}, q'_p)

$$i.e. \quad \frac{dq'}{d\epsilon_s} = 0 \quad when \quad \epsilon_s = \epsilon_{sp} \tag{5.15}$$

By introducing these three conditions into (5.12), the following expressions were obtained for the three constants

$$q_L^* = \frac{q_L q_p (2-\beta+\beta f^2) - 2q_p^2 f^\beta}{(2-\beta)q_L + (\beta f^2 - 2f^\beta)q_p} \tag{5.16}$$

where $f = \epsilon_{sL}/\epsilon_{sp}$.

$$c = \frac{2(k-1)}{\beta}\epsilon_{sp}^{2-\beta} \tag{5.17}$$

$$d^2 = \frac{(2-\beta)(k-1)}{\beta k}\epsilon_{sp}^2 \tag{5.18}$$

where $k = q_p / q_L^*$. The mathematical derivations of (5.16), (5.17) and (5.18) are given in Appendix B. The parameter β was then determined to range from 0.3 to 0.6 by applying (5.12) to the test data.

Equation (5.12) together with (5.9), (5.10) and (5.11) generates a curved surface in q - p' - ϵ_s space, which is the **Effective Shear Resistance Surface** of the unfrozen sand.

5.3.3.2 The Effective Ice Shear Stress, q'_i

As discussed in **5.3.3**, it is assumed that the contribution of the sand skeleton to the shear resistance of frozen sand is the same as the shear resistance of the same sand in an unfrozen state. The effective shear resistance of frozen sand at peak and large strain states may be expressed by $q'_p=M_p\, p'_{fro} + C_p$ and $q'_L=M_L\, P'_{fro} + C_L$ respectively. The constants M_p and M_L which represent the contributions from the sand skeleton were determined in **5.3.3.1** as $M_p = 1.42$ and $M_L = 1.07$. The parameters C_p and C_L represent the contributions which stem from the ultimate shear resistance of the ice. It was assumed that the ultimate shear resistance of ice, q'_i, depends solely on temperature, therefore for a constant temperature, C_p and C_L may be replaced by q'_i.

$$C_p = C_L = q'_i = Constant \qquad (5.19)$$

The effective ice shear stress, q_i', may be determined from creep tests. From (5.8), we have

$$q'_i = q'_{fro} - q' \qquad (5.20)$$

From the definition of q'_{fro} as shown in Fig.5.2, we have

$$q'_{fro} = q - q_e \qquad (5.21)$$

Combining (5.21) with (5.20) produces

$$q'_i = q - q' - q_e \qquad (5.22)$$

It is noted that q_e approaches zero towards the end of attenuating creep. In a creep test, q is known, and q' may be determined from (5.12), and therefore q_i' may be obtained from the stress and strain at the end of attenuating creep. Table 1 is a compilation of all the data required to determining the effective ice shear stress, q_i'.

Table 1 Calculation of effective ice shear stress q'_i.

	Step	p (kPa)	q (kPa)	ϵ_{su} (%)	p_e (kPa)	p'_i (kPa)	p' (kPa)	q' (kPa)	q'_i (kPa)
MST2	1	280	120	0.1469	0.0	20.5	259.5	95.48	24.5
MST4	1	70	60	0.1638	0.0	20.5	49.5	24.65	35.3
	2	70	120	1.9	15.26	20.5	34.24	53.87	66.1
MST5	1	420	240	0.5127	52.92	20.5	346.58	228.5	11.5
	2	420	480	1.431	14.28	20.5	385.22	407.46	72.5
The average value of the effective ice shear stress, q'_i, is									**42** kPa

In the table, ϵ_{su} is the ultimate creep strain at the end of attenuating creep. Since none of the tests were carried out to ceasation of creep, the value of ϵ_{su} used was obtained by curve-fitting the test creep curves and extrapolating the curves to t=10 years to ensure that most of the attenuating creep had been accounted for. The equations and the parameters used to fit the data are given in Appendix A, and the fitted curves are shown in Figs.5.5 - 5.9 together with the experimental data. Parameter p_e is the pore ice pressure that still existed at t=10 years, while p'_i is the effective ice pressure as defined in Fig.4.2. The values of p_e were

obtained by evaluating volumetric creep using the consolidation model developed in Chapter 4 and assuming that the degree of consolidation, U_c, at t=10 years is equal to the degree of shear creep at the same time. The values of p'_i were obtained from the experimental data by comparing the ultimate p-ϵ_v relationship for frozen sand to the isotropic compression curve for the sand in an unfrozen state. The stresses p' and q' are respectively the effective mean normal and shear components sustained by the sand skeleton. The values of p' were obtained from $p'=p-p_e-p'_i$, and the values of q' were obtained from the q'-p'-ϵ_s relationship developed in **5.3.3.1** for the sand. There was some scatter in the calculated values of effective ice shear stress, q'_i. This is to be expected for experimental data. An average value of q'_i = 42 kPa was taken and used for the frozen sand tested at a temperature of -3°C.

5.3.3.3 ESRS for the Frozen Sand

With all the parameters in (5.4), (5.5) and (5.6) determined, the peak shear strength envelope of the frozen sand may be expressed as:

$$q'_p = 41.9 + 1.42 p'_{fro} \qquad (5.23)$$

and the large strain shear strength envelope of the frozen sand may be expressed as:

$$q'_L = 41.9 + 1.07 p'_{fro} \qquad (5.24)$$

while the shear strain taken to reach the peak shear stress may be expressed as:

$$\epsilon_{sp} = 2.25 + 0.18 \left(\frac{p'_{fro}}{8.9} \right)^{0.64} \qquad (5.25)$$

where the stress is in kPa, and the strain is in percent.

A typical ϵ_s - q'_{fro} curve for a given effective mean normal stress, p'_{fro}, takes the shape of Line [2] in Fig.5.2. The curve may be expressed by the set of equations used for the ESRS of the unfrozen sand.

$$q'_{fro} = q_L^* \frac{\epsilon_s^2 + c\epsilon_s^{\beta}}{\epsilon_s^2 + d^2} \qquad \textbf{(5.26)}$$

Where β is a parameter to be determined experimentally, and q^*_L , c and d are three intermediate variables which were introduced to ensure that (5.26) satisfied the following three requirements:

(a) The ϵ_s - q'_{fro} relationship given by (5.26) must pass through the peak shear strength point (ϵ_s , q'_p).

$$\textit{i.e.} \quad q'_{fro} = q'_p \quad \textit{when} \quad \epsilon_s = \epsilon_{sp} \qquad \textbf{(5.27)}$$

(b) The ϵ_s - q'_{fro} relationship given by (5.26) must pass through the large strain shear strength point (ϵ_s , q'_L).

$$\textit{i.e.} \quad q'_{fro} = q'_L \quad \textit{when} \quad \epsilon_s = \epsilon_{sL} \qquad \textbf{(5.28)}$$

(c) the effective shear stress, q'_{fro}, reaches its maximum value at the peak shear strength point (ϵ_{sp} , q'_p).

$$i.e. \quad \frac{d\,q'_{fro}}{d\epsilon_s}=0 \quad when \quad \epsilon_s=\epsilon_{sp} \tag{5.29}$$

As in the case of the sand in an unfrozen state, expressions for the parameters q^*_L, c, and d were obtained by utilizing the above three requirements. The expressions are as follows:

$$q^*_L=\frac{q'_L\,q'_p(2-\beta+\beta f^2)-2f^{\beta}(q'_p)^2}{(2-\beta)q'_L+(\beta f^2-2f^{\beta})q'_p} \tag{5.30}$$

where $f=\epsilon_{sL}/\epsilon_{sp}$, and ϵ_{sL} is the shear strain at the "large strain" state, which is assumed to be about 15%.

$$c=\frac{2(k-1)}{\beta}\epsilon_{sp}^{2-\beta} \tag{5.31}$$

where $k=q'_p/q'_L$, and

$$d^2=\frac{(2-\beta)(k-1)}{\beta k}\epsilon_{sp}^2 \tag{5.32}$$

The mathematical derivations of (5.30), (5.31) and (5.32) are given in Appendix B. A three dimensional view of **ESRS** for the frozen sand is shown in Fig.5.3.

5.3.4 Shear Induced Excess Pore Ice Pressure

5.3.4.1 Introduction

Shear induced excess pore ice pressure is a new concept presented by the writer. There has been no previous work done on this subject, and currently there is no technology available to measure it. The assumption that the shear induced excess pore ice pressure in a frozen sand under a fully undrained condition is the same as the excess pore water pressure that is generated in unfrozen sand under the same state and stress conditions provides an indirect method to determine the shear induced excess pore ice pressure. Shear induced excess pore water pressure in an unfrozen sand was investigated by undrained, constant σ_3, triaxial tests. A mathematical modelling is presented in this section. The excess pore ice pressure was then calculated by considering the joint effect of shear deformation and isotropic consolidation. (The consolidation model for the frozen sand was given in Chapter 4.)

5.3.4.2 Shear Induced Excess Pore Water Pressure In Unfrozen Sand

The shear induced excess pore water pressure in unfrozen sand may be expressed according to the state parameter of the sand. From triaxial tests performed on the sand reported in Chapter 3, a steady state line (or critical state line) was obtained by analyzing the relationship between the specific volume, v, and the effective mean normal stress, p', at the large strain state. Fig.5.14 shows the **Steady State Line** of the sand in v - $ln\ p'$ space (Been and Jefferies, 1985). It may be expressed as:

$$v=N_s-\lambda\ lnp' \qquad \textbf{(5.33)}$$

The parameters λ and N_s were determined from the test data as $\lambda=0.0187$ and $N_s=1.8464$ as shown in Fig.5.14. By analyzing the stress-strain path of the sand in v -p' and ϵ_s - p' spaces,

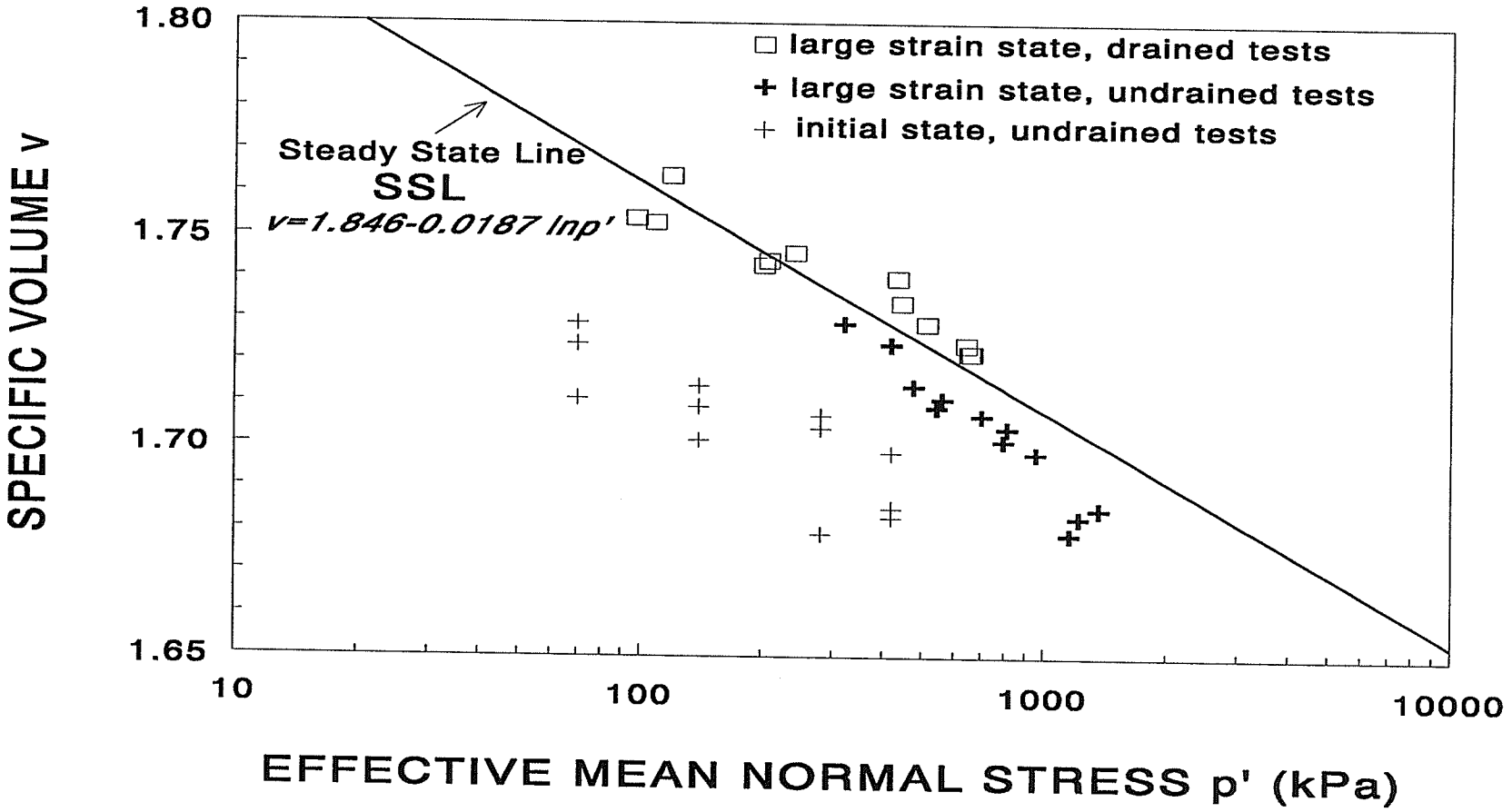

Fig.5.14 The specific volume versus effective mean normal stress at the large strain state.

the excess pore water pressures were modeled mathematically. Fig.5.15 shows the steady state line, SSL, and the stress-strain paths of a sample when it is sheared under an undrained condition. The initial state of the sample is represented by point O on the figure with $v = v_0$ and $p' = p'_0$. As shown in Fig.5.15, the state parameter, $\psi = v_0 - v_\lambda$, of the sand is smaller than zero. The state parameter may be expressed as

$$\psi = v_0 - (N_s - \lambda \ lnp'_0) \qquad (5.34)$$

As shown in Fig.5.15 when a sample of medium to dense sand is sheared under an undrained condition, the stress path in v - p' space is O-T-B-P-L-(S). Fig.5.16 shows the stress-strain path in ϵ_s - p' space. At the start of shearing, the sand has a tendency to contract. However the volume change is prevented in an "undrained" test, and therefore positive excess pore water pressure, Δu, is generated and the effective mean normal stress, p', decreases with increasing shear strain. This excess pore water pressure, Δu, reaches its maximum at point T as shown in Fig.5.16 (compressive pressure is referred to as positive). After this point, the dilatant medium to dense sand has a tendency to increase its volume, therefore negative excess pore water is generated. At point B, the generated negative pore pressure offsets the positive pore pressure, and p' becomes equal to the total mean normal stress, p. After point B, p' continues to increase until the sample fails at the point of large strain, L. The shear induced excess pore water pressure in ϵ_s - p' space is also shown in Fig.5.16.

Point T was termed the "point of phase transformation" by Ishihara, Tatsouka & Yasuda (1975) since the sample is contractive before the point and expansive after it for medium to dense sand. The state parameter at this point indicates whether the sand will be

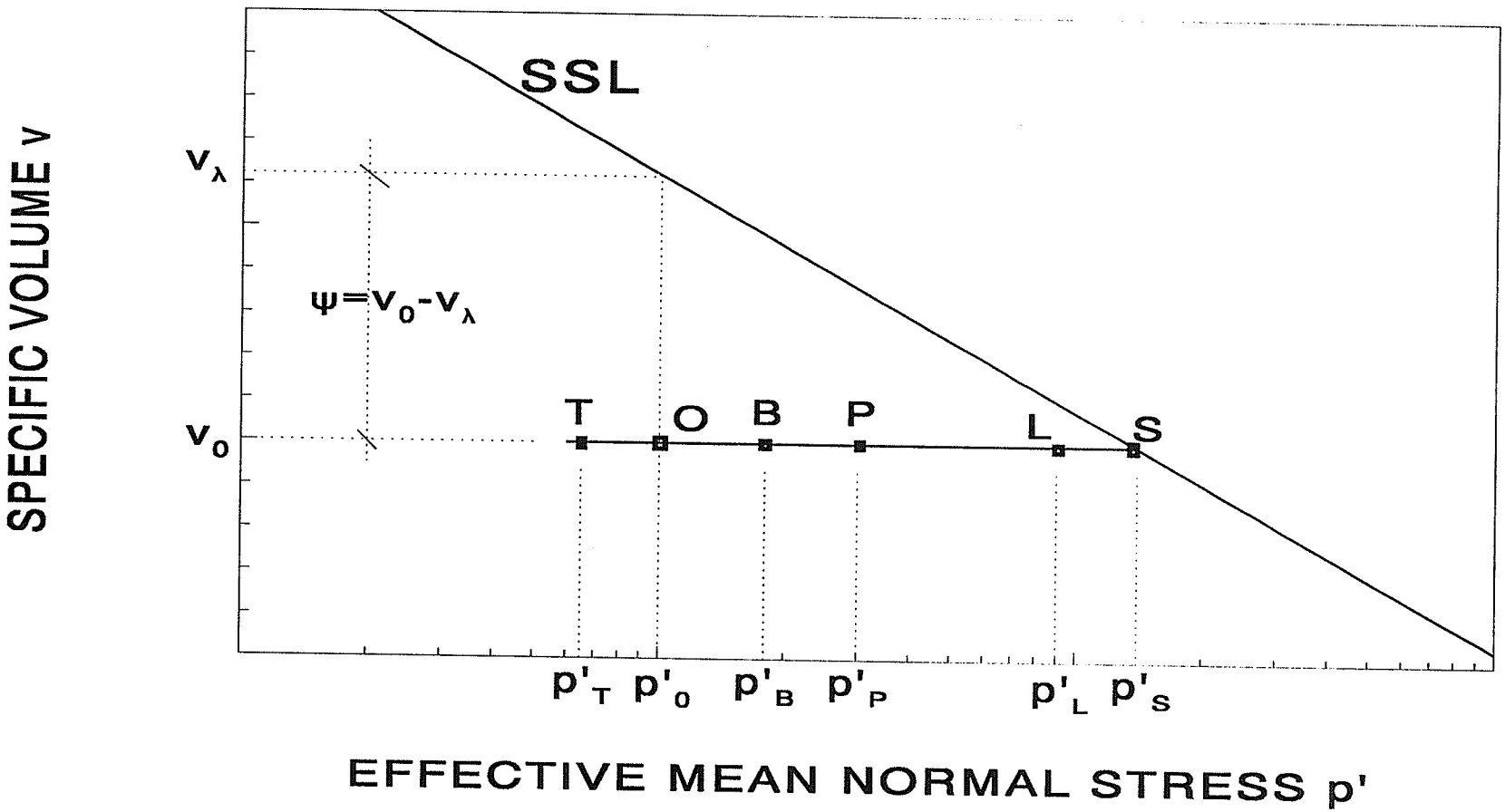

Fig.5.15 A schematic of stress-strain path in v - p' space for the unfrozen sand in an undrained triaxial test.

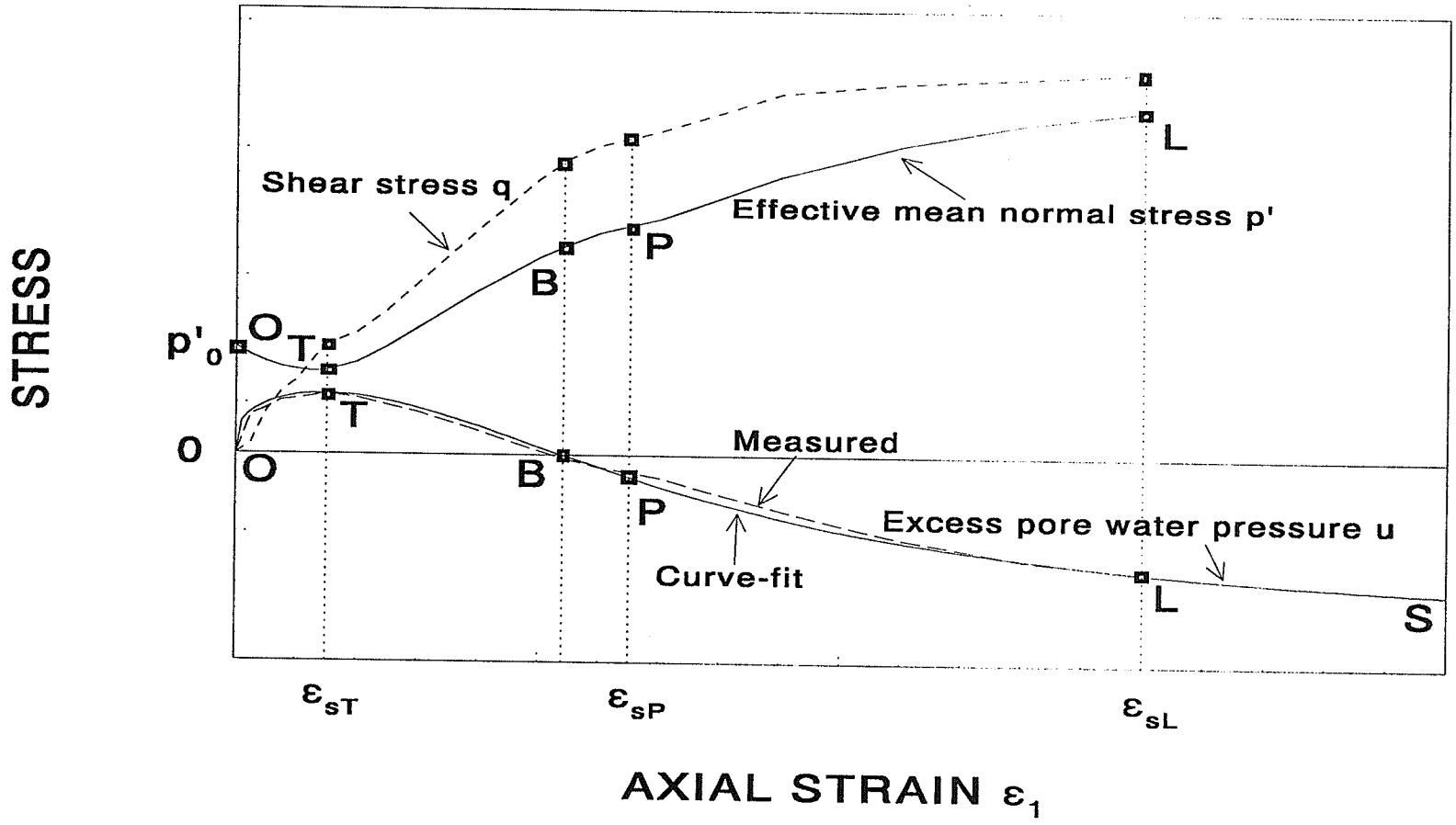

Fig.5.16 A schematic of stress-strain paths of the unfrozen sand in p' - ϵ_1, q - ϵ_1, and u - ϵ_1 spaces in an undrained triaxial test.

contractive or expansive with further shear deformation (Been and Jefferies, 1985).

Point P corresponds to the point of peak shear resistance. It was noted that there were no obvious "peak" points on the conventional $\Delta\sigma_1$ - ϵ_1 curves obtained from the tests since p' continued to increase after the stress path reached the Mohr-Coulomb line. There is, however, a peak shear resistance envelope, no matter whether the test is drained or undrained. The peak point may be found by calculating the ratio of q/p', and finding its maximum value. Point P may occur before or after point B depending on the dilatancy of the sample. The pore water pressure parameters at T, the phase transformation point, P, the "peak" shear resistance point, and L, the "large strain" point were analyzed and related to the state parameter ψ as shown in Fig.5.17. The relationships may be empirically expressed as follows:

at phase transformation point $$A_T=1.113+12.62\psi \quad (5.35)$$

at "peak" point $$A_P=0.339+5.75\psi \quad (5.36)$$

and at "large strain" point $$A_L=0.165+10.35\psi \quad (5.37)$$

It should be noted that the above correlations are valid only for the sand and the stress range tested. Since only a limited number of tests were performed and the range of the state parameter is narrow, the pore water pressure parameters were related to ψ simply by a straight line. Actually, the pore water pressure parameter at steady state may be obtained from the steady state line, **SSL**, directly as:

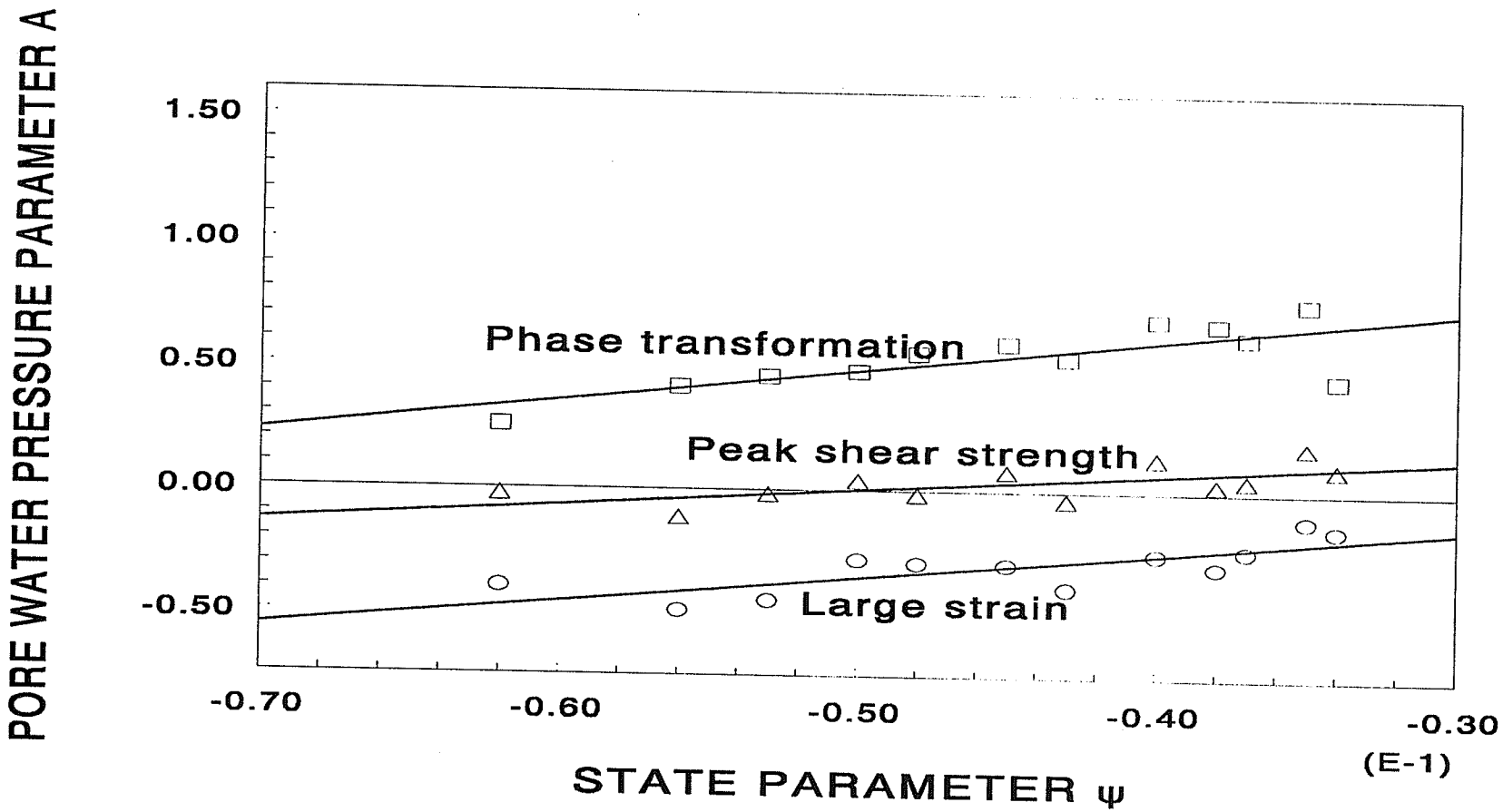

Fig.5.17 The relationships between pore water pressure parameter, A, and the state parameter, ψ, for the unfrozen sand at the state of phase transformation, the state of peak shear stress, and the large strain state.

$$A_s = \frac{1}{M_s}\left(e^{\frac{\psi}{\lambda} + \frac{M_s}{3} - 1}\right) \qquad \textbf{(5.38)}$$

However, for the large strain point, the pore water pressure predicted using (5.38) is always higher than that calculated from (5.37). The explanation for this phenomenon may be found from Fig.5.15 and Fig.5.16. The stresses from the undrained tests at about 15% of shear strain did not reach **SSL**. It reached point L and did not go far enough to reach point S. There is a gap between the stresses obtained from drained and undrained tests as shown in Fig.5.14, and the **SSL** used here is a compromise of the two. Equation (5.37) is adopted for predicting the excess pore water pressure since it is obtained directly from the tests.

The pore water pressure parameter A changes with shear strain continuously. Equations (5.35), (5.36) and (5.37) give the A values at three key points which are of practical interest. Actually, an A - ϵ_s relationship may be obtained from the experimental data. Fig.5.18 shows a typical A - ϵ_s curve which may be represented by a hyperbola as:

$$A = a_1 + \frac{a_2}{\epsilon_s + a_3} \qquad \textbf{(5.39)}$$

Since the A values at points T, P and L are known, a_1, a_2, and a_3 may be determined by solving 3 simultaneous equations if the shear strains at these points are also known. The shear strain at peak shear strength point, ϵ_{sp}, was given by (5,11), while the shear strain at large strain state, ϵ_{sL}, was assumed to be about 15% as discussed in **5.3.3.3**. The shear strain at the phase transformation point, ϵ_{sT}, may be empirically related to the effective mean normal

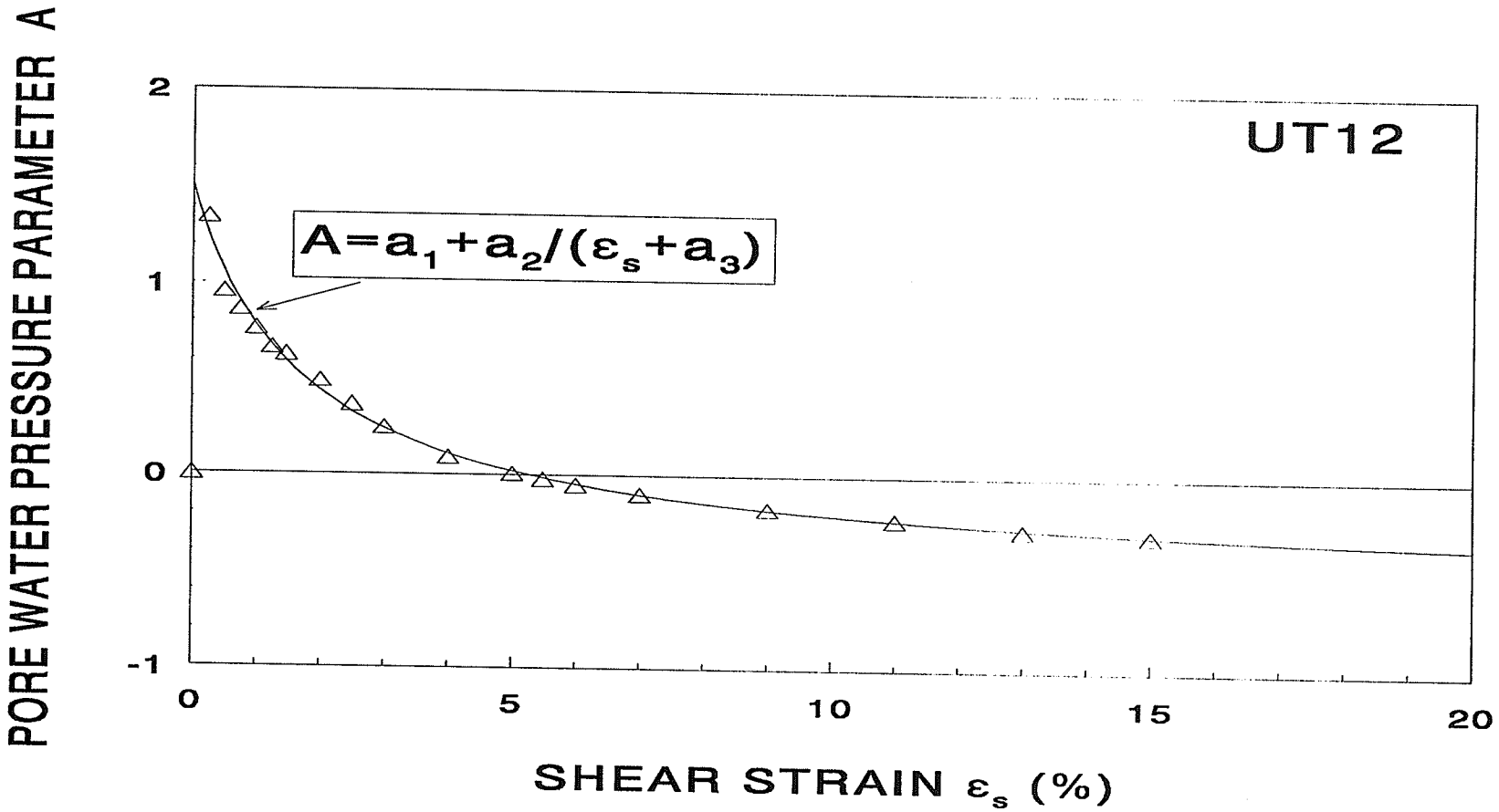

Fig.5.18 A typical curve of pore water pressure parameter versus shear strain for the unfrozen sand in an undrained triaxial test.

stress at the point as shown in Fig.5.19. A mathematical expression for the ϵ_{sT} - p'_T relationship is given as:

$$\epsilon_{sT} = \epsilon_{sT0} + \epsilon_{sTp}\left(\frac{p'_T}{p_{0T}}\right)^{\Lambda} \qquad \textbf{(5.40)}$$

with $\epsilon_{sT0} = 0.80$ %, $\epsilon_{sTp} = 0.065$ %, $p_{0T} = 5.76$ kPa and Λ=0.599139 for the data shown in Fig.5.19.

At the peak shear strength point, (5.11) is rewritten as:

$$\epsilon_{sp} = \epsilon_{sP0} + \epsilon_{sPp}\left(\frac{p'_p}{p_{0P}}\right)^{\zeta} \qquad \textbf{(5.41)}$$

with ϵ_{sP0}=2.25%, $\epsilon_{sPp} = 0.18$%, $p_{0P} = 8.9$ kPa and $\zeta = 0.642$.

In order to determine ϵ_{sT} and ϵ_{sp} from (5.40) and (5.41), the effective mean normal stresses at the phase transformation point T, p'_T, and the peak shear strength point P, p'_p, are needed. The relationship between p'_T and the shear resistance at point T, q'_T, is shown in Fig.5.11, and is expressed as:

$$q_T = M_T\, p'_T \qquad \textbf{(5.42)}$$

with M_T = **1.25** for the sand tested. For the peak shear strength envelope, (5.9) is rewritten as:

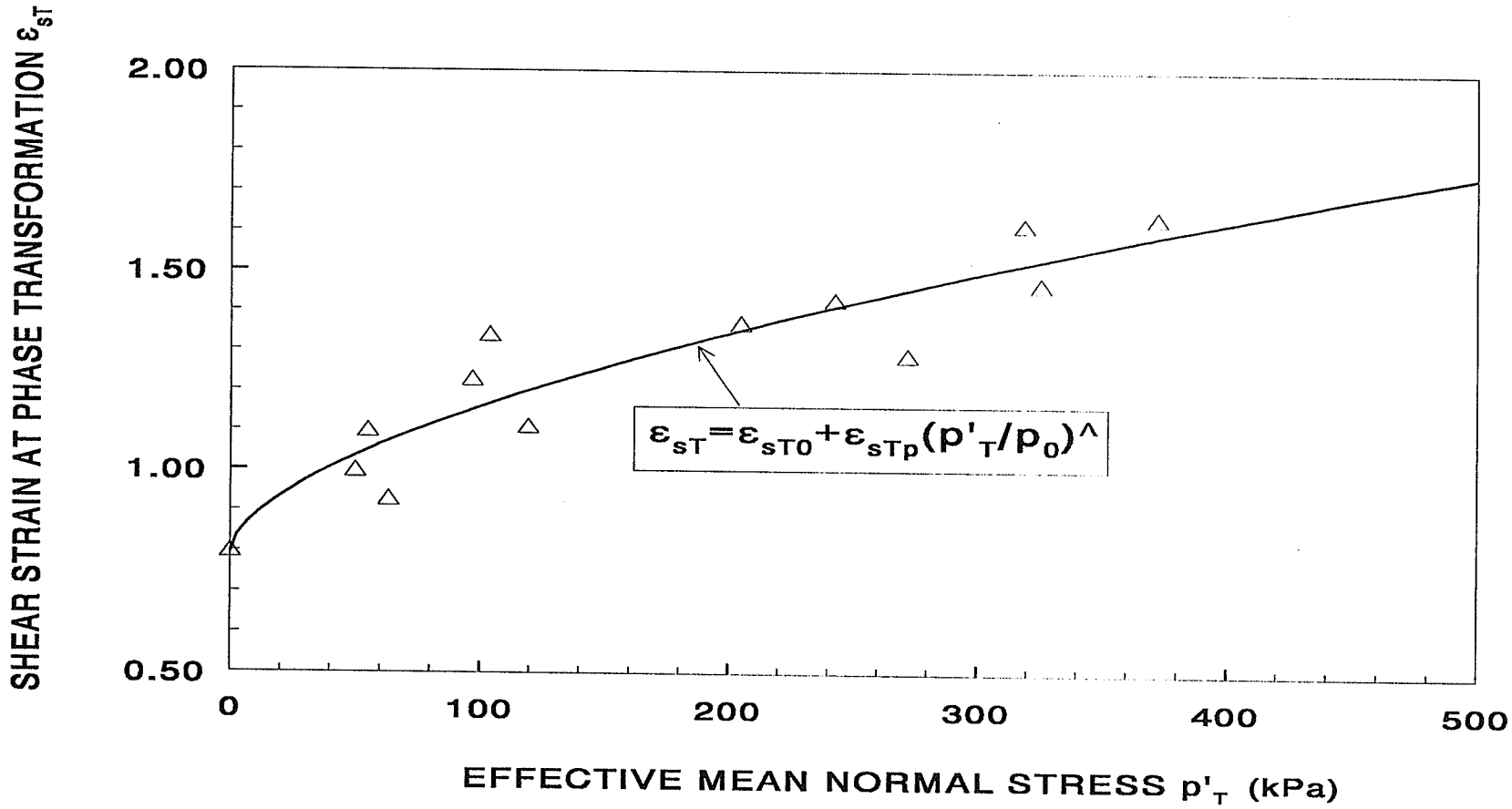

Fig.5.19 The relationship between the shear strain and the effective mean normal stress at the point of phase transformation for the sand in an unfrozen state.

$$q_p = M_p\, p'_p \tag{5.43}$$

The excess pore water pressure, Δu may be determined from the pore water pressure parameter, A as:

$$\Delta u = B(\Delta\sigma_3 + A(\Delta\sigma_1 - \Delta\sigma_3)) \tag{5.44}$$

For fully saturated sand, B=1.0, and (5.44) becomes

$$\Delta u = \Delta\sigma_3 + A(\Delta\sigma_1 - \Delta\sigma_3) \tag{5.45}$$

The effective mean normal stress at any point may be expressed as:

$$p' = p'_0 - (A - \frac{1}{3})(\Delta\sigma_1 - \Delta\sigma_3) \tag{5.46}$$

where p'_0 is the effective mean normal stress before shearing. Specifically, at point T, we have

$$p'_T = p'_0 - (A_T - \frac{1}{3})(\Delta\sigma_{1T} - \Delta\sigma_{3T}) \tag{5.47}$$

It should be noted that $\Delta\sigma_{1T} - \Delta\sigma_{3T} = q_T$. Therefore by substituting (5.42) into (5.47), the effective mean normal stress at phase transformation point, p'_T, is expressed as:

$$p'_T = \frac{p'_0}{1 + (A_T - \frac{1}{3})M_T} \tag{5.48}$$

By Following the same routine, the effective mean normal stress at peak point, p'_p, is given

by:

$$p'_p = \frac{p'_0}{1 + (A_p - \frac{1}{3})M_p} \tag{5.49}$$

By substituting (5.48) into (5.40) and (5.49) into (5.41), ϵ_{sT} and ϵ_{sp} are determined. Since parameters $A_T, \epsilon_{sT}, A_p, \epsilon_{sp}$ and A_L, ϵ_{sL} are all defined, the three parameters in (5.39), a_1, a_2 and a_3 may be determined by solving 3 simultaneous equations, and therefore the pore water pressure parameter A at any stress strain state may be determined by (5.39). Fig.5.18 shows the A - ϵ_s data for Test UT12. Both the measured values and the generated A - ϵ_s curve are shown in the figure and it is seen that the two matched very well. The excess pore water pressure at any stress-strain state may be calculated from (5.45) once the A value is determined.

5.3.4.3 The Shear Induced Excess Pore Ice Pressure in Frozen Sand

As discussed in **5.2.3**, the creep process of frozen soil is neither fully "drained" nor fully "undrained". It is partially drained. As assumed in **5.2.3**, if the frozen sand was sheared with no volume change, the Shear Induced Excess Pore Ice Pressure, SIEPIP, would be the same as the excess pore water pressure in the same sand in an unfrozen state as given by (5.41). If the frozen sand was sheared under a fully "drained" condition, there would be no SIEPIP. The real value of SIEPIP lies between these two extreme cases. The accurate calculation of SIEPIP starts with the calculation of the Shear Induced Excess Pore Water Pressure, SIEPWP, as discussed in the previous section. The creep process was separated into

a number of small strain steps. At the beginning of each step, the SIEPIP was first assumed to be equal to the SIEPWP, then adjusted by analyzing the volumetric creep (consolidation) that occurred during the step. Therefore, an iterative calculation was needed. Actually, the shear induced excess ice pore pressure, may be expressed as

$$\Delta u_f = F \Delta u \tag{5.50}$$

where F is a parameter depending on the relative magnitude of the rates of shear and volumetric creep. For the soil and the stress range tested here, it is about 0.8 to 0.95 at the beginning of the shear creep and gradually decreases as the volumetric creep continues. It also changes with changing total stress. Fig.5.20 shows the calculated SIEPIP for Test MST5. It is seen from the figure that at small strains the SIEPIP is close to the fully undrained condition, and at large strains it is close to the fully drained condition.

Once Δu_f is determined, p'_{fro} may be obtained from

$$p'_{fro} = p'_{fro0} + \Delta p - \Delta u_f \tag{5.51}$$

where p'_{fro0} is the effective mean normal stress at the beginning of the shear creep, and Δp is the increase of the total mean normal stress.

5.4 THE SHEAR CREEP RATE - EXCESS ICE SHEAR STRESS RELATIONSHIP

The effective shear stress, q'_{fro}, may be determined from **ESRS** once p'_{fro} is known.

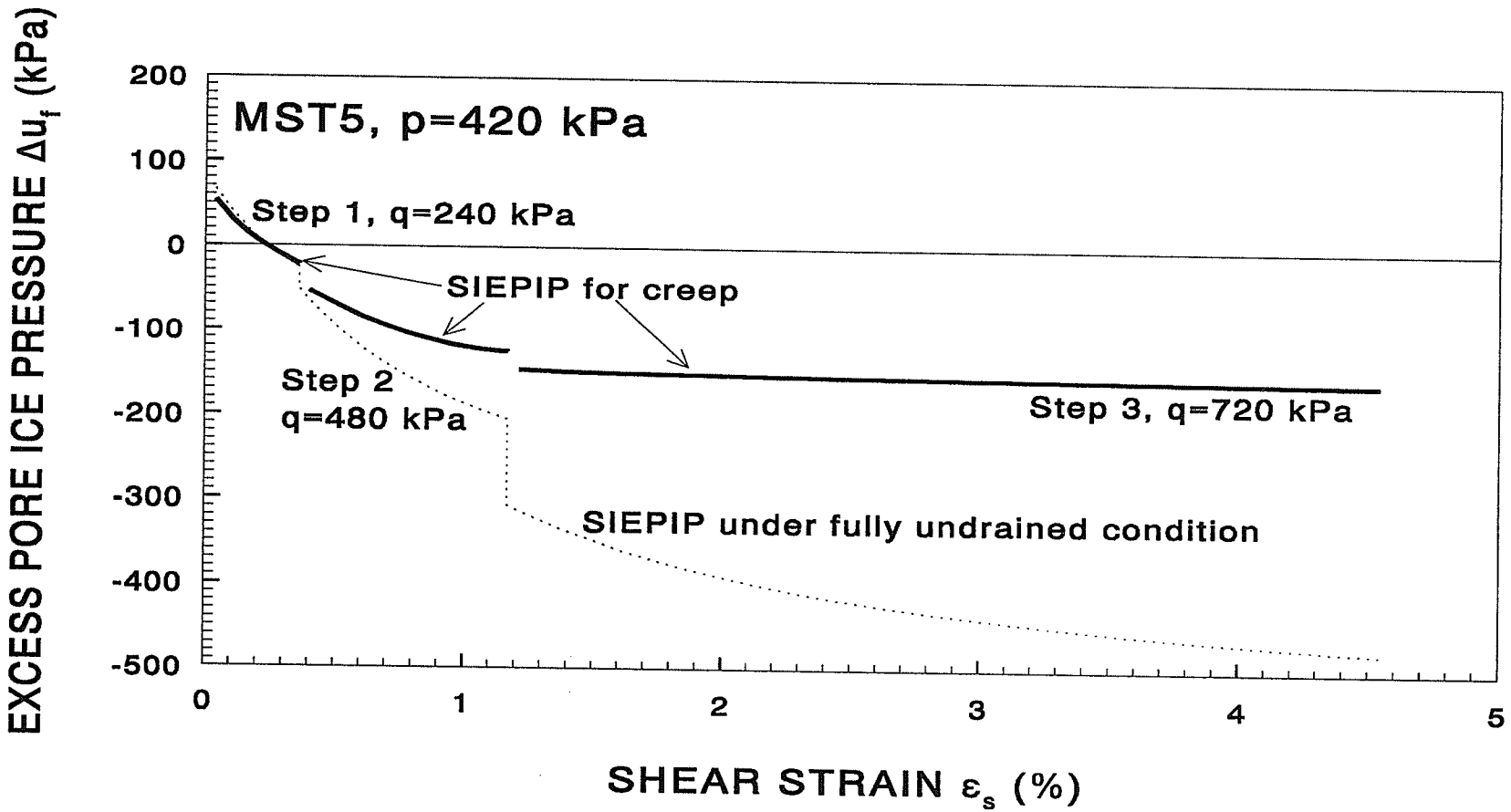

Fig.5.20 Calculated shear induced excess pore ice pressure of the frozen sand in the creep process, Test MST5.

Since the total shear stress, q, is known in the creep process, the excess ice shear stress, q_e, which is the driving force of shear creep, may be obtained from

$$q_e = q - q_{fro} \tag{5.52}$$

Fig.5.21 shows the excess ice shear stress versus the shear creep rate, $\dot{\epsilon}_{sc}$, for MST4 on a log - log scale. It is seen that all the data fell within a narrow band except for a few points during the early period of each loading step. This indicates that a power law relationship may exist between q_e and $\dot{\epsilon}_{sc}$. Fig.5.22 gives the q_e vs. $\dot{\epsilon}_{sc}$ data for MST5. The same pattern of the q_e - $\dot{\epsilon}_{sc}$ relationship occurred. By putting all the data on a single figure as shown in Fig.5.23, it is seen that all the data fell in a narrow band except those points from the starting periods of each stress increment. By ignoring those points, which will be dealt with later on, a power law relationship between $\dot{\epsilon}_{sc}$ and q_e was obtained as:

$$\dot{\epsilon}_{sc} = \dot{\epsilon}_{s0}\left(\frac{q_e}{q_0}\right)^n \tag{5.53}$$

where $\dot{\epsilon}_{s0} = 4.6623\times10^{-14}$ 1/s , $q_0 = 1.0$ kPa , and $n = 2.573$ for the frozen sand tested at the given temperature of -3°C. The test data collected here covered the stress range of q from 0 to 1000 kPa and p from 0 to 420 kPa, and the shear creep strain rate, $\dot{\epsilon}_{sc}$, from 10^{-11} to 10^{-6} 1/s. For stress-strain states outside of this range, the correlations should be confirmed experimentally before they are applied.

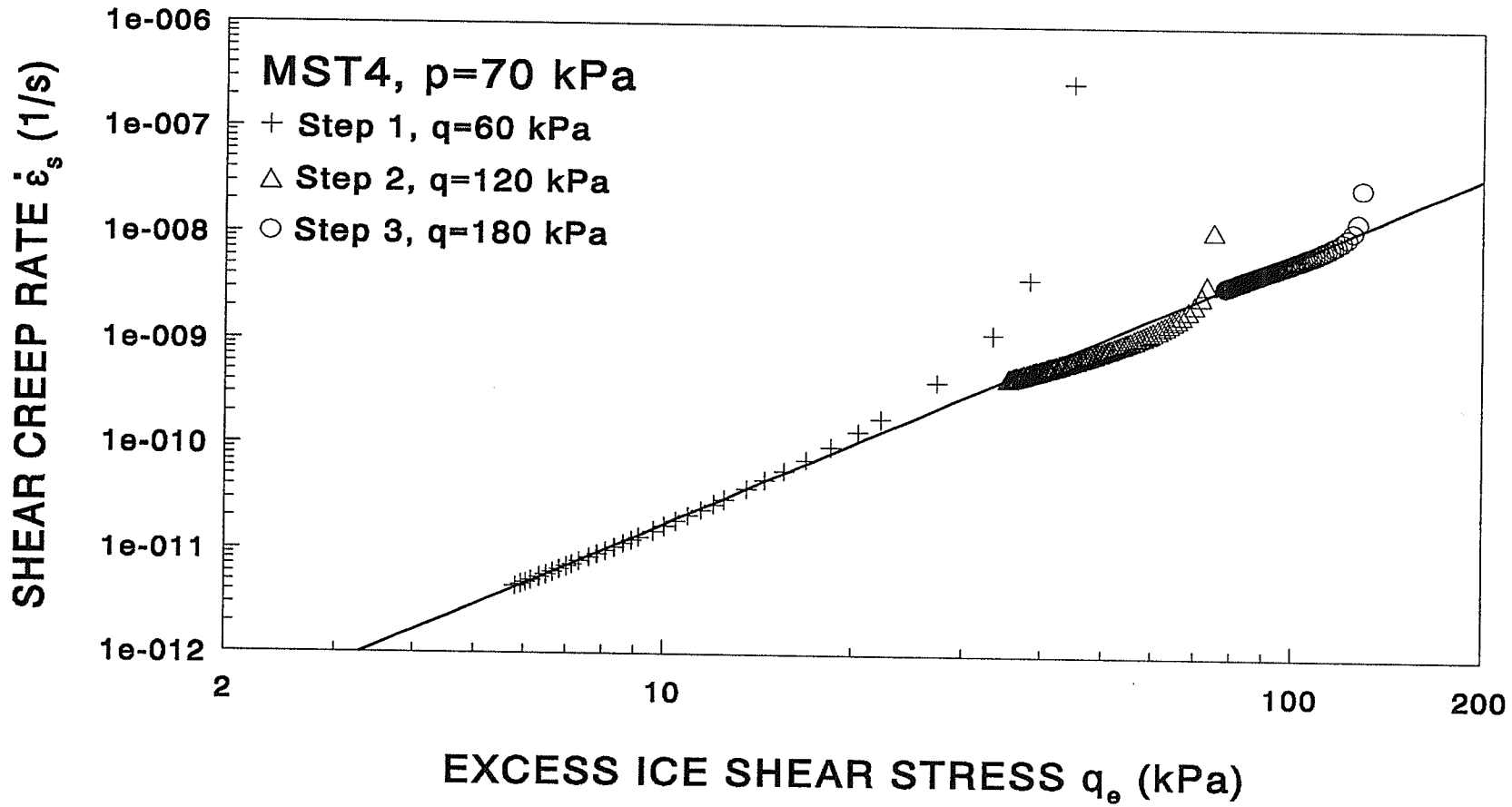

Fig.5.21 The relationship between shear creep rate and excess ice shear stress of frozen sand in a long-term triaxial creep test: Test MST4.

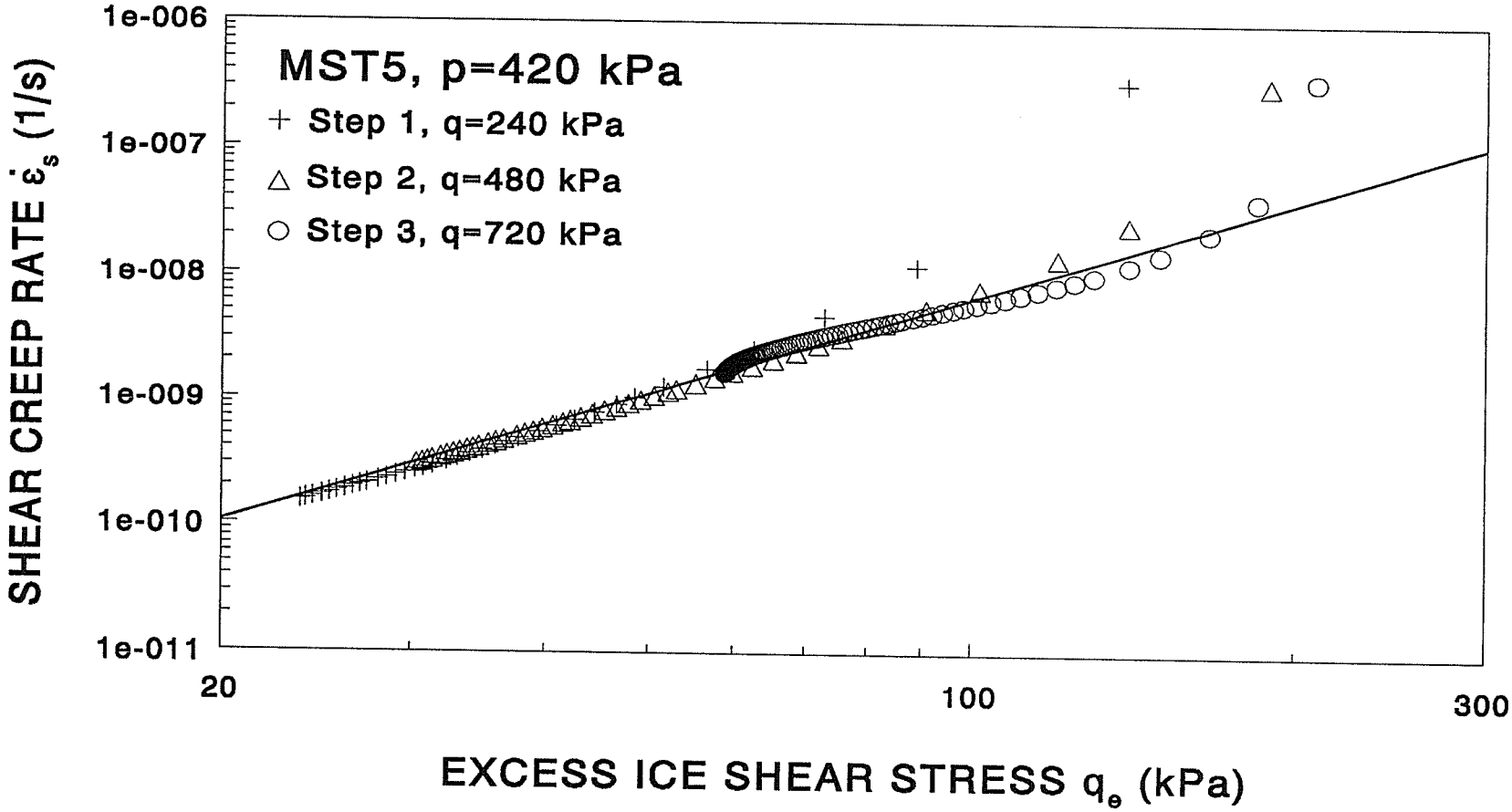

Fig.5.22 The relationship between the shear creep rate and the excess ice shear stress of the frozen sand in a long-term triaxial creep test: Test MST5.

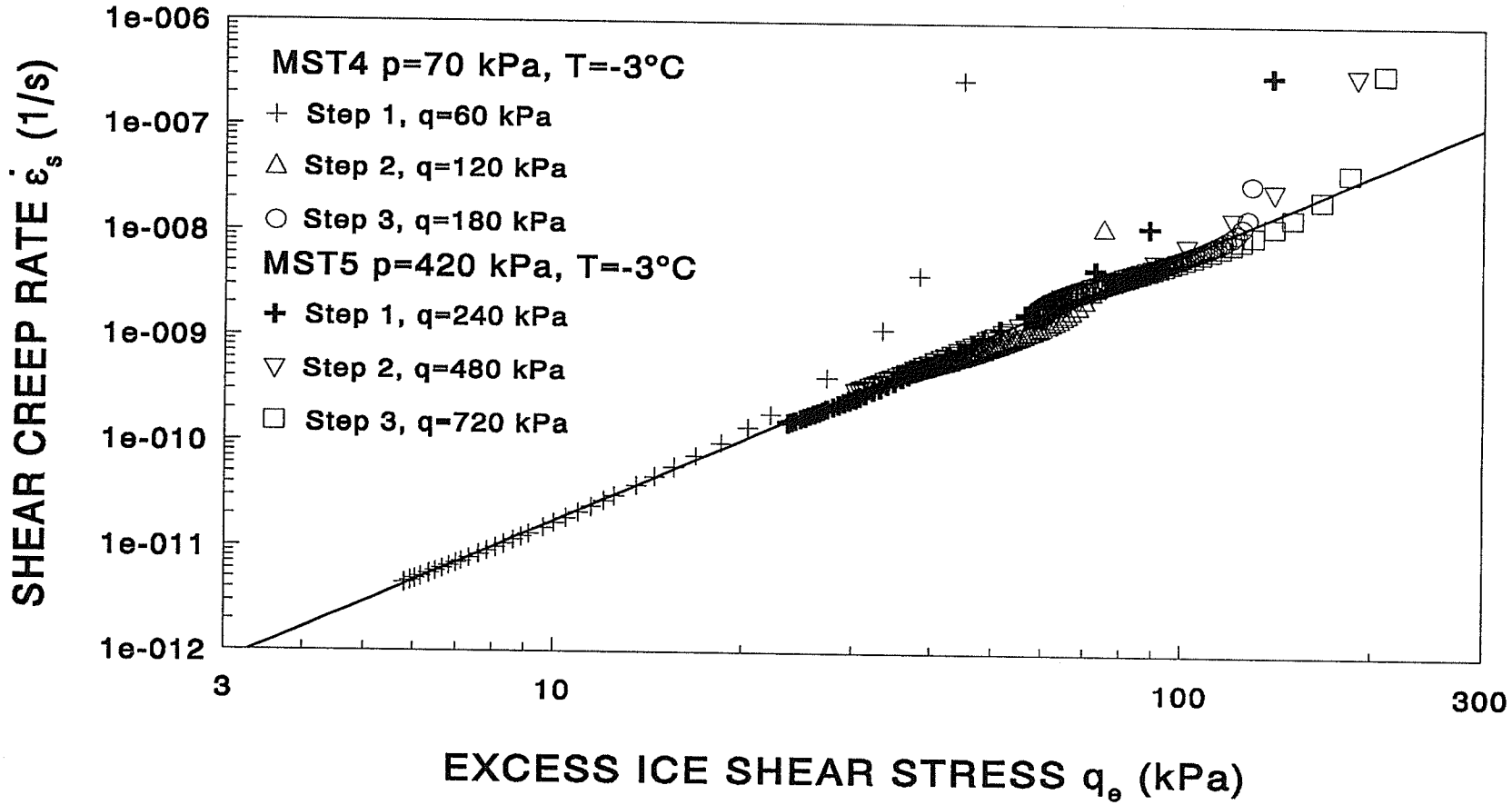

Fig.5.23 Summary of the data of shear creep rate versus excess ice shear stress data for MST4 and MST5.

5.4.1 The Transition Factor

As mentioned in the previous section, the $\dot{\epsilon}_{sc}$ - q_e relationship does not follow (5.48) at the start of a stress increment. This period lasts about 15 - 20 hours depending on the magnitude of the stress increment and several other factors. A suggested physical interpretation of this phenomenon is that the mechanism of creep during this period is different from that of the later periods. Consider pore ice from a metallurgical point of view. The frozen sand tested was at -3°C, and the corresponding homologous temperature of the pore ice was

$$T_h = \frac{T}{T_m} = \frac{273-3}{273} = 0.989 \qquad \textbf{(5.54)}$$

From a metallurgical point of view, the ice was very "hot" since its temperature was very close to its melting point. Fig.5.24 shows a "schematic version of a deformation map for a polycrystalline metal. It illustrates the stress/temperature regimes within which dislocation and diffusional creep processes are expected to be dominant. The boundaries between adjacent fields represents the conditions under which two or more processes may contribute equally towards the overall creep deformation." (Evans and Wilshire, 1985). Pore ice is also a polycrystalline material and has a similar creep mechanism. It is seen from the figure that the stress/temperature condition ($\sigma/E = 10^{-8}$-10^{-5}, and $T/T_m = 0.99$) for the pore ice tested falls within the lower right portion of the figure, which corresponds to diffusional creep (Nabarro-Herring creep). When diffusional creep dominates, the rate of molecule migration under stress

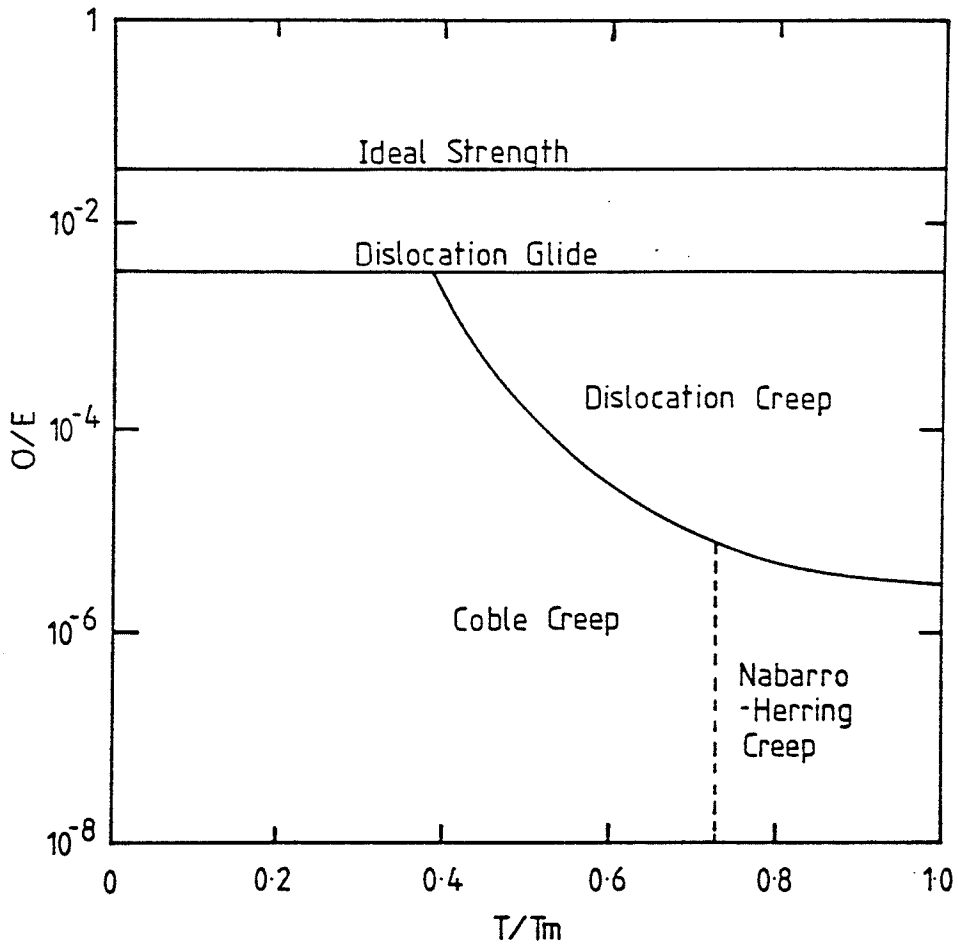

Fig.5.24 A schematic version of a deformation map for a polycrystalline metal illustrating the stress/temperature regimes within which dislocation and diffusional creep process may be expected to be dominant. The boundaries between adjacent fields then represent the conditions under which two or more processes contribute equally towards the overall steady-state creep rate. (After, Evans and Wilshire, 1985)

is proportional to the stress level and independent of time, and the relationship between the creep rate and the stress acting on the medium is usually expressed by a power law such as (5.53). The stress used here should be the average stress actually sustained by the ice matrix, which is the excess ice shear stress, q_e. It should be noted, however, that at the start of the creep process, due to the heterogeneity of the polycrystalline structure of the pore ice which produces localized stress concentration, not only diffusion, but also dislocation and grain-boundary sliding may contribute significantly to the creep process. The creep caused by dislocation and grain boundary sliding does not follow the same law as that followed by diffusional creep, and this may explain to a certain extent why (5.53) does not fit the data obtained from the starting period of the creep process. As the creep process goes on, the heterogeneity of the pore ice decreases dramatically and the diffusional creep becomes dominant quickly, and therefore the $\dot{\varepsilon}_{sc}$ - q_e relationship approaches (5.53). A new increment of total stress will increase the ice shear stress and may also cause some disturbances to the structure of the pore ice and trigger a new round of dislocation and grain boundary sliding activity. The data from three short-term constant p triaxial creep tests was used to find a solution to this issue. The creep curves from MST7, MST8 and MST9 are shown in Fig.5.7, Fig.5.8, and Fig.5.9. Each step of stress increment lasted for about 24 hours. By applying (5.53) to these data, the $\dot{\varepsilon}_{sc}$ - q_e relationship for these tests are shown in Fig.5.25, Fig.5.26 and Fig.5.27. As shown in the figures, the shear creep rate immediately after the loading is significantly higher than that predicted by (5.53). A **Transition Factor**, F_t, which is defined as the ratio of the transient creep rate over the creep rate predicted by (5.53), was introduced to model this behaviour. The $\dot{\varepsilon}_{sc}$ - q_e relationship may now be

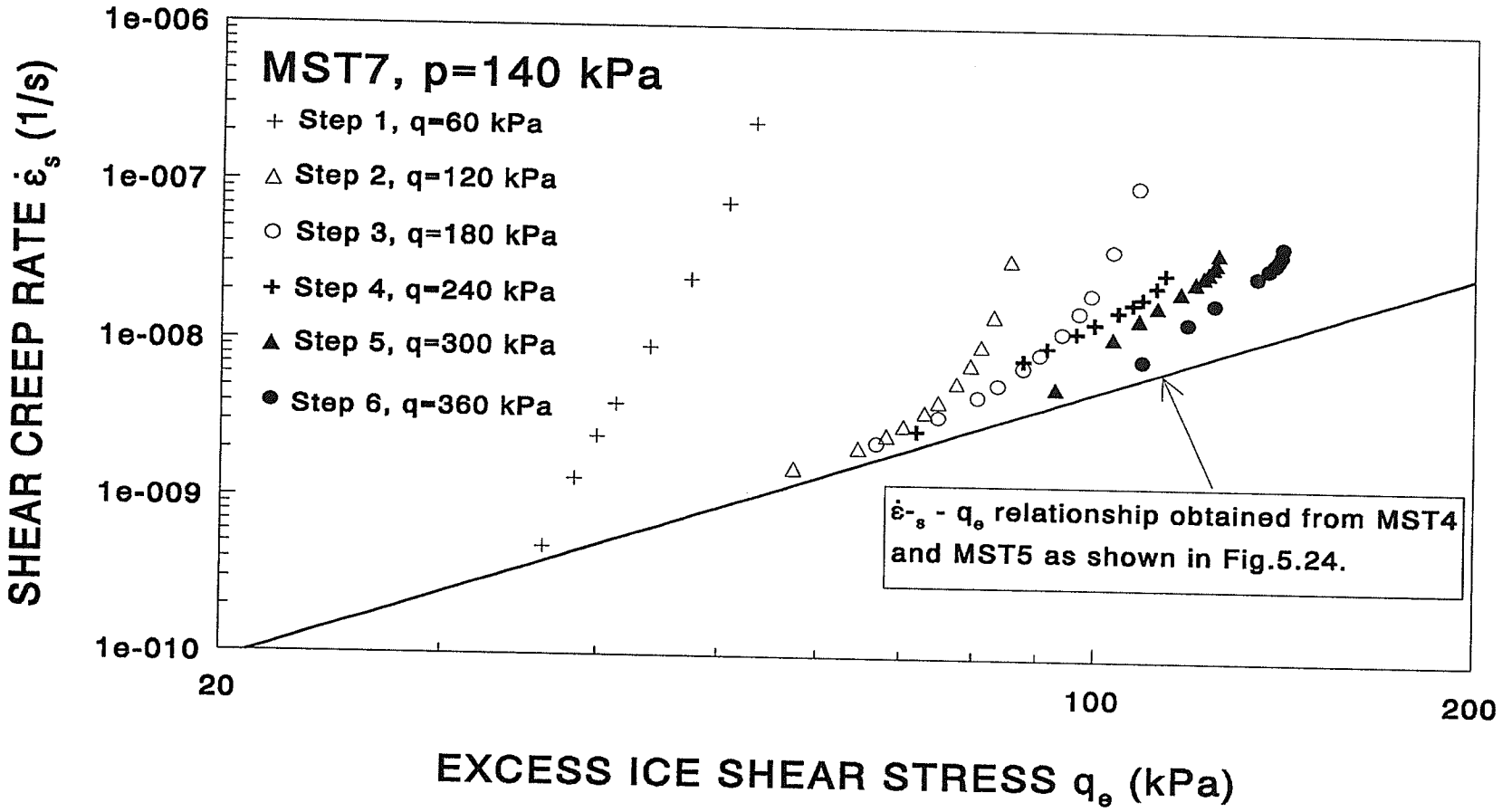

Fig.5.25 The relationship between shear creep rate and excess ice shear stress for short-term creep test MST7.

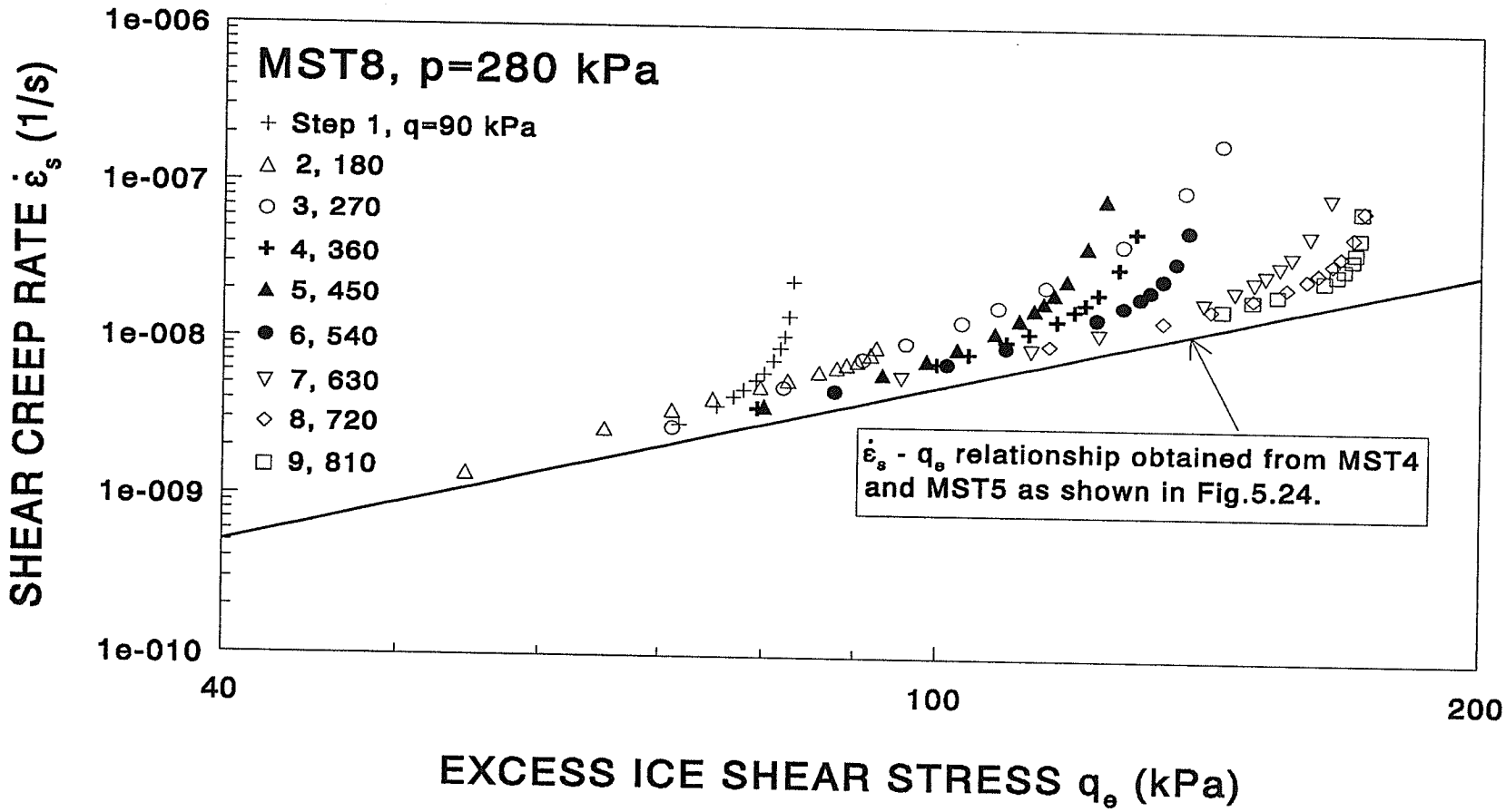

Fig.5.26 The relationship between shear creep rate and excess ice shear stress for short-term creep test MST8.

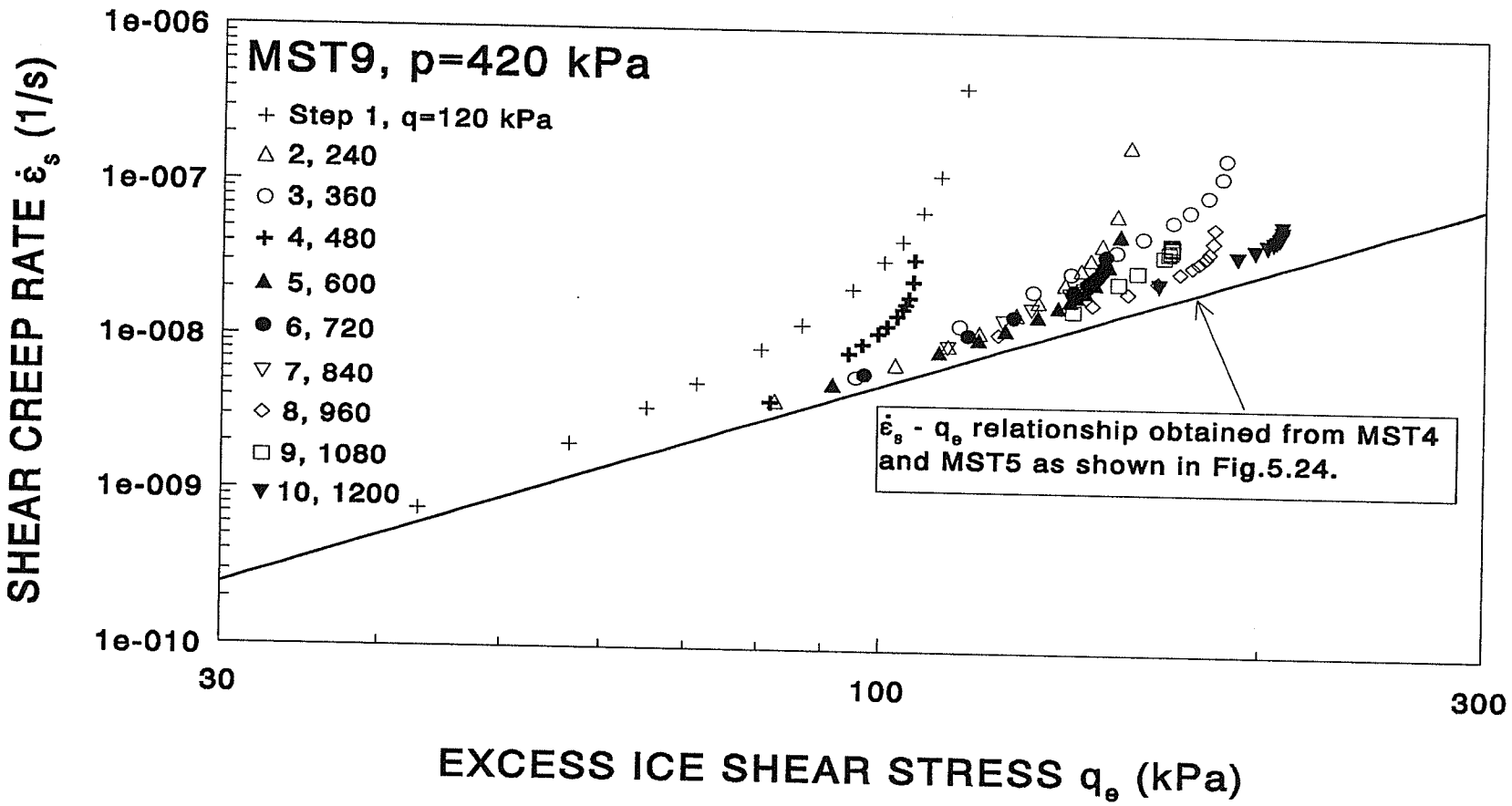

Fig.5.27 The relationship between shear creep rate and excess ice shear stress for short-term creep test MST9.

rewritten as

$$\dot{\epsilon}_{sc} = F_t \dot{\epsilon}_{s0} \left(\frac{q_e}{q_0} \right)^n \tag{5.55}$$

The transition factor, F_t, depends on the magnitude of the contribution from diffusional creep relative to the contributions from the dislocation creep and grain boundary sliding, which is characterized by the level of the ice shear stress and the heterogeneity of the pore ice. There has been very little study of this phenomena and an empirical method was used here. The transition factor F_t may be expressed as

$$F_t = exp\left[\left(\frac{\epsilon_{st}}{\epsilon_s - \epsilon_{sb}} \right)^{\eta} \right] \tag{5.56}$$

where ϵ_{sb} is the shear strain before the new stress increment was applied, and ϵ_{st} is called the **Transient Strain**, and η is a constant to be determined experimentally. Immediately after the application of a new stress increment, we have

$$\epsilon_s - \epsilon_{sb} = \Delta \epsilon_{si} \tag{5.57}$$

and

$$F_t = exp\left[\left(\frac{\epsilon_{st}}{\Delta \epsilon_{si}} \right)^{\eta} \right] \tag{5.58}$$

where $\Delta \epsilon_{si}$ is the instantaneous shear strain caused by the stress increment, and may be determined by (5.2). The transition factor F_t attains its maximum value at this moment, and

decreases to unity quickly as the shear strain increases. The **Transient Strain**, ϵ_{st}, is a measure of how quickly F_t approaches unity, and may be determined experimentally. The relationship between the **Transition Factor** F_t and the shear strain is given in Fig.5.28, Fig.5.29 and Fig.5.30 for tests MST7, MST8 and MST8 respectively. Since the data available for calibrating F_t was very limited, (5.56) was reduced to a simpler form by assuming η=1. The **Transient Strain**, ϵ_{st}, was related to the increment of the shear stress Δq as shown in Fig.5.31. It was empirically expressed by a straight line as:

$$\epsilon_{st} = \epsilon_{stq} \frac{\Delta q}{\Delta q_0} \qquad \textbf{(5.59)}$$

where $\epsilon_{stq} = 0.015973\%$, and Δq_0 =100 kPa as determined from the data shown in Fig.5.31.

The factors which affect F_t are more than just the stress increment Δq. Actually, for a given Δq, F_t at the early loading steps is generally greater than that at the later loading steps. One explanation to this phenomenon may be that the initial heterogeneity of the pore ice structure has a greater effect on the earlier loading steps than on the later ones because the initial heterogeneity gradually dissipates as the creep process goes on. The Δq - F_t relationship given by (5.54) is an empirical correlation based on the very limited data available here, and should be used with caution. More work needs to be done on this subject.

5.5 SUMMARY

This chapter discussed the behaviour of frozen soil under shear. Based on the fact that ice can carry shear stress, the concept of effective shear stress in unfrozen soil presented by

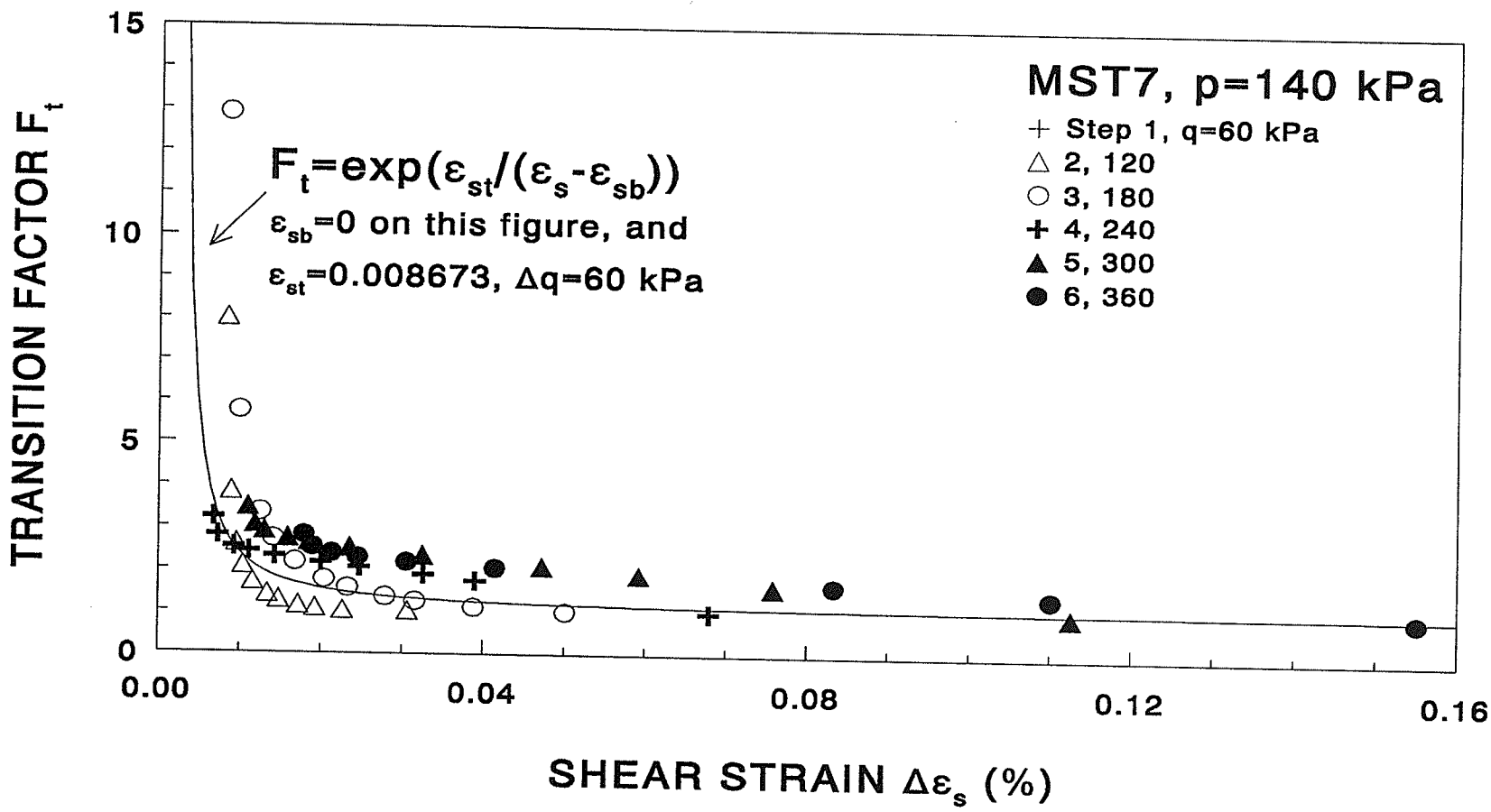

Fig.5.28 Relationship between transition factor, F_t, and shear strain increment, $\Delta\epsilon_s = \epsilon_s - \epsilon_{sb}$, for short-term creep test MST7.

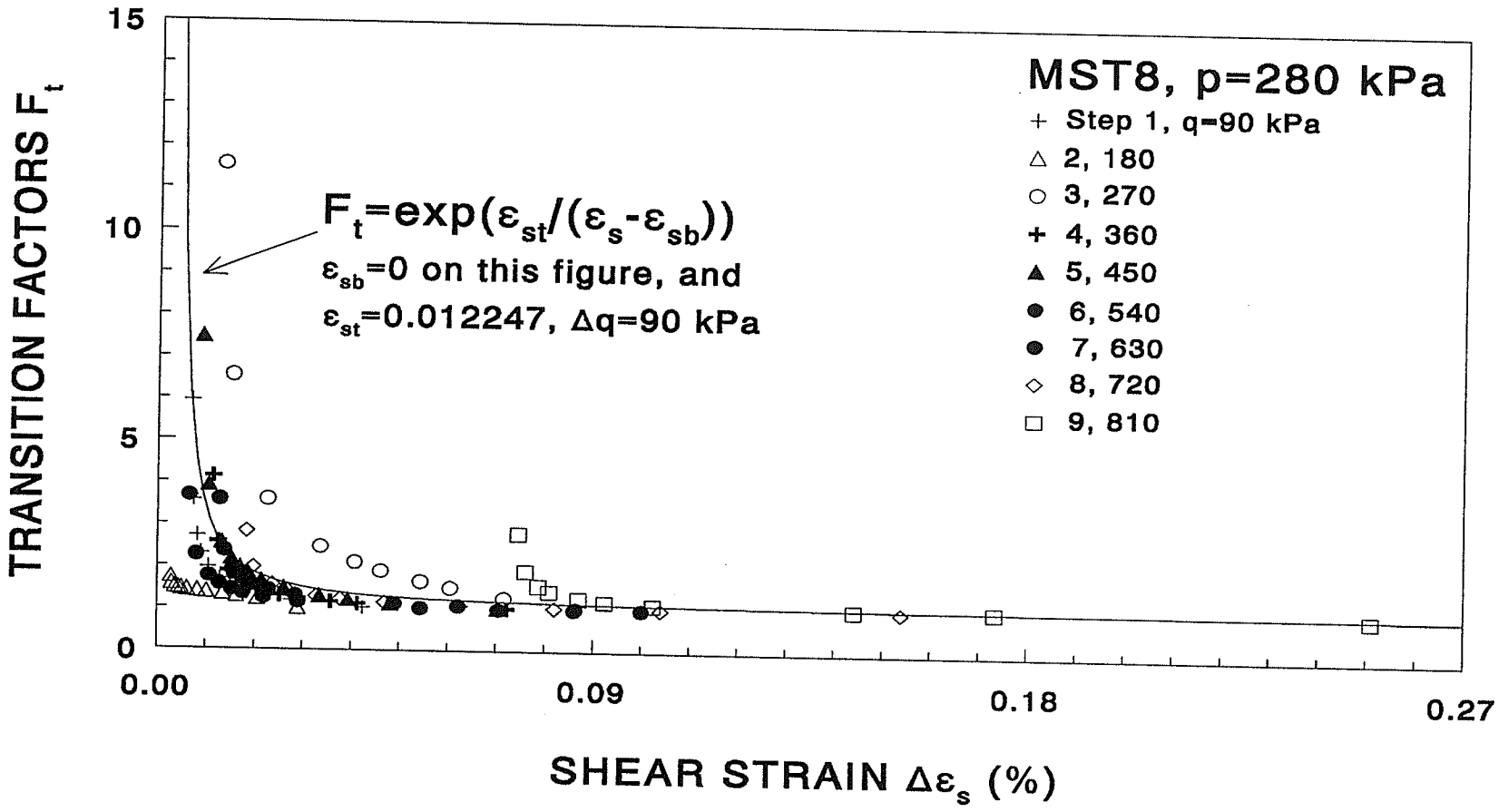

Fig.5.29 Relationship between transition factor, F_t, and shear strain increment, $\Delta\epsilon_s = \epsilon_s - \epsilon_{sb}$, for short-term creep test MST8.

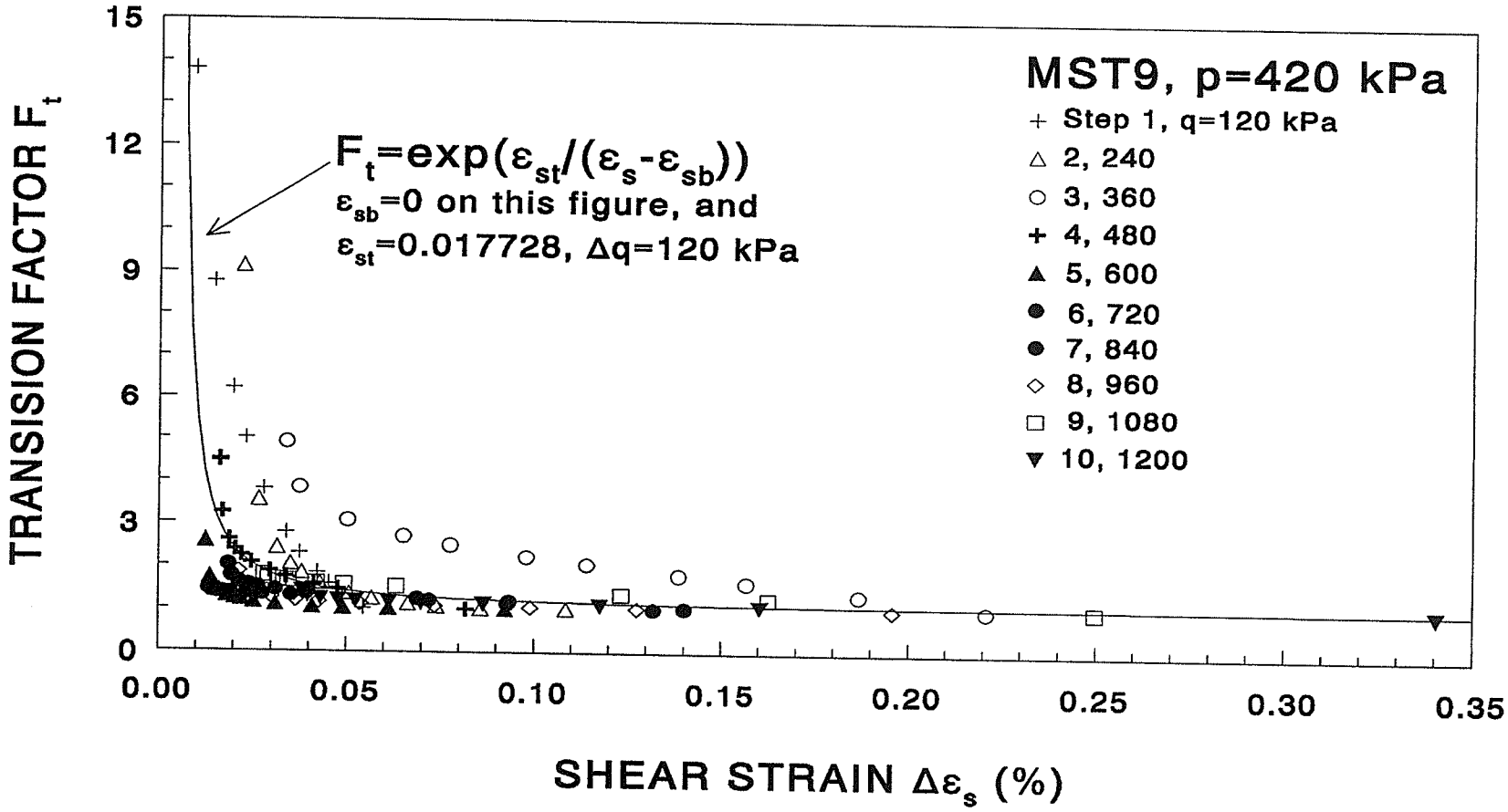

Fig.5.30 Relationship between transition factor, F_t, and shear strain increment, $\Delta\epsilon_s = \epsilon_s - \epsilon_{sb}$, for short-term creep test MST9.

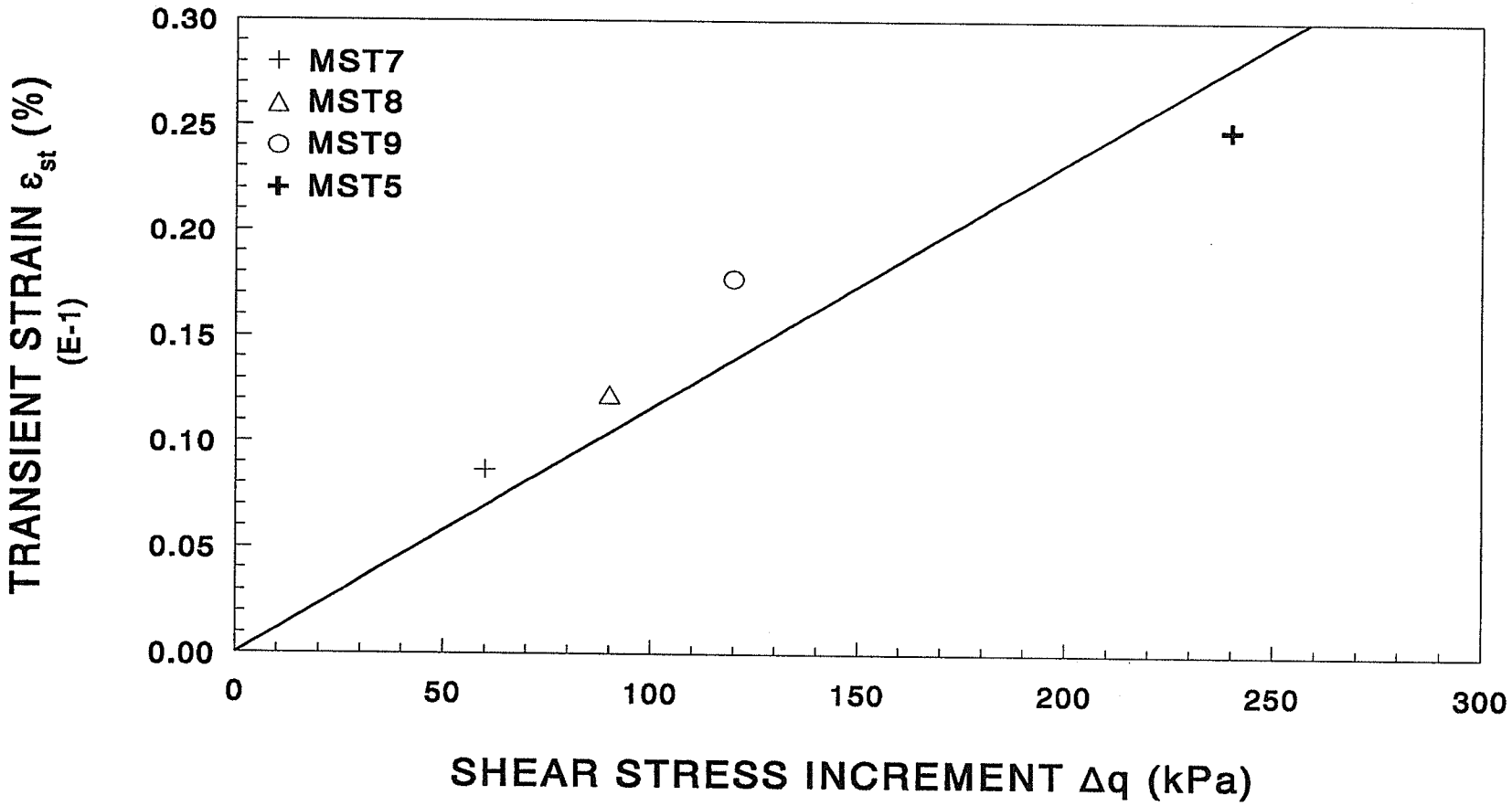

Fig.5.31 Relationship between transient strain, ϵ_{st}, and shear strain increment, Δq.

Terzaghi (1923) was extended to frozen soil. A generalized effective stress and an excess ice shear stress for frozen soil were defined. It is suggested that the excess ice shear stress is the true driving force of shear creep. A relationship between the effective mean normal stress, effective shear stress and shear strain was established by combining the data from both triaxial creep tests on frozen soil and conventional triaxial tests on the same soil in an unfrozen state. The shear induced excess pore ice pressure was determined by considering the joint effect of dilatancy of the soil skeleton and the volumetric creep of frozen soil. A power law relationship between the excess ice shear stress and the rate of shear creep was established, and a transition factor was introduced to account for the different modes of creep of the pore ice during the early period of loading. Together with the consolidation model developed in Chapter 4 for frozen soil under isotropic compression, the strain-hardening, strain-softening creep model developed in this chapter for frozen soil under shear stress produces a method to predict the deformation of frozen soil under a general stress-strain state and loading process. The next chapter will discuss the verification and the application of the model.

CHAPTER 6

THE MODEL AND ITS VERIFICATION

6.1 SUMMARY OF VOLUMETRIC AND SHEAR MODELS

The creep models developed in the previous two chapters, when coupled, provide a solution for the creep rate of a frozen soil as a function of the imposed general stress state. They are based on the concept that creep is the result of the existence of excess pore ice stress and that the pore ice can sustain a certain ultimate shear stress which is a function of its temperature. The total stress acting on frozen soil is shared between the pore ice and the soil skeleton, and it is tacitly assumed that the portion of the stress sustained by the soil skeleton is equal to the stress that it can sustain in an unfrozen state, and that the shear induced excess pore ice pressure in frozen soil would be the same as the shear induced excess pore water pressure in unfrozen soil under the same conditions.

6.1.1 Volumetric Creep Under Isotropic Compression

The governing equation for volumetric creep rate under isotropic compression is (4.12)

$$\dot{\epsilon}_{vc} = \frac{\alpha \epsilon_{vc0}}{t^*}\left(\frac{p}{p_0}\right)^m U_c^{\,1-\frac{1}{\alpha}}(1-U_c)^{1+\frac{1}{\alpha}} \qquad \textbf{(4.12)}$$

where α=0.6, ϵ_{vc0}=0.0402 %, p_0=1.0 kPa, and m=0.7661 for the soil tested. The expressions

for t^* is:

$$t^* = t_0^* \left(\frac{p}{p_0} \right)^{\theta} \tag{4.13}$$

where t_0^*=2.8323 hour, θ=0.81532 for the soil tested. The expression for U_c is:.

$$U_c = \left(1 - \frac{p_e}{p} \right)^m \left(\frac{p - K_i \epsilon_v}{p - p_e - K_i \epsilon_v} \right) \tag{4.11}$$

in which the instantaneous bulk modulus, K_i, was determined as 9.0×10^6 kPa.

6.1.2 Shear Creep

The governing equation for shear creep developed in Chapter 5 gives the rate of shear creep strain, $\dot{\epsilon}_{sc}$ as a function of the excess ice shear stress, q_e

$$\dot{\epsilon}_{sc} = F_t \dot{\epsilon}_{s0} \left(\frac{q_e}{q_0} \right)^n \tag{5.55}$$

where $\dot{\epsilon}_{s0} = 4.6623 \times 10^{-14}$ 1/s , $q_0 = 1.0$ kPa , and $n = 2.573$ for the soil tested. The transition factor, F_t, was expressed as

$$F_t = exp\left[\left(\frac{\epsilon_{stq} \dfrac{\Delta q}{\Delta q_0}}{\epsilon_s - \epsilon_{sb}} \right)^{\eta} \right] \tag{5.56}$$

where η=1.0, $\epsilon_{stq} = 0.016\%$, and Δq_0 =100 kPa for the soil tested.

The key variable in the governing equation, (5.55), is the excess ice shear stress, q_e. Two relationships are required to determine q_e.

(1) A relationship between the shear strain, ϵ_s, the effective shear stress, q'_{fro}, and the effective mean normal stress, p'_{fro}, of the frozen soil, which is called as the effective shear resistance surface, **ESRS**. It is mathematically expressed as

$$q'_{fro} = q_L^* \frac{\epsilon_s^2 + c\epsilon_s^{\beta}}{\epsilon_s^2 + d^2} \qquad \textbf{(5.26)}$$

(2) A relationship between the shear induced excess pore ice pressure, Δu_f, and the shear induced excess pore water pressure, Δu, for the soil in an unfrozen state.

$$\Delta u_f = F \Delta u \qquad \textbf{(5.50)}$$

Parameter F depends on the relative magnitudes of the rates of shear and volumetric creep. For the soil and the stress range tested here, it was about 0.8 to 0.95 at the beginning of the shear creep and gradually decreased to about 0.15 to 0.4 as the volumetric creep continued.

Once Δu_f is determined, the effective mean normal stress, p'_{fro} is known, the effective shear stress, q'_{fro} is then determined from (5.26), and the excess ice shear stress, q_e, is determined as

$$q_e = q - q_{fro} \qquad (5.52)$$

Once q_e is determined, shear creep strain, ϵ_{sc}, is obtained by integrating shear creep rate, $\dot{\epsilon}_{sc}$, over time. For each time step, q_e is calculated first, and then the increment of shear strain for that time-step is calculated from (5.55).

6.2 VERIFICATION OF THE MODEL

In order to verify the model and examine its predictive capability, the model was used to predict the creep curves of several triaxial creep tests that had been carried out experimentally. The test procedures and the results of these tests were discussed in Chapter 3 and section **5.3.1**.

As a first step, the model was used to predict the creep curves of tests MST4 and MST5. These data were used to calibrate a part of the model. However, since the calibration involved some assumptions and correlations which were independent of these data, a comparison was deemed to be useful. The experimental and the predicted creep curves for tests MST4 and MST5 are shown in Fig.6.1 and Fig.6.2. As can be seen from the figures, the experimental and the predicted creep curves matched very well. This indicates that the model which was calibrated using the data from both frozen and unfrozen soil tests is able to represent the results of individual creep tests.

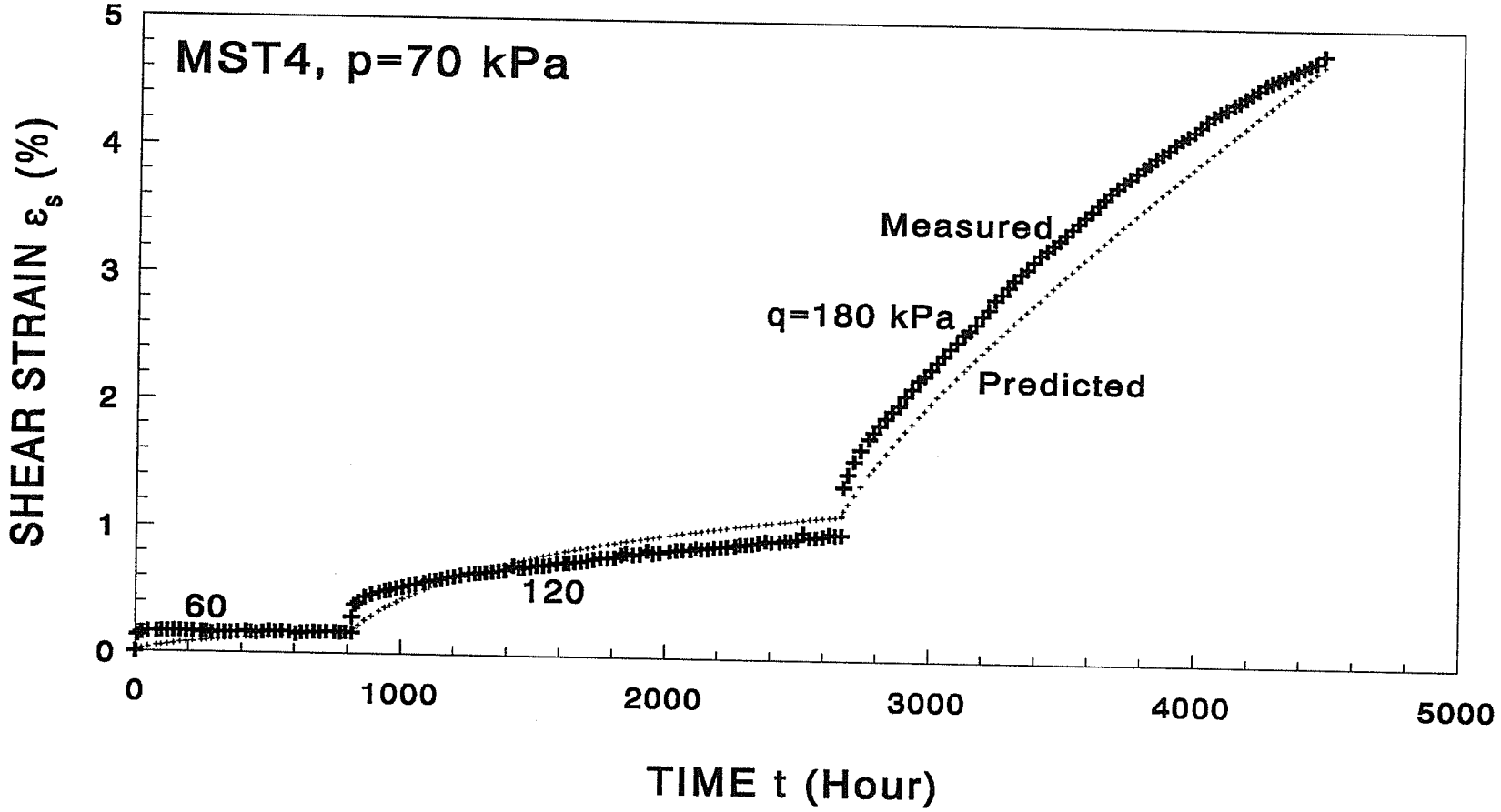

Fig.6.1 Measured and predicted shear strain versus time for constant *p*, multi-stage, triaxial creep test MST4.

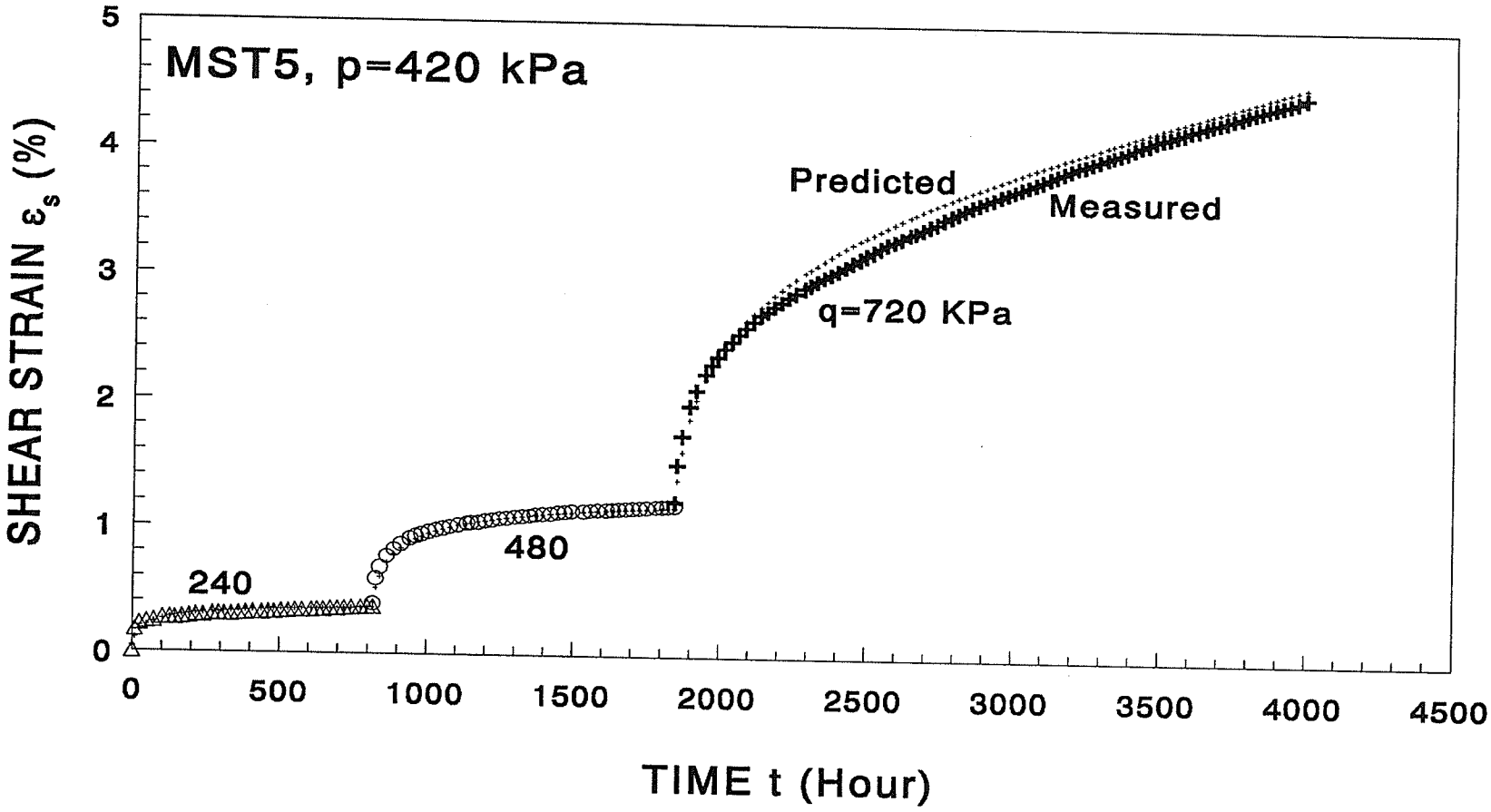

Fig.6.2 Measured and predicted shear strain versus time for constant *p*, multi-stage, triaxial creep test MST5.

The shear induced excess pore ice pressure was analyzed using the method and the correlations developed in **5.3.4**. The calculated shear induced excess pore ice pressure, SIEPIP, for MST4 is represented by the solid lines in Fig.6.3, while the calculated shear induced excess pore ice pressure of the same sand if it were sheared under a fully undrained condition is also shown in the figure by the fine broken line. The pore water pressures were calculated using the pore water pressure parameter A obtained from the undrained test data discussed in **5.3.4.1**. It is seen from the figure that SIEPIP was positive at the start of the creep process, and gradually changed to negative as the shear strain continued. This was because the frozen sand was contractive at small shear strains but expansive at large shear strains. It is also seen from the figure that at the start, the value of SIEPIP was close to the that obtained under a fully undrained condition, while at large shear strain, it was significantly smaller than that obtained under a fully undrained condition. This was because at the starting period the dissipation of SIEPIP due to volumetric creep was less significant than at large strains.

The second step was to use the model to predict the creep process of three independent constant p triaxial creep tests that were not used in the calibration. The experimental and the predicted creep curves for MST1, MST2 and MST3 are shown in Figs.6.4, 6.5 and 6.6 respectively. As shown in the figures, the experimental and the predicted shear strains matched fairly well. The relative difference between the experimental and the predicted shear strains was as high as 100% at some locations where the strain was small. However, the overall relative difference was less than 20%. Considering the scatter of the data from the tests on frozen sand and the limited resources available to develop this model,

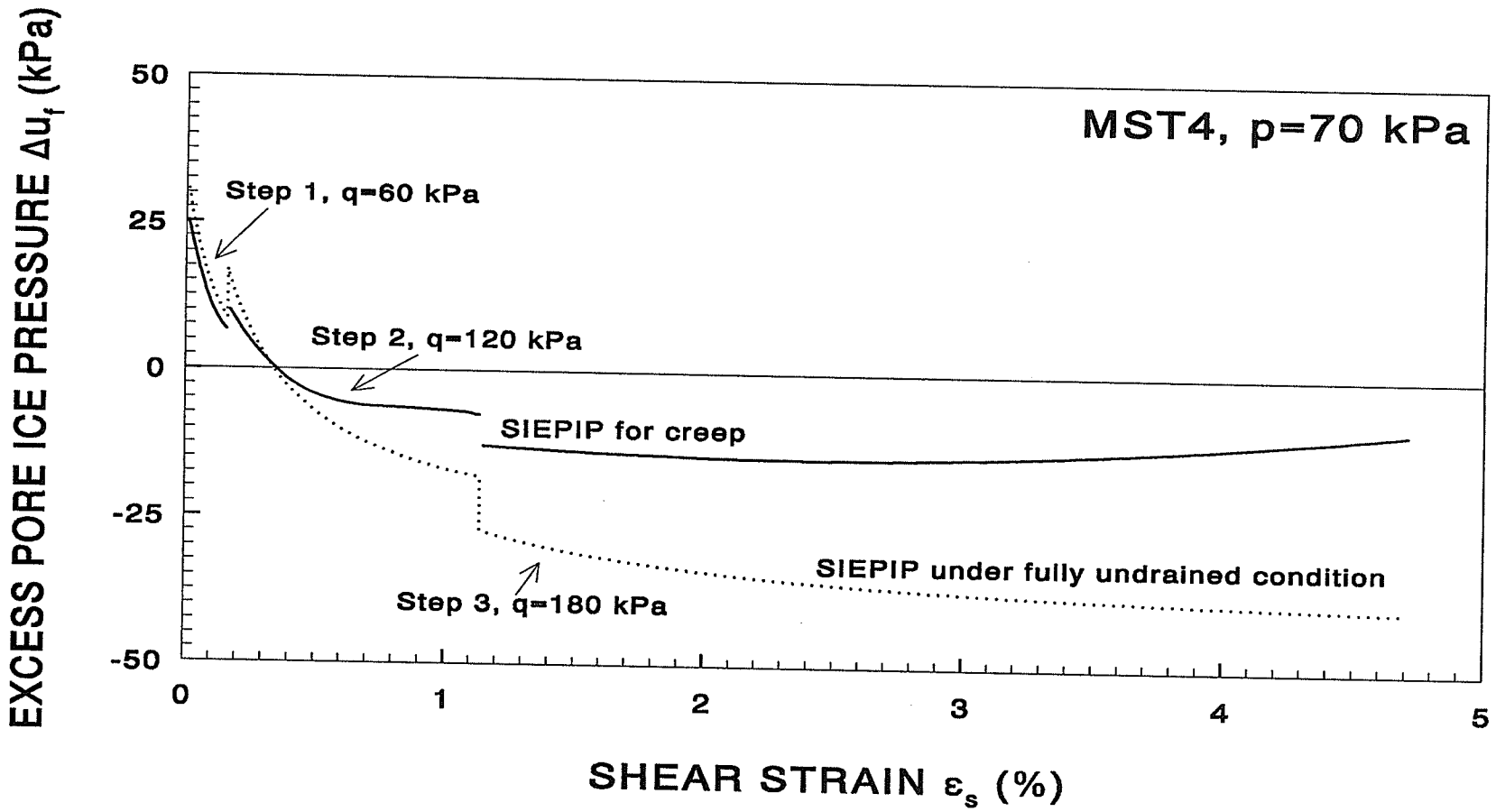

Fig.6.3 Calculated shear induced excess pore ice pressure of the frozen sand, Test MST4.

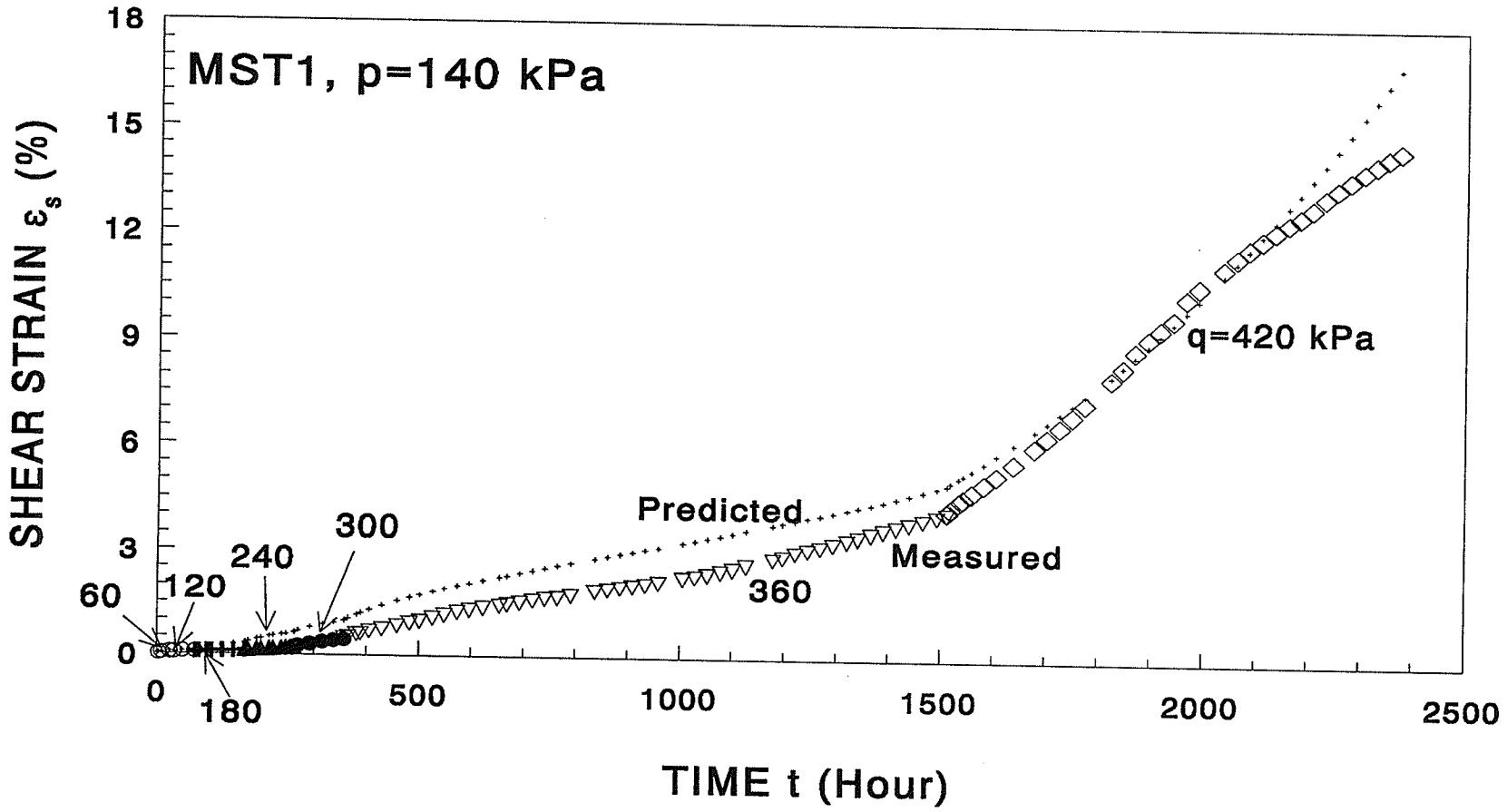

Fig.6.4 Measured and predicted shear strain versus time for constant *p*, multi-stage, triaxial creep test MST1.

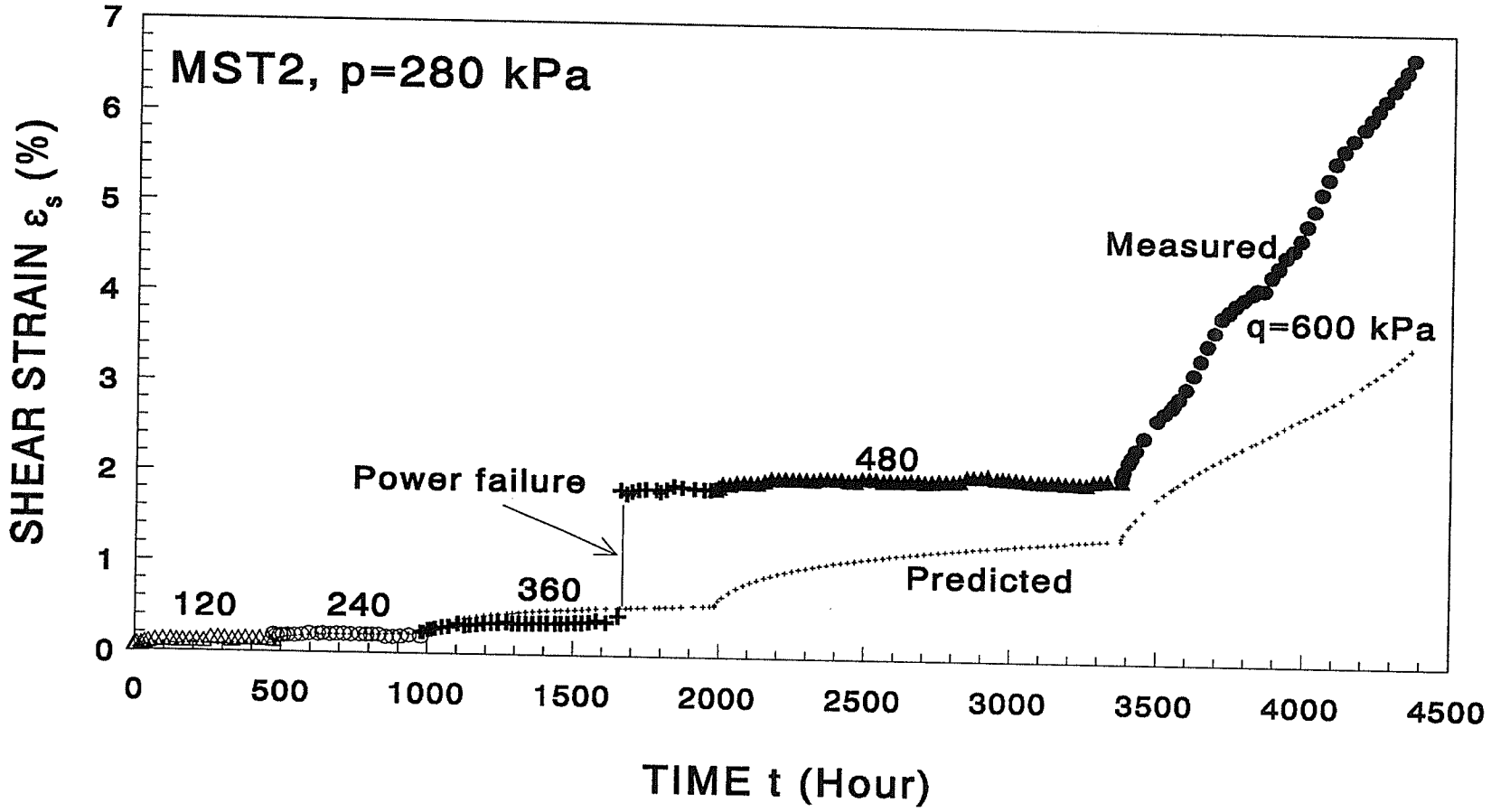

Fig.6.5 Measured and predicted shear strain versus time for constant p, multi-stage, triaxial creep test MST2.

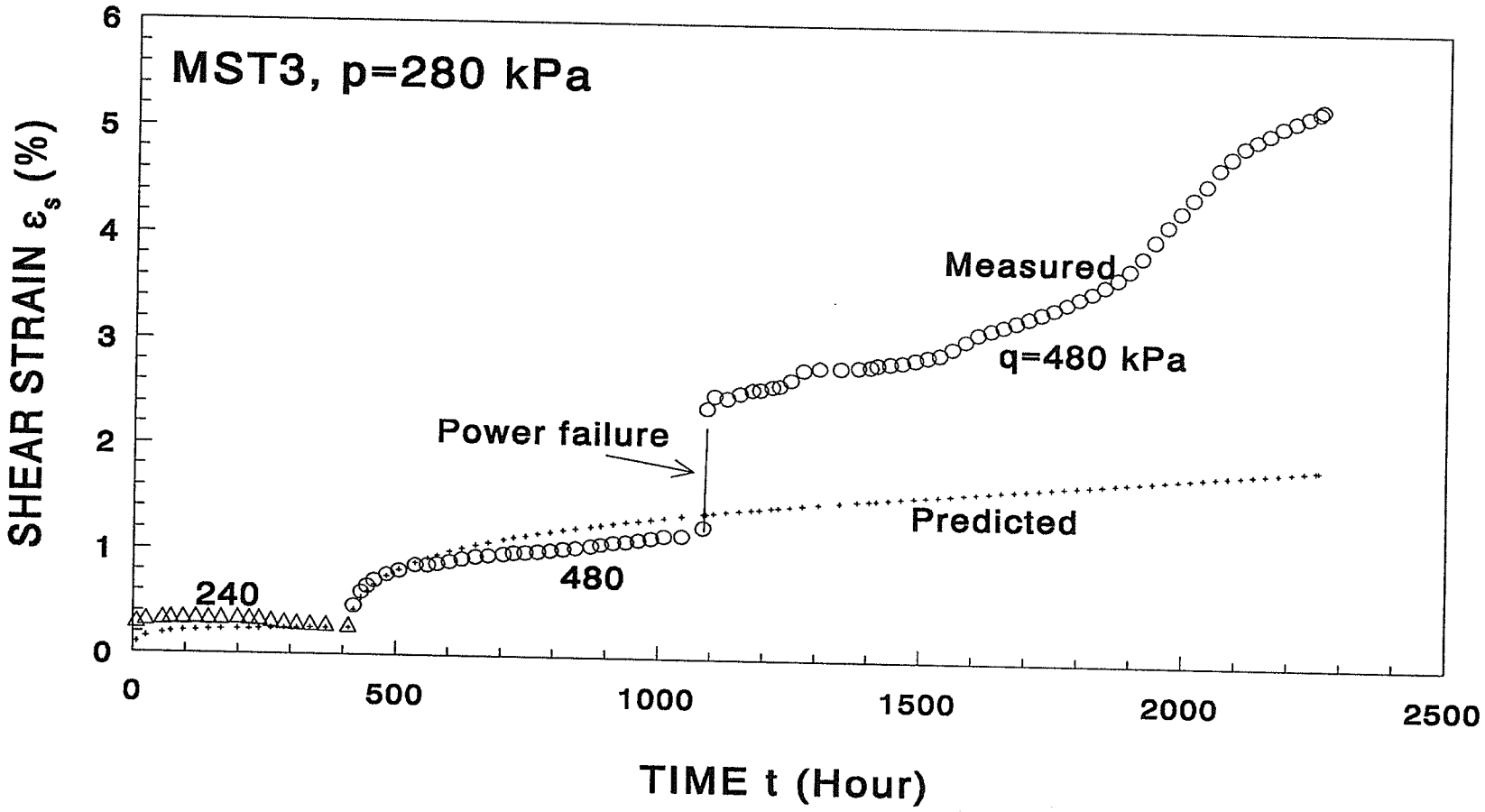

Fig.6.6 Measured and predicted shear strain versus time for constant *p*, multi-stage, triaxial creep test MST3.

this suggests that the predictive capability of the model is quite good. The effect of the mean normal stress on the shear creep of frozen sand was clearly shown by comparing the results of MST1 and MST2. The initial densities of the two samples were approximately the same, but MST2 was subjected to shear stresses which were four times as high as that of MST1. Test MST1 was carried out for about 2400 hours (100 days), and had a cumulative shear strain of 14.5%, while test MST2 lasted for about 4400 hours (183 days), and had a cumulative shear strain of only 6.7%. The explanation for the lower cumulative shear strain despite the higher shear stress level and longer time duration is that MST2 had a higher level of mean normal stress which resulted in higher effective mean normal stress. That is, its resistance to shear was greater. Consequently the excess ice shear stress, which was the driving force of the shear creep, was actually lower in test MST2 than in MST1 even though the total shear stress in MST2 was higher. The present model is thus able to rationally explain this apparent anomalous phenomenon.

The calculated shear induced excess pore ice pressures for MST1, MST2 and MST3 are shown in Fig.6.7, Fig.6.8 and Fig.6.9 respectively. In the figures, the thick solid lines represent the shear induced excess pore ice pressure in frozen soil, while the fine broken lines show the shear induced excess pore ice pressure under the condition of no volume change during creep. The fine broken lines were obtained by calculating the shear induced excess pore water pressure using the pore water pressure parameter, A, determined from the tests on unfrozen sand. The difference between the solid and the broken lines represent the reduction of the excess pore ice pressure due to volumetric creep.

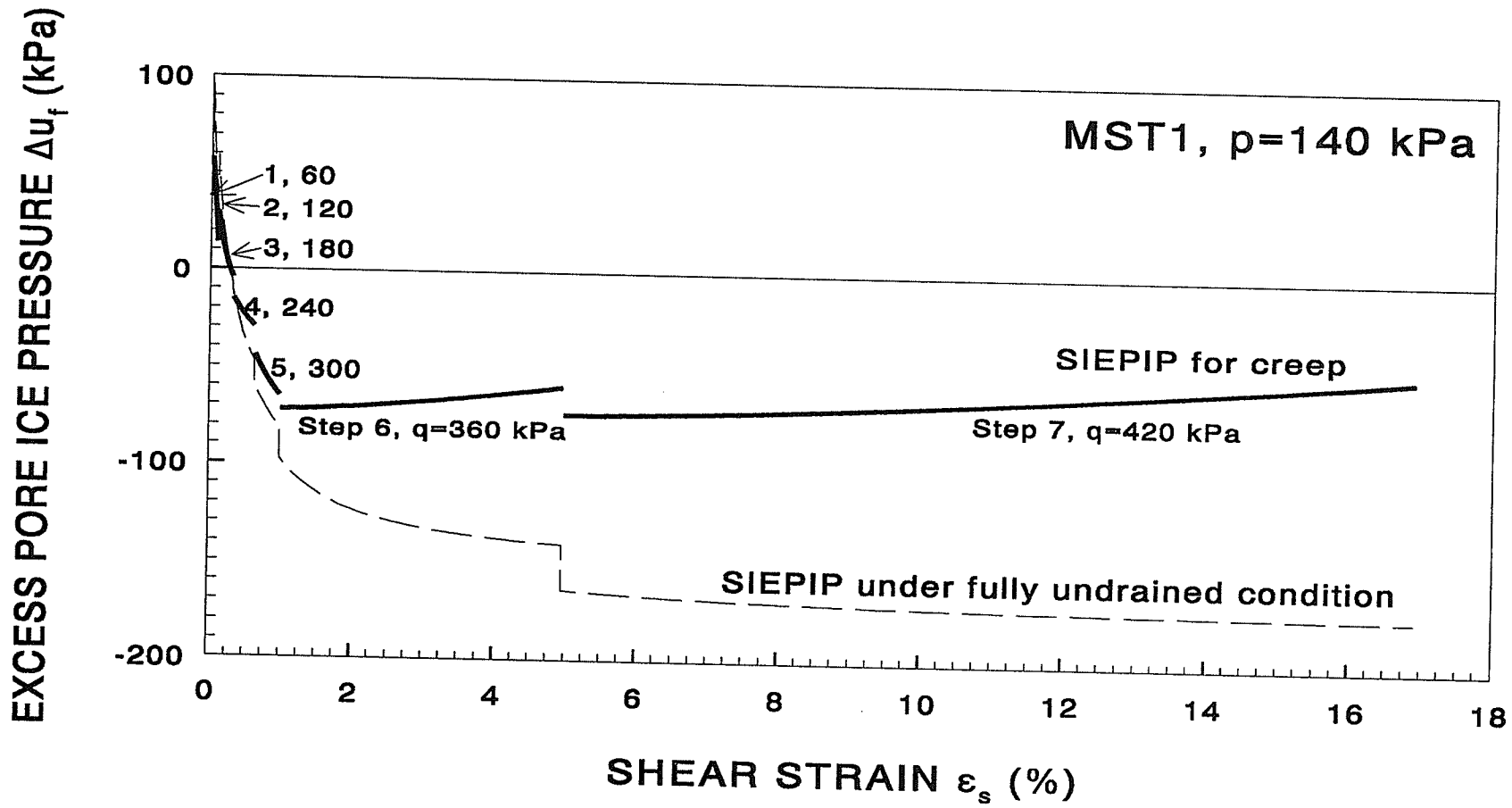

Fig.6.7 Calculated shear induced excess pore ice pressure of the frozen sand, Test MST1.

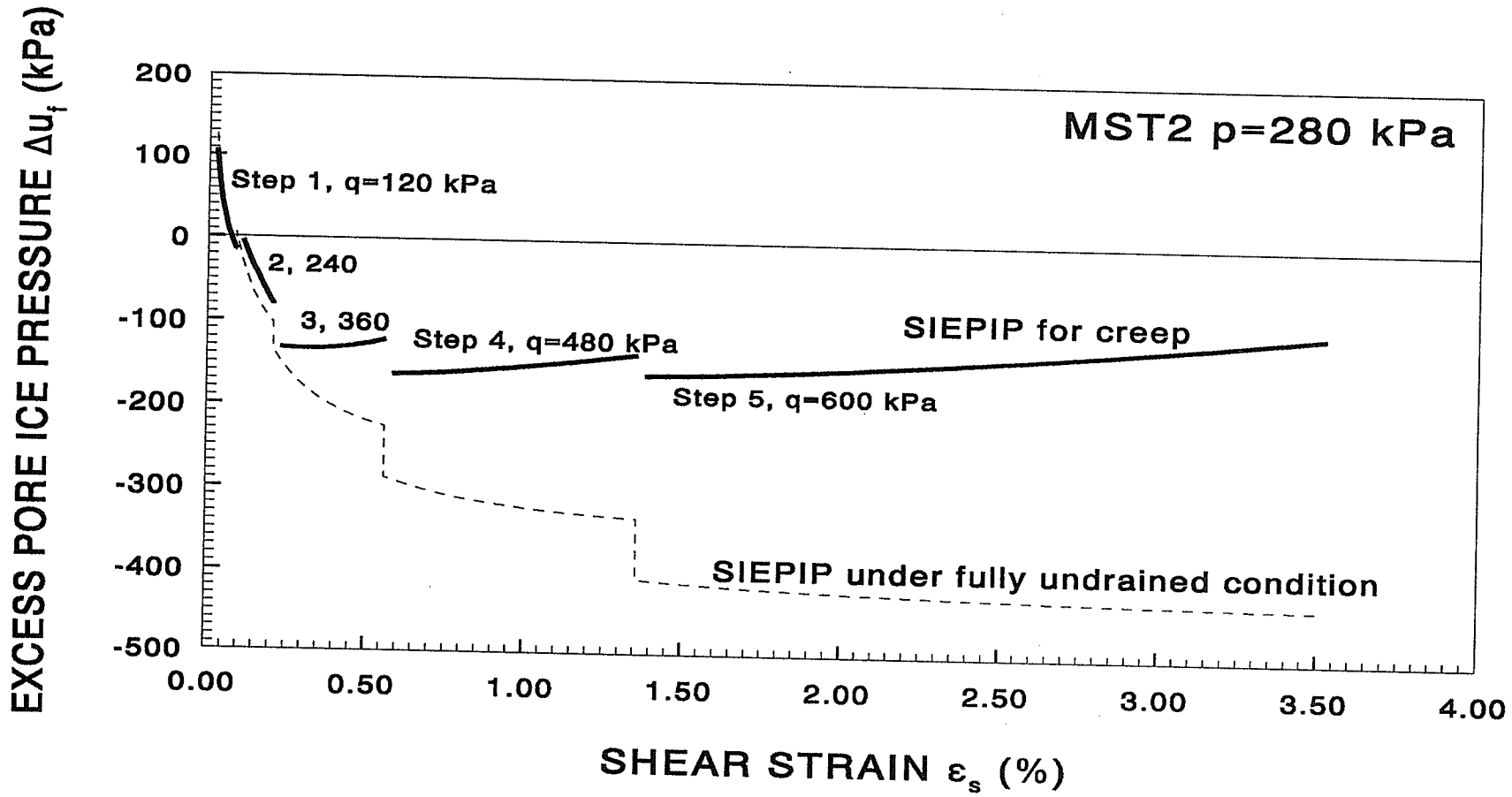

Fig.6.8 Calculated shear induced excess pore ice pressure of the frozen sand, Test MST2.

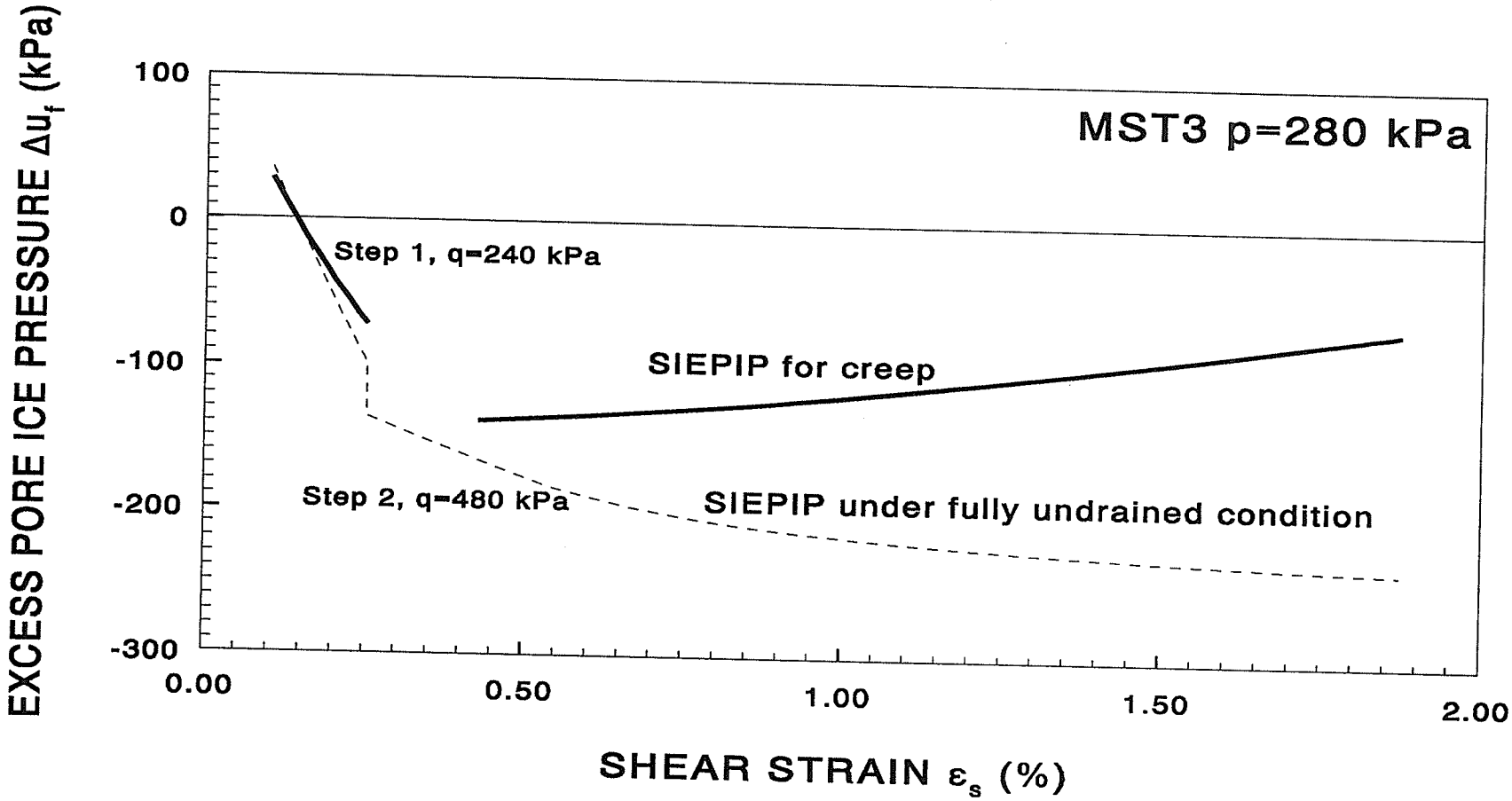

Fig.6.9 Calculated shear induced excess pore ice pressure of the frozen sand, Test MST3.

The last example in examining the predictive capability of the model was to use it to predict the performance of a constant σ_3 creep test, MST13. As mentioned previously, the model was calibrated using data from constant p tests. Test MST13 lasted 8400 hours (350 days) and the cumulated shear strain was only 2.8%. The experimental and the predicted creep curves for MST13 are shown in Fig.6.10. It is seen from the figure that the predicted creep curve is a fairly good representative of the experimental creep curve. The relative difference between the measured and the predicted shear strain was less than 10% for the time period of 0 to 6000 hours. While the calculated shear strain was 20 - 25% higher than that of measured for the time period later than 6000 hours. The temperature variation and the high stresses in these three loading steps may be part of the reason for the high relative difference.

The shear induced excess pore ice pressures for Test MST13 is given in Fig.6.11. The larger symbols represent the shear induced excess pore ice pressure, SIEPIP, while the smaller symbols show SIEPIP under fully undrained condition. The excess ice shear stress in test MST13 was considerably lower than that of the other tests, such as MST1 and MST4. Since MST13 was a constant σ_3 test, the total mean normal stress, p, increased at the same time as the shear stress, q, was increased. This resulted in an increasing effective mean normal stress, p'_{fro}, and effective shear stress, q'_{fro}. Therefore the newly increased q at each loading step was partially offset by the increasing q'_{fro}, and the actual increase of excess ice shear stress q_e was smaller than the increment of total shear stress, q. Also, the initial density of sample MST13 was a little higher than that of the others, and therefore this specimen was a little "stiffer" than the others. These two factors may account for the fairly small shear strain that occurred over such a long period of time.

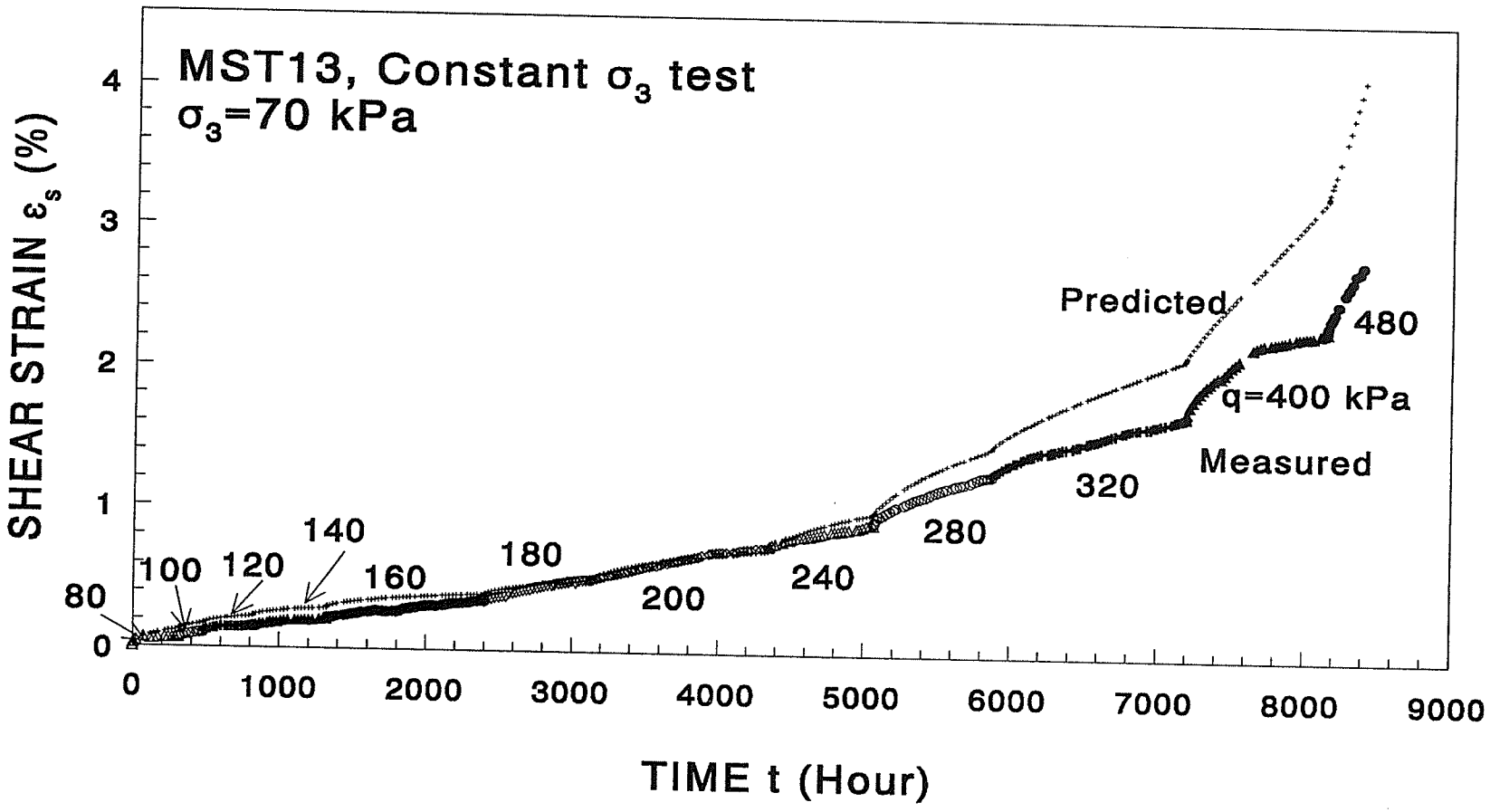

Fig.6.10 Measured and predicted shear strain versus time for constant cell pressure, multi-stage, triaxial creep test MST13.

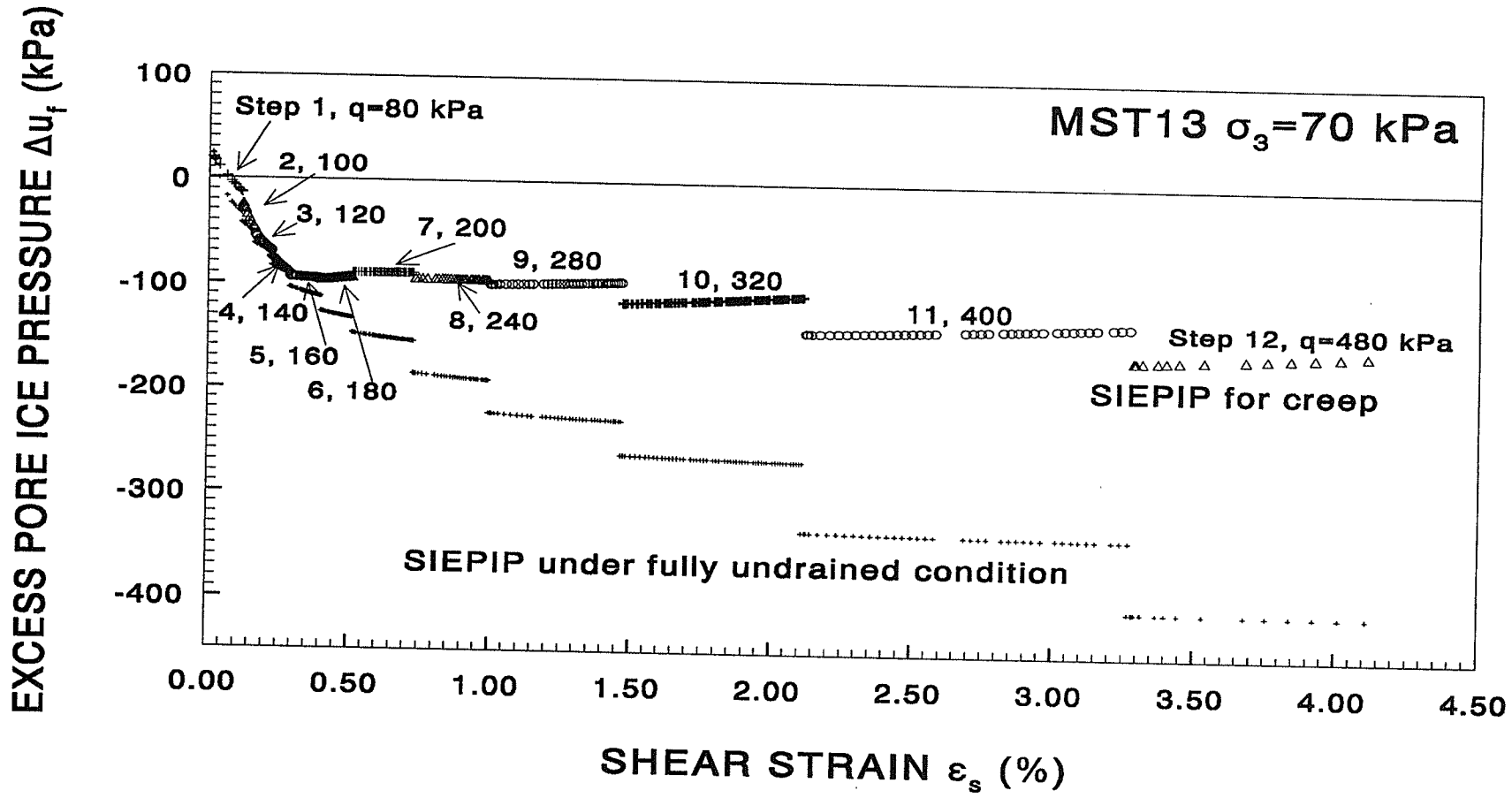

Fig.6.11 Calculated shear induced excess pore ice pressure of the frozen sand, Test MST13.

6.3 GENERALIZATION OF THE MODEL

6.3.1 General Stress-Strain State

The equations developed in the previous chapters were based on the stress and strain states that corresponded to the triaxial test, and the stress and strain components used were $p=(\sigma_1 + 2\sigma_3)/3$, $\epsilon_v = (\epsilon_1 + 2\epsilon_3)$, $q = \sigma_1 - \sigma_3$, and $\epsilon_s = 2(\epsilon_1 - \epsilon_3)/3$. When a general stress-strain state occurs, more general expressions for stress and strain components should be used, for example $p=(\sigma_1 + \sigma_2 + \sigma_3)/3$, $\epsilon_v = (\epsilon_1 + \epsilon_2 + \epsilon_3)$,

$q=\sqrt{\frac{3}{2}}\sqrt{(\sigma_1-p)^2+(\sigma_2-p)^2+(\sigma_3-p)^2}$ and $\epsilon_s=\sqrt{\frac{2}{3}}\sqrt{(\epsilon_1-\frac{1}{3}\epsilon_v)^2+(\epsilon_2-\frac{1}{3}\epsilon_v)^2+(\epsilon_3-\frac{1}{3}\epsilon_v)^2}$. The approach developed by Domaschuk and Wade (1969) may be followed for dealing with a general stress-strain state.

6.3.2 Expressions for Volumetric and Shear Creep Functions

The creep governing equations, (4.12) and (5.55), can also be introduced into the creep model developed by Domaschuk et. al. (1991) in which they utilized a bulk creep function, K_c, and a shear creep function, G_c, in their model. Creep functions K_c and G_c depended on soil properties, the imposed stress state, and time. The bulk creep function, K_c, was defined as

$$K_c=\frac{p}{\epsilon_v} \qquad (6.1)$$

while the shear creep function, G_c was defined as

$$G_c = \frac{q}{\epsilon_s} \tag{6.2}$$

The expressions for K_c, and G_c may be re-developed using (4.12 and (5.55) as follows.

Both volumetric strain, ϵ_v, and shear strain, ϵ_s, may be separated into an instantaneous component and a creep component as

$$\epsilon_v = \epsilon_{vi} + \epsilon_{vc} \tag{4.1}$$

and

$$\epsilon_v = \epsilon_{vi} + \epsilon_{vc} \tag{5.1}$$

as discussed in **4.3** and **5.2.1** respectively.

The volumetric creep strain, ϵ_{vc}, is obtained by integrating (4.12) over time. At any time, t, ϵ_{vc} is expressed as

$$\epsilon_{vc}(t) = \int_0^t \dot{\epsilon}_{vc}(t)dt = \int_0^t \frac{\alpha \epsilon_{vc0}}{t^*} \left(\frac{p}{p_0} \right)^m U_c^{1-\frac{1}{\alpha}} (1-U_c)^{1+\frac{1}{\alpha}} dt \tag{6.3}$$

Since the variables in the right hand side of (6.3) are functions of stress-strain state, the integration is usually carried out numerically rather than analytically.

An expression for the bulk creep function, K_c, discussed in the previously may be derived as follows:

By substituting (4.1) and (4.2) into (6.1), we have

$$\frac{p}{K_c} = \frac{p}{K_i} + \epsilon_{vc} \tag{6.4}$$

Substitute (6.3) into (6.4) and divide both side by p, we have

$$\frac{1}{K_c} = \frac{1}{K_i} + \frac{1}{p}\int_0^t \frac{\alpha \epsilon_{vc0}}{t^*}\left(\frac{p}{p_0}\right)^m U_c^{1-\frac{1}{\alpha}}(1-U_c)^{1+\frac{1}{\alpha}}dt \tag{6.5}$$

by following the same procedure, an expression for the shear creep function, G_c, may derived as:

$$\frac{1}{G_c} = \frac{1}{G_i} + \frac{1}{q}\int_0^t F_t \dot{\epsilon}_{s0}\left(\frac{q_e}{q_0}\right)^n dt \tag{6.6}$$

The creep functions can then be used in a finite element solution with each element characterized by its own set of K_c and G_c values. For example, a general stress-strain relationship may be written as

$$\sigma_{ij} = K_c \epsilon_{kk}\delta_{ij} + 2G_c\left(\epsilon_{ij} - \frac{1}{3}\epsilon_{kk}\delta_{ij}\right) \tag{6.7}$$

where σ_{ij} and ϵ_{ij} are stress and strain tensors respectively, and δ_{ij} is Kronecker delta.

The application of the model developed in this thesis to a real engineering project was beyond the scope of this thesis. Chapter 8 will discuss the future work for further development of this creep model.

CHAPTER 7

ICE - DRY SAND PENETRATION TESTS

7.1 INTRODUCTION

An important concept inherent in the model developed in the previous chapters is that ice is a viscous material that flows under shear stress. Since the rate of flow of ice is low under the stress level usually encountered in engineering practice, the term 'flow' is not usually used. However, experiments on ice showed that when a hard object was forced into ice, the deformation of ice around the hard object followed a similar pattern as water flowing around an obstacle, except that the rate of flow is slow. Sego and Morgenstern (1983, 1985) performed punch indentation tests on ice and developed a flow law for the rate of punch indentation. Rahman (1988) performed ball penetration tests, and Kenyon (1994) performed laterally loaded bar tests on ice. The experimental works stated above dealt with the flow of ice around large objects. However, more directly related investigations of the flow or movement of ice through soil are needed for understanding the creep behaviour of frozen soil. Tests of ice penetrating dry sand were performed by the writer for this purpose. Since detailed research of this subject was beyond the scope of this thesis, only a preliminary study was carried out and the results are included in this chapter. The purpose of the tests was to obtain a qualitative understanding of the phenomenon rather than to establish a quantitative relationship.

7.2 Penetration Test of Ice into Dry Sand

Two penetration tests, IS1 and IS2, were performed to explore the possibility and the rate of ice flow through a sand skeleton. The tests were performed in a cold chamber using an ordinary oedometer. Basically, a layer of sand was placed in the bottom half of the oedometer ring, and a layer of ice was placed in the upper half. Load was applied to the ice through the loading cap. A schematic of the test setup is shown in Fig.7.1.

The sand used for Test IS1 was the same medium sand that was used in the triaxial tests, which were discussed in Chapter 3, while the sand used in Test IS2 was a coarser uniform, coarse-grain, quartz-carbonate sand with grain diameters ranging between 1.2 and 2.0 mm (#14 and 10 sieves). The latter sand was obtained by sieving.

The ice samples were prepared in a plexiglass mould having the same inner diameter as that of the oedometer ring. Distilled water was gradually poured into the mould until the water reached the preset level of about 10 mm. The plastic mould together with the water was then put into a plexiglass container with a tightly sealed lid. A vacuum pressure of 50 kPa was applied to the container to extract any air bubbles from the water. The suction was maintained for twenty four hours. The mould was then moved out of the container and insulation was placed around the mould and on its top. The bottom of the mould was not insulated. The mould was put into a freezer which was kept at a temperature of -20°C and the water was frozen unidirectionally from the bottom to the top. After the ice sample was formed, the mould along with the ice sample was put inside the cold chamber set at -5°C for more than

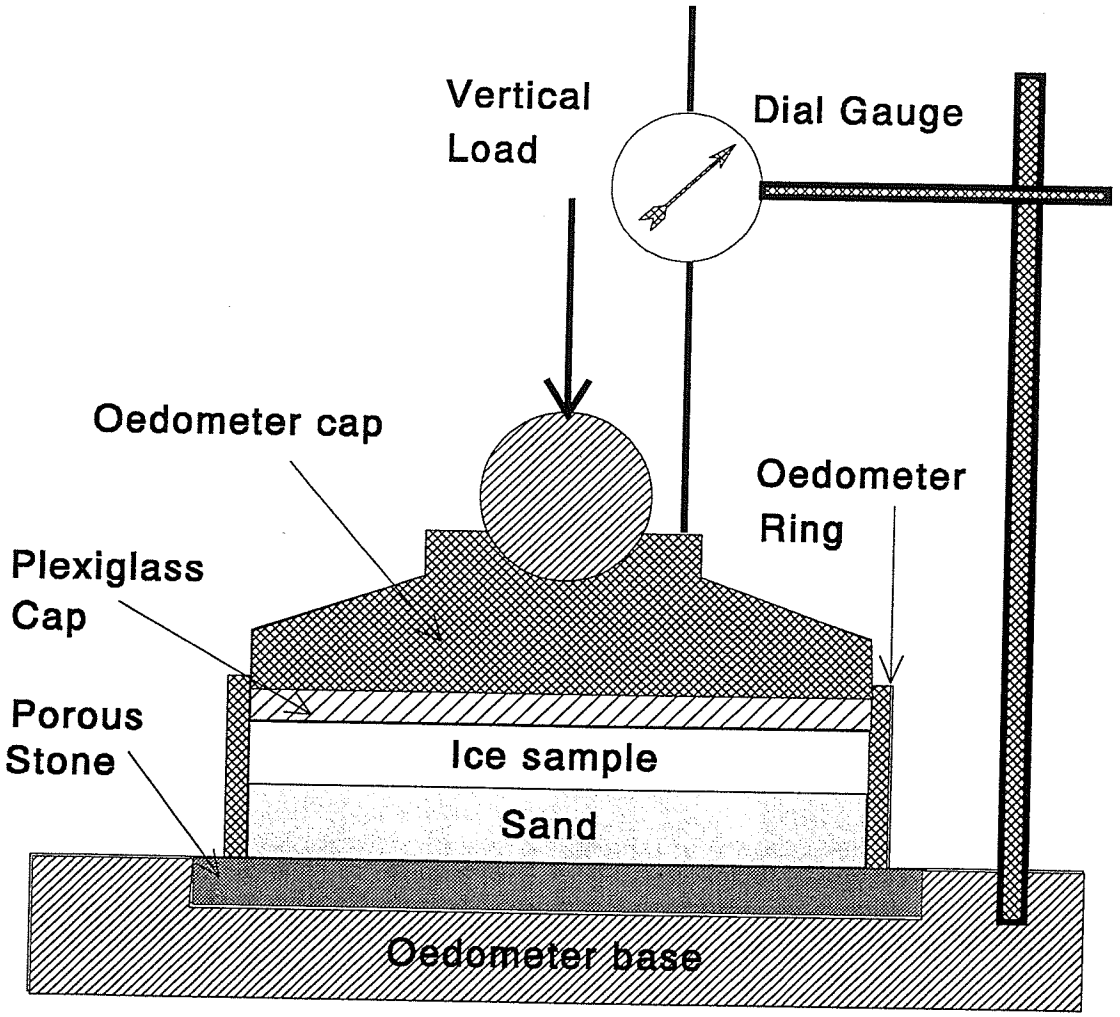

Fig.7.1 A schematic of the test setup for ice-dry sand penetration test.

twenty four hours to allow the specimen to reach temperature equilibrium. The specimen was then removed from the mould and trimmed to a height of 7.5 mm.

The first step of the test was to consolidate the dry sand as follows. As shown in Fig.7.1, a porous stone was inserted in the base of the oedometer, and then a layer of dry sand was placed on the porous stone. The sand had been oven-dried and had then been placed inside the cold chamber for more than a day before it was used in the test. After the sand was put in the oedometer, the loading cap was put on the top of the sand and a dial gauge was mounted to measure the displacement. A vertical load of 11.5 kN was applied and the vertical displacement of the cap was measured. The load was maintained for about two hours to allow time for the sand to consolidate. The load was then removed gradually and the vertical displacement during the unloading was also recorded. This step was performed to take the consolidation effect of the sand out of the penetration testing.

After consolidation, the cap of the oedometer was removed and the prepared specimen of ice was put on the top of the sand. A plexiglass disk was placed on top of the ice, and the cap of the oedometer was placed on the plexiglass as shown in Fig.7.1. The dial gauge for the displacement measurement was installed on the top of the oedometer again. A load was gradually applied until it reached the predetermined level and the vertical displacement was recorded together with the load. Test IS1 was a two-stage test with a vertical load of 6.37 kN corresponding to a vertical stress of 2.02 MPa for the first stage which lasted for three days and a vertical load of 11.5 kN corresponding to a vertical stress of 3.63 MPa for the next stage which lasted for 182 days.

Test IS2 was set up in the same manner as Test IS1. However, it was an single-stage test with a vertical load of 7.5 kN corresponding to a vertical stress of 2.34 MPa. The test lasted for 175 days, and the vertical displacements were recorded with time.

Fig.7.2 shows the displacement versus time data for both tests. The elastic displacement due to the deformation of test equipment and sand layer are deducted from the total penetration displacement, therefore the displacements shown in Fig.7.2 represent the penetration of the ice into the sand. The following three preliminary observations can be made from the test results:

(1) The rate of penetration was high at the start of loading for both tests. This is mainly because the contact area between sand particles and ice was small at that time, and therefore the contact stress was high, thus resulting in a high penetration rate.

(2) The rate of penetration decreased with time in both tests. Within the first three days, the penetration rate of IS1 which had finer sand and lower stress level was significantly smaller than that of IS2 which had coarser sand and higher stress level. This was expected since the contact area between sand particles and ice for coarser sand (IS2) was smaller than that for finer sand (IS1) at this stage, therefore the contact stress for the coarser sand was higher than that for finer sand. After three days, the stress level for IS1 was increased to 3.63 MPa which was significantly higher than the stress acting on IS2.

Because of the very limited amount of data, the effect of stress versus the effect of

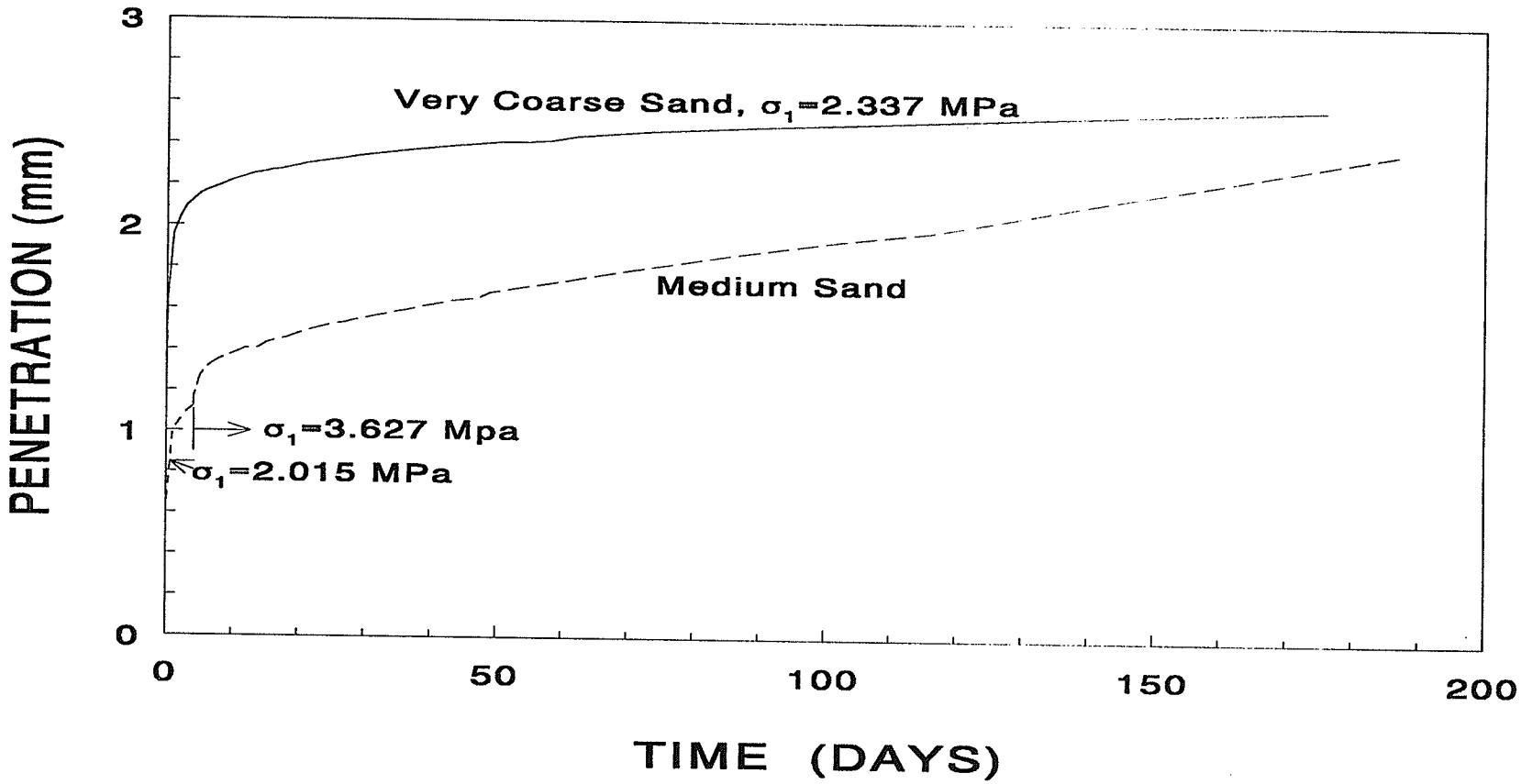

Fig.7.2 Penetration versus time in ice-sand penetration tests.

grain size could not be analyzed. However, the test results support the concept that ice under stress will move within a soil skeleton.

CHAPTER 8

CONCLUSIONS AND RECOMMENDATIONS

8.1 CONCLUSIONS

Based on the premise that ice can sustain both normal and shear stresses, the concept of effective stress was introduced into the behaviour of frozen soil and a corresponding constitutive creep model was developed. The total stress was separated into a component carried by the soil skeleton and a component carried by the pore matrix. The pore matrix consisted of both the unfrozen water and the pore ice. No distinction was made between pore ice pressure and pore "unfrozen" water pressure. It was tacitly assumed that the creep behaviour of the frozen soil was dictated by the excess pore matrix stress and the creep characteristics of the ice. The creep behaviour of the frozen soil was separated into its response to changes in the volumetric component of stress, which was represented by the mean normal stress, and its response to changes in the shear component of stress which was represented by the deviate stress. The model was calibrated using triaxial test data and was verified by applying it to triaxial test results that were not used in the calibration and in which the stress paths were different from those used in the calibration. The stages of development, calibration, and verification of the model are presented below.

1. It was assumed that an increase in hydrostatic stress caused a corresponding excess pore ice pressure which induced volumetric creep that continued until the excess ice pressure was dissipated. The relationship between the rate of volumetric creep strain and excess

pore ice pressure was represented by Eq.(4.12).

$$\dot{\epsilon}_{vc} = \frac{\alpha \epsilon_{vc0}}{t^*}\left(\frac{p}{p_0}\right)^m U_c^{1-\frac{1}{\alpha}}(1-U_c)^{1+\frac{1}{\alpha}} \qquad (4.12)$$

2. The parameters required for the calibration of the above relationship were taken from the results of isotropic compression tests performed on a sand in both the unfrozen and frozen states.

3. It was assumed that an increase in the total shear stress resulted in an increase in the pore ice shear stress which was separated into an excess ice shear stress and a sustainable shear stress. The excess ice shear stress was the cause of shear creep which continued until the pore ice shear stress was reduced to the sustainable magnitude. The rate of shear creep strain was related to the excess ice shear stress by a power law relationship Eq.(5.55).

$$\dot{\epsilon}_{sc} = F_t \dot{\epsilon}_{s0}\left(\frac{q_e}{q_0}\right)^n \qquad (5.55)$$

4. The parameters required for the calibration of the above equation were taken from constant mean normal stress, triaxial creep tests on a frozen sand and conventional triaxial tests on the sand in an unfrozen state.

5. The predictive capability of the two governing equations was assessed by generating solutions for 5 different triaxial creep tests for which there were experimental data, and comparing the predicted strains with the measured strains.

(a) Eq.(4.12) was used to generate a creep curve for a multi-stage, isotropic compression creep test, which had stress levels of 50, 100, 150, 200, and 300 kPa and a total time duration of 4466 hours. The maximum variation between the generated and the experimental data was 6%.

(b) Eq.(5.55) together with (4.12) was used to generate 3 creep curves for three multi-stage, constant mean normal stress, triaxial creep tests. The average variation between the experimental and the predicted shear strains was 17.3% for Test MST1, 5.2% for Test MST2, and 9.2% for Test MST3. Part of the variation was attributed to temperature and density differences between the samples used in the calibration and those used in the verification study.

(c) Eq.(5.55) and (4.12) were used to generate a creep curve for a multi-stage, constant cell pressure, triaxial creep test which lasted 8400 hours (350 days) and in which the cumulated shear strain was 2.8%. The maximum variation between the measured and the predicted shear strains was about 10% for the time period of 0 to 6000 hours. After 6000 hours, the variation increased, and the predicted shear strains were about 20-25% higher than the measured strains.

6. Although the stress components used in the development, calibration and verification of the model were based on the triaxial stress state, the model can accommodate a more general stress state by replacing the components with more general expressions, such as those used by Domaschuk and Wade (1969).

7. The model also provides a rational method of incorporating stress changes during the creep process. This was accomplished by expressing strain rates in terms of the stress history, and the prevailing state of strain. Current models express strain and strain rate in terms of time, which does not provide a rational means of accommodating stress changes, since time is not a measure of the changes in creep properties that occur with strain.

8. Separating applied stresses into a component carried by the soil skeleton and a component carried by the pore matrix, offers a conceptual model that explains the cause and duration of creep of frozen soils. It has been demonstrated that such a model can be developed from a theoretical basis, and that it has reasonable predictive capability. However, it requires more extensive development in order for it to become a practical method of dealing with the creep of various types of frozen soils and for a range of soil temperatures.

8.2 RECOMMENDATIONS FOR FURTHER STUDY

The model developed in this study is fundamentally different from the models developed in the past. New parameters were introduced, and therefore more extensive research is required to establish a better data base for those parameters. The study was limited to a single soil, (a sand) at a single temperature, and therefore more experiments should be performed on different types of soils and at different temperatures. The following specific suggestions are made for future development of this model.

1. More single-stage, isotropic compression creep tests are required to establish a more

representative relationship between the ultimate volumetric strain and hydrostatic pressure. By comparing the difference between the ultimate volumetric strain - hydrostatic pressure curve of a frozen soil with the isotropic compression curve of the soil in an unfrozen state, the value of the effective ice pressure, p_i, which represents the hydrostatic pressure sustained by the ice matrix at the ultimate state of volumetric creep, may be obtained.

2. More single-stage, constant mean normal stress triaxial creep tests are required to establish a more representative relationship among mean normal stress, shear stress and the ultimate shear strain of frozen soil.

3. Shear tests on ice are required to obtain a relationship between the ultimate sustainable shear stress of ice and temperature.

4. Studies should be performed on different types of soil and at different temperatures to establish the dependency of the parameters of the model on the soil types and temperature.

5. The effect of anisotropy of frozen soil on the creep behaviour should be studied.

REFERENCE

1. Alkire, B.D., and Andersland, O.B. 1973. The effect of confining pressure on the mechanical properties of sand-ice materials. J. Glaciology. **12**(66): 469-481.

2. Andersland, O.B., and Akili, W. 1967. Stress effect on creep rates of a frozen clay soil. Géotechnique, **17**: 27-39.

3. Andersland, O.B., and AlNouri, I. 1970. Time dependent strength behaviour of frozen soils. J. Soil Mech. Found. Div. ASCE **96**(SM4): 1249-1265.

4. Assur, A. 1979. Some promising trends in ice mechanics. Physics and Mechanics of Ice : IUTAM Symp., Copenhagen, ed. P. Tryde. Berlin: Springer-Verlag, pp.1-15.

5. Azizi, F. 1989. Primary creep of polycrystalline ice under constant stress. Cold Regions Science and Technology. **16**: 159-165.

6. Baker, T. H. W. 1979. Strain rate effect on the compressive strength of frozen sand. Proc. First Int. Symp. on Ground Freezing, Bochum, Germany, ed. H. L. Jessberger. Amsterdam: Elsevier. pp. 223-231.

7. Been, K., and Jefferies, M.G. 1985. A state parameter for sane. Geotechnique, **35**(2): 145-156.

8. Bourbonnais, J., and Ladanyi, B. 1985a. The mechanical behaviour of frozen sand down to cryogenic temperatures. Proc. 4th Int. Symp. on Ground Freezing, Sapporo, Japan. Rotterdam: A.A. Balkema, Vol. 1, pp. 235-244.

9. Bourbonnais, J., and Ladanyi, B. 1985b. The mechanical behaviour of a frozen clay down to cryogenic temperatures. Proc. 4th Int. Symp. on Ground Freezing, Sapporo, Japan. Rotterdam: A.A. Balkema, Vol. 2, pp. 237-244.

10. Bragg, R.A., and Andersland, O.B. 1980. Strain rate, temperature and sample size effects on compressive and tensile properties of frozen sand. Proc. 2nd Int. Symp. on Ground Freezing, Trondheim, Norway, Vol. 1, 34-47.

11. Čadek, J. 1988. Creep in Metallic Materials. Materials Science Monographs, 48, Amsterdam - Oxford - New York - Tokyo: Elsevier.

12. Chadwick, G.A., and Smith, D.A. 1976. Grain Boundary Structure and Properties. London: Academic Press.

13. Chamberlain, E.J., Groves, E., and Perham, R. 1972. The mechanical behaviour of

frozen earth materials under high pressure triaxial test conditions. Geotechnique **22**(3): 469-483.

14. Cole. D. M. 1986. Effect of grain size on the internal fracturing of polycrystalline ice. U.S. Army Cold Regions Research and Engineering Laboratory, CRREL Rep. 86-5.

15. Cole, D. M. 1988. Crack nucleation in polycrystalline ice. *Cold Regions Science and Technology*. **15**(1): 79-87.

16. Cole, D. M. 1989. Microfracture and the compressive failure of polycrystalline ice. Proc. IUTAM/IAHR Symp. Ice-Structure Interaction. St. John's, Newfoundland, Canada.

17. Conrad, H. 1961. Experimental evaluation of creep and stress rupture. Mechanical behaviour of materials at elevated temperatures. ed. J. E. Dorn. McGraw-Hill, New York, pp. 149-217.

18. Domaschuk, L., Shields, D.H., Man, C-S., and Yong, E. 1983. Creep Behaviour of frozen saline silt under isotropic compression. Proc. 4th Int. Conf. on Permafrost, Fairbanks, Alaska. Washington, D.C.: Academy Press, pp. 238-243.

19. Domaschuk, L., Shields, D.H., and Rahman, M. 1991. A model for attenuating creep of frozen sand. Cold Regions Science and Technology. **19**: 145-161.

20. Domaschuk, L., and Wade, N.H. 1969. A study of bulk and shear moduli of sand. J. Soil Mech. Found. Eng. ASCE, **95**(SM2): 561-582.

21. Evans, R.W., and Wilshire, B. 1985. Creep of Metals and Alloys. London: The Institute of Metals.

22. Eyring, H. 1936. Viscosity, plasticity and diffusion as example of absolute reaction rates. Journal of Chemical Physics, 4(4): 283-291.

23. Fish, A. M. 1980. Kinetic nature of the long-term strength of frozen soils. Proc. 2nd Int. Symp. on Ground Freezing, Trondheim, Norway, Vol. 1, 98-108.

24. Fish, A. M. 1982. Deformation and failure of frozen soils and ice at constant and steadily increasing stresses. Proc. 4th Canadian Permafrost Conference, Calgary, Alberta, Canada. pp. 419-428.

25. Fish, A. M. 1983. Thermodynamic model of creep at constant stresses and constant strain rates. U.S. Army Cold Region Research and Engineering Laboratory, CREEL Report 83-33.

26. Fish, A. M. 1985. Creep strength, strain rate, temperature, and unfrozen water

relationship in frozen soil. Proc. 4th Int. Symp. on Ground Freezing, Sapporo, Japan. Rotterdam: A.A. Balkema, Vol. 2, pp. 29-36.

27. Fish, A. M. 1987. Shape of creep curves in frozen soils and polycrystalline ice. Canadian Geotechnical Journal, **24**: 623-629.

28. Frenkel, J. 1946. Kinetic Theory of Liquids. London: Oxford Press.

29. Fish, A.M., and Assur, A. 1984. Discussion paper, Tertiary creep model for frozen sand, by J.M. Ting. Journal of Geotechnical Engineering, ASCE **110**(9): 1373-1378.

30. Gardner, A.R., Jones, R.H., and Harris, J. S. 1984. A new creep equation for frozen soils and ice. Cold Regions Science and Technology. **9**: 271-275.

31. Glasstone, S., Laidler, K.J., and Eyring, H. 1941. The Theory of Rate Processes. New York: McGraw-Hill.

32. Gold, L.W., and Krausz, A.S. 1971. Investigation of the mechanical properties of St. Lawrence River ice. Canadian Geotechnical Journal, **23**(8): 163-169.

33. Gold, L. W. 1973. Activation energy for creep of columnar grained ice. Physics and Chemistry of Ice, eds. E. Whalley, S. J. Jones, and L. W. Gold, pp. 362-364.

34. Gold, L.W., and Sinha, N.K. 1979. The rheological behaviour of ice at small strain. Physics and Mechanics of Ice : IUTAM Symp., Copenhagen, ed. P. Tryde. Berlin: Springer-Verlag, pp.117-128.

35. Goughnour, R.R., and Andersland, O.B. 1968. Mechanical properties of a sand-ice system. J. Soil Mech. Found. Eng. ASCE **94**(SM4): 923-950.

36. Hawkes, I., and Mellor, M. 1972. Deformation and fracture of ice under uniaxial stress. Journal of Glaciology. **11**(61): 103-131

37. Haynes, F.D. 1978. Strength and deformation of frozen silt. Proc. 3rd Int. Conf. on Permafrost, Edmonton, Alberta, Canada. Ottawa: National Research Council of Canada, Vol. 1, pp. 656-661.

38. Haynes, F.D., and Karalius, J.A. 1977. Effect of temperature on the strength of frozen silt. U.S. Army Cold Regions Research and Engineering Laboratory, CREEL Rep. CR77-03.

39. Haynes, F.D., Karalius, J.A., and Kalafut, J. 1975. Strain rate effect on the strength of frozen silt. U.S. Army Cold Regions Research and Engineering Laboratory, Technical Report 350.

40. Herrin, M., and Jones, G.E. 1963. The behaviour of bituminous materials from the viewpoint of the absolute rate theory. Proc. tech. Sess. Ass. Asph. Pav. Technol., **32**: 82-105.

41. Hooke, R. LeB., Dahlin, B.B., and Kauper, M.T. 1972. Creep of ice containing dispersed fine sand. Journal of Glaciology. **11**(63): 327-336.

42. Hult, J.A.H. 1966. Creep in Engineering Structures. Waltham Mass.: Blaisdell.

43. Ishihara, K., Tatsouka, F., and Yasuda, S. 1975. Undrained deformation and liquefaction of sand under cyclic stresses. Soils and Foundations, Japanese Soc. Soil Mech. Found. Eng. **15**(1): 29-44.

44. Jones, S.J., and Parameswaran, V.R. 1983. Deformation behaviour of frozen sand-ice material under triaxial compression. Proc. 4th Int. Conf. on Permafrost, Fairbanks, Alaska. Washington, D.C.: Academy Press, pp. 560-565.

45. Kalifa, P., Ouillon, G., and Duval, P. 1992. Microcracking and the failure of polycrystalline ice under triaxial compression. Journal of Glaciology, **38**(128):65-76.

46. Kauzman, W. 1941. Flow of solid metals from the standpoint of the chemical-rate theory. Trans. Am. Inst. Min. Metall. Engrs, **143**: 57-81.

47. Kenyon, R.M. 1994. Lateral Creep Behaviour of Discrete "Winkler" Pile Elements in Ice. Ph.D. thesis, The University of Manitoba, Winnipeg, Manitoba, Canada.

48. Ladanyi, B. 1972. An engineering theory of creep of frozen soils. Canadian Geotechnical Journal, **9**(1): 63-80.

49. Ladanyi, B. 1981. Mechanical behaviour of frozen soils. Proceedings, International Symposium on Mechanical Behaviour of Structured Media, Ottawa, Canada, May 18-21, 1981, Part B. pp. 205-245.

50. Ladanyi, B., and Morel, Jean-Francois. 1990. Effect of internal confinement on compression strength of frozen sand. Canadian Geotechnical Journal, **27**: 8-18.

51. Le Gac, H., and Duval, P. 1978. Constitutive relations for the non elastic deformation of polycrystalline ice. Physics and Mechanics of Ice : IUTAM Symp, Copenhagen, ed. P. Tryde. Berlin: Springer-Verlag, pp. 51-59.

52. Mclean, D. 1957. Grain Boundaries in Metals. Oxford: Clarendon Press.

53. Mellor, M. 1979. Mechanical properties of polycrystalline ice. Physics and Mechanics of Ice: IUTAM Symp, Copenhagen, ed. P. Tryde. Berlin: Springer-Verlag, pp. 217-245.

54. Mellor, M., and Cole, D.M. 1982. Deformation and failure of ice under constant stress or constant strain-rate. Cold Regions Science and Technology. **5**: 201-219.

55. Norton, F.H. 1929. Creep of Steel at High Temperature. New York: McGraw-Hill.

56. Odqvist, F.K.G. 1966. Mathematical Theory of Creep and Creep Rupture. Oxford Mathematical Monographs. Oxford: Clarendon Press.

67. Parameswaran, V.R. 1980. Deformation behaviour and strength of frozen sand. Canadian Geotechnical Journal **17**(1): 74-88.

58. Perkins, T.K., and Ruedrich, R.A. 1973. The mechanical behaviour of synthetic permafrost. Soc. Pet. Eng. J. AIME **13**(4): 211-220.

59. Perkins, T.K., and Ruedrich, R.A. 1974. A study of factors influencing the mechanical properties of deep permafrost. Journal of Petroleum Technology. **26**:1167-1177.

60. Pewe, T.L. 1983. Alpine permafrost in the contiguous United States. Arctic and Alpine Research, **15**(2): 145-156.

61. Pusch, R. 1977. Rate process theory and clay microstructure. Proc. 9th International Conference in Soil Mechanics, Tokyo, pp. 223-227.

62. Pusch, R. 1979. A physical clay-creep model and its mathematical analogy. Proc. 3rd Int. Conf. Numerical Methods Geomech., Aachen, Vol. 1, pp. 485-491.

63. Pusch, R., and Feltham, P. 1980. A stochastic model of the creep of soils. Géotechnique, **30**(4): 497-506.

64. Rahman M. 1988. A constitutive model for creep of a frozen sand. Ph.D. Thesis, The University of Manitoba, Winnipeg, Manitoba, Canada.

65. Rein, R.G., Hathi, V.V., and Sliepcevich, C.M. 1975. Creep of sand ice system. J. Geotech. Eng. Div. ASCE **101**(GT2): 115-128.

66. Rist, M.A., and Murrell, S.A.F. 1994. Ice triaxial deformation and fracture. Journal of Glaciology, **40**(135): 305-318.

67. Rowe, P.W. 1962. The stress-dilatancy relation for static equilibrium of an assembly of particles in contact. Proc. Roy. Soc. A, Vol. 269.

68. Sayles, F.H. 1968. Creep of Frozen sands. U.S. Army Cold Regions Research and Engineering Laboratory, Technical Report 190.

69. Sayles, F.H. 1973. Triaxial and creep tests on frozen Ottawa sand. Proc. North American Contribution, 2nd Int. Conf. on Permafrost, Yakutsk, U.S.S.R. Washington, D.C.: National Academy of Science, pp. 384-391.

70. Sayles, F.H. 1988. State of the art: Mechanical properties of frozen soil. Ground Freezing 88: 5th Int. Symp. on Ground Freezing, Nottingham, ed. R. H. Jones and J. T. Holden: Balkema-Rotterdam-Brookfield, pp. 143-165.

71. Sayles, F.H., and Carbee, D.L. 1981. Strength of frozen silt as a function of ice content and dry unit weight. Engineering Geology **18**: 55-66.

72. Sayles, F.H., and Haines, D. 1974. Creep of frozen silt and Clay. U.S. Army Cold Regions Research and Engineering Laboratory, Technical Report 252.

73. Sego, D.C., and Morgenstern, N.R. 1983. Deformation of ice under low stresses. Canadian Geotechnical Journal, **20**: 587-602.

74. Sego, D.C., and Morgenstern, N.R. 1985. Punch indentation of polycrystalline ice. Canadian Geotechnical Journal, **22**: 226-233.

75. Shields, D.H., Domaschuk, L., Azizi, F., and Kjartanson, B. 1989. Primary creep parameters for ice as measured in-situ. Cold Regions Science and Technology. **16**: 281-290.

76. Shoji, H., and Higashi, A. 1978. A deformation mechanism map of ice. Journal of Glaciology, **21**(85): 419-427.

77. Sinha, N.K. 1978. Short-term rheology of polycrystalline ice. Journal of Glaciology, **21**(85): 457-473.

78. Sinha, N.K. 1979. Grain-boundary sliding in polycrystalline materials. Philosophical Magazine A, **40**(6): 825-842.

79. Sinha, N.K. 1984. Intercrystalline cracking, grain-boundary sliding, and delayed elasticity at high temperature. Journal of Material Science, **19**: 359-376.

80. Sinha, N.K. 1988. Crack-enhanced creep in polycrystalline material: strain-rate sensitive strength and deformation of ice. Journal of Materials Science, **23**: 4415-4428.

81. Sinha, N.K. 1989a. Elasticity of natural types of polycrystalline ice. Cold Regions Science and Technology. **17**: 127-135.

82. Sinha, N.K. 1989b. Ice and steel - A comparison of creep and failure. Mechanics of Creep Brittle Materials -1, eds. A. C. F. Cocks and A. R. S. Ponter, London:

Elsevier, pp. 201-212.

83. Sinha, N.K. 1989c. Microcrack-enhanced creep in polycrystalline material at elevated temperature. Acta Metall. **37**(11): 3107-3118.

84. Smith, L.L., and Cheatham, J.B. 1975. Plasticity of ice and sand ice systems. J. Eng. for Industry. **97**(2): 479-484.

85. Sunder, S.S., and Wu, M.S. 1990a. Crack nucleation due to elastic anisotropy in polycrystalline ice. Cold Regions Science and Technology. **18**: 29-47.

86. Sunder, S.S., and Wu, M.S. 1990b. On the constitutive modelling of transient creep in polycrystalline ice. Cold Regions Science and Technology. **18**: 267-294.

87. Terzaghi, K., and Peck, R.B. 1948. Soil Mechanics in Engineering Practice. New York: John Wiley.

88. Ting, J.M. 1981. The creep of frozen sands: Qualitative and quantitative Models. Ph.D. thesis, Massachusetts Institute of Technology. Cambridge, Mass. U.S.A.

89. Ting, J.M. 1983. Tertiary creep model for frozen sands. Journal of Geotechnical Engineering, ASCE, **109**(7): 933-945.

90. Ting, J.M., Martin, T.R., and Ladd, C.C. 1983. Mechanism of strength for frozen sand. Journal of Geotechnical Engineering, ASCE, **109**(10): 1286-1302.

91. Tsytovich, N.A. 1975. The Mechanics of Frozen Ground, New York: McGraw-Hill, New York.

92. Vialov, S.S. 1959. Rheological properties and bearing capacity of frozen soils. US Army Cold Regions Research and Engineering Laboratory, Translation 74.

93. Vyalov, S.S. 1973. Long term failure of frozen soil as a thermal activated process. Proc. U.S.S.R. Contribution, 2nd Int. Conf. on Permafrost, Yakutsk, U.S.S.R. Washington, D.C.: National Academy of Science, pp. 222-228.

94. Weaver, J. S. 1979. Pile foundations in permafrost. Ph.D. Thesis, University of Alberta, Edmonton.

95. Weertman, J. 1973. Creep of ice. Physics and Chemistry of Ice, eds. E. Whalley, S. J. Jones, and L. W. Gold, pp. 320-337.

96. Wijeweera H., and Joshi, R.C. 1990. Compressive strength behaviour of fine-grained frozen soils. Canadian Geotechnical Journal, **27**: 472-483.

97. Wijeweera H., and Joshi, R.C. 1991. Creep behaviour of fine-grained frozen soils. Canadian Geotechnical Journal, **28**: 489-502.

98. Zaretskiy, Y.K., and Vialov, S.S. 1971. Structural mechanics of clayey soils. Soil Mechanics and Foundation Engineering, Moscow. **8**(3):153-160.

99. Zhan, Caizhao, Evgin, E., and Sinha, N.K. 1994. A three dimensional anisotropic constitutive model for ductile behaviour of columnar grained ice. Cold Regions Science and Technology. **22**: 269-284.

100. Zhu, Y., and Carbee, D.L. 1983. Creep behaviour of frozen silt under constant uniaxial stress. Proc. 4th Int. Conf. on Permafrost, Fairbanks, Alaska. Washington, D.C.: Academy Press, pp. 1507-1512.

101. Zhu, Y., and Carbee, D.L. 1984. Uniaxial compressive strength of frozen silt under constant deformation rates. Cold Regions Science and Technology **9**: 3-15.

102. Zhu, Y., and Carbee, D.L. 1987. Tensile strength of frozen silt. U.S. Army Cold Region Research and Engineering Laboratory, CREEL Report 87-15.

103. Zhu, Y., Zhang, J., and Shen, Z. 1988. Uniaxial compressive strength of frozen medium sand under constant deformation rates. Proc. Ground Freezing 88: 5th Int. Symp. on Ground Freezing, Nottingham, ed. R. H. Jones and J. T. Holden: Balkema-Rotterdam-Brookfield, pp. 225-232.

APPENDIX A

Curve-fit of Multi-stage, Constant p', Triaxial Creep Curves Using Eq.(5.7)

Temperature fluctuations and other disturbances which existed during the experiments caused some scatter in the creep test data. The results from Tests MST4, MST5, MST7, MST8, and MST9 were chosen to calibrate the shear creep equations. In order to smooth out the scatter caused by experimental disturbances and obtain more representative data for the creep rates, the multi-stage creep curves were separated into incremental shear strain versus incremental time, and each stage was fitted by Eq.(5.7).

$$\epsilon_s = \epsilon_{si} + \epsilon_{scu} \frac{\bar{t}^{\xi}}{1 + \bar{t}^{\xi}} \tag{5.7}$$

where $\bar{t} = t/t_s$, t is the real time, and t_s is a reference time. Eq.(5.7) may be rewritten as

$$\epsilon_s = \epsilon_{si} + \epsilon_{scu} \frac{t^{\xi}}{t_s^{\xi} + t^{\xi}} \tag{5.7a}$$

Using least square scheme, constants ϵ_{si}, ϵ_{scu}, ξ, and t_s were obtained for each step of the creep curves. TABLE 1 shows the values of these constants for the long-term triaxial creep tests MST4 and MST5, while TABLE 2 shows the values of the constants for each step of the short-term triaxial creep tests MST7, MST8, and MST9.

TABLE 1. Calculated values of parameters ϵ_{si}, ϵ_{scu}, ξ, and t_s of Eq.(5.7) for long-term creep tests MST4 and MST5.

Test	Step	ϵ_{si} (%)	ϵ_{scu} (%)	ξ	t_s (Hours)
MST4	1	0.0598	0.104	1.5	5.912
	2	0.0093	2.21	0.49	6382.5
	3	0.3166	15.99	0.832	8075.6
MST5	1	0.0235	0.56	0.334	262.9
	2	0.0369	1.075	0.527	150.5
	3	0.0708	139.9	0.413	1.957×10^7

TABLE 2. Calculated values of parameters ϵ_{si}, ϵ_{scu}, ξ, and t_s of Eq.(5.7) for short-term creep tests MST7 and MST8, and MST9.

Test	Step	ϵ_{si} (%)	ϵ_{scu} (%)	ξ	t_s (Hours)
MST7	1	0.0495	0.0375	0.5271	3.134
	2	0.0086	0.6206	0.6122	4587.8
	3	0.0081	0.2452	0.561	379.0
	4	0.0076	0.1087	0.912	18.2
	5	0.011	0.1899	0.9393	19.45
	6	0.0185	0.2601	1.0065	20.83
MST8	1	0.008	0.0867	0.99	36.1
	2	0.0015	0.049	0.9521	20.23
	3	0.0131	0.1458	0.6329	22.31
	4	0.0082	0.1468	0.75	35.41
	5	0.0102	0.2637	0.6675	136.74
	6	0.0113	0.2372	0.7841	64.01
	7	0.0058	0.3222	0.74	77.67
	8	0.0179	0.525	0.813	85.97
	9	0.073	13.61	0.813	4810.0
MST9	1	0.0175	0.0675	0.625	1.917
	2	0.0238	0.16	0.7018	19.56
	3	0.0391	0.2657	0.8868	8.17
	4	0.0141	0.13	0.9278	24.16
	5	0.014	0.242	0.8073	55.25
	6	0.0181	0.2339	0.9358	26.55
	7	0.0135	0.3452	0.9839	41.17
	8	0.021	0.4942	0.9032	48.51
	9	0.0272	0.5939	0.9892	39.48
	10	0.0312	1.15	0.8983	74.55

APPENDIX B

Mathematical Expression of the Stress-strain Curve for a Medium to Dense Sand

The following figure shows a schematic of a stress-strain curve for a medium to dense sand or overconsolidated clay under constant effective mean normal stress.

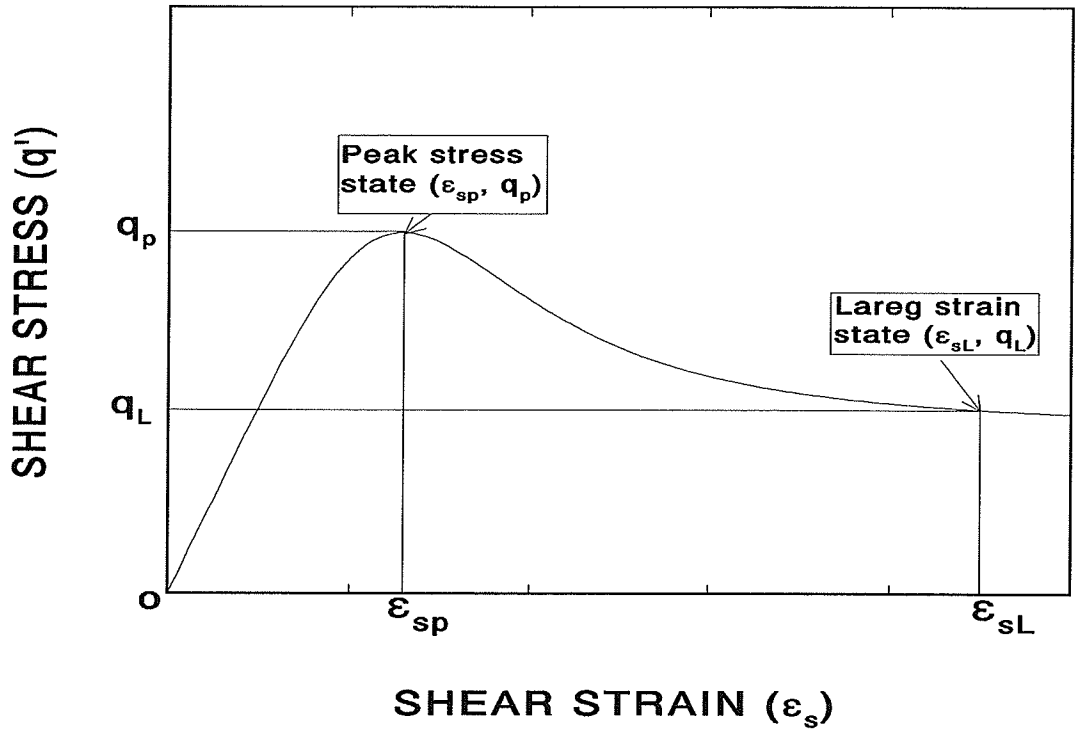

The curve shows a peak shear strength, q_p, which is greater than the large strain shear strength, q_L. This type of behaviour is typical for dense sand or overconsolidated clay due to the effect of dilatency. In order to provide a mathematical expression for this type of stress-strain relationship, Eq.(5.12) is introduced.

$$q' = q_L^* \frac{\epsilon_s^2 + c\epsilon_s^{\beta}}{\epsilon_s^2 + d^2} \tag{5.12}$$

Where q_L^*, c, d and β are constants. Parameters q_L^*, c and d are introduced to ensure that the curve produced by (5.12) goes through the peak strength state point, (ϵ_{sp}, q_p), the large strain state point, (ϵ_{sL}, q_L), and obtains its maximum value at the peak strength state, as discussed in **5.3.3.1**. Once the known conditions at points (ϵ_{sp}, q_p) and (ϵ_{sL}, q_L) are satisfied, the curve is fairly close to the measured stress-strain curve. Parameter β is introduced to bring the theoretical curve given by (5.12) closer to the measured curve. The values of β were found to be between 0.3 to 0.6 for the sand tested here. Since (5.12) is not sensitive to the β value, a fixed value of β=0.45 was used for the sand studied.

Parameters q_L^*, c and d are determined as follows:

(I) Differentiate (5.12) with respect to ϵ_s

$$\frac{d(q')}{d\epsilon_s} = q_L^* \frac{(\epsilon_s^2 + d^2)(2\epsilon_s + c\beta\epsilon_s^{\beta-1}) - (\epsilon_s^2 + c\epsilon_s^{\beta})2\epsilon_s}{(\epsilon_s^2 + d^2)^2} \tag{B.1}$$

Combining the items in (B.1) and simplifying it, we have

$$\frac{d(q')}{d\epsilon_s} = q_L^* \frac{2d^2\epsilon_s + d^2c\beta\epsilon_s^{\beta-1} + c\beta\epsilon_s^{\beta+1} - 2c\epsilon_s^{\beta+1}}{(\epsilon_s^2 + d^2)^2} \tag{B.2}$$

(II) Impose three known conditions stated in **5.3.3.1**, which are (1) $q' = q_p$ when $\epsilon_s = \epsilon_{sp}$, (2)

$q' = q_L$ when $\epsilon_s = \epsilon_{sL}$, and (3) $dq'/d\epsilon_s = 0$ when $\epsilon_s = \epsilon_{sp}$.

By substituting condition (1) into (5.12), we have

$$q_p(\epsilon_{sp}^{\ 2} + d^2) = q_L^*(\epsilon_{sp}^{\ 2} + c\epsilon_{sp}^{\ \beta}) \tag{B.3}$$

By substituting condition (1) into (5.12), we have

$$q_L(\epsilon_{sL}^{\ 2} + d^2) = q_L^*(\epsilon_{sL}^{\ 2} + c\epsilon_{sL}^{\ \beta}) \tag{B.4}$$

By substituting condition (3) into (B.2), we have

$$2d^2\epsilon_{sp} + cd^2\beta\epsilon_{sp}^{\ \beta-1} - c(2-\beta)\epsilon_{sp}^{\ \beta+1} = 0 \tag{B.5}$$

By solving simultaneous equations (B.3), (B.4) and (B.5), the expressions for q_L^*, c and d are obtained as

$$q_L^* = \frac{q_L q_p(2-\beta+\beta f^2) - 2q_p^{\ 2} f^\beta}{(2-\beta)q_L + (\beta f^2 - 2f^\beta)q_p} \tag{5.16}$$

where $f = \epsilon_{sL}/\epsilon_{sp}$.

$$c = \frac{2(k-1)}{\beta}\epsilon_{sp}^{\ 2-\beta} \tag{5.17}$$

$$d^2 = \frac{(2-\beta)(k-1)}{\beta k}\epsilon_{sp}^{\ 2} \tag{5.18}$$

where $k = q_p / q_L^*$. Variables q_p, q_L, ϵ_{sp}, and ϵ_{sL} may be obtained experimentally, and they are function of effective mean normal stress.